University of Nottingham
UK | CHINA | MALAYSIA

Biotechnology and Biological Sciences Research Council

Development of Genetic Tools for the Chemolithoautotroph *C. metallidurans* CH34: Harnessing Synthetic Biology to Expand Knowledge of Extracellular Electron Transfer

Federico Turco, MSc

Thesis submitted to the University of Nottingham for the degree of Doctor of Philosophy

December 2021

Declaration

Unless otherwise acknowledged, the work presented in this thesis is my own. No part has been submitted for another degree at the University of Nottingham or any other institute of learning

Federico Turco, December 2021

Abstract

Synthetic biology is based on engineering principles by assembling characterized genetic parts to redesign organisms with new abilities that can be used for the benefit of society.

Among the list of microbial chassis under investigation for industrial purposes, the facultative chemolithoautotroph *Cupriavidus metallidurans* CH34 exhibits a series of qualities that makes it ideal for applications such as bioremediation, bioprocessing and generation of bioelectricity in Microbial Fuel Cells (MFCs). Nevertheless, the lack of genetic tools for strain development and for the study of fundamental physiological mechanisms, currently represents a bottleneck to boost commercial applications of *C. metallidurans* CH34.

The main aim of this study was to develop a "toolkit starter-pack" to investigate physiological processes, such as extracellular electron transfer (EET) in *C. metallidurans* CH34 and to expand the repertoire of genetic tools available for its exploitation in the biotechnology industry. Firstly, Plasmid Addiction Systems (PASs) were developed and assessed in continuous growth conditions for stable plasmid maintenance and heterologous protein expression. Unfortunately, none of the PASs developed during this study achieved stable plasmid maintenance. Failure to develop a stable plasmid-based expression platform further highlighted the necessity of developing suitable tools and methodologies for chromosomal alterations, including chromosomal integrations of heterologous genes. Inducible and constitutive promoter libraries were built and characterized that served the dual purpose of i) providing a first comprehensive list of biological parts for regulation of protein expression and ii) to use these parts to optimize a CRISPR-Cas9 system that would allow efficient chromosomal alterations in *C. metallidurans* CH34. Subsequently, a single-plasmid

CRISPR-Cas9 system that can be delivered by electroporation was successfully developed for fast, marker-less genome editing of *C. metallidurans* CH34. To my knowledge, this is the first marker-less genome editing tool developed for this organism that allows for precise gene deletions and integration of heterologous DNA. The genome editing system was validated and further exploited to study the mechanisms of EET in *C. metallidurans* CH34. Deletion targets were selected based on candidate genes encoding for type IV pili which are believed to be among the major actors for EET to solid surfaces in *G. sulfureducens*. As it was hypothesised that type IV pili might fulfil the same function in *C. metallidurans* CH34, single (Δ*pilA*, Δ*pilE*) and double deletions strains (Δ*pilAE)* were generated using the newly developed CRISPR-Cas9 system. The strain *C. metallidurans* CH34 Δ*pilAE* was further studied by means of Cyclic Voltammetry using disposable Screen-Printed Carbon Electrodes (SPCEs). No difference in current generation was found in deletion strains when compared to the wild type *C. metallidurans* CH34, suggesting that the type IV pilins were not involved in EET. Nevertheless, it was discovered that *C. metallidurans* CH34 was capable of generation of extracellular currents thanks to the use of both electroactive soluble mediators and molecules adsorbed on the electrode surface.

Future work should include bolstering of the genetic toolbox by i) implementation of multiplex CRISPR-Cas9 systems for editing of multiple genes and expansion of the inducible and constitutive promoter libraries for precise regulation of gene expression ii) further elucidation of the EET mechanisms by means of omics disciplines and genetic studies of thick electrogenic biofilms of *C. metallidurans* CH34 in MFCs and iii) use of the tools developed to generate mutant strains for increased extracellular electron transfer.

Altogether this work represents a significant advancement in terms of development of genetic tools and knowledge regarding EET mechanisms adopted by *C. metallidurans* CH34 that hopefully will bolster its exploitation in MFCs and other fields of biotechnology.

Acknowledgments

Firstly, I would like to express my gratitude to my supervisors, Prof. Frankie Rawson, Dr. Katalin Kovacs, and Prof. Phil Hill for all the precious advice and the support during critical stages of my PhD.

Secondly, I would like to thank my family for the support and encouragement. You brought me up nourishing curiosity and backing my desire to study and live abroad. All this would have not been possible if it wasn't for your support.

The biggest thanks to my partner Sara. Without your love, patience and support I don't know if I would have made it. Sharing this journey and going through the pandemic with you has been an incredible bonding and learning experience that motivated me to become a better person.

List of abbreviations

5-FOA = 5 Fluoroorotic Acid

AnO_2 = Anaerobic

Ar = Arabinose

BES = Bioelectrochemical Systems

CAT = Chloramphenicol Acetyltransferase

cPCR = Colony PCR

Chl = Chloramphenicol

CE = Counter Electrode

CV = Cyclic Voltammetry

DET = Direct Electron Transfer

DMR = Dissimilatory Metal Reducing

DSB = Double Strand Breaks

EET = Extracellular Electron Transfer

EDP = Entner-Doudoroff Pathway

EMP = Embden-Meyerhof Pathway

ETC = Electron Transport Chain

FC = Flow Cytometry

FCI^+ = Ferrocyanide

FCI = Ferricyanide

FMN = Flavin Mononucleotide

GHG = Greenhouse Gases

GMB = Genetically Modified Bacteria

GOI = Gene of Interest

HR = Homologous Recombination

iPCR = Inverse PCR

Kan = Kanamycin

LB Gen^+ = LB agar plates supplemented with gentamycin 10 μg/mL

LB IND = LB agar plates supplemented with Gentamycin 10 μg/mL, tetracycline 20 μg/mL, theophylline 5 mM and arabinose 0.1%

LB Tc^+ = LB agar plates supplemented with tetracycline 20 μg/mL

MES = Microbial Electrosynthesis Systems

MET = Mediated Electron Transfer

MFC = Microbial Fuel Cells

MIC = Minimal Inhibitory Concentration

Mtr = metal-reducing

MIC = Minimal Inhibitory Concentration

MGE = Mobile Genetic Elements

NADH = Nicotinamide Adenine Dinucleotide Hydride

NHEJ = Non-Homologous-End Joining

ncRNAs = non-coding RNAs

PAS = Plasmid Addiction System

PHB = Polyhydroxybutyrates

PI = Propidium Iodide

Pip = Piperacillin

PST = Plasmid Stability Test

RE = Reference Electrode

RBS = Ribosome Binding Site

SAM = Single Assembled Monolayer

TCA = Citric Acid Cycle

SD = Standard Deviation

SGMM = 0.4% Sodium-Gluconate Minimal Media

2% SGMM = 2% Sodium-Gluconate Minimal Media

SPCE = Screen Printed Carbon Electrodes

SPE = Screen Printed Electrode

TA = Toxin-antitoxin

Tc = Tetracycline

TEA = Terminal Electron Acceptor

Th = Theophylline

WB = Western Blot

WE = Reference Electrode

List of Figures

List of Tables

Table of Content

1 -Industrial Microbiology as Fundamental Tool to Solve the Climate and Energy Crisis

1.1 The Bioeconomy Revolution to Solve the Climate and Social Emergencies

Since the dawn of the industrial revolution, economic development and environmental degradation have been deeply intertwined due to the overexploitation of fossil fuels and natural resources. This has rapidly led to a critical situation which has manifested as major economic, social, and environmental crisis where the health and wealth of future generations are at stake. Therefore, the current economic model which led us to this precarious position needs rapid re-thinking and modernization in favour to a new system - the Bioeconomy, defined as the conversion of waste streams and renewable resources into valuable products such as food, chemicals and biofuels[1]. Development of a Bioeconomy system entails an integrated approach where all the industrial sectors move toward the common goal of sustainable growth to ensure food security, improve public health and nutrition, make industrial processes more efficient and cleaner in the effort to mitigate climate change[2]. One of the leading sectors for development of this new economic system is biotechnology which in recent years has been transforming several key industrial fields like agriculture, health and manufacturing[3]. A good example of the role of biotechnology in the development of a circular Bioeconomy strategy is the exploitation of biotechnological techniques for development of the agricultural industry. Biotechnology helps to improve the safety and quality of the agricultural sector by connecting all the aspects of the production chain. This stems from i) development of environmentally safe products for plant growth promotion and defence against pests ii) genetic engineering of crops for addition of valuable nutrients that prevents malnutrition and diet-related diseases such as the creation of rice enriched with vitamins or folate[4,5] or improved tolerance to stress of the same crop[6] and iii) conversion of organic wastes from agricultural residues into valuable biofuels by means of microbial activity in apposite vessels

called bioreactors. Therefore, by looking at the example of the circular Bioeconomy revolving around the agricultural business, it can be stated biotechnology carries a fundamental role in solving the current climatic and social issues by improving the quality of the products and lowering the environmental costs.

1.2 Microbial Biotechnology as Core Activity for Development of the Bioeconomy for Tackling Environmental Degradation & Climate Change

Despite the term Microbial Biotechnology being of contemporary origin, the exploitation of microorganisms for human needs is an ancient activity deeply rooted within civilization. Without having the knowledge of microbial life, our ancestors used biotechnological processes to produce beer, wine, and bread. In the 20th century, thanks to the rise of recombinant DNA technologies, modified microorganisms started to be considered for production of chemicals of industrial interest and nowadays Microbial Biotechnology is one of the fastest growing industries. Among the first examples of rational genome engineering to exploit microorganisms for bioprocessing, is the use of recombinant *E. coli*[7] and *S. cerevisae*[8] for production of human insulin. Currently, the use of recombinant bacteria for production of biopharmaceuticals account for 30% of the related market[9] and many other applications resulting from microbial biotechnology research are rising, including the use of bacteria for tumor-killing[10], sensing toxic chemicals[11], producing biofuels[12], clean-up of wastewaters[13], self-healing concrete[14], carbon capture[15] and production of bioelectricity[16]. As climate change and environmental degradation is regarded to be one of the biggest challenges the human species had to face so far, several microbial based biotechnological solutions are growing within the bioeconomy strategy for green production of chemicals, biofuels, and bioenergy. These include i) exploitation

of autotrophic organisms that can be engineered to convert polluting greenhouse gases (GHGs) such as CO_2 into biofuels and/or valuable compounds[17], ii) biosynthesis of valuable chemicals and biofuels by means of bacteria able to grow on low values carbon sources and engineered *ad hoc* for the task[18] and iii) production of bioenergy by means of *wild type* or engineered microbial community-driven fermentation of biomass wastes[19]. Moreover, since the early 2000s attention has been rising for generation of bioelectricity and valuable chemicals while simultaneously treating wastewaters by exploitation of "electroactive" microorganisms able to exchange electrons with extracellular electron donors &/or acceptors in devices known as Bioelectrochemical Systems (BES).

1.3 Bioelectrochemical Systems for the Circular Bioeconomy & as Research Tool

Bioelectrochemical Systems (BES) integrate microorganisms in electrochemical technologies to improve the bacterial reducing or oxidizing metabolism thereby promoting the interconversion between chemical and electrical energy[20]. The first ever BES was built by Michael Cresse Potter in 1911, a Professor of Botany at the University of Durham, who observed microbial-driven degradation of different organic substrates led to generation of electricity in electrochemical cells with platinum electrodes[21]. Such a type of BES is called Microbial Fuel Cell (MFC) which holds significant potential for applications such as treatment of wastewaters with simultaneous production of electricity[22]. This is of particular importance since deterioration of freshwater streams and increasing amount of toxic wastewaters poses significant issues to the availability of this fundamental resource to future generations[23]. MFCs typically consists of anodic and cathodic materials (electrodes), microorganisms and a fuel (organic matter). Conversion of chemical into electrical

energy is achieved when bacteria degrade organic matter liberating protons which travel to the cathodic compartments via a semipermeable membrane and transmitting electrons to apposite RedOx components synthesised by the bacteria themselves. Electrons are then transferred to the anode (which requires removal of terminal electron acceptors such as O_2 and NO_3) connected through an external circuit to a cathode where eventually O_2 is reduced to produce H_2O (Figure 1, see also section 2.4 of the material and methods for details of the mechanisms of electron transfer).

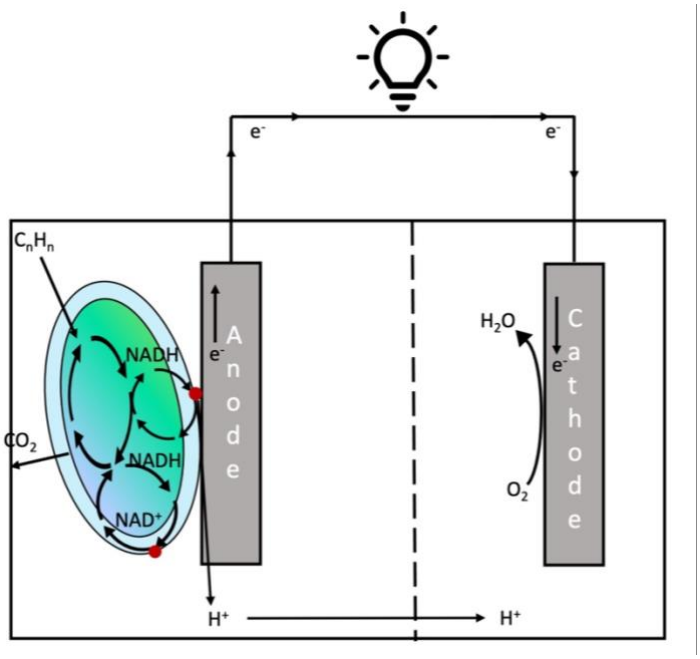

Figure 1- Scheme of a MFC Bacteria grow at the anode, oxidise organic matters and transmits electrons (e^-) to the anodic surface by means of apposite RedOx molecules (red dots). In the process protons are liberated, which travel through the cathodic compartment via the semipermeable membrane (dashed line). The electrons are transmitted through an external circuit to the cathode where they reduce O_2 to H_2O.

Compared to anaerobic digestors, where low value biomass derived from agricultural or urban wastes is converted into gases (mainly CH_4), MFC offers some specific advantages such as the direct conversion of organic compounds in electricity and the ability of working at room temperature[24]. Alternatively to MFCs, Microbial

Electrosynthesis (MES) devices exploit bacteria at the cathode that can reduce CO_2 to industrially relevant compounds such as alcohols and carboxylic acids[25]. Nonetheless, BES struggles to find commercial applications due to low yield of valuable products (MES)[26] or low power output (MFC)[27] and the often prohibitive costs of electrode materials[28]. To circumvent the low power output and product yield, a synthetic biology approach can be used where bacterial species-specific genetic toolboxes are used to enhance the flux of electrons between the electrodes and the bacteria[29]. However, there is a wide phylogenetic difference among "electromicrobes", which in turns reflects a different set of molecular mechanisms for EET[30]. This implies that to increase or alter the RedOx metabolism by means of synthetic biology techniques, it is of paramount importance to expand our understanding of the underlying mechanisms of bacterial extracellular electron transfer.

Regardless the limitation of the low power/product output that prevents BES to be placed in the market, their importance as device to study the electrophysiological aspects of microorganisms remains invaluable and it should be explored further[31].

1.4 Development of Bacterial Strains for Biotechnological Applications

As mentioned in section 1.2, bacterial-based biotechnology is a promising field of biotechnology. Prokaryotes can be used for many applications such as conversion of cheap organic waste substrates or GHGs as into valuable chemicals[24,32,] and production of electricity in MFCs[33]. However, as often wild type organisms are inefficient catalysts, genetic engineering needs to be performed for introduction of synthetic pathways and for general strain improvement. Development of successful industrial strains is a time and resource-consuming activity and the overall process

herein reviewed can be divided into three sub-processes called upstream, midstream and downstream (Figure 2)[34].

Upstream process: During the upstream phase, a suitable microbial host is selected based on its metabolic characteristics. This phase includes generation of genetic tools for modulation of heterologous protein expression and genetic engineering, construction of biosynthetic pathways, removal of competitive pathways and genes that can negatively impact production of the target molecules. During this phase the tools generated can also be exploited to gain better insight on the physiology of the microorganism of interest. Ideally, the tools generated should fulfil the concept of "standard" borrowed from mechanical and electronic engineering. This concept determines the manipulation of microorganisms by using (standard) genetic parts that are well characterized in a wide variety of prokaryotes and which activity is well defined and can be orthogonally transferred to other systems. Considerable effort has so far been invested by the scientific community into the establishment, characterization, and registration of standard genetic parts. One notable example is the creation of the Registry of Standard Biological Parts (BioBricks) by the International Genetically Engineered Machine (iGEM) fundation[35].

Midstream process: During the midstream phase, the engineered bacteria is tested in biotechnologically relevant conditions, such as by growth in bioreactors. A cheap carbon source is used together with a chemically defined growth medium for evaluation of growth and production performance. During this phase, scale-up experiments are crucial to determine the ability to produce a chemical in industrial-like settings.

Downstream process: During this phase, the end-product is separated from the cells and purified from possible contaminants.

As implementation of prokaryotes for bioprocessing is an extremely time and cost-demanding process, it does not come as surprise that there are few examples of efficient industrial bacterial-driven bioprocesses. These includes the development of *E. coli* strains capable of generating high concentrations of L-threonine[36], L-valine[37] and 1,4-butanediool[38]. Despite the richness in metabolic diversity of prokaryotes that can be exploited for several biotechnological applications, very few prokaryotic species other than *E. coli* can be listed as being able to produce the yields necessary in industrial contexts. Some of these bacteria are *Pseudomonas putida*[39] *Corynebacterium glutamicum*[40] and *Bacillus subtilis*[41]. The poor diversity of industrial prokaryotic strains is mostly due to the fact different bacterial species show dramatically different levels of activity of regulatory elements and tools for genome engineering so that each prokaryotic species needs a tailored genetic toolbox.

Therefore, to create robust and efficient microbial strains for bioprocessing, it is of paramount importance to develop strain-specific Genetic Toolboxes that can be exploited to modulate expression of heterologous genes, generate knockouts & knock-ins to gain insight into the physiology of the selected chassis and implement synthetic metabolic pathways.

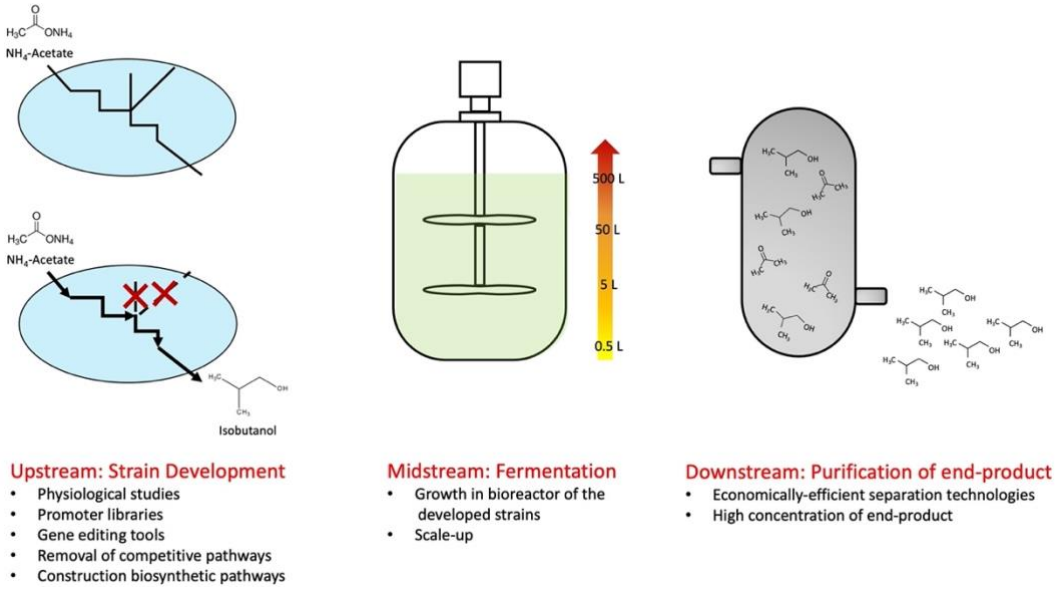

Figure 2- Representation of the upstream, midstream, and downstream steps for industrial implementation of microbial strains for bioprocessing: The example considers metabolic engineering of a bacterial chassis for production of isobutanol using acetate as carbon source in industrial settings. Upstream phase: On the left panel a chosen microbial chassis is subjected to metabolic engineering, metabolic pathways are represented by black lines. A genetic engineering approach is then used for deletion of competing pathways (red crosses) to maximise the production of isobutanol. Midstream phase: the engineered microorganism is tested for growth and production of the desired chemical in fermentation bioreactors. A stepwise volume increase is recommended. Downstream phase: purification of isobutanol is eventually performed and the product can be commercialized. Adapted from[42].

1.5 *Cupriavidus metallidurans* CH34

1.5.1 General Features of *Cupriavidus metallidurans* CH34

C. metallidurans CH34 is a facultative anaerobic chemolithoautotroph soil β-proteobacterium belonging to the family of the *Burkholderiacaea.* It thrives in different oligotrophic environments connected to anthropic activities, which are normally abundant in heavy metals and other toxic contaminants, it is capable of oxidizing gluconate and other carbon sources such as lactate, citrate, and acetate, but cannot use glucose for its central carbon metabolism as it lacks the specific transporter[43]. *C. metallidurans* CH34 was isolated in 1976 from sediments of a decantation basin in the metallurgical plant in Engis, near Liège (Belgium) in the

Meuse valley[44] (Figure 3). This peculiar geographical region has seen human presence since the 11th century, who heavily benefited from the exploitation of local zinc and copper ores up to the early 1900s, when finally local ores became exhausted. Therefore, it is very likely exploitation of the local mines for production of Copper- and Brass-ware was a factor leading to the selection of bacterial strains able to survive in environments with high concentration of heavy metals[45]. Moreover, since its discovery *C. metallidurans* strains have been isolated in disparate environments, from gold mines in Australia[46], to clinical settings[47] and even in the International Space Station[48] thereby highlighting the capability of these strains to grow in environments with low nutrient availability and to adapt to different kinds of environmental conditions.

Figure 3- Map of the River Meuse basin with its network of canals and location of main metal extraction and manufacturing industries: the marker 3) shows the "Metallurgie de Prayon" factory where *C. metallidurans* CH34 was isolated in 1976. Adapted from[45]. Permission to use the figure obtained from publisher.

The genetic material of *C. metallidurans* CH34 is divided into one chromosome of 3.9 megabases (Mb) (CHR1), a chromid of 2.5 Mb (CHR2) and two megaplasmids

pMOL28 and pMOL30 of 171 Kb and 233 Kb respectively. While CHR1 bears all the housekeeping genes necessary for replication and growth of the organisms, the chromid has characteristics in between the ones of a chromosome and a plasmid such as i) carrying some "core" genes which are on the main chromosomes in other prokaryotes ii) having a plasmid-like replication and partitioning system and iii) bearing a vast array of accessory genes. CHR2 carries genes responsible for specialized biosynthesis, such as the ones involved in synthesis of carotenoid or genes for catabolic functions like those necessary for utilization of acetone[43] and a vast array of Resistance-Nodulation-Division (RND) pumps involved in efflux of heavy metals[45]. From the evolutionary point of view, it is possible the presence of genes for catabolism of alternative carbon sources and for the efflux of heavy metals in CHR2 allowed colonization of oligotrophic environments with moderate concentrations of heavy metals[49]. pMOL28 contains genes for resistance to nickel, cobalt, chromate, and mercury, while pMOL30 has resistance determinants for zinc, cadmium, cobalt, mercury, lead, silver, and copper. It is believed acquisition of these plasmids, which carry resistance genes that mainly code for RND and P-type ATPase efflux pumps which are able to process high concentrations of heavy metals, might have occurred more recently to adapt to increasing 21vailability of pollutants in the environment as result of anthropic activities[49].

A peculiar aspect of *C. Metallidurans* CH34 is the presence of a considerable amount of Mobile Genetic Elements (MGEs) of which 13 are present in CHR1, 4 on CHR2, 3 on pMOL28 and 2 on pMOL30. The fact that most of these MGEs have not been characterized, few are reported to bear the necessary information for interesting accessory functions. For example, CMGI-1 (Genomic Island) is involved in heavy metal resistance while CMGI-2 and CMGI-3 (belonging to the Tn*4371* transposon

family) give *C. metallidurans* CH34 the ability to use H_2 as energy source (hydrogenotrophy). CMGI-2 and CMGI-3 are further responsible of providing genes for metabolism of aromatic compounds and fixation of CO_2 via the Calvin-Benson-Bassham cycle. Moreover, pMOL30 and pMOL28 possess CMGI-30 and CMGI-28 which provides *C. metallidurans* CH34 with the ability to withstand mM concentrations of heavy metals[43].

1.5.2 Potential Biotechnological Applications of *C. metallidurans* CH34 & Limitation to Its use in Industrial Contexts

C. metallidurans CH34's genetic flexibility is based on the high number of genomic islands and the competency to easily exchange DNA with the environment, resulting in evolution of many interesting features for biotechnological applications. Beyond the resistance to high concentrations of heavy metals, intriguing characteristics include the ability to i) oxidise toluene, benzene, xylene and ethylbenzene (BTEX)[50], ii) grow on low values organic compounds like acetate and iii) grow chemolithoautotrophically by using CO_2 and H_2 as carbon and energy source, iv) being responsible for the biomineralization process of gold[51], v) be able to transmit electrons outside the cells[52] and accept electrons from extracellular environment[53], and vi) the presence of genes for the synthesis of PHB (a polymer that can be used as biodegradable bioplastic). These features highlight *C. metallidurans* CH34 as an ideal candidate for green biotechnological applications like bioremediation, bioprocessing for production of valuable chemicals, biomining, biosensor development, MFC and MES devices. Despite the benefits that successful industrial exploitation of *C. metallidurans* CH34 would carry to the bioeconomy, there is a general lack of studies focusing on potential applications of this microorganism. These studies include the

exploitation of wild type *C. metallidurans* CH34 for bioremediation of contaminated soils or wastewaters[54] and production of electricity coupled to oxidation of toluene in MFC setup[52]. Furthermore, few studies used a genetic engineering approach for different applications. For example, *C. metallidurans* CH34 was engineered to build bioluminescent biosensors in which the light output was proportional to the concentration of heavy metals[55] or to express mouse metallothioneins or phytochelatins for bioremediation of soils and wastewaters contaminated with heavy metals[56,57].

Cupriavidus necator H16 is a hydrogen oxidizing chemolithoautotrophic bacterium, which shares many metabolic features with *C. metallidurans* CH34[58]. Despite the similarity of *C. metallidurans* CH34 with *C. necator* H16, the literature is mainly abundant with successful examples of metabolic engineering for production of chemicals, biofuels and PHB of the latter[58]. This predilection stems from several studies where the basic genetic toolbox for heterologous protein expression and genome engineering in *C. necator* H16 were developed[59–61], a necessary step for the implementation of non-model organisms in biotechnology[62]. While genetic engineering of *C. metallidurans* CH34 was successful by means of mini-Tn*5* transposons[55,57], the current state of the art technique relies on allelic exchange and is dependent on insertion of a tetracycline or kanamycin resistance cassette in the chromosomal DNA[55]. Although this can be later excised using *Cre-Lox* technology, the procedure is laborious and time consuming (see section 1.6.3.1 for details on Allelic Exchange). Furthermore, there are no extensive studies for implementation of synthetic and heterologous constitutive and inducible promoters. In fact, the only publication attempting to provide a list of regulatory elements in *C. metallidurans* CH34 highlights the activity of the P_{pan} from *B. subtilis* and the native P_{czI} promoter.

While the former showed high expression of EGFP, the latter showed little activity in *C. metallidurans* CH34[63]. These factors are still a major hindrance to encouraging the biotechnology community to study and use recombinant strains of *C. metallidurans* CH34 for industrial applications.

1.6 Essential Genetic Tools for Implementation of the Microbial Chassis concept in Biotechnology

During the upstream phase of implementation of industrial bacterial strains, there are several tools spanning different scientific disciplines that need to be developed for successful exploitation of industrial strains. These can be divided into: i) Genetic Molecular Tools such as shuttle vectors for successful expression of recombinant DNA and genome engineering systems, ii) Synthetic Biology Tools such as those necessary for control of protein expression, iii) Omics Data which are needed for simultaneous identification of gene functions and iv) Genome Scale metabolic models useful to predict the outcome of metabolic engineering experiments of the selected prokaryote (Figure 4)[33].

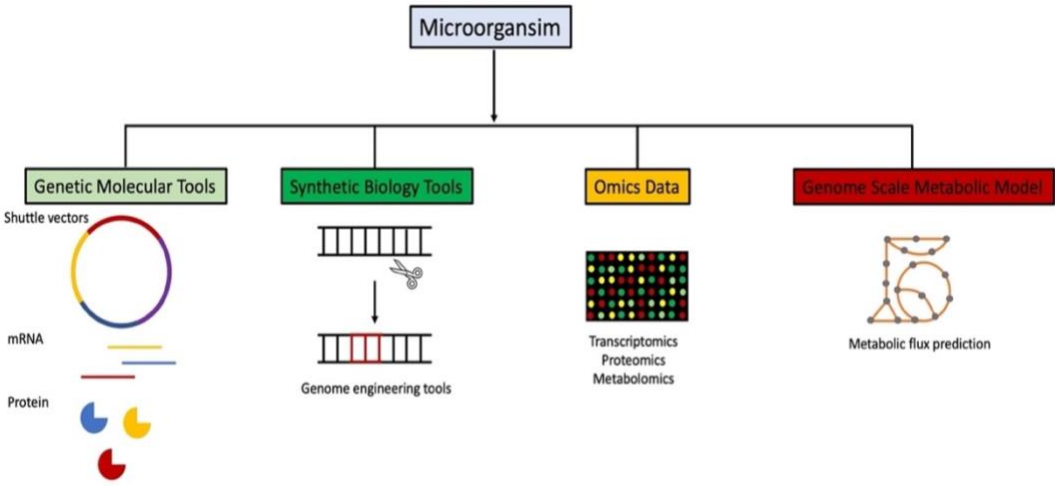

Figure 4- Representation of the necessary tools for implementation of a selected microorganism in biotechnological settings: genetic tools such as shuttle vectors for expression of recombinant proteins, synthetic biology tools for genome engineering, omics data and related genome scale metabolic models for metabolic flux predictions are herein represented.

In this thesis, I focused on the specific section of the upstream phase, development of Genetic Molecular and Synthetic Biology Tools for exploitation of *C. metallidurans* CH34 in the biotechnological industry. More specifically, I studied development of:

i) *Shuttle Vectors & technologies for plasmid maintenance*: Plasmid vectors able to replicate in *E. coli* and the microorganism under investigation. These can be coupled to Plasmid Addiction Systems, which allow stable plasmid maintenance and heterologous protein expression.

ii) *Genetic tools for tuning of gene expression:* which includes a variety of regulatory elements such as sense RNA[64], dCas9[65], ncRNA[66] RBSs and promoters. Implementation of both inducible and constitutive promoters with a wide range of activities would be preferable.

iii) *Genome engineering toolbox:* such as HR-mediated allelic exchange and CRISPR-Cas technologies. For most of the prokaryotes, both systems rely

on HR-driven allelic exchange. A homologous template is provided to the selected chassis which triggers recombination and cause the desired mutation (deletion, insertion or SNV) by exploitation of endogenous enzymes. However, the two differ in the way selection of the recombinant clones occur. While HR-driven allelic exchange requires the use of a counterselection gene, usually an antibiotic cassette, CRISPR-Cas systems exploit the nuclease activity of the Cas proteins to achieve killing of the non-recombinant isolates and has been shown to result in high efficiency of isolation of recombinant clones in eukaryotes[67].

The tools herein presented will be discussed in more details in the following sections.

1.6.1 Shuttle Vectors and Plasmid Maintenance

Shuttle vectors are multicopy plasmids able to replicate in two or more hosts and are usually comprised of i) an *E. coli*-specific and secondary host-specific origin of replications ii) an antibiotic resistance cassette to ensure selection of transformants and when necessary, iii) genes involved in conjugative transfer of the plasmid. Cloning of heterologous genes is firstly performed using conventional laboratory *E. coli* strains such as DH5α and later plasmids are transferred to the selected chassis to test for gene expression and product accumulation. While this is a widely used approach, there are several issues with plasmid-based expression of heterologous proteins which can severely impact product yields in alternative hosts other than *E. coli*. Extrachromosomal multicopy vectors are in fact widely reported to suffer from structural instability[68] or effects caused by mutations in the GOI that results in loss of product and segregational instability[69], caused by phenomena like metabolic burden, plasmid multimerization and plasmid loss. Metabolic burden is due to the requirement

of extra ATP for plasmid replication, expression of antibiotic cassettes and other genes cloned in the plasmid[70,71] while plasmid multimerization is caused by recombination of homologous sequences of the multi-copy plasmids. Furthermore, addition of antibiotics is often required to allow selection of the cell population bearing the plasmid, which is costly and can lead to unwanted presence of antibiotic traces after downstream purification of the product of interest. Even the use of relatively low copy number origins of replication such as ColE1 and pBR322 (~15-20 copies/cell) have been associated with a decrease of growth rate connected to metabolic burden and plasmid loss in model organism *E. coli*[70]. The issue of plasmid instability can at times be overcome by means of stabilising tools such as Plasmid Addiction Systems (PASs).

1.6.1.1 Plasmid Addiction Systems for Stable Inheritance of Recombinant Plasmids for Heterologous Protein Expression

Plasmids have a major importance in microbial evolution and adaptation as they confer the ability to resist anti-microbials[72] and degrade non-canonical carbon-based molecules to sustain their growth[73]. Plasmids have evolved Plasmid Addiction Systems (PASs) as regulation mechanisms to ensure their transmission to daughter cells. These are based on a dedicated partitioning system and/or the presence of so-called *selfish* DNA (Toxin-Antitoxin systems, Tas) which ensures equal distribution of the number of plasmid copies in the daughter cells and post-segregational killing (PSK) of plasmid-less cells respectively. PSK systems that can be found in nature are made of a stable toxin and an unstable antitoxin. TA systems exists in three forms: based on the nature of their constituents these can be protein-regulated, antisense RNA-regulated and restriction modification systems. Different types of TA have been used by the scientific community for applications such as molecular cloning[74] and to

reach high yield of protein expression *in vivo*[75] but the underlying working mechanisms remains the same. The unstable antitoxin is produced in higher amount compared to the toxin, so that if the plasmid is present there is enough product to neutralize the toxin. However, if the plasmid is lost the antitoxin is degraded more quickly by the host's protease and the toxin eventually kills the plasmid-less cells (Figure 5). Alternatively, metabolism-based PASs can be used to couple bacterial growth, plasmid maintenance and heterologous protein expression. For example, an addiction system for efficient production of cyanophycin from a plasmid system was engineered in *C. necator* H16. This was based on development of a strain of *C. necator* H16 that lacks the *eda* gene coding for the KDPG-aldolase, and subsequent complementation of the gene *in trans* together with the *cphA* gene from *Synechocystis sp*. PCC6308[76]. In another case, *pyrF* (orotidine-5phosphate decarboxylase) and *proC* (pyrroline-5-carboxylate reductase) auxotrophic markers producing enzymes participating in the uracil and arginine/proline metabolism respectively, were successfully used to achieve stable plasmid-based protein production in *P. fluorescens*[77]. Therefore, PAS tools can be used to ensure high protein expression and plasmid maintenance in industrial microbial strains where plasmid stability is an issue.

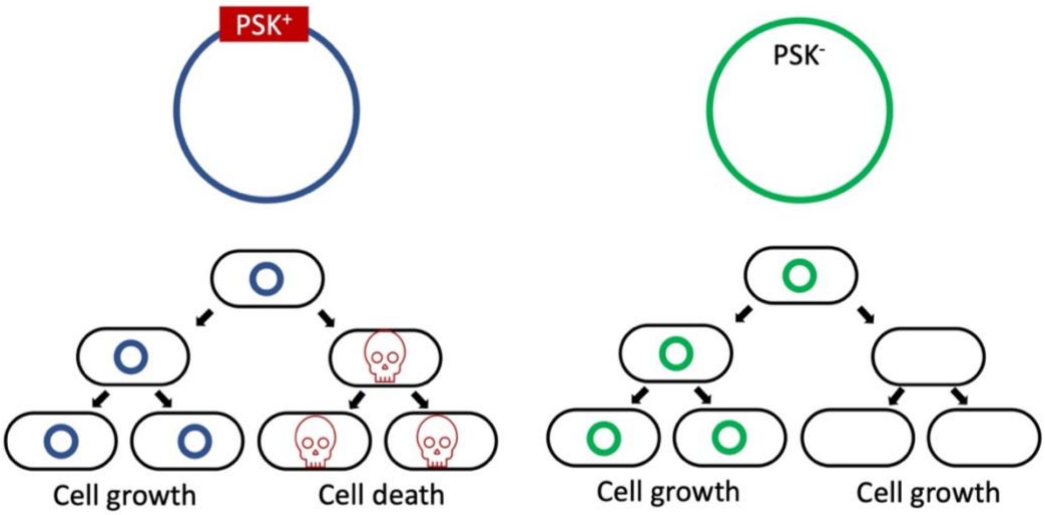

Figure 5- Schematic representation of the post-segregational killing system: Left panel represent a plasmid (blue) endowed of the PSK system (red cassette). The system ensures cell survival only if the plasmid persists in the cell. Right panel represents a plasmid (green) without the PSK. Plasmid-less cells will therefore be able to replicate.

1.6.2 Regulatory Elements for Fine Tuning of Heterologous Gene Expression

Production of desired chemicals from synthetic metabolic pathways require expression of different genes and in industrial context, high yields are required for economical viable production. Nevertheless, the highest yields are not obtained with the highest concentration of key enzymes in the cell, but rather by fine regulation of expression levels of the different genes composing the given pathways[78]. Regulatory sequences such as promoters, ncRNA and RBSs can be characterized for fine optimization of expression of the GOIs. Promoters are DNA sequences to which the holoenzyme RNA polymerase binds and transcribe the RNA molecules. The RNA polymerase is composed of the apoenzyme, made up of four subunit and a catalytic centre with a Mg^{2+} ion as well as a σ factor. The σ factor is necessary for recruitment of the RNA polymerase on the promoter sequence and for transcription initiation. After initiation, the σ factor dissociates from the RNA polymerase and elongation of the RNA transcript occurs. Recognition of the promoter sequence occurs at specific

locations called the -10 and -35 sequence, which indicate the position in reference to the transcription start site. There are different σ factors that are used by bacteria to regulate gene expression under different environmental conditions. These are distinguished by their molecular weight. For example, in *E. coli* the σ^{70} has a molecular weight of 70 kDa and regulates expression of housekeeping genes, while the σ^{28} and σ^{32} are involved in expression of genes involved in flagellar synthesis and heat shock response respectively[79]. The final RNA product may contains the coding sequence of a gene (mRNA) or may have other functions such as those of tRNA, rRNA or ncRNA[79,80]. Promoters can be constitutive if they are always active, or tuneable when a specific molecule is needed to activate or repress gene transcription (Figure 6A). Constitutive promoters normally regulate expression of housekeeping genes and work at constant rate, thereby producing the same amount of product[81]. On the other hand, tuneable promoters respond to a specific activation/repression agent for example internal metabolites, sugars, metals or physical stimuli for example temperature or light[81] (Figure 6B). Ideally, an inducible promoter should have low or no basal expression, its induction should be high, but expression levels should be tunable based on the concentration of the inducer. Moreover, expression levels of proteins can be regulated at translation or posttranscriptional level. At translational level engineering of RBSs results in altering the energetics of interaction between the ribosome and its binding site, allowing differences in the expression level of several-fold[82] while ncRNAs have been used to modulate gene expression at posttranscriptional level by acting as *cis* regulatory elements[83,84]. Therefore, as engineering of metabolic pathways requires expression of several genes, development of inducible and constitutive

promoter libraries with a diverse activity range is a first fundamental step for implementation of novel microbial chassis in industrial biotechnology[78].

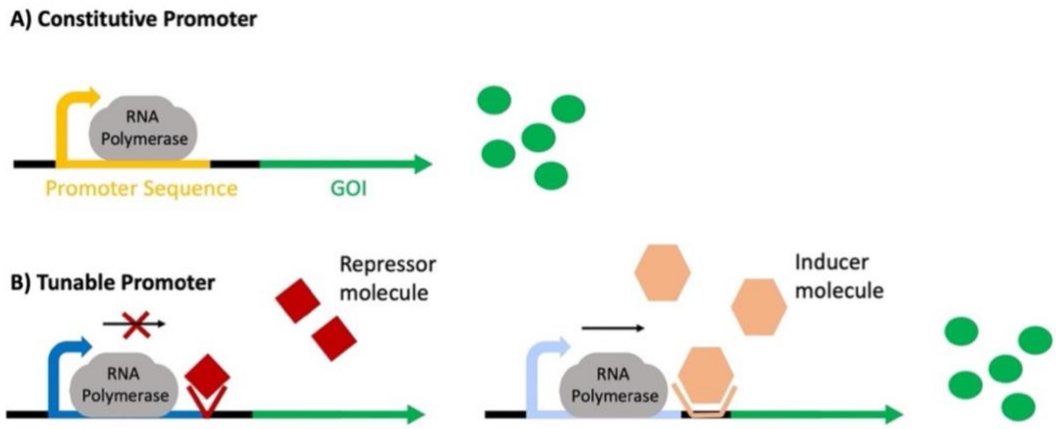

Figure 6-Representation of the working mechanisms of constitutive and inducible promoters: A) Constitutive promoters are always active, the RNA polymerase (grey) binds the promoter sequence (yellow) and express the GOI (green). B) tunable promoter which expression is prevented upon presence of a repressor molecule (red) (left panel) and tunable promoter which expression is induced by an inducer molecule (dark pink) (right panel) are represented.

1.6.3 Genetic Tools for Genome Engineering: Homologous Recombination mediated Allelic Exchange and CRISPR-Cas systems

1.6.3.1 Allelic Exchange

Allelic exchange is widely used for genome engineering of prokaryotes of industrial interest such as *C. glutamicum*[85], *C. acetobutylicum*[86] and *C. necator* H16[87] and it still is the only approach for engineering promising cell factories such as *C. metallidurans* CH34[88]. HR-mediated allelic exchange is based on conjugation of a suicide plasmid built with homology arms of DNA identical to the gDNA of the host to be modified, DNA carrying the desired mutation and genes necessary for counterselection and selection of the transformants. During the first single crossover event, the whole plasmid is integrated in the genome and the plasmid-specific antibiotic selection can be used to screen for candidates, which underwent this first

process. A rare second crossover event can occur and depending on whether it happens between the same region of homology of the first crossover event or between the homologous sequences as placed in the recombineering plasmid, can result in wild type revertant or recombinant isolates respectively (Figure 7). The counterselection determinant is used to discriminate between cells which underwent successfully the second recombination event. Different counterselection methods are used with some of the most commonly used being the *sacB*[87] or the *pyrF*[86] genes or antibiotic resistance genes[88]. Often the use of two antibiotic resistance genes on the suicide vector, allow direct isolation of double crossover mutants. For example, if kanamycin and tetracycline resistance gene cassettes are cloned into the backbone of the vector, and between the sites for homologous recombination, by screening for resistance to tetracycline (when the resistance gene is inserted into the gDNA) and susceptibility to kanamycin, desired mutant strains can be screened. Such is the case of *C. metallidurans* CH34[88], *Lactobacillus plantarum*[89] and *Staphylococci*[90] (Figure 7A). However, introduction of antibiotic cassettes in chromosomal DNA severely limits the amount of genome editing possible in a single strain to the number of the antibiotics to which the bacterium of interest is susceptible. To circumvent this problem, recombinase-specific *loxP* sites can be inserted flanking the antibiotic cassette followed by transient introduction of a plasmid expressing the *cre* recombinase, which eventually leads to excision of the unwanted gene leaving a small DNA scar behind[89] (Figure 7B). Allelic exchange HR-driven genome modification tools are therefore extremely inefficient and time-consuming methodologies for development of microbial strains for industrial applications.

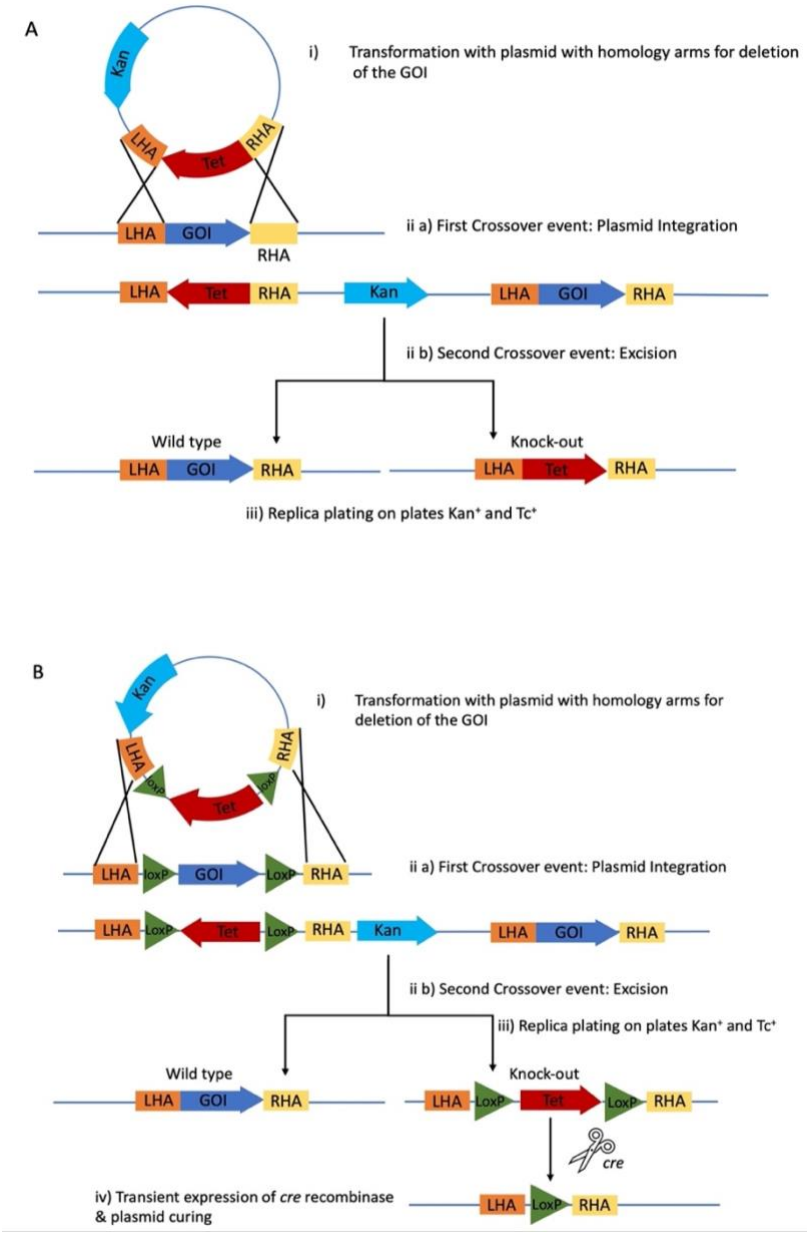

Figure 7- Schematic representation of allelic exchange for generation of modified strains of C. *metallidurans* CH34: A) i) A plasmid with kanamycin and tetracycline resistance cassettes cloned in the backbone and in between the homology arms respectively is conjugated in *C. metallidurans* CH34. Ii a) during the first crossover event the whole plasmid is integrated in the gDNA. ii b) In a second crossover event the plasmid is excised from the chromosome either resulting in reversion to the wild type or generation of the desired knockout strain with a tetracycline cassette replacing the GOI. iii) by replica plating on Kan^+ and Tet^+ plates it is possible to individuate recombinant knockout clones. B) Generation of knockouts of *C. metallidurans CH34* and excision of the antibiotic cassette via *cre-loxP* recombinase. i)-iii) are the same steps as if removal of antibiotic cassette is not to be performed. Iv) a plasmid with *cre* recombinase is delivered *in C. metallidurans* CH34 for transient expression of the *cre* recombinase and is subsequently cured, leaving a single P-lox site as scar.

1.6.3.2 CRISPR-Cas Systems

The CRISPR-Cas (Clustered Regularly Interspaced Short Palindromic Repeats-Crispr Associated Proteins) systems is an adaptive immune response system found in prokaryotes which was applied as genome editing technique for eukaryotic cells in the early 2010s by Emmanuelle Charpentier and Jennifer Doudna[91]. The system turned out to have a revolutionary impact on life sciences, allowing high precision modification of animal, plants and prokaryotic DNA and it further contributed to the development of cancer therapies and techniques for curing inherited disease, thereby allowing its creators to be awarded the Nobel Prize in Chemistry[92]. The CRISPR system was discovered between the late 1980's and early 1990's independently in different parts of the world[93,94] and is nowadays found in 45% of the known bacteria species. The CRISPR-Cas system is composed of short palindromic repeats of 28 to 37 bp separated by spacers matching the nucleic acid sequence of infectious agents and sized between 32-38 bp[95], an AT-rich leader sequence involved in acquisition of new spacers[96], and *cas* genes coding for proteins with helicase and nuclease motifs which are involved at different stages of the immune response which together constitutes the effector protein module[67,68, 97,98] (Figure 8).

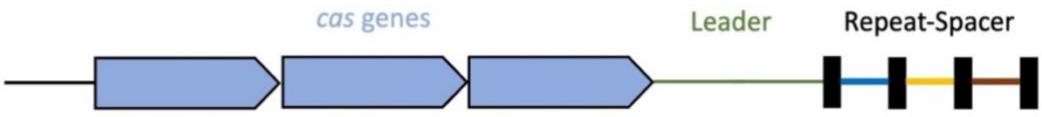

Figure 8- Organisation of the CRISPR Locus: the *cas* genes and the leader sequence are reported as blue boxes and a green line respectively. The DNA repeats and spacer sequences are represented as black vertical boxes and coloured thick lines respectively.

A study in 2007 showed that after changing the spacer sequences in the CRISPR array of *S. thermophilus* with spacer matching DNA of different bacteriophage,

immunity against the viruses was triggered upon infection, thereby highlighting for the first time the role of the CRISPR-Cas systems in adaptive immunity[99]. Consequently, it was discovered that after transcription of the CRISPR-RNA array with all the spacers, a Cascade of Cas proteins was responsible for processing of the transcript into a mature crRNA molecules each containing one spacer without the repeats, which then formed a complex with the Cas proteins[100]. Today the immune defence mechanism is recognized to occur in three stages called adaptation, expression, and interference. During adaptation, Cas1 and Cas2 nucleases i) identify a short and specific nucleotide sequence of the infecting agent called protospacer, and ii) integrate new spacers into the CRISPR array between the repeats. This provides the CRISPR-Cas system with a nucleotide sequence complementary to the invading virus, which can be used upon a second infection to trigger the immune response. Spacers were found to not be randomly selected from the viral DNA sequence, but rather adjacent to a Protospacer Adjacent Motif (PAM) which sequence varies depending on the Cas protein(s) involved[101]. In the expression phase the crRNA is generated firstly by means of RNA polymerase transcribing the CRISPR locus and secondly by a maturation step during which the CRISPR effector proteins processes the long transcript, resulting in mature crRNA complementary to the DNA of the infectious agent. In the last step called Interference, the crRNA complexed with the Cas protein(s) leads cleavage of the exogenous DNA after recognition of the PAM site and the complementary DNA strand (Figure 9). The PAM site is of paramount importance for the Cas proteins to be able to direct DNA cleavage and without it the protospacer

introduced in the bacterial chromosome might instead be targeted leading to cell death[102].

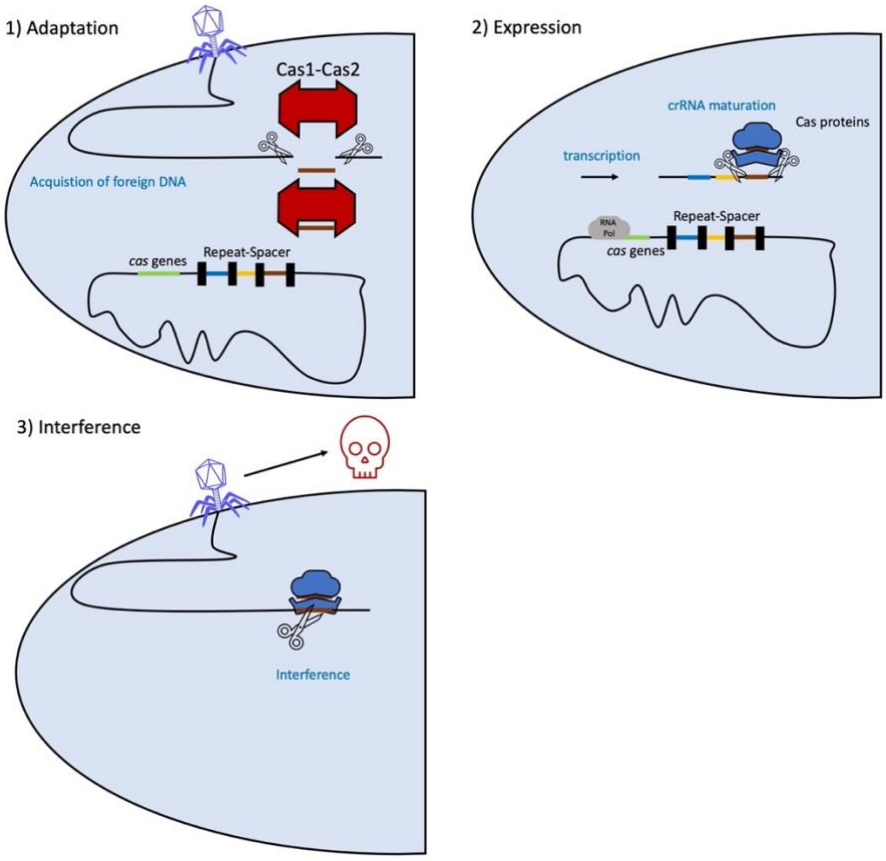

Figure 9- Stages of CRISPR-Cas mediated immune defence system of prokaryotic cells: 1) Adaptation: A virus inject its genetic material inside the cell. The genetic material is cleaved by Cas1-2 protein (red) and acquired as spacer into the CRISPR array (coloured thick lines). 2) Expression: The CRISPR array is expressed, and the crRNA undergoes a maturation process carried out by the Cas proteins. 3) Interference: upon re-infection the Cas protein(s) (blue) complexed with the crRNA (brown) leads to recognition and excision of viral genetic material.

As CRISPR-Cas systems are present in different bacteria genera, it is not surprising they show high diversity in terms of genomic architecture, gene composition and sequence homology, rendering necessary a rational classification system. The most used classification system considers the signature *cas* genes in the effector module, sequence similarity of Cas proteins common among CRISPR-Cas types of different organisms and the genetic organization of the CRISPR-Cas loci.

Therefore, two main classes are identified, each encompassing different types: Class 1 includes type I and III which share a rather complex organization of multiple *cas* genes largely not characterized and a rare type IV with a less elaborate composition. Class 2 systems on the other side have a simpler architecture and are composed of a single large multifunctional effector protein. This class contains the famous type II system with the signature Cas9 protein and the less known types V and VI systems.

Given the simplicity of the Class 2 System II CRISPR-Cas9, several research groups studied the molecular mechanisms for targeted DNA cleavage with the aim to exploit it as a tool for genome engineering. Compared to other systems, where only the crRNA is necessary to target and destroy the infectious agent, an additional small RNA called trans-activating crRNA (tracrRNA) is transcribed as antisense RNA compared to the transcription direction of the *cas* genes and the Repeat-Spacer array. The tracrRNA and the primary crRNA form base pairing and are further processed by the host RNaseIII to produce the mature crRNA which constitute the Cas9-crRNA complex ready to cleave phage DNA[103] (Figure 10). During interference, the Cas9-crRNA complex scouts the foreign genome for the protospacer sequence (complementary to the spacer) adjacent to the NGG PAM site and performs a double strand cleavage at the 5' of the PAM site by using the HNH and RuvC nuclease domains. In 2012, it was demonstrated that the crRNA and tracrRNA could be combined into a single guide RNA (sgRNA), which could be recognized by Cas9 leading to programmable site-specific double strand break (DSB) of eukaryotic cells[91]. Once DSB has been introduced, the Non-Homologous-End-Join (NHEJ) or HR repair systems can re-ligate the DNA causing permanent modification of its sequence. While the NHEJ simply disrupt the sequence where the DSB occurred, the HR pathway can perform precise InDels and single-nucleotide mutations by using an appropriate

homologous DNA template. Despite the programmable two-components CRISPR-Cas9/sgRNA system have been extensively exploited for introduction of the desired mutations across the eukaryotic domain[104–108], to date its use for genome engineering of prokaryotic systems is still not widespread due to the need for diverse regulatory elements to control *cas9* and gRNA expression in different microorganism[109].

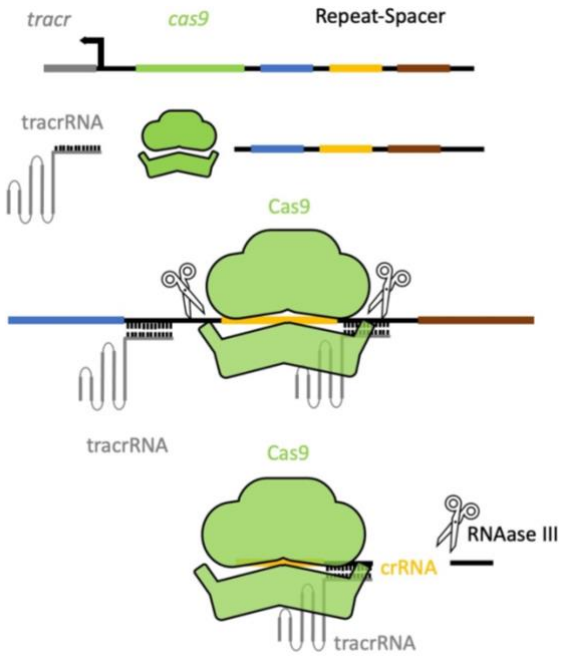

Figure 10- Schematic representation of the class 2 System II CRISPR-Cas9 mediated maturation of the crRNA: After transcription of the tracrRNA and the CRISPR array, the Cas9 protein processes the spacer::tracrRNA complex that is further matured thanks to the endogenous RNAase III enzyme. The colour coding is: green for *cas9,* grey for the tracr RNA and yellow for the crRNA.

1.7 Cellular Respiration & Extracellular Electron Transfer

1.7.1 General Features of Cellular Respiration

Bacteria have evolved to adapt to the most challenging environmental conditions and as consequence developed a vast array of pathways to obtain energy for their metabolic functions. In heterotrophic aerobic or anaerobic prokaryotes, energy is obtained from the oxidation of organic compounds. In the case of heterotrophs, these are directly taken up by the cell and oxidised via either the

Embden-Meyerhof-Parnas pathway (EMP, also known as the biochemical standard for glycolysis) or the Entner-Doudoroff pathway (EDP). Chemolithoautotrophs, can alternatively fix CO_2 via the Calvin-Benson-Bassham pathway (CBB) to produce sugars that are fed into the central carbon metabolism. While both EMP and EDP serve the purpose of oxidizing glucose to yield pyruvate, ATP and NADH, they differ in two aspects. Firstly, The EDP relies on the unique 6-phosphogluconate dehydratase aldolase and 2-keto-deoxy-6-phosphoglcuonate (KDPG) aldolase as well as other common enzymes and secondly the EDP produces 1 ATP, 1 NADH and 1 NADPH per molecule of glucose processed while the EMP yields 2 ATP and 2 NADH for each glucose catabolized. Pyruvate is then decarboxylated by the pyruvate dehydrogenase to generate Acetyl-CoA, which is the starting molecule for the Citric Acid Cycle (TCA). The TCA cycle is used by aerobic- and anaerobic-respiring microbes (it is not used by fermentative prokaryotes which respiration mechanism will not be covered in this thesis) to generate energy in form of ATP or GTP, precursors of amino acids, NADH and $FADH_2$. Eventually NADH and $FADH_2$ are fed into the Oxidative Phosphorylation Pathway or Electron Transport Chain (ETC), which is herein discussed in more detail (Figure 11).

The ETC is the “core” part of the respiratory chain where most of the ATP is generated and is composed of an array of enzymes and other organic molecules embedded in the cytoplasmic membrane having gradually higher RedOx potential. Despite different microorganisms have different multidomain RedOx proteins located on the periplasmic membrane, the general mechanism remains similar. NADH is oxidized to NAD^+ by means of a NADH dehydrogenase (N_{DH}) having a Flavin Mononucleotide (FMN) as prosthetic group which relay electrons to the Succinate Dehydrogenase (SDH), the only enzyme common between the TCA cycle and the

ETC). SDH carries out oxidation of $FADH_2$ to FAD in a two-step reaction involving oxidation of succinate to fumarate and acquiring more electrons in the process. Following, electrons are transferred to the Cytochrome bc_1 complex (bc_1), to the Cytochrome-C © and eventually to the Cytochrome C oxidase (C_{ox}) which is responsible for reducing O_2 thereby forming H_2O. During this process, the protons liberated in the oxidation of NADH and $FADH_2$ are pumped by the N_{DH}, bc_1 and C_{ox} to the periplasmic space forming a proton gradient which drives synthesis of ATP thanks to an enzyme called ATP synthase[110] (Figure 11).

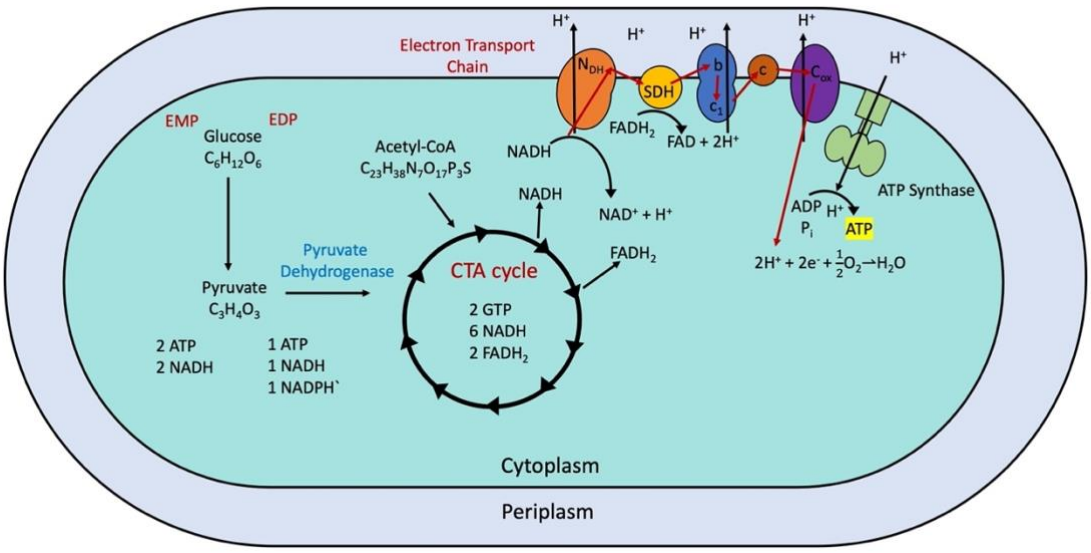

Figure 11- Schematic Representation of the Central Carbon Cycles and the Electron Transport Chain in a Bacterial Cell: simplified representation of the central carbon pathways that leads to feeding reducing equivalents (NADH and $FADH_2$) to the Electron Transport Chain. Colour coding is: orange for the N_{DH}, yellow for the SDH, blue for the bc_1, dark orange for the C and purple for the C_{ox}. Detailed description of the ETC is in the text[110].

Overall, for each molecule of glucose completely oxidised to CO_2 in aerobic conditions, a theoretical maximum of 38 ATP molecules can be obtained of which 34 are produced during the ETC only, thereby highlighting the importance of this process in generating energy. While higher eukaryotes and several prokaryotes are obligate aerobes, bacteria adaptability resolves in the desirable ability to use alternative

terminal electron acceptors to molecular oxygen in the electron transport chain (ETC)[111,112] such as nitrate[113], sulfate[43] or sulfur[114]. Nevertheless, as these molecules possess a lower reduction potential than oxygen, less ATP is produced by anaerobic bacteria despite still making use of the electron transport chain.

1.7.2 Dissimilatory Metal-Reducing Microorganisms

While for decades it was believed microbes could only reduce soluble electron acceptors diffusing in the periplasmic space, this perception started to change in the late 1980's when Dissimilatory Metal-Reducing (DMR) bacteria, capable of reducing insoluble (and therefore membrane-impermeable) metal oxides, were reported for the first time. Observations of DMR first came from the study of geochemical cycling of insoluble metal oxides in two separate locations. At Oneida Lake, NY the formation of insoluble reduced manganese minerals in the anoxic sediments of the lake during the warm season was noticed. The process was discovered to be many orders of magnitude greater than it could be explained just by abiotic chemistry alone and it was eventually labelled as microbial-driven reduction of insoluble manganese oxides by means of the organism *Shewanella oneidensis* MR1[115]. Almost concurrently, a Mn(IV) and Fe(III) reducing bacteria, lately named *Geobacter sulfureducens* was isolated from the sediments of the Potomac river (Maryland)[116]. Despite these exciting discoveries, the scientific community was initially reluctant to accept the possibility of solid extracellular electron acceptors but had soon start to welcome this alternative means of respiration when external mediator-less EET was demonstrated as to be the cause of anodic currents in MFC devices inoculated with *Shewanella sp.*[117]. Later, *Shewanella oneidensis* was described to rely on outer membrane cytochromes and flavins as soluble electron carriers[118,119] (Figure 13A), while *Geobacter sulfureducens*

was proposed to use an array of cytochromes and conductive nanowire for EET without the use of soluble electron carriers[120,121] (Figure 13B). Beside these well-studied organisms, EET is also reported for other bacteria such as *Therminicola,* proposed to use a cytochrome-based system[122], *Clostridium ljungdahlii* which was shown capable of EET but which molecular mechanisms remain unknown[123] and *Pseudomonas* species which were reported to use phenazines and cytochromes for a mixed EET mechanism[124,125]. Therefore, two types of EET can be described, namely mediated Electron Transfer (MET) and Direct Electron Transfer (DET). In MET the cell produces soluble electron mediators, such as flavins that are involved in transporting electrons between the cell and the solid electron acceptor, while in DET cells are directly connected via proteinaceous structures to the oxidant. DET can be further subdivided into i) short range when transfer occurs via outer membrane cytochromes in direct contact with a solid oxidizer and ii) long range when electron transfer occurs via proteinaceous conductive appendices called nanowires (Figure 12) which are the focus of part of this thesis.

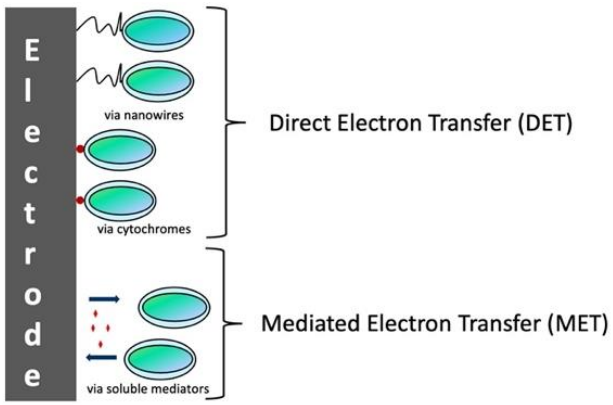

Figure 12- Mechanisms of extracellular electron transfer to anodic surface: the figure shows DET and MET mechanisms to a solid electrode. The electrode is represented in grey while cells are reported in light blue. DET can occur via nanowires (curvy black lines) or via cytochromes (red circles). MET results from the presence of soluble mediators travelling from the cell to the electrode and vice versa (red squares).

Shewanella oneidensis MR1 DET relies on the metal-reducing (Mtr) pathway composed of the MtrB decaheme-associated outer membrane protein, the multiheme cytochromes MtrA, OmcA, MtrC, CymA, Fcc_3, and a small tetraheme cytochrome STC. Briefly, EET starts in the Electron Transport Chain, where the quinol pool receives electrons from the NADH-dehydrogenase and transmits them to the CymA cytochrome which is inserted in the inner membrane but faces the periplasm[126]. CymA transfers electrons to the periplasmic proteins Fcc_3 and STC which travel to the inner side of the MtrB-bound cytochrome complex, donating electrons which are firstly transmitted to the MtrC/MtrA cytochromes[127] and are eventually transmitted to the extracellular electron acceptor when direct contact is established with the terminal electron acceptor[128–130]. Alternatively *Shewanella oneidensis* MR1 can secrete soluble carriers such as flavins that mediate electron transport between the cell and the extracellular environment[118] (Figure 13A). *Geobacter sulfureducens* DET also begins with the menaquinone pool of the ETC which passes electrons to the diheme cytochrome C peroxidase MacA protein, responsible of electron transfer from the

periplasmic membrane to the periplasmic cytochrome PpcA which eventually transmits electrons to different outer membrane-bound cytochromes OmcB (Porin-like protein), OmcS and OmcZ (Figure 13B).

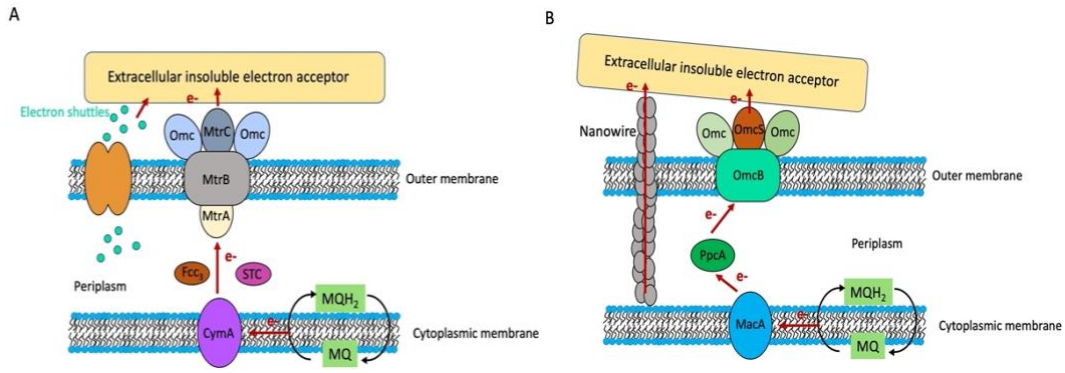

Figure 13-Schematic Representation of the Link Between ETC and the Extracellular Electron Transfer Pathways in *Shewanella Oneidensis* MR1 and *Geobacter Sulfureducens sp.*: In both organisms the quinol pol of the ETC is responsible for transmitting electrons to the components of the EET pathways. A) In *S. oneidensis* MR1 EET occurs via both DET and MET mechanisms in B) *G. sulfureducens* only DET mechanism occur via either membrane bound cytochromes or conductive nanowires. Adapted from[131]. Permission to use the figure obtained from the publisher.

While EET in *Shewanella* requires the cells to be in close contact with the solid terminal electron acceptor and forms thin electroactive-biofilm on the electrode surface[132], *G. sulfureducens* is shown to form thick biofilms capable of EET which can occur both at short and long ranges depending on the stage and thickness of biofilm formation. The process of EET is thought to involve a wide range of cytochromes and proteinaceous nanowires which composition is highly debated. On the one hand it is believed these nanowires are monomer of the type IV PilA protein which is thought to be conductive due to the high content of aromatic amino acids that confer "metal-like" conductivity to the pili[133]. On the other hand, it is believed the conductive appendices that have been mistaken for two decades as conductive pili are nothing else than filaments made of OmcS and OmcZ cytochromes involved in long-

range EET in thin and thick mature (>50μM) electroactive biofilms respectively[134] (Figure 14).

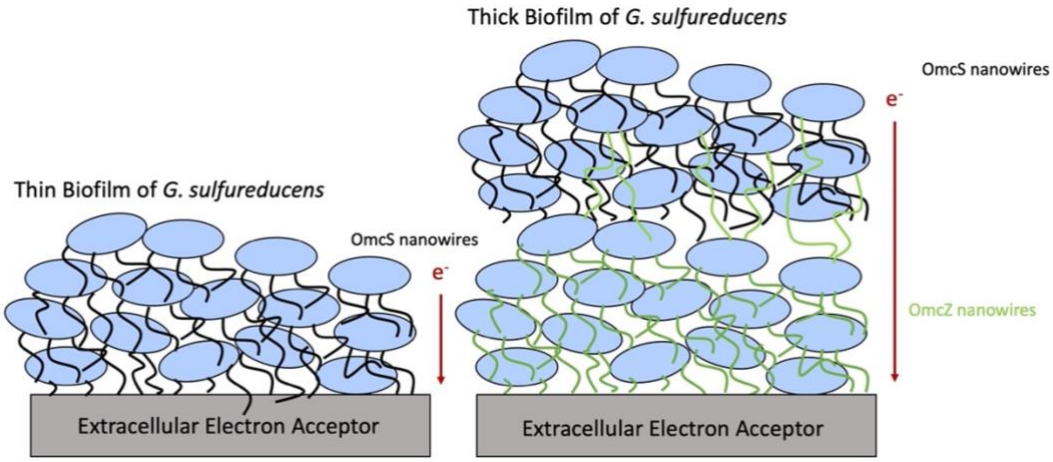

Figure 14- Schematic Representation of the Involvement of OmcS and OmcZ Nanowires During Different Stages of Biofilm Formation of *G. sulfureducens*: Left panel represents a thin biofilm of *G. sulfureducens* (light blue ovals) with OmcS-based nanowires (black) as main actors in EET with the extracellular solid electron acceptor (grey rectangular shape). Right panel represents the nanowires-mediated EET mechanisms in thick biofilms. OmcS-based nanowires (made of polymers of cytochrome-S, black) and OmcZ-based nanowires (made of polymers of cytochrome-Z, green) are expressed and involved in the process of electron transfer. Movement of electrons is shown as a red arrow. Adapted from[135]. Permission to use the figure obtained from the publisher.

1.7.3 Controversy on the Composition of the Proteinaceous Nanowires of *G. sulfureducens*

PilA from *G. sulfureducens* has been postulated to exhibit high similarity to the N-terminal of other type IV pili and has an α-helix structure and high content of aromatic amino acids which stacking would provide a metal-like conductivity[136]. While the idea of a PilA-based bacterial nanowire as a fundamental component for long-range EET is exciting from the biological point of view and the potential applications as green electronic material, twenty years of extensive research on the subject still has not fully elucidated whether this protein is really directly involved in generation of high currents and EET when forming thick biofilms on electrode

surfaces, or if the pilins are composed of cytochromes with stacked heme centers being the major factor contributing to long range EET. Following are a list of active research groups giving support to both the hypotheses.

Arguments and evidence supporting the theory of a type IV conductive e-pili

The first motivation to enquire on the role of type IV pili in Extracellular electron transfer came from the observation that *Geobacter metallireducens* up-regulated transcription of *pilA* when grown in presence of insoluble Mn(IV) or Fe(III). Upregulation was not seen when soluble Fe(III) citrate was supplemented to the growth media[137] which was subsequently also confirmed for *G. sulfureducens*[138]. The hypothesis of type IV pili being involved in EET found further confirmation in the following facts:

i) When adding insoluble Fe(III) oxide to cells initially grown on fumarate (*pilA* expression conditions when no insoluble Fe(III) oxides are added to growth media) iron particles would group along the pili, which was found to have a ohmic current response[138] thereby suggesting PilA is conductive and is needed for EET to insoluble metal oxides.

ii) Growth of *G. sulfureducens* and Δ*pilA* strains in the anodic chamber of a MFC device under current-generating conditions led to lower current peaks for the knockout strain compared to the *wild type* counterpart[139] thereby indicating a fundamental role of PilA in EET.

iii) Knockout of the *omcS* gene (coding for outer membrane cytochrome S), after initial decrease in current production, eventually results in production of high currents in *G. sulfureducens* which would indicate the role of OmcS in current generation is at least marginal, probably confined to the short

range electron transfer requiring direct contact of the cell with the insoluble electron acceptor[121].

iv) Substitution of the five aromatic amino acids in the PilA monomer severely impacted conductivity of the biofilm, Fe(III) reduction and overall nanowire conductivity and the pili filament[133]. Which raises the question on why such a phenotype would appear if PilA was not involved in EET.

v) Adaptive evolution on current-producing *G. sulfureducens* yielded strain KN400 which produced higher currents when compared to its wild type counterpart. Higher current production was correlated with lower and higher level of OmcS and PilA respectively[140] which again would support the theory of a e-pili.

vi) Recently, it was found that *G. sulfureducens* Δ*omcBESTZ* strain produced conductive appendages postulated to be e-pili. As all the known cytochromes involved in EET were knocked-out, this would strengthen the theory of an e-pili[141].

Arguments & evidence supporting the theory of cytochrome-based nanowires

i) The presence of a conductive e-pili has never been structurally proven and the only evidence supporting this theory are of genetic nature (i.e knockout study which do not consider the contribution of OmcS and OmcZ cytochromes[135]. Furthermore, conductivity of PilA has only been measured throughout its section, never for the whole length of the filament[142]. These arguments imply there is simply not enough evidence to conclude PilA assemble for generation of conductive e-pili.

ii) *G. sulfureducens* deletion strains of OmcS were reported to produce high currents after adaptation in MFCs, thereby discarding initially the role of cytochromes in EET[121]. However, recent discovery of OmcZ conductive nanowires with conductivity 1000-fold higher than OmcS would compensate loss of the latter[134] thereby explaining why current generation is recovered after a time lag in *G. sulfureducens* Δ*omcS* strain.

iii) Strain KN400 was also found to overexpress OmcZ, which would support a theory of cytochrome-based rather than pilin-based nanowire involved in EET[134].

iv) Computational models and conductivity prediction calculations do not match experimental results if nanowires are assumed to be e-pili. Indeed, it was predicted stacking of aromatic amino acids in e-pili would be too spaced for allowing high rate of electron flow as it has been measured in *G. sulfureducens*[143].

v) Lastly, in September 2021 it was postulated the genes GSU1496 and 1497 of *G. sulfureducens* coding for the N and C terminal portion of canonical type IV pili, were instead more similar to type II secretion pseudo-pili and were involved in translocation of OmcS and OmcZ to the outer membrane rather than forming extracellular conductive pili. Furthermore, the structural analysis of nanowires correlated with model predictions for cytochrome-based nanowires[144].

1.7.4 Extracellular Electron Transfer in *C. metalllidurans* CH34

Regarding *C. metallidurans* CH34, two early studies on gold detoxification and biomineralization mechanisms hinted at its ability for EET. *C. metallidurans* CH34

was shown to grow as biofilm on gold mineral ores in natural environments[145] and it was demonstrated Au(III) complexes were taken up by the cells and reduced eventually to Au(0) in the periplasm thanks to enzymes of the *CopABCD* operon involved in Cu detoxification[146,147]. Furthermore, when grown as biofilm on a sand column supplemented with Au(III), the biofilm was shown to be embedded by proteinaceous filaments, thought to be conductive nanowires used to breath excess electrons outside the cell (Figure 15), which hinted type IV pili might be used by *C. metallidurans* CH34 for Extracellular Electron Transfer[51]. More recent studies investigated the possibility to use *C. metallidurans* CH34 in MFC. It was firstly screened as possible candidate for microbial electrosynthesis at the cathode, where however it was shown to be unable to consume significant current[53]. Then, it was proved to be able of coupling toluene oxidation to anodic current production in mediator-less MFC in anaerobic conditions[52]. Lastly, *C. metallidurans* CH34 was isolated at the anode of a MFC acclimatized with sulphate-reducing sludge and once more, anodic currents were observed[148]. However, these studies aimed to answer the question about "If" *C. metallidurans* CH34 is capable of producing/consuming current rather than "how" and to date its mechanisms for EET has not been elucidated.

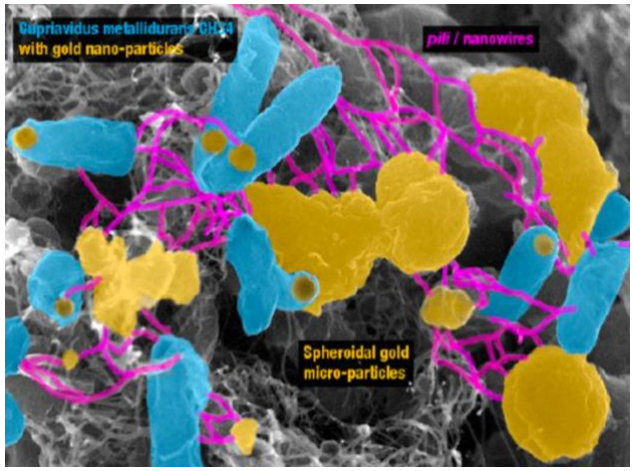

Figure 15- Secondary Electrons Microscopy image of *C. metalllidurans* CH34 growing as biofilm in sand column amended with soluble Au(I) Thiosulfate: *C. metallidurans* CH34 picks up toxic soluble gold from solution and precipitate it as micro-particles of solid Au(0). The biofilm (blue) is shown to be embedded in proteinaceous filaments (pink), proposed to be nanowires used to rely excess electrons outside the cells, improving overall electron flow according to the authors[51]. Permission to use the figure obtained from the publisher.

1.8 Goals & Objectives of This thesis

C. metallidurans CH34 represents an ideal candidate for biotechnological applications that can serve the purpose of the circular Bioeconomy. These include MFC devices, bioremediation of wastewaters contaminated with heavy metals or recalcitrant carbon-based chemicals and bioprocessing of high value chemicals from reduction of CO_2.

However, lack of tools to efficiently engineer its genomic DNA, knowledge of functional synthetic promoters and plasmid stability for heterologous protein expression and scarce understanding of alternative respiration pathways, currently limits the biotechnological potential of the industrial community for *C. metallidurans* CH34. The goals of this thesis were the i) development of a Synthetic Biology Toolbox for *C. metallidurans* CH34 and the ii) exploitation of the Toolbox to gain insight into

the EET mechanisms of *C. metallidurans*. The objectives established to achieve the goals were the i) Development of PASs for stable plasmid maintenance for heterologous protein expression, ii) Development of promoter libraries and a CRISPR-*cas* system generation of mutant strains of *C. metallidurans* CH34, iii) Development of a novel synthetic biology approach for increased EET between the electrodes surface and the cells and the iv) Exploitation of the CRISPR-*cas* tool to study the mechanisms *C. metallidurans* CH34 uses for EET.

2 -General Materials & Methods

This chapter lists the general materials and describes the methodologies used to carry out this study. Given the multidisciplinary nature of this work, each subsection will contain a brief description of the purpose of the methodology. Furthermore, each experimental chapter (I.E Chapter 3, Chapter 4, Chapter 5 and Chapter 6) contains a separate Material and Methods section specific to that section.

2.1 Microbiology Techniques

This section describes the material and the procedures employed to grow and transform the bacterial strains used in this study.

2.1.1 Preparation of Growth Media

LB media composition was as follows: 20 g/L NaCl, 10g/L yeast extract and 20 g/L tryptone. For solid medium 15 g/L of bacteriological agar no.1 (Oxoid ™) was added prior to autoclaving.

Minimal medium (MM) composition was as follows: 9g/L Na_2HPO_4 x 12 H_2O, 1.5 g/l KH_2PO_4, 0.5 g/L NH_4Cl, 0.2 g/L $MgSO_4$ x 7H_2O, 20 mg/L $CaCl_2$ x 2 H_2O, 1.2 mg/L Fe(III)NH_4-citrate and 1 mL/L of SL7 trace element solution which composition was; 25% (W/v) HCl 1.2 mL/L, H_3BO_3 62 mg/L, $CoCl_2$ x 6H_2O 190 mg/L, $CuCl_2$ x 2H_2O 17 mg/L, $MnCl_2$ x 4H_2O 100 mg/L, Na_2MoO_4 x 2 H_2O 36 mg/L, $NiCl_2$ x 6H_2O 24 mg/L and $ZnCl_2$ 70 mg/L. The pH was adjusted to 6.9. For Na-Gluconate Minimal Medium (SGMM), 0.4% Na-Gluconate (wt/vol) was added followed by filter sterilization. SGMM agar was prepared by adding 15 g/L agar no. 1 (Oxid ™) followed by sterilization by autoclave.

2.1.2 Bacterial Strains Growth & Storage

All the bacterial strains used in this study are listed in Table 1. Bacterial cultures were grown in LB overnight supplemented with appropriate antibiotic, 1 mL was transferred to three Microbank vials and mixed by inversion. The liquid was then removed leaving the porous beads colonized by bacteria and the vials were immediately stored at -80 ˚C. The procedure for uracil auxotrophs of *C. metallidurans* CH34 involved the use of SGMM Gen^+ supplemented with 20 µg/mL of uracil.

Table 1-List of strains used in this study

Species	Strain	Description	Source
Escherichia coli	DH5α	F– *end*A1 *gln*V44 *thi*-1 *rec*A1 *rel*A1 *gyr*A96 *deo*R *nup*G *pur*B20 φ80d*lacZ*Δ M15 Δ(*lacZYA-argF*)U169, *hsd*R17($r_K^- m_K^+$), Δ–	NEB
	S17-1	Ec294:: [RP4-2(Tc::Mu)(Km::Tn7)] [3] Tp^r, Sm^r, tra^+ recA, *pro*, *res*	[149]
	One Shot™ Pir2	F- Δ*lac*169 *rpoS*(Am) *rob*A1 *cre*C510 *hsd*R514 *end*A r*ec*A1 *uid*A(Δ*Mlu*I)::*pir*	ThermoFIsher
Cupriavidus metallidurans	NG7	ΔpMOL28 ΔpMOL30 Incp-1α	Biodiscovery Institute, NG7 2RD, Nottingham, UK
	CH34 (DSMZ 22839)		German Collection of Microorganisms and Cell Cultures, Braunschweig, Germany

Species	Strain	Description	Source
Cupriavidus metallidurans	CH34 Δ*pyrE*	Δ*pyrE,* evolved on SGMM plates supplemented with 5-FOA	This study
	CH34 Δ*pyrE*	Δ*pyrE,* generated with CRISPR-Cas9 system developed in this study	
	CH34 Δ*pilAE*	Δ*pilAE,* generated with CRISPR-Cas9 system developed in this study	
	CH34 Δ*pilA*	Δ*pilA,* generated with CRISPR-Cas9 system developed in this study	
	CH34 Δ*pilE*	Δ*pilE,* generated with CRISPR-Cas9 system developed in this study	
	CH34 Δ*pilAE::gfp*	Δ*pilAE::gfp,* generated with CRISPR-Cas9 system developed in this study	
	CH34 Δ*pilAE::λgfp*	Δ*pilAE::λgfp,* generated with CRISPR-Cas9 system developed in this study	

2.1.3 General Growth Conditions of *E. coli* and *C. metallidurans* CH34

E. coli strains were herein used for plasmid propagation, molecular cloning, and inter-species bacterial conjugation of plasmids. Growth was initiated by streaking one bead from the cryo-stock onto LB agar plates supplemented with appropriate antibiotic and was incubated at 37 ˚C overnight. A single colony was inoculated with 1 µL loop into 5mL liquid LB supplemented with appropriate antibiotic concentration for plasmid maintenance and grown aerobically in a shaking incubator at 200 rpm overnight.

C. metallidurans CH34 & *C. metallidurans* NG7 (derivative strain of *C. metallidurans* CH34 discovered in this study, see Chapter 4) growth was initiated by streaking one bead from the cryo-stock onto LB agar plates supplemented with appropriate antibiotic and was incubated at 30 ˚C for 48-72 hours. A single colony was inoculated with a 1 µL loop into 5mL liquid LB supplemented with appropriate

antibiotic concentration for plasmid maintenance and grown aerobically in a shaking incubator at 200 rpm for 48-72 hours.

Table 2 shows the concentrations of the different antibiotics used for *E. coli* and *C. metallidurans* for plasmid maintenance.

Table 2-Type and concentration of antibiotic for different strains used in this study

Antibiotic	**Plasmid backbone**	**Concentration (μg/mL)**			**Solvent**
		E. coli	*C. metallidurans* CH34	*C. metallidurans* NG7	
Tetracycline	pMTL71301 pMTL74311	20	20	/	50% ethanol
Chloramphenicol	pMTL71101	50	50	500	Ethanol
Gentamycin	all	/	10	/	H_2O

2.1.4 Heat-Shock transformation of *E. coli* DH5α

50 μL aliquots of *E. coli* DH5α competent cells (NEB) were thawed from the -80 ˚C freezer for 15 minutes on ice. 2 μL of ligation mixture or Hi-Fi® reactions were added to the cells and further incubated for 30 minutes on ice. Heat shocked followed by placing the vials with the cell in a water bath heated at 42 ˚C. The cells were then placed on ice for 2 minutes, supplemented with 950 μL SOC, transferred to a 50 mL Falcon tube and incubated for 1 hr at 200 rpm at 37 ˚C. 100 μL were spread on LB agar plates with appropriate antibiotic. The rest of the culture was collected by

centrifugation at 4000 rpm for 5 minutes, the supernatant discarded, the pellet resuspended in 100 µL of fresh LB and plated on LB agar plates with appropriate antibiotic.

2.1.5 Preparation of Electrocompetent of *E. coli* S17-1 Cells

E. coli S17-1 was grown overnight as described in section 2.1.3. 1 mL of culture was used as inoculum for 100 mL of pre-warmed LB media at 37 ˚C in 250 mL E-Flasks. The flasks were incubated at 37 ˚C at 200 rpm until OD_{600} of 0.5-1.0 was reached. Flasks were incubated on ice for 15 minutes, transferred to four 50 mL Falcon tubes and centrifuged at 4000g for 15 minutes at 4 ˚C. supernatant was discarded, and pellet was resuspended in 25 mL of chilled de-ionised H_2O. This step was repeated twice. Pellets were resuspended in 500 µL of 2 mL 10% glycerol in de-ionized H_2O and combined in one 50 mL falcon tube in a final volume of 2 mL 10% glycerol in de-ionized H_2O. The culture was centrifuged at 4000g for 15 minutes at 4 ˚C, supernatant was discarded, pellet resuspended in 300 mL of 10% glycerol in de-ionized H_2O and cells were split in 50 µL aliquots in 1.5 mL Eppendorf tubes and eventually stored at -80 ˚C.

2.1.6 Transformation of Electrocompetent *E. coli* S17-1 Cells

An aliquot of electrocompetent *E. coli* S17-1 cells were mixed with 2 µL of DNA in a pre-chilled 0.2 cm gap electroporation cuvette (Thermofisher™). The cells were electroporated at 2.5 kV, 200 Ω, 25 µF using a MicroPulser Electroporator (Biorad®). After electroporation, 950 µL of SOC (Thermofisher ™) was added to the cell suspension, which was then incubated at 37 ˚C for 1 hour at 200 rpm. 100 µL were spread on LB agar plates with appropriate antibiotic. The rest of the culture was

collected by centrifugation at 4000 rpm for 5 minutes, the supernatant discarded, the pellet resuspended in 100 µL of fresh LB and plated on LB agar plates with appropriate antibiotic.

2.1.7 Preparation of Electrocompetent Cells of *C. metallidurans sp.*

A single colony from LB plate was used to start an overnight culture in 7.5 mL of LB media at 200 rpm and 30 ˚C. The culture was divided into four 1.5 mL Eppendorf tubes, collected by centrifugation at 4000 rpm at RT and washed two times in 300 mM sucrose in de-ionized H_2O. Following another centrifugation step, the culture was resuspended in 50 µL of 300 mM sucrose and either immediately used or stored at -80 ˚C. The protocol was adapted from Choi and colleagues[150].

2.1.8 Transformation of Electrocompetent Cells of *C. metallidurans sp.*

An aliquot of electrocompetent *C. metallidurans* cells were mixed with 1 µg of DNA and transferred to a 0.2 cm gap electroporation cuvette. The cells were electroporated at 2.5 kV, 200 Ω, 25 µF using a MicroPulser Electroporator (Biorad®). After electroporation, 950 µL of LB was added to the cells which were then incubated at 30 ˚C for 2 hours at 200 rpm. 100 µL were spread on LB agar plates with appropriate antibiotic. The rest of the culture was collected by centrifugation at 4000 rpm for 5 minutes, the supernatant discarded, the pellet resuspended in 100 µL of fresh LB and plated on LB agar plates with the appropriate antibiotic.

2.1.9 Conjugation of Plasmids into *C. metallidurans*

E. coli S17-1 transformed with the appropriate plasmid, was incubated in LB with the appropriate antibiotic and as already described. *C. metallidurans* CH34 was grown

in LB as described. 1 mL of each culture was centrifugated at 4000 rpm for 5 minutes to collect the pellets. The cells were resuspended in LB with the purpose of removing the antibiotics. Cells were eventually resuspended in 500 μL of LB and mixed in a ratio 1:1 according to their OD_{600}. Cells were centrifuged at 4000 rpm for 5 minutes, resuspended in 30 μL of LB media and spotted on LB agar plate for mating. Mating was performed at 30 ˚C for 6 hr. The cell mixture was then resuspended in 200 μL of PBS and plated on LB agar or SGMM agar plates with tetracycline and gentamycin and incubated for 72 hours.

2.2 DNA Manipulation

This section provides a list of the plasmids and oligonucleotides used in this study. Furthermore, a comprehensive description of the molecular biology techniques is herein described.

2.2.1 Plasmids and Oligonucleotide Primers

All the plasmids and oligonucleotides used in this thesis are listed in Table 3 & 4 respectively.

Table 3-List of plasmids used in this study

Plasmid	relevant features*	Reference
	General plasmids	
pMTL71301	Tc^R, pBBR1 origin	[151]
pMTL71101	Cm^R, pBBR1 origin	[151]
pMTL74311	Tc^R, IncP origin, *trfA* R271A	[151]
	Chapter 3	
pUT-mini-Tn5-cm	R6K ori, IncP origin of transfer, Tn5, Cm^R, Bla^R	[152]
p*SNAP*	*SNAP* CDS	This study
pARAbad-ZigG-EC	*aidA-C* CDS	[153]
pMTL71101_pMTL71101_P_{BAD}_*aidA-C*	Cm^R, pBBR1 origin, P_{BAD}_*SNAP_aidA-C*	This study
pUT-mini-Tn5-cm_P_{BAD}_*SNAP_aidA-C*	R6K ori, IncP origin of transfer, Tn5, Cm^R, Bla^R, P_{BAD}_*SNAP_aidA-C*	This study

Table 3-List of plasmids used in this study: continuation from previous page

Plasmid	relevant features*	Reference
	Chapter 4	
pUC57_P_{pan}	Amp^R, pUC origin, P_{Pan} promoter	This study
pMTL71101_P_{pan}*mRFP1*_P_{trpsyn}*pyrE*FA1090	Cat^R, pBBR1 origin, P_{pan}-*mRFP1* & P_{trpsyn}-*pyrE*FA1090 expression platforms, complementation uracil auxotrophy	This study
pMTL71301_P_{pan}*mRFP1*_P_{trpsyn}*pyrE*FA1090	Tc^R, pBBR1 origin, P_{pan}-*mRFP1* & P_{trpsyn}-*pyrE*FA109*0* expression platforms, complementation uracil auxotrophy	This study
pMTL71301_P_{pan}*mRFP1*_P_{trpsyn}*pyrE*FA1090	Tc^R, pBBR1 origin, P_{pan}-*mRFP1*, P_{trpsyn}*pyrE*FA1090 (*pyrE* from *N. gonorrhoeae* FA1090)	This study
pMTL71101_P_{pan}*mRFP1*_P_{trpsyn}*pyrE*FA1090	Cm^R, pBBR1 origin, P_{pan}-*mRFP1*, P_{trpsyn}*pyrE*FA1090 (*pyrE* from *N. gonorrhoeae* FA1090)	This study
pMTL74311Low	Tc^R, IncP origin restored to low copy, ColE RNAII pol rep	[1]
pMTL74301Low_*parCBADE*	Tc^R, IncP origin restored to low copy, *parCBADE* from IncP-1α	This study
pMTL74301Low	Tc^R, IncP origin restored to low copy	This study

[2,2]Plasmid was cloned by Dr. Marco Garavaglia

Table 3-List of plasmids used in this study: continuation from previous page

Plasmid	relevant features*	Reference
	Chapter 5	
pRECas1_Cpas_sgRNAonly	Cm^R; P_{fdx}*-E-*cas9*-P_{araE}-sgRNA-editing template (*phaC1 C. Necator* H16)	Not published[2]
pRECas1-IIRE	Cm^R; P_{fdx}*-E-*cas9*-P_{araE}-sgRNA-editing template (*spoIIE),* engineering of *Clostridia Sp.*	[84]
pMTL74311_Ribocas_Δ*phaC*1	Tc^R, IncP origin, *trfA* R271A, P_{fdx}, Riboswitch E, AraE-sgRNA editing template (*phAC*1 *C. metallidurans* CH34) engineering *C. metallidurans* CH34, 13.7kb	This study
pMTL74311_*cas9*_Δ*phaC*1	Tc^R, IncP origin, *trfA* R271A, P_{BAD}, Riboswitch E, P_{AraE}-sgRNA editing template (*phaC*1 *C. Necator* H16) engineering *C. necator* H16[3]	Not published
	P_{fdx}-Riboswitch library	
pMTL71301_P_{fdx}RBE_*mRFP1*	Tc^R, IncP origin, *trfA* R271A, P_{fdx}, Riboswitch E, *mRFP1*	This study
pMTL71301_P_{fdx}RBF_*mRFP1*	Tc^R, IncP origin, *trfA* R271A, P_{fdx}, Riboswitch F, *mRFP1*	This study

[2,2]Plasmid was cloned by Dr. Marco Garavaglia

Table 3-List of plasmids used in this study: continuation from previous page

Plasmid	relevant features	Reference
pMTL71301_P_{fdx}RBG_*mRFP1*	Tc^R, IncP origin, *trfA* R271A, P_{fdx}, Riboswitch G, *mRFP1*	This study
pMTL71301_P_{fdx}RBH_*mRFP1*	Tc^R, IncP origin, *trfA* R271A, P_{fdx}, Riboswitch H, *mRFP1*	
pMTL71301_P_{fdx}RBI_*mRFP1*	Tc^R, IncP origin, *trfA* R271A, P_{fdx}, Riboswitch I, *mRFP1*	
pMTL71301_P_{fdx}RBJ_*mRFP1*	Tc^R, IncP origin, *trfA* R271A, P_{fdx}, Riboswitch J, *mRFP1*	
pMTL71301_P_{fdx}RBL_*mRFP1*	Tc^R, IncP origin, *trfA* R271A, P_{fdx}, Linker, *mRFP1*	
P_{BAD}-Riboswitch library		
pMTL71301_P_{BAD}RBE_*mRFP1*	Tc^R, IncP origin, *trfA* R271A, P_{BAD}Riboswitch E, *mRFP1*	This study
pMTL71301_P_{BAD}RBF_*mRFP1*	Tc^R, IncP origin, *trfA* R271A, P_{BAD}, Riboswitch F, *mRFP1*	
pMTL71301_P_{BAD}RBG_*mRFP1*	Tc^R, IncP origin, *trfA* R271A, P_{BAD}, Riboswitch G, *mRFP1*	
pMTL71301_P_{BAD}RBH_*mRFP1*	Tc^R, IncP origin, *trfA* R271A, P_{BAD}, Riboswitch H, *mRFP1*	

Table 3-List of plasmids used in this study: continuation from previous page

Plasmid	relevant features	Reference
pMTL71301_P_{BAD}RBF_*mRFP1*	Tc^R, IncP origin, *trfA* R271A, P_{BAD}, Riboswitch F, *mRFP1*	This study
pMTL71301_P_{BAD}RBG_*mRFP1*	Tc^R, IncP origin, *trfA* R271A, P_{BAD}, Riboswitch G, *mRFP1*	
pMTL71301_P_{BAD}RBH_*mRFP1*	Tc^R, IncP origin, *trfA* R271A, P_{BAD}, Riboswitch H, *mRFP1*	
pMTL71301_P_{BAD}RBI_*mRFP1*	Tc^R, IncP origin, *trfA* R271A, P_{BAD}, Riboswitch I, *mRFP1*	
pMTL71301_P_{BAD}RBJ_*mRFP1*	Tc^R, IncP origin, *trfA* R271A, P_{BAD}, Riboswitch J, *mRFP1*	
pMTL71301_P_{BAD}RBL_*mRFP1*	Tc^R, IncP origin, *trfA* R271A, P_{BAD}, Riboswitch L, *mRFP1*	
Knockouts experiments; generation ΔpyrE, ΔpilAE, ΔpilA, ΔpilE, ΔpilAE::gfp and ΔpilAE:λgfp		
pMTL74311_P_{BAD}RBIC9_Δ*pyrE*	Tc^R, IncP origin, *trfA* R271A, P_{BAD}-E-*cas9*-J23119-sgRNA-editing template(*pyrE*), engineering *C. metallidurans* CH34, 13.7 kb	This study
pMTL74311_P_{BAD}RBIC9_Δ*pilAE*	Tc^R, IncP origin, *trfA* R271A, P_{BAD}-E-*cas9*-J23119-sgRNA-editing template(*pilAE*), engineering *C. metallidurans* CH34, 13.7 kb	
pMTL74311_P_{BAD}RBIC9_Δ*pilA*	Tc^R, IncP origin, *trfA* R271A, P_{BAD}-E-*cas9*-J23119-sgRNA-editing template (*pilA*), engineering *C. metallidurans* CH34, 13.7 kb	

Plasmid	relevant features*	Reference
Knockouts experiments; generation ΔpyrE, ΔpilAE, ΔpilA, ΔpilE, ΔpilAE::gfp and ΔpilAE:λgfp		
pMTL74311_P_{BAD}RBIC9_Δ*pilAE::λgfp*	Tc^R, IncP origin, *trfA* R271A, P_{BAD}-E-*cas9*-J23119-sgRNA-editing template (*pilAE::λgfp*), engineering *C. metallidurans* CH34, 13.7 kb	This Work
pMTL74311_P_{BAD}RBIC9_Δ*pilAE::gfp*	Tc^R, IncP origin, *trfA* R271A, P_{BAD}-E-*cas9*-J23119-sgRNA-editing template (*pilAE*::*gfp*), engineering *C. metallidurans* CH34, 14.5 kb	

Table 3-List of plasmids used in this study: continuation from previous page

Table 4-List of oligos used in this study

Primer name	Primer sequence (5'-3')	Function	Template
Chapter 3			
Pbad_71101NotI_Fw	caggaaacagctatgaccgcggccgcttatgacaacttgacggc	Amplification of P_{BAD}	pMTL71301_P_{BAD}_*mRFP1*
Pbad_SNAP_Rv	ctttgtccattactgcaaatgcatttcc		
SNAP_PBAD_Fw	atttgcagtaatggacaaagactgcgaaatgaagcgc	Amplification of *snap*	pSNAP
SNAP_AIDA_Rv	tgttattcacacccagcccaggcttgcc		
AIDA-C_SNAP_Fw	caatgcttccattgttattcacacccagccca	Amplification of a*idA*	pARAbad-ZigG-EC[154]
AIDA-C_71101XhoI_Rv	agcttgcatgtctgcaggcctcgagtcagaagctgtattttatcc		
AIDA_Fw	tacggtacgtggtatcagaatgg	cPCR to confirm transformation	pMTL71101_P_{BAD}_*SNAP_aidA*
AIDA_Rv	ttcaccttccaggatgcacgaata		
SNAP_71101NotI_Fw	acagctatgaccgcggccgcatggacaaagactgcgaaatgaagcgc	Cloning of promoter-less pMTL71101_*SNAP_aidA*	pSNAP
Pbad_pUTNotI_Fw	gatccccgggaattcgtcgacaagcttcggccgcctaggccgcttcacgaggcagacctcatc	Cloning of pUT-mini-Tn5-cm_P_{BAD}_*SNAP_aidA*	pMTL71101_P_{BAD}_*SNAP_aidA*
AIDA-C_pUTNotI_Rv	Ccagtgggcaagttgaaagcacttgtgtataagagtcagaattccacaaattgttatc		
pUTCm_Sq_Fw	gttcaggacgctacttgtgta	Screening for absence of pUT-mini-Tn5Cm backbone	gDNA of *C. metallidurans* NG7
Omega_Cat_Sq_Rv	gtctcttgatcagatctggccgcc		
Omega_Cat_Sq_Fw	ataattacagccattgcctggttgc	Screening for presence of *snap* tag expressing operon	
AraC_Rv	ccgtcggtcgcaatgttggttt		
fdx_Sq_Fw	gaagcctgcatttgcaggcttctt	iPCR	
Omega_Cat_Sq2_Rv	gtctcttgatcagatctggccgcc		
Omega_Cat_Sq3_Rv	ccggtgattgattgagcaagc	Sequencing of the iPCR product to confirm insertion site	gDNA of *C. metallidurans* NG7 Tn5 mutants
Block_SNAP_Sq_Fw	aatagcgaagaggcccgcaccg		

Table 4-List of oligos used in this study: continuation from previous page

Primer name	Primer sequence (5'-3')	Function	Template
Chapter 4			
PyrE400Up_Fw	ttgtgggcgatgttcacgtcac	Amplification of *pyrE* gene from *C. metallidurans* CH34 for detection of mutations in the *pyrE* gene	gDNA *C. metallidurans* NG7 & *C. metallidurans* CH34
PyrE400Dw_Rv	ggaatacatctgtgcccagcc		
PyrF400Up_Fw	ttcgggatggttcgagcgc	Amplification of *pyrF* gene from *C. metallidurans* CH34 for detection of mutations in the *pyrF* gene	
PyrF400Dw_Rv	cgaacatggtgatctggcatctgtt		
pMTL71101/71301_P_{Pan}*mRFP1*_P_{trpsyn}*pyrE*FA1090			
Pan_71101NotI_fw	tttatcaggaaacagctatgaccgcgttcggtatcgaaagccg	Amplification of P_{pan} promoter for expression of *mRFP1*	pUC57_P_{pan}
Pan_rfp_rv	gatcacaaggaggacgttatatggcgagtagcgaa		
RFP_Pan_fw	caaggaggacgttatatggcgagtagcgaagac	Amplification of *mRFP1* under control of P_{pan}	pMTL71101_P_{BAD}_*mRFP1*[4]
RFP_71101PvuI_Rv	tcaggctgcgcaactgttgggaagggcgatttaagcaccggtggagtg		
P_{trpsyn}_PyrEFA1090_71101FseI_Fw	atttgcaggcttcttatttttatggctgttgacaattaatcatcgaactag	Amplification of *pyrE* gene of *N. gonorrhoeae* FA1090	gDNA of *N. gonorrhoeae* FA1090
PyrEFA1090_BBa0012_71101AscI_Rv	ggcagtacggcgtagaataagcgaaaaaaccccgccgaagcgggggttttttgcgccggccagtgggcaagttgaaaaat		
Pan_71301NotI_Fw	gcaggcttcttatttttatgttaagcaccggtggagtg	Amplification of P_{pan} *mRFP1*_P_{trpsyn}*pyrE* FA1090 block	pMTL71101_P_{Pan}*mRFP1*_P_{trpsyn}*pyrE*FA1090
PyrEFA1090_71301AscI_Rv	gcgctcctgcggccggccggatttttcaacttgcccactg		
pMTL74311Low			
Trfa271mut_Fw	acgcggaagcggtgcagcagc	Amplification of pMTL74311 for generation of pMTL74311Low	pMTL74311
Trfa271mut_Rv	cctggaccgtggcaagaaaacg		
pMTL74301_*ParCBADE*			
parCABDE_74301AscI_Fw	caggcttcttatttttatggaaaagccgggcactgccc	Amplification of *parCABDE*	gDNA *C. metallidurans* NG7

[4] Built by Dr. Giorgia Tibaldero during her PhD

Table 4-List of oligos used in this study: continuation from previous page

Primer name	Primer sequence (5'-3')	Function	Template
pMTL74301Low			
74301_Fw	ggaggcgcgccataaaaataagaagc	Amplification of pMTL74311Low for generation of pMTL74301Low	pMTL74311Low
74301_Rv	gataaccgtattaccgcctttgagtgag		
Chapter 5			
pMTL74311_RiboCas_Δ*phaC*1			
RiboCas_74311EcoRI_Fw	tccatatgaccatgattacgtcagtcacctcctagctg	Amplification of the RiboCas regulon (P_{fdx}_*cas*9/P_{AraE}).	pRECas1_Cpas_sgRNAonlyPhaC1
RiboCas_AraE_Rv	gaaaactcctccttaagatttatatatg		
SIBS_sgPhaC1SpeI_Fw	aatcttaaggaggagttttcgactagtcgtattggttgacgggctcggttttagagctagaaatagcaag	Amplification SIBS RNA with addition of sgRNA targeting *phaC*1. Introduce *Spe*I restriction site 5' of sgRNA	pRECas1_Cpas_sgRNAonlyPhaC1
SIBS_LHAPhaC1_Rv	catttgcaggcttcttatttttatggcgcggcac		
LHA_PhaC1_Fw	ttatttttatggcgcggcacatgcgggc	Amplification of *phaC*1 LHA	gDNA *C. metallidurans* CH34
LHA_PhaC1_Rv	cttatgaagctgttgcctcgcaatgtagacgctgtcaatgc		
RHA_PhaC1_Fw	cgaggcaacagcttcataagggccggcc	Amplification of *phaC*1 RHA. Introduce *Asc*I restriction site 3' of RHA	
RHA_PhaC1_Rv	tgagattatcaaaaaggaggggcgcgccccgtgccggtcttgtcga		
LHA_PhaC1_SqFw	acgcgccatggtggtgtc	Binds outside HA of *phaC*1. Screening of *phaC*1 KO	
LHA_PhaC1_SqRv	gccgacatcacgaccacagc		
PhaC1_Rv	aggcattcgtccaggcct	Binds inside *phaC1*. Screening of *phaC*1 KO	
Riboswitch Library[5]			
Arac_pbad_gt_Fw	ccttcttcacgaggcagacctcagcctgcaggcaggataaaaaaattgtagataaattttataaaatag	Amplification of AraC-P_{BAD} sequence including CD0164 terminator for HiFi ® assembly with Riboswitch Library. Rv primer has homology arms for universal Linker	pMTL71101_P_{BAD}_*mRFP1*
Arac_pbad_gt_Rv	tgagtcgtattggtaccatggagaaacagtagagag		

[5]Highlighted blue sequence corresponds to the linker sequence. Orange coloured letters, correspond to the riboswitch

Table 4-List of oligos used in this study: continuation from previous page

Primer name	Primer sequence (5'-3')	Function	Template
RbD_RFP_fw	ctactgtttctccatggtaccaatacgactcactataggttccggtgataccagcatcgtcttgatgcccttggcagcaccctgctaaggtaacaacaagatggcgagtagcgaagac	Forward amplification of RbD riboswitch for HiFi ® assembly with P_{BAD} promoter and *mRFP1*. Has homology arms for universal linker	pMTL71101_P_{BAD}_*mRFP1*
Rb_RFP_rv	gccagtgccaagcttgcatgtctgcaggcctcgagttaagcaccggtggagtg	General primer for reverse amplification of *mRFP1* for HiFi® assembly with pMTL710301 digested with *Xho*I	
Lk_RFP_fw	ctactgtttctccatggtaccaatacgactcactataggttccatggcgagtagcgaagac	Amplify *mRFP1* with addition of Linker (Lk)	
RbE_RFP_fw	tgtttctccatggtaccaatacgactcactataggttccggtgataccagcatcgtcttgatgcccttggcagcaccctgctaaggaggtaacaacaagatggcgagtagcgaagac	Amplification of *mRFP1* with addition of Lk_RiboswitchE	
RbF_RFP_fw	ctactgtttctccatggtaccaatacgactcactataggttccggtgataccagcatcgtcttgatgcccttggcagcaccctgctaaggaggtaacaacatggcgagtagcgaagac	Amplification of *mRFP1* with addition of Lk_RiboswitchF	
RbG_RFP_fw	ctactgtttctccatggtaccaatacgactcactataggttccggtgataccagcatcgtcttgatgcccttggcagcaccctgctaaggaggtaacttaatggcgagtagcgaagac	Amplify *mRFP1* with addition of Lk_RiboswitchG	
RbH_RFP_fw	ctactgtttctccatggtaccaatacgactcactataggttccggtgataccagcatcgtcttgatgcccttggcagcaccctgctaaggaggtgtgttaatggcgagtagcgaagac	Amplify *mRFP1* with addition of Lk_RiboswitchH	
RbI_RFP_fw	ctactgtttctccatggtaccaatacgactcactataggttccggtgataccagcatcgtcttgatgcccttggcagcaccctgctaaggaggtcaacaagatggcgagtagcgaagac	Amplify *mRFP1* with addition of Lk_RiboswitchI	
RbJ_RFP_fw	tgtttctccatggtaccaatacgactcactataggttccggtgataccagcatcgtcttgatgcccttggcagcaccctgctaagggagtgtacgaccaatggcgagtagcgaagac	Amplify *mRFP1* with addition of Lk_RiboswitchJ	

Table 4-List of oligos used in this study: continuation from previous page

Primer name	Primer sequence (5'-3')	Function	Template
Constitutive promoter library			
Pan_71301NotI_Fw	caggaaacagctatgaccgcgttcggtatcgaaagccg	Amplification of P_{Pan}	pUC57_P_{pan}
Pan_mRFP1_Rv	tactcgccatataacgtcctccttgtgatc		
mRFP1_Pan_Fw	aggacgttatatggcgagt	Amplification of *mRFP1*. Common for all constructs	pMTL71101_ P_{BAD}_*mRFP1*
mRFP1_71301NheI_Rv	gcaggcttcttatttttatgttaagcaccggtggagtg		
λmRFP1NotI_Fw	caggaaacagctatgaccgctaacaccgtgcgtgttgactattttacctctggcggtgataatggttgcatgtactaaggaggtcat	Amplification of *mRFP1* λ promoter as spacer sequence	
PA0284_mRFP1_Fw	caggaaacagctatgaccgcgtcttcattcaaggttttcccatggactgttgttctagtcg	Amplification of PA0284 promoter	[6]gDNA *C. metallidurans* NA4
PA0284_mRFP1_Rv	tactcgccatgcgacctccccacgcgc		
mRFP1_PA0284_Fw	gggaggtcgcatggcgagtagcgaagac	Amplification of *mRFP1* with homology arms to PA0284	pMTL71101_ P_{BAD}_*mRFP1*
mRFP1_71301NotI_Fw	tactcgccatgcgacctccccacgcgc	Cloning of promotorless *mRFP1*	pMTL71101_ P_{BAD}_*mRFP1*
AraE_71301NotI_Fw	caggaaacagctatgaccgctttatatttagtcccttgcc	Amplification of P_{AraE}	pRECas1_IIE
AraE_mRFP1_Rv	tactcgccatgaaaactcctccttaagatttatatatg		
mRFP1_AraE_Fw	aggagttttcatggcgagtagcgaagac	Amplification of *mRFP1* with homology arms to AraE	pMTL71101_ P_{BAD}_*mRFP1*
mRFP1_J23119_71301 NotI_Fw	caggaaacagctatgaccgcttgacagctagctcagtcctaggtataatgctagcaaggaggacgttatatggcgagtagcgaagac	Amplification of *mRFP1* with spacer sequence for addition of P_{J23119}	
mRFP1_Ptrpsyn_71301 NotI_Fw	caggaaacagctatgaccgcctgttgacaattaatcatcgaactagttaactagtacgcacaacagatcacaaggaggacgttatatggcgagtagcgaagac	Amplification of *mRFP1* with spacer sequence for addition of P_{trpsyn}	

Table 4-List of oligos used in this study: continuation from previous page

Primer name	Primer sequence (5'-3')	Function	Template
Cloning of plasmid pMTL74311_RBIC9_Δ*pyrE* & characterization of isolates			
Cas9RBI_74311EcoRI_Fw	tccatatgaccatgattacgaattctcagtcacctcctagctg	Amplification of *cas9* with P_{BAD}RBI construct with spacer for insertion of P_{J23119}	pMTL74311_Cas9_Δ*phaC1*[7]
Cas9J231119sgRNA_Rv2	gtgcaaagcggatgaaggacactagtgctagcattataccta ggactgagctagctgtcaatct agatttttttggggcg		
SIBS_J23119_ Fw	gtccttcatccgctttgcacgtttagagctagaaatagcaag	Amplification of SIBS RNA scaffold with spacer sgRNA for targeting of *pyrE*	pMTL74311_Cas9_Δ*phaC1*[8]
SIBS_LHAPyrE_RV	gcttcttatttttatggcggctgaacttc		
LHAPyre_SIBS_Fw	ttttatggcggctgaacttctcgtccttgtagatc	Amplification of LHA from gDNA	gDNA *C. metalliduransis* CH34
LHAPyre_RHA_Rv	gccggacgaccttagccagttgttcaa		
RHAPyre_LHA_Fw	accttagccagtttgttcaaccagggcgcgatg	Amplify RHA from gDNA	
RHAPyre_74311AscI_Rv	atccgcgcgctggtgctgggcgcgcctccttttgataatctca		
LHAUp_pyrE_Fw	gggatgcgcacatcacaac	cPCR of putative *pyrE* knockouts	
RHA_pyrE_Rv	gatcattgacgacgtgatctccg		
PyrE_Fw	aagatgacgcagcagacga	Primer used for Sanger sequencing of *pyrE* knockouts	
PyrE_Rv	gatcattgacgacgtgatctccg		
Cloning of plasmid pMTL74311_RBIC9_Δ*pilAE* & characterization of isolates			
SgRNA1_RBIC9SpeI_Fw	tcctaggtataatgctagcactagtaatgtatcgattctcggcatgttttagagctagaaatagcaagtt	Amplification of SIBS scaffold with spacers for insertion of sgRNA targeting *pilAE*	pMTL74311_RBIC9_ΔpyrE, *Spe*I/*Asc*I fragments
SIBS_LHAPilA_Rv	ttcatcgtcgtcgccggtcacgccataaaaataagaagcctgcatttg	Amplification of LHA to *pilAE*	gDNA *C. metalliduransis*CH34 *wild type* and pilins knockouts
RHAPilE_LHA_Fw	aggggtcaacggcgcgccttaatccgggggcggtctag	Amplification of RHA to *pilAE*	
RHA_RBIC9AscI_Rv	tgagattatcaaaaaggaggcttttccagcagcagcacc		

Table 4-List of oligos used in this study: continuation from previous page

Primer name	Primer sequence (5'-3')	Function	Template
Cloning of plasmid pMTL74311_RBIC9_Δ*pilAE* & characterization of isolates			
PilA_Up2_Fw	gagcctgccgtacctgaaga	Fw primer binds outside *pilA* LHA. Rv primer binds inside *pilE* RHA	gDNA *C. metallidurans* CH34 *wild type* and pilins knockouts
PilEDw_Rv	ccatccgctggttcgaagaa		
PilA_Up3_Fw	ccagcagaagaaggccattttctgg	binds outside the homology arms for identification of knockouts	
RHA_Dw4_Rv	gaaacctgatcaccggactggagtt		
PilA _sq_Rv	ttacccgactcactcgctttcg	Binds inside *pilA*. Knockout screening	
PilE_Sq_Rv	atcgaggaatgtatcgattctcgg	Binds inside *pilE*. Knockout screening	
pMTL74311_RBIC9_Δ*pilA* & characterization of isolates			
sgRNAPilA_RBIC9_Fw	ggtataatgctagcactagtcgactcactcgctttcgcgcagggttttagagctagaaatagcaagtta	Amplification of SIBS scaffold with spacers for insertion of sgRNA targeting *pilA*	pMTL74311_RBIC9_Δ*pyrE*, *Spe*I/*Asc*I fragments
SIBSPilA_LHA_Rv	tcgccggtcacgccataaaaataagaagcctg		
LHAPilA_SIBS_Fw	//	Amplification of LHA to *pilA*	gDNA *C. metallidurans* CH34 *wild type* and pilin knockouts
LHAPilA_SIBS_Rv	tccatatgaccatgattacgaattctcagtcacctcctagctg		
RHAPilA_LHA_Fw	aaaggggtcaacggtagctagcattacgtcc	Amplification of RHA to *pilA*	
RHAPilA_AscI_Rv	ggtcatgagattatcaaaaaggaggcgcgccaaggtgttcttcgaaccag		
pMTL74311_RBIC9_Δ*pilE* & characterization of isolates			
SIBSPilE_RBISpeI_Fw	tcctaggtataatgctagcactagtgcagtagcggctccatcgcgtgggttttagagctagaaatagcaag	Amplification of SIBS scaffold with spacers for insertion of sgRNA targeting *pilA*	pMTL74311_RBIC9_Δ*pyrE*, *Spe*I/*Asc*I fragments
SIBSPilE_LHA_Rv	cgattctttccgccataaaaataagaagcc		
LHAPilE_SIBS_Fw	ttttatggcggaaagaatcgtcgaggcttc	Amplification of LHA to *pilE*	gDNA *C. metallidurans* CH34 wild type and pilin knockouts

Table 4-List of oligos used in this study: continuation from previous page

Primer name	Primer sequence (5'-3')	Function	Template
pMTL74311_RBIC9_Δ*pilAE*::*gfp* & characterization of isolates			
GFP_RBIC9_Fw	aaatgaaaaggggtcaacgg atgcgtaaaggagaagaac	Amplification of *gfp* for substitution with *pilAE*	pUT*gfp* (Donated by Rob Van Houdt, SCK-CEN, Mol, Belgium)
GFP RBIC9_RV	agaccgccccggattaaggt tatttgtatagttcatccatgc		
pMTL74311_RBIC9_Δ*pilAE*::λ*gfp* & characterization of isolates			
PrGFP_RBIC9_Fw	aaatgaaaaggggtcaacggt aacaccgtgcgtgttgactattt tacctctggcggtgataatggtt gcatgtactaaggaggtcatat gcgtaaaggagaagaac	Amplification of λ*gfp* for substitution with *pilAE*	

Table 5-List of spacers used in this study

Spacer target	Spacer oligo sequence (5'-3')	Plasmid reference
phaC1	cgtattggttgacgggctcg	pMTL74311_RiboCas_Δ*phaC1*
pyrE	gtccttcatccgctttgcac	pMTL74311_RBIC9_Δ*pyrE*
pilAE/pilAE::gfp/pilAE::λgfp	aatgtatcgattctcggcat	pMTL74311_RBIC9_Δ*pilAE/* pMTL74311_RBIC9_Δ*pilAE::gfp/* pMTL74311_RBIC9_Δ*pilAE:: λgfp*
pilA	cgactcactcgctttcgcgcagg	pMTL74311_RBIC9_Δ*pilA*
PilE	gcagtagcggctccatcgcgtgg	pMTL74311_RBIC9_Δ*pilE*

2.2.2 DNA Extraction

Plasmid DNA was purified using QIAprep Spin Miniprep Kit (Qiagen) following manufacturer recommendations from 5 mL of an overnight culture.

Genomic DNA was isolated by means of GenElute™ Bacterial Genomic DNA Kit (Sigma-Aldrich) according to manufacturer's recommendations from 1.5 mL of an overnight culture.

2.2.3 Restriction Digestions & Amplification of DNA via PCR

Restriction enzymes from NEB were used according to manufacturer's instructions by typically performing reactions in 20 µL volume with 1 unit of enzyme for 1-2 hours at 37 ˚C.

All primers designed were ordered from IDT (Leuven, Belgium). Lyophilized oligonucleotides were resuspended in de-ionized H_2O at 100 pmol/µL. Primers were designed by following published recommendations[155] and melting temperature was calculated by using NEB online tool (https://tmcalculator.neb.com/#!/main). Q5 High-Fidelity DNA Polymerase (NEB) was used for amplification of DNA fragments to be used for cloning purposes. PCR amplification of DNA fragments from purified plasmids or genomic DNA was performed by using 1ng of DNA template. Taq Master Mix (NEB) was used for screening of colonies via colony PCR. All the polymerases kit were used according to manufacturer's instructions.

2.2.4 Agarose Gel Electrophoresis

1% TAE agarose gel were prepared by mixing 1g of agarose with 1x TAE buffer (40mM Tris-Acetate, 1 mM EDTA) and 1:1000 SYBR safe DNA Gel Stain (ThermoFisher Scientific). 5-20 µL of PCR samples or restriction digestions were loaded per each well with 1-4 µL of loading dye (Gel Loading Dye, Purple (6x)). The gels were run for 60 minutes at 100 V and visualized by using Gel Doc™ XR+ (BioRad). QuickLoad® 1 kb Extended DNA Ladder was used as DNA ladder marker.

2.2.5 Gel Extraction, DNA Purification & Quantification

Fragments of DNA resulting from PCR or restriction digestion ran on 1% TAE agarose gels in TAE buffer, were excised, and purified using Zymoclean™ Gel DNA Recovery Kit (Zymo Research) according to manufacturer's instructions. A SimpliNano™ spectrophotomer (GE Healthcare Life Sciences) was used for quantification of DNA.

2.2.6 Plasmid Assembly

NEBbuilder® HiFi DNA Assembly Master Mix was used to build the plasmids in this study according to manufacturer recommendations. Primers for fragments amplification were designed with NEBuilder online tool (https://nebuilder.neb.com/#!/). The kit allows assembly of multiple DNA fragments that can be generated via either PCR or restriction digestion in few steps. For example, if two fragments are to be inserted into a backbone the general procedure applied in this thesis is the following:

i) Digestion and gel purification of the desired backbone

ii) PCR amplification of the desired DNA fragments. Primers are designed to have at least 25 bp homology arms that allow the upstream and downstream fragments to overlap with each other and with the plasmid backbone. The PCR fragments are then gel-purified

iii) Addition of the fragments into the HiFi® mastermix followed by incubation as per instruction from the manufacturer

benchling.com was used for digital DNA sequence editing and for all the *in silico* steps necessary for molecular cloning. This included primers design, virtual DNA digests, and Sanger sequencing alignments.

Ligation reactions of DNA fragments were performed with T4 DNA ligase according to manufacturer's instructions. Ligation reaction was performed at 4 ˚C overnight with molar ratio vector to insert 1:3. Following incubation, 2µL of ligation mixture were transformed in DH5α competent cells (NEB) as described in section 2.1.4. Eventually all the plasmids were transformed in *E. coli* DH5α unless otherwise stated.

The construction procedures specific to each plasmid are reported in the appropriate experimental section.

2.3 Bioinformatics

This section describes the bioinformatic tools exploited to compare genomic sequences of the bacterial strains used in this study.

2.3.1 Whole Genome Sequencing & protein alignment

CLC Genomics Workbench was used for analysis of Illumina Sequencing data. The genome of *C. metallidurans* CH34[156] downloaded from NCBI was used as reference to map paired trimmed end with parameters specified in Table 6 previously optimized by Dr Alex Grosse (University of Nottingham). The accessions numbers are as follows: NC_007971 (pMOL30), NC_007972 (pMOL28), NC_007973 (CHR1), NC_007974 (CHR2. chromid).

Clustal Omega was used for alignment of amino acid sequences with default parameters.

Table 6-Parameters used in CLS genomics for mapping of trimmed reads to the reference genome

Mapping feature	Value
Masking Mode	No Masking
Match Score	1
Mismatch cost	2
Insertion cost	3
Deletion cost	3
Insertion open cost	6
Insertion extend cost	1
Deletion open cost	6
Deletion extend cost	1
Mapping feature	Value
Length fraction	0.5
Similarity fraction	0.8
Non-specific match handling	Map randomly
Parameter	Value
Ploidy	1
Ignore positions with coverage above	100,000
Ignore broken pairs	Yes
Ignore specific matches	Reads
Minimum coverage	35
Minimum count	5
Minimum variant frequency (35%)	35
Require presence in both forward and reverse reads	Yes
Base quality filter	Yes
Neighbourhood radius	5
Minimum central quality	20
Minimum neighbourhood quality	15
Read direction filter	Yes
Direction frequency (%)	5
Parameter	Value
Relative read direction filter significance (%)	1
Read position filter	No
Remove pyro-error variants	No

2.4 Electrophysiological Techniques

This section reports the principle of electrochemistry fundamental to understand the experiments performed in chapter 6 for investigation of EET in *C. metallidurans* CH34.

2.4.1 Principles of Electrochemistry

To understand and critically evaluate the electrophysiology experiments performed in this thesis, an overview at the basic electrochemical principles will be herein presented.

Electricity is defined as the movement of electrons across chemical species. During oxidation a substance is “oxidised” and generates electrons and protons, while during reduction electrons are transferred to a substance which is therefore “reduced”. The amount of energy necessary to move electrons from the reduced to the oxidised chemical is called potential (E). The potential difference is the driving force for Extracellular Electron Transfer, and it is necessary for electrons to move from a substance A (reducing agent) to a substance B (oxidizing agent) (Figure 16)[154].

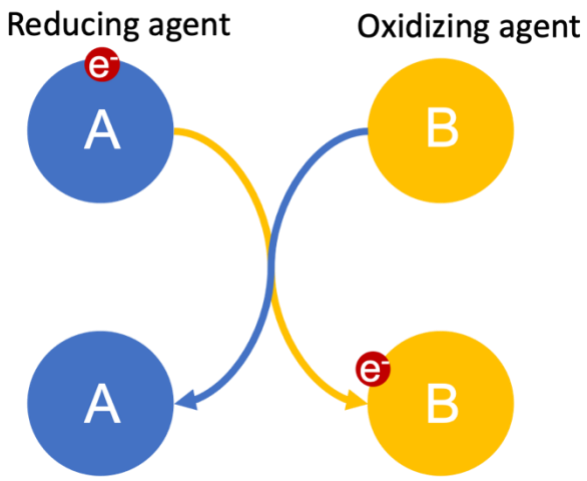

Figure 16-Schematic representation of RedOx mechanism: In blue and yellow are the reducing and oxidizing agents respectively. Adapted from[154].

Electrochemistry studies the relationship between the passage of electrons and chemical changes. Electrochemical reactions are controlled in a cell that includes the electrically active species (the analyte), an electrolyte, and the electrodes. A commonly used electrode setup in electrochemistry experiments is the "three electrodes system", which rely on a Working Electrode (WE) and a Counter Electrode (CE) where the reaction of interest and the opposite reaction occur respectively, and a Reference Electrode (RE), which composition and electrochemical potential are fixed. This arrangement is necessary to maintain the potential of the system at the WE constant. A potentiostat can also be used to simultaneously apply potential across the electrodes and measuring the passage of currents. By convention, in an electrochemical cell oxidation and reduction occur at the anode and cathode respectively. In the example reported in Figure 17, a potential more positive than the potential of A^- is applied at the WE to induce oxidation of A^-, which donate an electrode to the WE (anode) travelling through an external circuit to the CE (cathode) where reduction of B to B^- occurs[154].

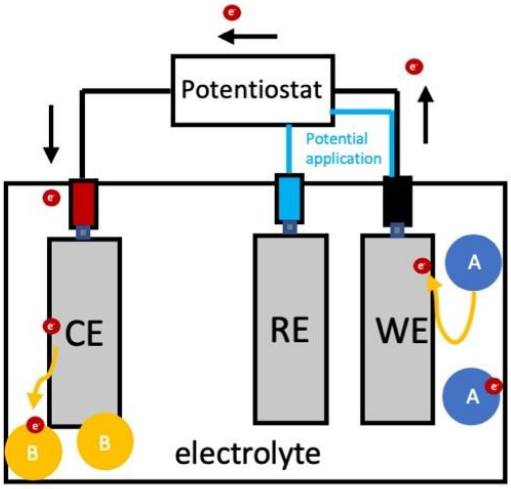

Figure 17-Schematic representation of an electrochemical cell: chemical species A^+ is oxidized to A at the WE (anode in this case), electrons travel through an external circuit and reach the CE (cathode), thereby reducing B^+ to B. Adapted from[154].

More specifically, electron transfer between an electrode and a chemical species in solutions occurs when the potential of the electrochemical cell is sufficient to i) promote transfer of an electron between the working electrode and the Lowest Unoccupied Molecular Orbital (LUMO) of the species of interest, thereby catalysing a reduction or ii) promote transfer of one electron between the Highest Occupied Molecular Orbital (HOMO) of the species in solution and the working electrode, phenomenon called oxidation. In the example of reduction of ferrocyanide ($[Fe(CN)_6]^{4-}$ (FCI^+) to ferricyanide ($[Fe(CN)_6]^{3-}$ (FCI), by appropriately changing the voltage at the electrode, a driving force is created such that the electrons in the electrodes are at higher energy than the LUMO of FCI^+, thereby leading to reduction to FCI (equation 1) at the cathode:

$$\text{equation 1: } FCI^+ + e - \rightleftharpoons FCI$$

2.4.2 The Electrode-Solution Interface

When a metal is immersed in a conductive solution (electrolyte), a potential is established at the electrode/solution interface[150]. Therefore, to understand better the phenomena at the electrode surface, a brief description of phenomena occurring at the electrode-solution interface is herein presented.

Assuming the electrode surface is charged positively a double layer of charge ions is present at the electrode-solution interface. These are the Inner Helmholtz plane (IHP) composed of negatively charged ions, and the Outer Helmholtz plane (OHP) constituted by ions loosely attracted to the surface. After the OHP, the diffusion layer (Nernst layer), comprised of ions free to diffuse to the electrode and eventually the bulk solution completes the overview of the electrode-surface interface. Upon application of a potential, the ions in the double layer undergo a redistribution which result in generation of a capacitative current that does not reflect a RedOx mechanism. The currents rising from RedOx reactions such as the ones causing reduction of FCI^+ to FCI are instead called faradaic currents and are the focus of part of this study. The overall magnitude of a faradaic current depends on the rate of the RedOx reaction at the electrode-analyte interface which is influenced by two elements:

i) Mass transport: the rate at which the reactants and products are transported to and from the electrode surface
ii) Electron transfer kinetic at electrode surface: the rate at which electrons are relayed between the electrode and the chemical species in solution

On the electrode surface, the rate at which the reaction occurs is defined by the slowest process in the system. In the simplest scenario, a reaction which occur rapidly is

limited by the mass transport of the chemical species to the electrode and such reactions are called mass transport-limited[154].

2.4.3 Cyclic Voltammetry

Cyclic voltammetry is one the most widely used techniques to obtain qualitative and quantitative information form electrochemical reactions. It consists in linear scan of the potential at the WE by means of a triangular potential waveform. Potential is usually scanned between two vertexes (E1 and E2 in Figure 18A) and back as function of time and is referred to as potential against the RE. The graph obtained depends on the type of WE used in the electrochemical system but generally gives information regarding the reduction and oxidation of chemical species, weather the RedOx reaction is controlled by diffusion and the potential at which these reactions occur. Figure 18C shows a typical voltammogram of FCI^+ taken from the experimental data presented in section 6.4.1. This also represents a typical CV that can be obtained from a diffusion-controlled reaction at a macroelectrode. Here, a potential window was selected, and faradaic currents were observed upon scanning in both directions. In the voltammogram, the presence of capacitative current can be observed, but the faradaic processes exceed the magnitude of the capacitative currents thereby producing measurable peaks. Eventually reduction (I_{rd}) and oxidation (I_{ox}) current peaks, peak potentials (E_{ox}, E_{rd}) and peak separation (ΔE) can be calculated as illustrated in Figure 18B. For better understanding of the electrochemical RedOx reaction occurring at the electrode-solution interface, the canonical FCI^+-FCI reduction will be herein explained by interpreting the main steps of the negative scan (from positive to negative potential). When the potential E_1 is applied at the WE, the Nernst diffusion and the double layers are setup (i). At this point the concentration of

FCI^+ and FCI is consistent. Changing potential at the WE lead to rise of a capacitative current due to rearrangement of the double layer (ii). When the potential becomes negative enough, FCI^+ is reduced at the electrode interface to FCI, thereby giving rise to a steep peak that can be identified as faradaic current (iii). During this step FCI^+ diffuses to the electrode surface according to Fick's laws and the concentration of the FCI/FCI^+ RedOx couple can be calculated according to the Nernst equation. Eventually a current peak is established (I_{rd}) (iv). At this point the WE have become saturated with FCI^+, the RedOx reaction is said to be diffusion-limited according to Nernst equation and the current starts to decay (v) (Figure 18C). Eventually the potential is reversed at E_2 and the opposite occurs during the positive scan[155].

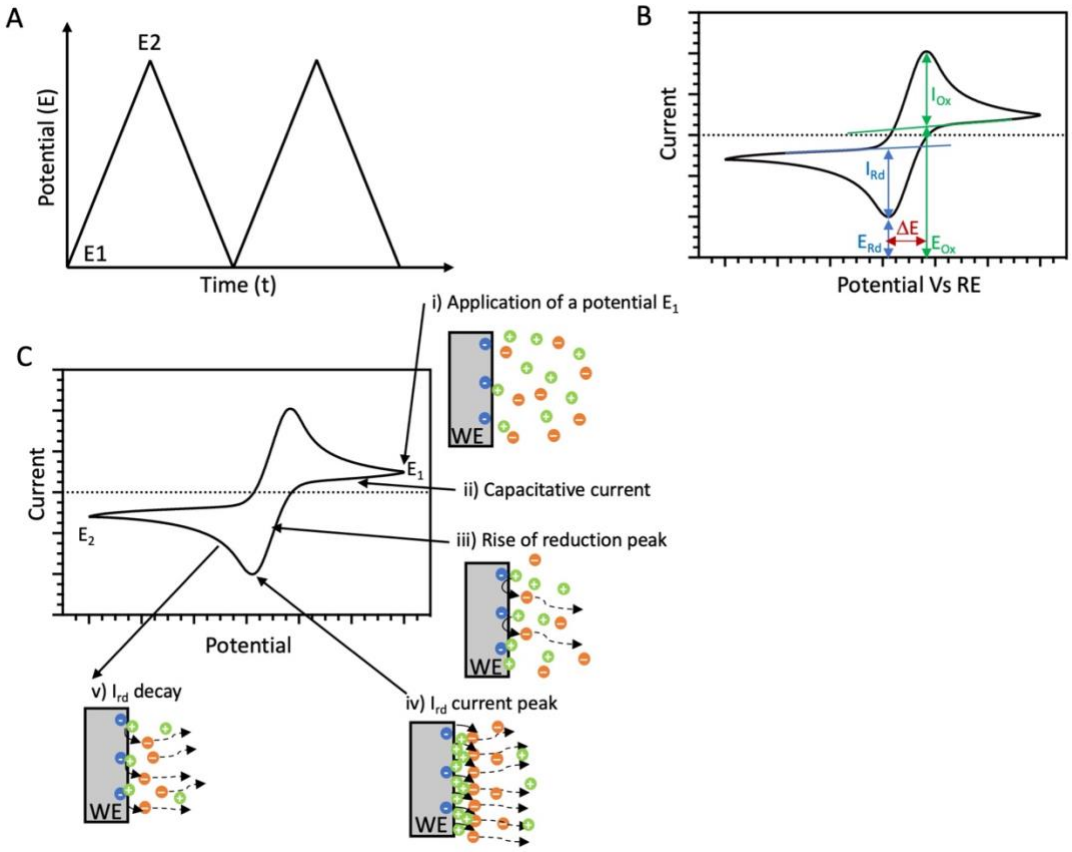

Figure 18-Representation of cyclic voltammogram features and peak calculation: A) typical triangular waveform of applied potential in function of time during CV, B) typical voltammogram of a diffusion- limited RedOx mechanism by using FCI^+ as analyte. I_{Rd}, I_{Ox} and ΔE are coloured in blue, green, and red respectively. C) voltammogram of FCI^+ with a diagram of the main mechanisms occurring at the electrode surface: Detail description of the underlying mechanism is in the text. adapted from[155].

2.4.3.1 Role of scan rate

Another useful tool that can be used to gather information on the RedOx mechanisms at the electrode-electrolyte interface during CV experiments is the scan rate. The scan rate is a measure of how fast the applied potential is scanned and is measured in Volts/Seconds. The scan rate affects the peak currents because it influences the size of the diffusion layer. At high scan rates the diffusion layer will be thin, thereby increasing the concentration of electron carriers which can be oxidised or reduced at the electrode surface. Once a diffusive mechanism has been confirmed

by the features of the voltammogram, the diffusion gradient and the concentration of the analyte can be determined with the Randles-Sevcik equation. Although there are different versions of this equation that can be used depending on if the mechanisms observed is fully reversible or not, the scope of the electrochemical studies in this thesis are mainly of qualitative nature and the elements of this equation will not be herein discussed. Nevertheless, the application of the Randles-Sevcik law makes also possible to graphically determine and confirm the nature of the electrochemical mechanism. For diffusive electron carriers, a linear dependence between the current peaks and the square root of the scan rate is established while if the phenomenon witnessed is related to a thin film of molecules adsorbed on the electrode surface, a linear relationship will be established between the current peak and the scan rate[155].

2.4.3.2 Interpretation of Voltammetry Curves

The interpretation of a voltammogram can provide several information such as the reversibility of the process and if the mechanism is associated with freely diffusive species in solution or adsorbed on the electrode surface. The tools necessary for interpretation of the voltammograms recorded in this study are herein presented.

An electrochemical reaction can be considered reversible, irreversible, quasi-reversible or electrocatalytic depending on the rate at which electrons transfer between the chemical species in solution and the electrode surface, and if the electron transfer step is followed by a chemical reaction. In the literature the concepts of "reversibility" and "irreversibility" are tied to the rate of electron transfer, where the former and the latter phenomena corresponds to a fast and slow transfer kinetics respectively in relation to the mass transfer. In the case of a fast diffusion-limited reversible reaction (like the single electron transfer mechanism that results in reduction of FCI^+ to FCI),

a CV scan will present i) ratio I_{ox}/I_{rd} equal to 1 ii) the current peak potentials distanced (ideally) 59 mV, iii) a classical "duck shaped" voltammogram and iv) no shift of the peak potentials correlated with change of the scan rate. Irreversible electrochemical reactions are limited by the slow electron transfer kinetics. This implies significantly large "overpotentials" are necessary to drive electron transfer between the electrode and the analyte. Therefore, if the potential window is large enough to display both the RedOx peaks, a typical voltammogram will show i) current peaks potential separated more than 59 mV and ii) shift of the peak potentials to higher values. In a quasi-reversible reaction, the current can be limited by both mass and charge transfer and the smallest of the two factors controls the type of reaction observed. For slow scan rates a quasi-reversible system resembles the features of reversible RedOx species, but for higher scan rates the shape of the voltammograms recalls an irreversible reaction with considerable peak potential separation. A typical voltammogram for each of the mechanisms is shown in Figure 19. Furthermore, some organic compounds show a phenomenon called electrocatalytic (EC) effect when studied by means of CV. Upon electron exchange, these molecules form reactive charged species which can react with other substrates in solution. The following chemical reaction (marked with the letter "C" in the acronym EC) results in decreased amount of product generated in the forward scan, which eventually results in a decreased current peak during the reverse scan. At low scan rate an EC mechanism will show display the behaviour just mentioned. However, if the scan rate is increased the time scale of the experiment "outrun" the chemical conversion and the system will move toward a Nernstian response (I.E reversibility)[155] Figure 20.

Eventually, this information can be transferred to electroactive biofilms since bacteria are reported to use MET or DET via use of diffusible RedOx mediators or

membrane bound cytochrome, which from the electrochemical point of view behave like diffusion-limited or surface-adsorbed mechanisms respectively[155].

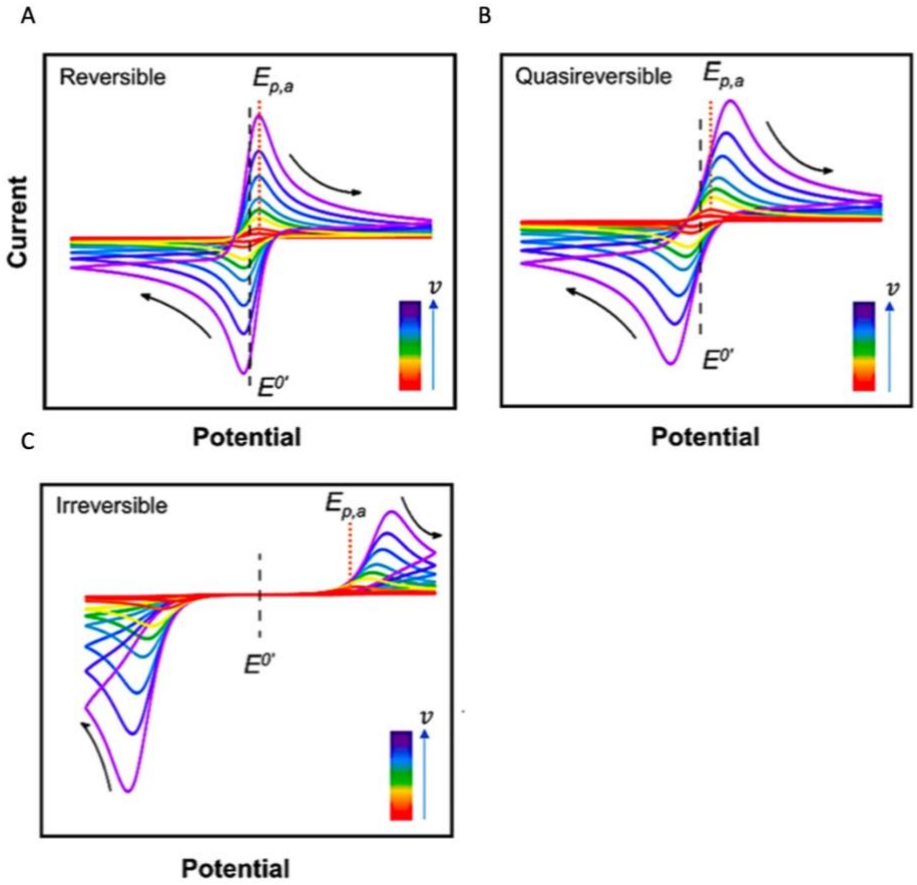

Figure 19-Voltammograms of A) Reversible B) Quasi-reversible and C) Irreversible RedOx mechanisms as function of the scan rate: the anodic peak potential of the CV curve recorded at the lowest scan rate (red) is reported as $E_{p,a}$. E_0 represent the formal potential, herein not discussed. Adapted from[156].

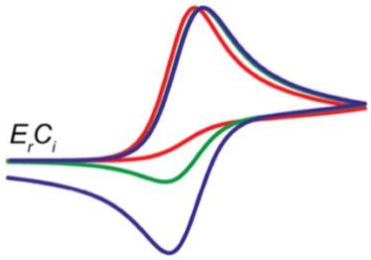

Figure 20-Voltammogram of an E_rC_i mechanism: The voltammogram represent the case of a reversible electron transfer (E_r) followed by an irrebversible chemical reaction (C_i). the scan rte values are v=100 mV/s (red), 1V/s (green) and 10 V/s (blue). Adapted from[155].

2.5 Statistical Test

All statistical tests were performed with Prism. Mann-Whitney Non-parametric Unpaired two tailed test was used unless alternatively specified.

For comparison of current peaks (see sections 0) Mann-Whitney non-parametric one tailed unpaired test was used since a difference in the specific range of negative (reductive currents) or positive (oxidative currents) was expected.

3 -Outer Membrane Expression of SNAP-tag for Increased Extracellular Electron Transfer Between *C. metallidurans* and the Electrode Surface

3.1 Background: Strategies for Improvement of Extracellular Electron Transfer Between Bacteria and Electrode Surface

Low power output is the major limitation to the use of MFCs at commercial scale and is determined by the low rate of electron transfer between the electroactive biofilm and electrode surface. MFC power output can be influenced by many factors including device configuration[157], type of substrate, microorganisms, electrode material and shape[158]. Nevertheless, augmented EET and formation of biofilm always influences positively the production of electricity and other relevant parameters in MFC such as removal of pollutants[159]. Approaches to increase power output of MFC can be based on engineering of the biofilms by genetic manipulation or surface modification of the electrodes. Examples of genetic manipulation include modification of the components directly involved in EET or alternative approaches like manipulation of quorum sensing pathways. For example, co-expression of the genes clusters responsible for synthesis of flavins and the cytochrome-porin complex (fundamental for reduction of Fe(III) and Mn(IV) in *Shewanella oneidensis* MR1 and alteration of quorum sensing signalling in *P. aeruginosa* resulted in increased electricity production in MFCs[160,161].

Electrode modification as alternative approach to increase the rate of electron transfer between the biofilm and the electrode has recently been proposed. This is based on the concept that increasing bacterial adherence to the electrode facilitates electron transfer and therefore power output[162]. Anode surface modification studies report increased electricity production in several instances. For example, MnO_2, Pd or Fe_3O_4 nanoparticles mixed with carbon black were used for preparation of "doped" electrodes for removal of ibuprofen and carbamazepine from wastewaters in MFC[163]. Degradation of the drugs and increased electricity production could be observed in the

fuel cells with the modified electrodes compared to the control where simple black carbon electrodes were employed[163]. However, to the best of my knowledge there is no study considering a merged approach where both genetic and surface modifications of bacteria and electrodes are contemplated.

In this chapter, a combined genetic and surface modification design was considered as a possibility to increase the extracellular electron transfer rate between *C. metallidurans* CH34 and the anodic surface. The strategy was based on genetic modification of *C. metallidurans* CH34 with an outer surface expression system resulting in the expression of a SNAP-tag[164] and surface functionalization of the electrode with Self-Assembled-Monolayers (SAM) carrying a functional O^6-benzylguanine (the ligand for the SNAP-tag).

Display of recombinant proteins on the outer membrane of Gram-negative bacteria by means of protein complexes called autotransporters is a promising technology that can be used for several biotechnological applications such as biocatalysis[165], live vaccine delivery[166] and bioremediation[57,167]. Autotransporters are typical of Gram-negative bacteria and are composed of an N-terminal signal peptide which promotes translocation of the translated peptide in the periplasm, a passenger protein which is eventually displayed on the bacterial surface, a β-barrel protein responsible for extrusion of the passenger domain (translocation domain) and a flexible linker which connects the passenger to the inner side of the translocation domain[168]. The Adhesin Involved in the Diffuse Adherence (AIDA-I) autotransporter was discovered in the enteropathogenic *E. coli* EPEC strain and it was reported to be involved in mediating attachment of the bacteria to the host cells in a mechanism called diffused adherence. After it was discovered the AIDA-I system possessed autocatalytic activity, which resulted in cleavage of the C-termini thereby leaving the

β-barrel translocation domain AIDA-C embedded in the outer membrane, it was postulated that fusion of different passenger proteins to AIDA-C could be performed for biotechnological applications and subsequently several reports used the AIDA-C system for successful expression of recombinant protein outside the outer membrane of Gram negative bacteria[154,169,170].

On the other hand, SAM are associations of molecules that adsorb spontaneously in ordered pattern on surface[174]. SAM molecules consist of a head, tail, and functional group. The head is usually made of phosphonates, thiols, or silanes, with the choice of the head group employed dependent on the downstream application as its role is to lead the adsorption process on the surface of interest. Alkanethiols are one of the most extensively studied SAM which are made of a thiol (S-H) tail, an alkyl $(C\text{-}C)^n$ group and a functional tail group[171]. Given their cheap and versatile nature, SAM have been employed mainly for chemical sensing[172] and electronics[173].

Here, I describe the experimental strategy and expression test of the AIDA-C translocation domain fused to a SNAP-tag protein for enhanced biofilm formation of *C. metallidurans* CH34 on the electrode surfaces with the aim to increase EET for increasing power output in MFCs. Functionalization of the electrode surface with Alkanethiols with O^6-benzylguanine (the ligand for the SNAP tag) was part of the PhD project of another PhD student, it was herein introduced for clarification purposes only and it will not be further discussed.

3.2 Experimental Strategy

The aim of this section is to describe the strategy adopted for development of a strain of *C. metallidurans* CH34 with increased capability of forming biofilm at the electrode surface for augmented electron transfer between bacteria and the electrode

surface. The idea relied on the use of the autotransporter AIDA-C for display of the SNAP-tag on the outer membrane. The SNAP-tag derives from a mutated version of the human O^6-alkylguanine-DNA alkyltransferase (hAGT) gene which forms a strong covalent bond with the synthetic O^6-benzylguanine. The genetic construct was composed of an operon under control of the P_{BAD} promoter driving expression of the SNAP tag as passenger protein connected to the AIDA-C β barrel via its native linker. The signal sequence native to the EPEC *E. coli* strain AIDA-C protein was placed in front of the SNAP tag to ensure translocation in the periplasmic space. Parallel to the genetic modification of *C. metallidurans* CH34, the electrode surface would have been modified with SAM functionalized with O^6-benzylguanine functional groups by another PhD student. Beside the ligand for the SNAP tag, the SAM to be used would have been endowed of a head group which nature was based on the electrode material. Figure 21 shows a model of the synhetic biofilm formation in the case of a gold anode and SAM enriched with a sulfur head group, which can be absorbed on gold surfaces where chemical bonds are formed between the electrode and the SAM sulfur group, thereby ensuring stable modification of the electrode[171].

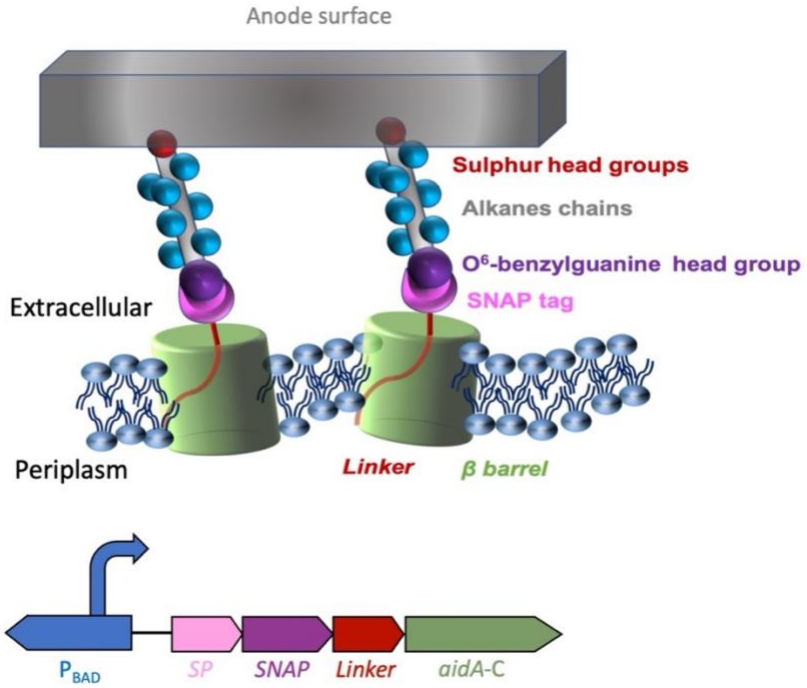

Figure 21-Model of the synthetic biofilm initiation of *C. metallidurans* CH34 on gold electrodes functionalized with SAM: Top panel shows the interaction between the SNAP tag (pink) and the electrode functionalized with SAM bearing sulphur head groups and O^6-benzylguanine for creation of chemical bonds with the electrode surface and the SNAP tag respectively. The bottom panel shows organization of the operon for expression of the AIDAc β barrel and the passenger protein SNAP-tag. The colour coding is: blue for the P_{BAD} promoter, pink for the Signal Peptide, purple for the *SNAP* tag, red for the linker and green for the *aidA-C* gene.

3.3 Aim of the Study

The aim of this study was to propose and test an interdisciplinary approach, combining synthetic biology and surface chemistry modification, for increased biofilm formation of *C. metallidurans* CH34 on the electrode surface and increased EET between the cells and the electrode. This was performed by:

i) Cloning and testing expression of the *aidA-C*-SNAP-tag system in model organism *E. coli* DH5α.

ii) Test and optimise the system in *C. metallidurans* CH34 for further characterization of enhanced synthetic biofilm on the electrode surface.

3.4 Materials and Methods

3.4.1 Antibiotic Susceptibility Test

The antibiotic susceptibility test was performed on the in-house strain of *C. metallidurans* CH34 ordered from DSMZ in 2015, prior to my arrival in the lab. As this strain has never been used since and I had no previous experience in working with *C. metallidurans,* an antibiotic screening test was performed with antibiotics reported in the literature for effective selection of transformants of *C. metallidurans* CH34 namely tetracycline[174], kanamycin[174] and chloramphenicol[56] in the attempt to confirm suitable antibiotics for the selection of transformants. Liquid cultures of *C. metallidurans* were spread on LB plates supplemented with 1500 μg/mL, 20μg/mL and 400 μg/mL of kanamycin, tetracycline, and chloramphenicol respectively. Cultures of *E. coli* DH5α were used as negative control to ensure the antibiotic stocks were still effective.

3.4.2 Construction of Plasmids for Expression of the SNAP-Tag

This section describes the procedure and the materials used for cloning of plasmid pMTL71101_P_{BAD}_*SNAP*_*aidA-C*, for outer membrane expression of the *SNAP* tag. A schematic representation of the cloning procedure is shown in Figure 22. pMTL71101 was digested with *Not*I and *Xho*I. plasmids pMTL71301_P_{BAD}_*mRFP1*, pARAbad-ZigG-EC\[153] and pSNAP were used as templates for amplification of the P_{BAD} promoter, *aidA-C* and SNAP-tag respectively with primer pairs PBAD_71101NotI_Fw/P_{BAD}_SNAP_Rv, SNAP_PBAD_Fw/SNAP_AIDA-C_Rv.

and AIDA_SNAP_Fw/AIDA_711010XhoI_Rv the two fragments were then assembled for generation of pMTL71101_P_{BAD}_*SNAP_aidA-C*. Vector pMTL71101_*SNAP_aidA-C* was also built in the same way, but by using primer pairs SNAP_71101*Xho*I_Fw/ SNAP_AIDA-C_Rv to exclude P_{BAD} promoter from the finl plasmid.

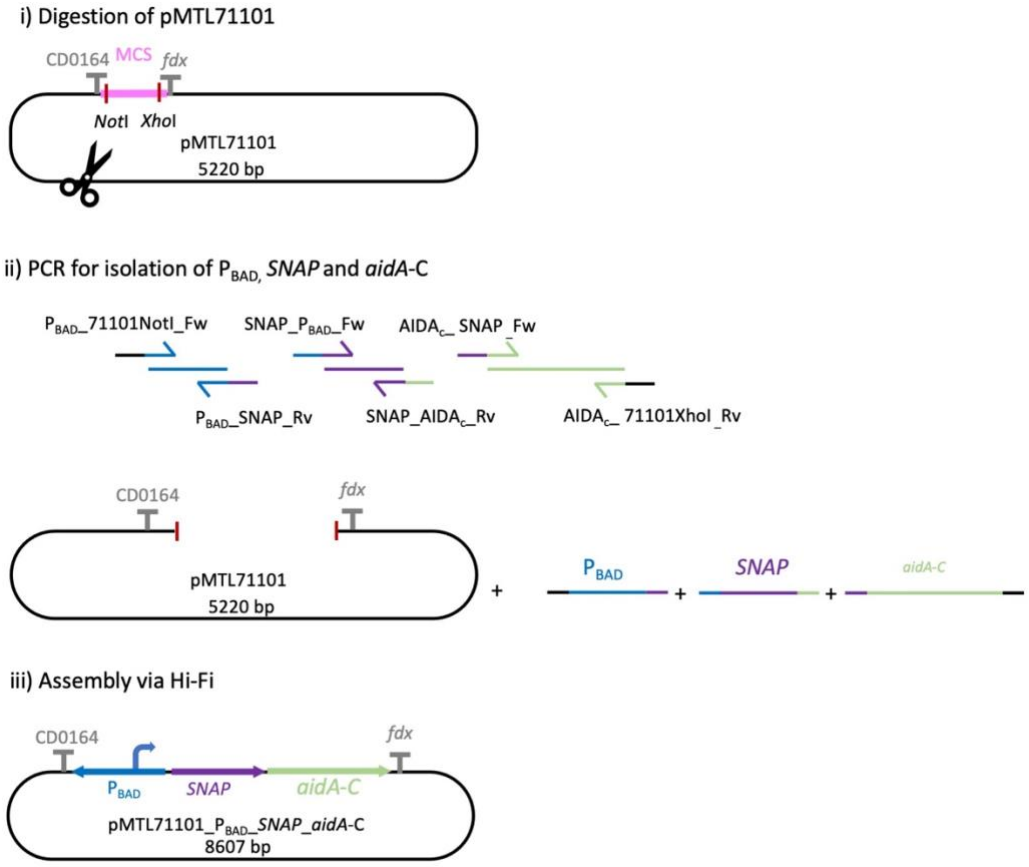

Figure 22- Cloning strategy of pMTL71101_P_{BAD}_*SNAP_aidA-c*

: Detailed description is in the text. Colour coding is: grey for the terminators, purple for the *SNAP* tag, light green for *aidA*-C.

Next, plasmid pUT-mini-Tn5-cm- P_{BAD}_*SNAP_aidA-C* was constructed for transposon-mediated integration of the *SNAP_aidA-C* construct in the genomic DNA of *C. metallidurans* CH34. A schematic representation of the cloning procedure of pUT-mini-Tn5-cm- P_{BAD}_*SNAP_aidA-C* is reported in Figure 23. plasmid pUT-mini-

Tn5-cm was linearized with *Not*I while the P_{BAD}_*SNAP_aidA-C* operon was isolated via PCR from pMTL71101_P_{BAD}_*SNAP_aidA-C* with primer pairs P_{BAD}_pUTNotI_Fw/AIDA-C_pUTNotI_Rv. The fragments were assembled for generation of pUT-mini-Tn5-cm- P_{BAD}_*SNAP_aidA-C*. This was then transformed in *E. coli* Pir2 for cloning of plasmids with conditional R6K origin of replication.

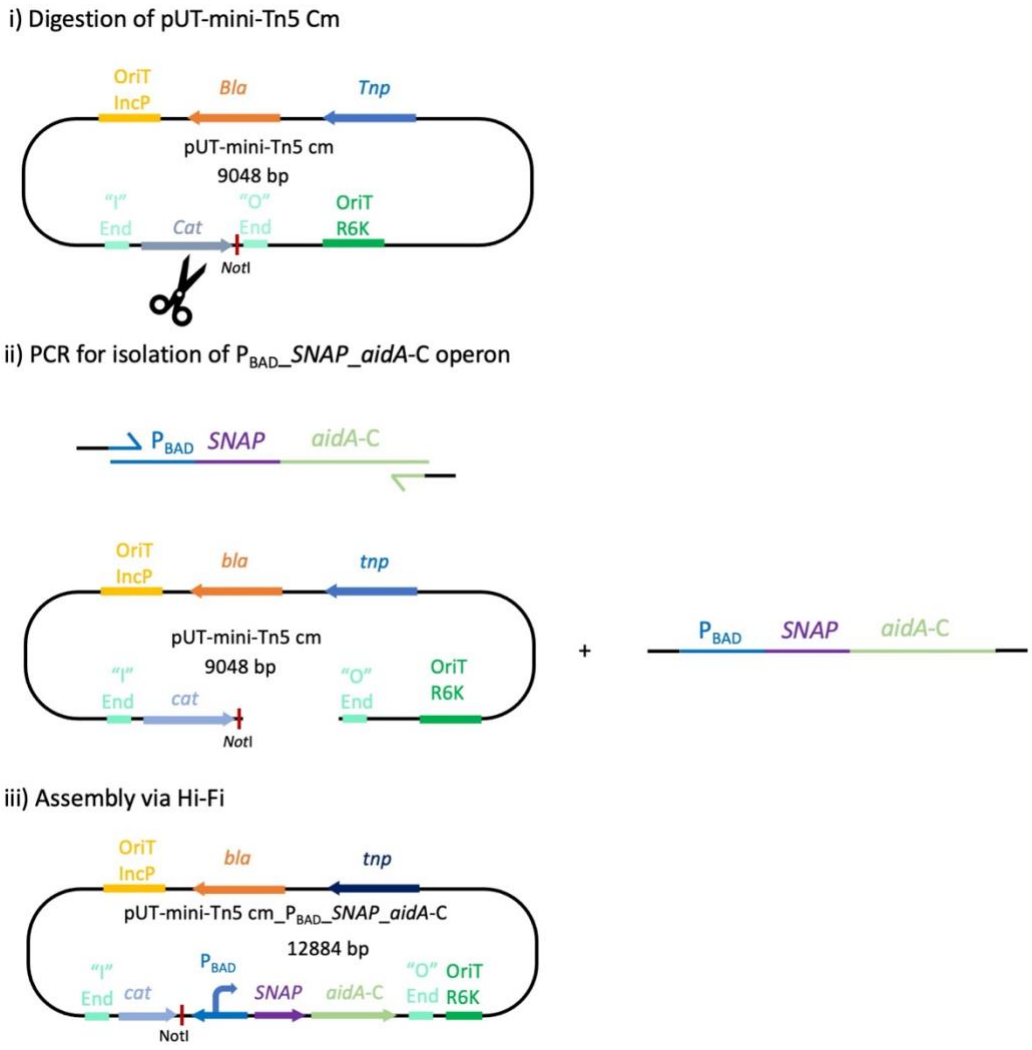

Figure 23-Cloning strategy of pUT-mini-Tn5-cm_P_{BAD}_*SNAP_aidA*-C: Description of the cloning steps and main features of the plasmid are in the text. The colour coding is yellow for the OriT, orange for the *bla* gene, dark blue for the *tnp* gene, light teal for the "I" and "O" ends, blue for the PBAD promoter, purple for the *SNAP*-tag, light green for the *aidA*-C and dark green for the R6K OriT.

3.4.3 Expression of SNAP-tag and Protein Analysis

This section describes the conditions and techniques used to express and verify expression of the SNAP tag. For expression of the SNAP protein, *E. coli* DH5α and *C. metallidurans* NG7 were transformed with pMTL71101_P_{BAD}_*SNAP_aidA-C* and pMTL71101_*SNAP_aidA-C* and selected on LB Cm 25 and 500 μg/mL respectively. cPCR was performed with primers AIDA-C_Fw/Rv to confirm successful transformation. Clones positive to cPCR were inoculated in 5mL LB media supplemented with chloramphenicol and grown for 48 hours at 200 rpm and 30 ˚C. Cultures were setback at OD_{600} 0.1 in 100mL E-Flasks with 10 mL LB media with chloramphenicol. When OD_{600} reached 0.5, cultures were induced with 0.1% L-arabinose and grown in the same conditions for 18 hours. For expression of the *SNAP*-tag from the transposon mutants *C. metallidurans* NG7_P_{BAD}_*SNAP*1 & *C. metallidurans* NG7_P_{BAD}_*SNAP*2 the same procedure was followed.

3.4.3.1 SDS PAGE and Western Blot

Western blotting was firstly used to verify successful expression of the SNAP tag. To do so, 1 mL of each culture were collected in 1.5 mL Eppendorf® tubes and centrifuged at 14000 rpm for 5 minutes to collect the cells. These were then resuspended in a normalized amount of BugBuster® (Merck Millipore) calculated with the formula suggested by the manufacturer. Halt™ Protease inhibitor (Thermofisher), Benzoase (Thermofisher) and rLysozime (Millipore) were added at ratios 1:50, 1:10000 and 1:100 according to manufacturer instructions. The tubes were incubated at RT with gentle shaking on a Rocking platform shaker (VWR). Membrane and cytoplasmic fractions were separated by centrifugating at 14000 rpm for 20 minutes. The cytoplasmic fractions were collected and 10 μL were resuspended in an

equal amount of SDS-page loading buffer (5 µL LDS, 2 µL Nupage, 3 µL H_20). Membrane fractions were resuspended in 75 µL of PBS and 10 µL of these were added to 10 µL of SDS page loading buffer, Color Prestained Protein Standard, Broad Range (NEB) was used as molecular ladder. Samples were boiled at 100 ˚C for 10 minutes, chilled on ice for 10 minutes and spun down at 14000 rpm for 10 minutes. Samples were loaded on 4-12% polyacrylamide gel Tris-Glycine (Invitrogen) and run at 80 V in MES buffer. Staining was done with Comassie blue brilliant (Sigma).

SDS-page gels were transferred onto Trans-Blot® Turbo™ PVDF membrane by means of Turbo blot system (Biorad). Membranes were washed with TBS once and blocked with TBS 5% BSA 5% no-fat milk at RT for 1 hr. Following, the membranes were washed three times in TBST and incubated in TBS 5% BSA with anti-SNAP (NEB, Rabbit) 1:2000 overnight at 4 ˚C. Membranes were washed again in TBST for three times and incubated at RT for 1 hr with TBS 5% BSA anti-rabbit (Signaling technologies) 1:2000. Three washes were performed with TBST. Detection was done by means of TMB (Sigma).

3.4.4 Confocal Microscopy: Detection of the SNAP-tag

Secondly, expression of the SNAP tag was further investigated by means of confocal microscopy. To do so, 1mL of the Induced liquid cultures of *E. coli* DH5α and *C. metallidurans* CH34 transformed with pMTL71101_P_{BAD}_*SNAP_aidA-C* and pMTL71101_*SNAP_aidA-C* were collected by centrifugation at 5000 rpm for 10 minutes and washed twice in PBS. Staining of DNA, outer membrane and SNAP-tag were performed with 1:1000 DAPI, 5µM SNAP-Surface® Alexa Fluor® 647 (NEB) and 5µM FM™ 1-43 Dye (Thermofisher) in PBS for 30 minutes in the dark at RT. After staining, cells were collected by centrifugation at 2000 rpm for 10 minutes,

washed twice in PBS and eventually resuspended in 100 µL of Fluoromount-G™ water based Mounting Medium (ThermoFisher). 5 µL of cell suspension was placed on 18 mm Borosilicate Glass Square Coverslip (FisherScientific) and mounted on a Frosted Microscope slide (ThermoScientific). Images were taken with a Zeiss Elyra Super Resolution Microscope using a Plan-Apochromat 63x/1.4 Oil DIC M27 objective. SIM (Structured Illumination Microscopy) mode was used with the following settings. Three tracks were setup for lasers 642 nm, 405 nm and 488 nm for excitation of the Alexa Fluor® 647 (NEB), DAPI and FM™ 1-43 at 4%, 2%, 2% power respectively. Exposure for the same lasers was 150 ms, 150 ms and 200 ms. SRM (Super Resolution Microscopy) and SIM (Structured Illumination Microscopy) grating periods were 28 µm, 42 µm and 34 µm for the blue (DAPI), green (FM™ 1-43) and Alexa Fluor® 647 respectively while bandpass filters employed were BP 420-480 + LP 750 for the blue channel, LP655 for the red channel and BP570-620 + LP 750 for the green channel.

3.4.5 Integration of PBAD_*SNAP_aidA-C* regulon via delivery of pUT-Mini-Tn5-cm_P$_{BAD}$_*SNAP_aidA*-C Plasmid in *C. metallidurans* NG7

pUT-Mini-Tn5-Cm_P$_{BAD}$_*SNAP_aidA-C* was electroporated in *E. coli* S17-1λpir which was selected on LB agar plates supplemented with chloramphenicol 25 µg/mL. *E. coli* S17-1λ pir transformed with the plasmid in object and *C. metallidurans* NG7 were grown and conjugated according to the protocol described in section 2.1.9. Selection of exconjugant of *C. metallidurans* NG7 was performed on LB agar supplemented with chloramphenicol 500 µg/mL *C. metallidurans* NG7. *C. metallidurans* NG7 conjugated with un-transformed *E. coli* S17-1λpir was used as negative control. cPCR was firstly performed on clones growing on LB Cm^+ plates

with primers pair pUTCm_Sq_Fw/Omega_Cat_Sq_Rv binding in the backbone of the pUT-mini-Tn5-cm transposon and in the *cat* gene respectively and primer pairs Omega_Cat_Sq_Fw/AraC_Rv. These primer pairs had the respective function to exclude presence of the plasmid backbone and confirm presence of the operon expressing SNAP-tag in the gDNA of *C. metallidurans* NG7. Following, the gDNA of the mutant clones of *C. metallidurans* NG7 was extracted. The gDNA was then digested with *Ehe*I (Thermofisher) for 4 hours at 37 ˚C and ligated with T4 ligase (NEB) at 4˚ C overnight. 2 µL of circular DNA were then used as template for iPCR with primer pairs Omega_Cat_Sq2_Rv/RepA1_Sq_Fw. 10 minutes and 55 ˚C were used as extension time and annealing temperature respectively. The PCR products were run in 1% agarose gel, the gel fragment excised and purified and sent for sanger sequencing with the same primers used for the iPCR to confirm site of insertion. depicts the delivery of the genetic construct expressing the SNAP tag as well as the PCRs strategies used to confirm insertion site.

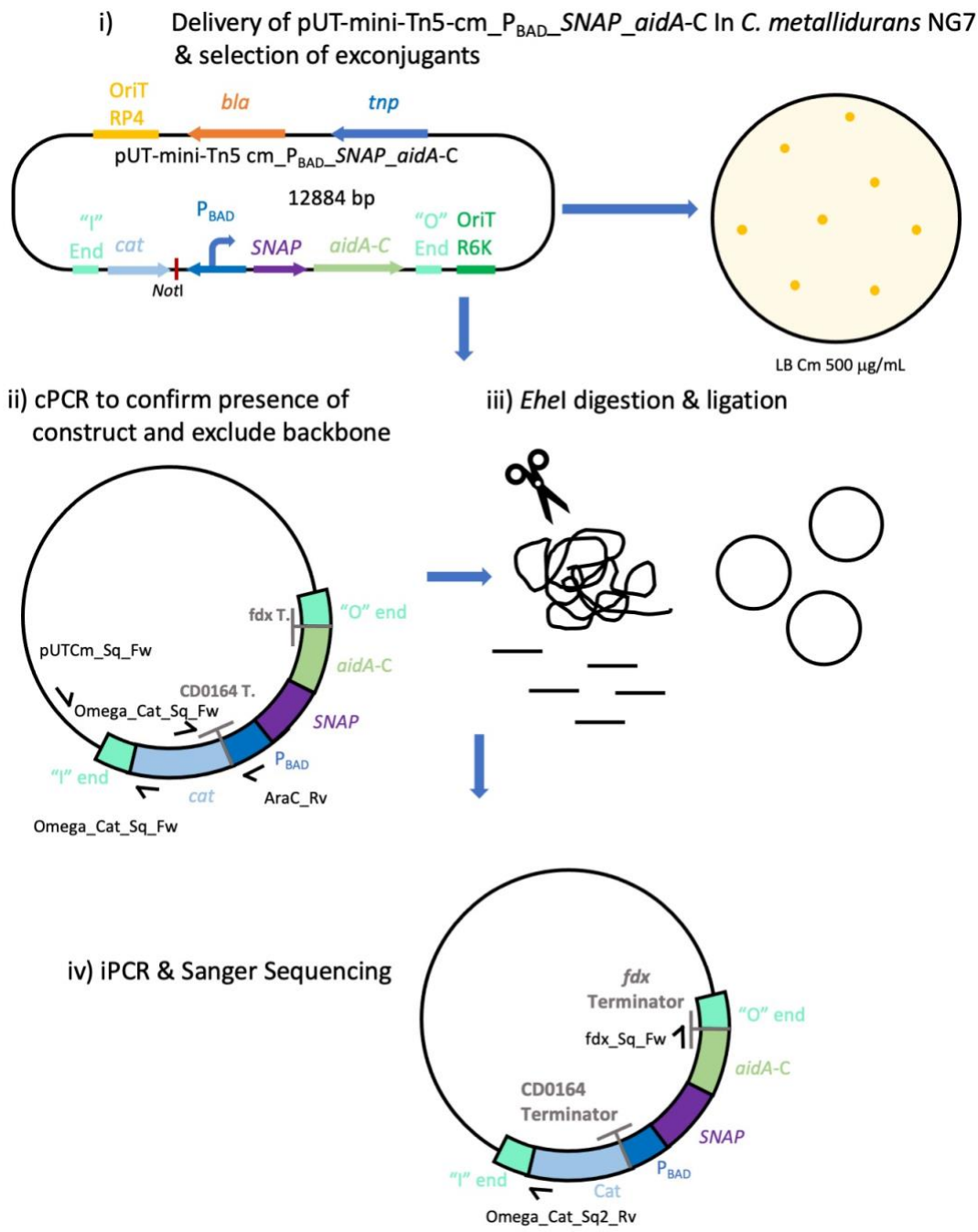

Figure 24-Protocol for isolation of transposon mutants of *C. metallidurans* NG7 for insertion of the P$_{BAD}$_*SNAP_aidA-C* expression block: Description of the steps of the protocols is in the text. Colours are the same as in Figure 24. The terminator sequences are shown in grey.

3.5 Results & Discussion

3.5.1 Screening of Effective Antibiotics for Selection of Transformants of *C. metallidurans* NG7

C. metallidurans grew on every antibiotic with every concentration, except chloramphenicol 400 µg/mL where it showed only small colonies. As *E. coli* did not grow in any of the conditions the phenotype was entirely attributed to *C. metallidurans*. Since this phenotype was not described elsewhere for *C. metallidurans* CH34, our in-house strain was re-named *C. metallidurans* NG7. Eventually chloramphenicol 500 mg/mL was selected as suitable concentration for selection of transformants isolates of *C. metallidurans* NG7.

3.5.2 Plasmid-based Autotransporter-Mediated Outer Membrane Expression of the SNAP-tag in *E. coli* DH5α & *C. metallidurans* NG7

3.5.2.1 Cloning of the Autotransporter-mediated Outer Membrane Display of the SNAP tag

Cloning of pMTL71101_P_{BAD}_*SNAP_aidA-C* was performed as described in section 3.3.1 and is shown in Figure 22. Sanger sequencing was used to confirm the nucleotide sequence of the plasmid. pMTL71101_*SNAP_aidA*-C (promotorless) was cloned as a negative control as described in section 3.4.2. Maps of plasmids pMTL71101 and pMTL71101_P_{BAD}_*SNAP_aidA*-C can be seen in figure S1 with relevant restriction sites (pMTL71101 only).

3.5.2.2 Plasmid-Driven Expression test of the SNAP-tag Cassette in *E. coli* DH5α and *C. metallidurans* NG7

To understand if the construct built in the previous section was functional, pMTL71101_P$_{BAD}$_*SNAP*_*aidA*-C and pMTL71101_*SNAP*_*aidA*-C were transformed into *E. coli* DH5α. Three single colonies were propagated, induced, and subjected to Western Blot and Super Resolution Confocal Microscopy as described in sections 3.4.3. The Western blot (WB) did not show exclusive specificity of protein bands related to the presence of the SNAP-tag, but multiple bands appeared in both cytoplasmic and membrane fraction of the cultures transformed with the plasmid expressing the SNAP-tag and the negative control. Observation of non-specific bands is a common problem encountered when performing WB with polyclonal antibodies (such as the Anti-SNAP used in this study). Polyclonal antibodies are known to recognize multiple epitopes of a target protein, which in turns amplify the likelihood of cross-reactivity with non-target proteins[175]. Nevertheless, a specific band of around 72 KDa could be observed in the membrane fraction (OM) of the samples transformed with pMTL71101_P$_{BAD}$_*SNAP*_*aidA*-C but not in the ones transformed with the negative control thereby showing the autotransporter-SNAP-tag system was successfully expressed in *E. coli* DH5α.

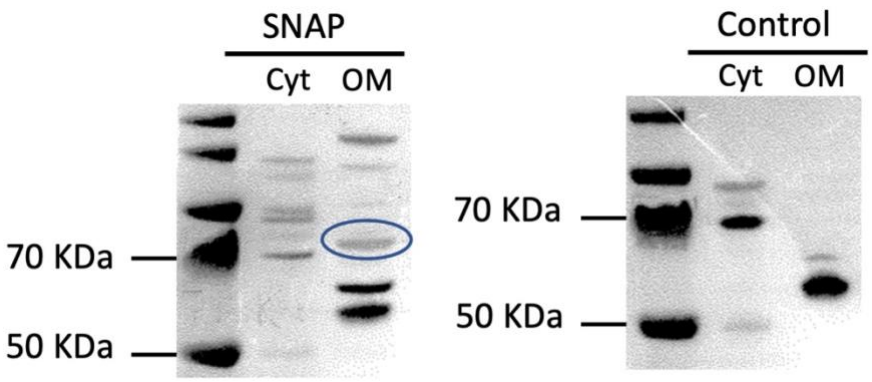

Figure 25-Western Blot of the SNAP tag protein expressed in *E. coli* DH5α: On the left and right panels respectively are *E. coli* DH5α transformed with pMTL71101_P_{BAD}_*SNAP_aidA*-C and pMTL71101_*SNAP_aidA* C -. For each WB lanes 1, 2 & 3 were loaded with protein standard ladder, cytoplasmic and outer membrane fractions respectively

Moreover, Super Resolution Microscopy micrographs showed fluorescence of the fluorophore conjugated with O^6-benzylguanine in *E. coli* DH5α transformed with the plasmid expressing the SNAP tag, while no fluorescence could be observed in the negative control. This further confirmed the results shown by the WB and expression of the SNAP tag was deemed to be successfully achieved (Figure 26A & Figure 26B respectively).

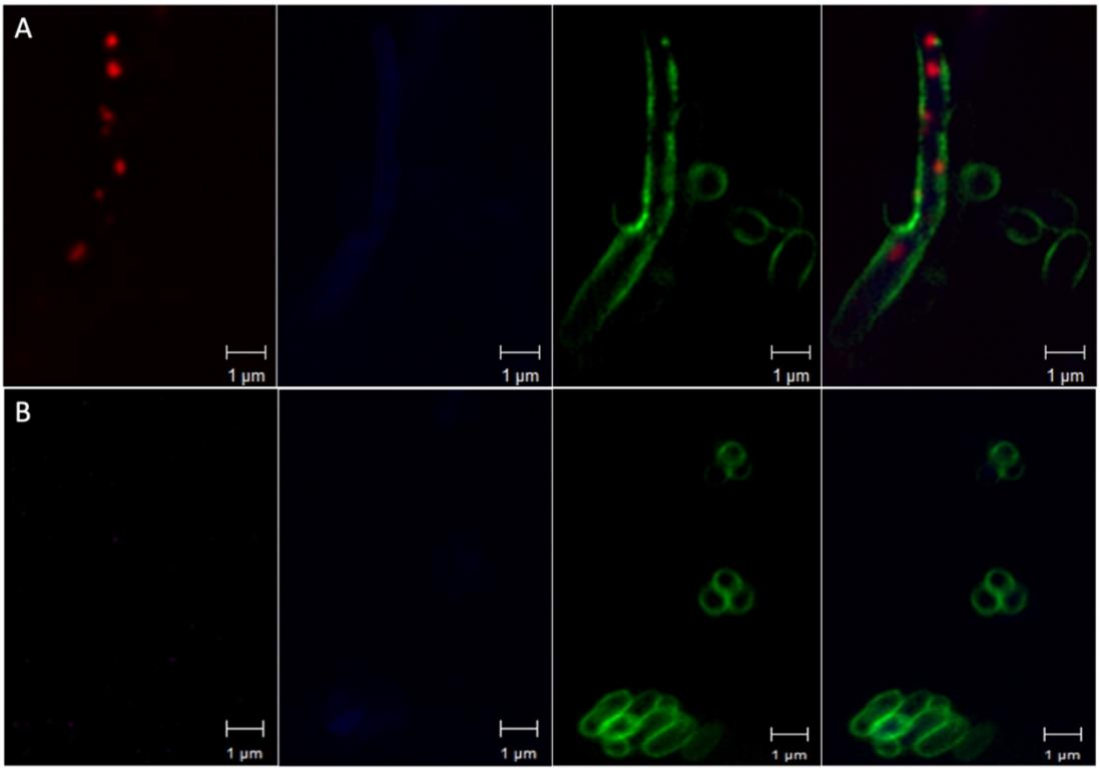

Figure 26-Confocal microscopy of the SNAP tag expressed in *E. coli* DH5α: A) transformed with pMTL71101_P_{BAD}_*SNAP_aidA*-C and B) pMTL71101_*SNAP_aidA-C*. From Left to right the channels relative to the SNAP-tag, DAPI, FM 1-43 and merged are visible for A). For B only the merged channel can be visualized.

The same plasmids were electroporated in *C. metallidurans* NG7 via electroporation and a negative control (no plasmid) was also introduced in the transformation step. A high background was observed in the negative control, with tiny colonies growing on LB plates supplemented with chloramphenicol. Therefore, to confirm presence of the expression and promotorless control plasmid, cPCR was performed as reported in section 3.4.5. After confirmation of the presence of the plasmids, the cultures were subjected to the same protocol for WB and confocal microscopy as used for *E. coli*. However, expression was not detected in any of the isolates tested (n=3, to shown). Since the transformation control did produce colonies on selection plates, lack of expression of the SNAP-tag was attributed to plasmid loss due to overcoming of antibiotic resistance. Consequently, it was decided to integrate

the P_{BAD}_*SNAP*_*aidA*-C expression cassette in the genome of *C. metallidurans* NG7. In the literature, two studies employed a genetic engineering approach by endowing *C. metallidurans* CH34 of IgA autotransporter from *N. gonorrhoeae* for surface display of mouse metallothioneins and phytochelatins for bioremediation of contaminated soils and waters[57,167]. The issue of plasmid loss was addressed by integration of the AT-passenger cassette in the chromosomal DNA[57] or by testing of the *hok-sok* post-segregation TA system, thereby highlighting stable plasmid maintenance is an issue to overcome if *C. metallidurans* CH34 is to be considered as chassis for biotechnological applications.

3.5.2.3 Transposon-Mediated Integration of the SNAP-tag Expression Cassette in *C. metallidurans* NG7

Next, it was decided to integrate the P_{BAD}_*SNAP*_*aidA*-C operon in the chromosomal DNA of *C. metallidurans* NG7 to ensure stable protein expression. To do so, the mini Tn*5* suicide plasmids developed by Victor De Lorenzo[152] was used. These plasmids are composed of the conditional R6K origin of replication, IncP origin of transfer and a *tnpA* transposase gene responsible for translocation of the DNA fragments lying in between the "I" and "O" recognition sites. Furthermore, these were built in several versions having different antibiotic resistance cassettes, also included between the transposition sites. Therefore, after transformation the isolates subjected to the transposition event could be screened by their resistance to whatever antibiotic cassette was inserted between the transposase recognition sites. Plasmid pUT-mini-Tn5-cm_P_{BAD}_*SNAP*_*aidA*-C (cat cassette) was constructed as reported in section 3.3.1 and as shown in Figure 23. Following cloning, the protocol for the transposon-

mediated insertion of P_{BAD}_*SNAP_aidA-C* was adapted from De Lorenzo and Timmis[152] as described in section 3.3.4.

After delivery of the transposon plasmid, growth of exconjugants was observed on LB plates supplemented with chloramphenicol 500 µg/mL. Fifteen exconjugants were subjected to cPCR as mentioned above and six of the isolates tested produced an amplicon following PCR performed with primer pairs Omega_Cat_Sq_Fw/AraC_Rv (approximately 900 bp) while no amplification was observed with primer pairs pUTCm_Sq_Fw/Omega_Cat_Sq_Rv thereby confirming insertion of the SNAP-tag expression cassette and loss of the suicide plasmid respectively (Figure 27A). The iPCR showed amplification only in two of the isolates positive to the cPCR which were renamed *C. metallidurans* NG7_P_{BAD}_*SNAP*1 and *C. metallidurans* NG7_P_{BAD}_*SNAP*2 respectively (1&2 in Figure 27A & B). However, this does not imply necessarily no insertion occurred in the other isolates, but rather extension time of the iPCR was too short to amplify digested fragments[176].

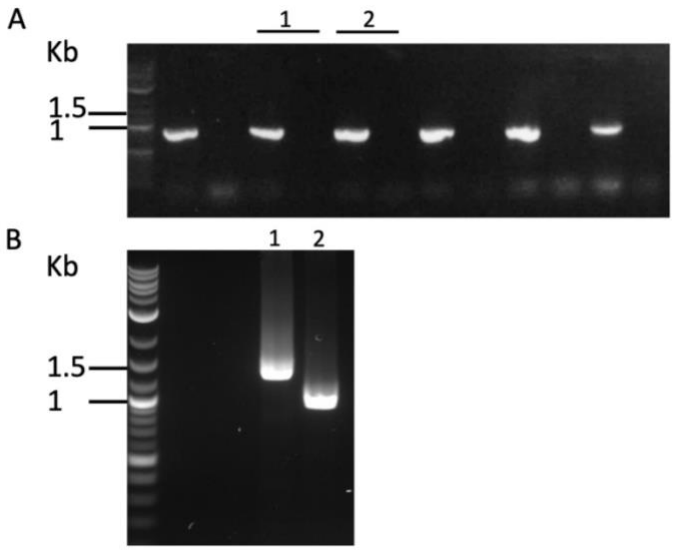

Figure 27-PCRs of transposon mutant isolates of C. *metallidurans* NG7: A) cPCR of exconjugants of *C. metallidurans* NG7 showing successful specific amplification of integration cassette and absence of backbone. B) iPCR of fragments of *Ehe*I digested and ligated gDNA of transposon mutants of *C. metallidurans* NG7.

Sanger sequencing revealed the site of insertion for isolate 1 & 2 was Rmet_3610, and Rmet_3253 coding for a tRNA modification GTPase and a putative transporter subunit respectively. Site of insertion with Sanger sequencing data is shown in Figure 28 for the representative transposon mutant isolate *C. metallidurans* NG7_P_{BAD}_*SNAP*1. Continuity of the chromatogram between the "I"/"O" ends and Rmet_3610 shows the Tn5-mediated insertion of the SNAP-tag expression block was successful (Figure 28)

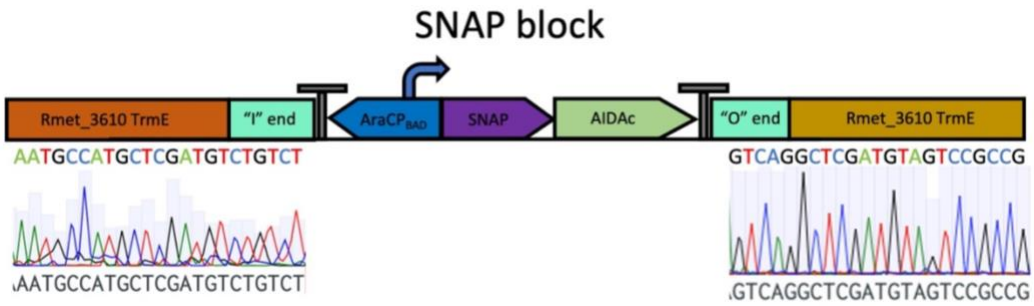

Figure 28-Sanger sequencing data demonstrating insertion of the *SNAP*-tag expression cassette: Chromatograms of the Sanger sequencing results of the iPCR sample relative to *C. metallidurans* NG7_P_{BAD}_*SNAP*1 shows integration of the transposon in the chromosomal DNA in Rmet_3610. Colour coding is the same as in Figure 20 and Figure 21.

Next, expression of the SNAP-tag was tested for the two transposon mutants in the same conditions used for *E. coli* DH5α pMTL71101_P_{BAD}_*SNAP*_*aidA*-C. However, no protein was detected by either WB or Super Resolution Confocal Microscopy. Failure of expressing the recombinant SNAP-tag in *C. metallidurans* NG7 from both multicopy plasmid system and chromosomal insertion might have happened for different reasons. Plasmids for heterologous protein expression are known to be unstable due to phenomena such as segregational and structural stability. Segregational stability refers to a phenomenon in which the plasmids are not evenly distributed to the daughter cells upon cellular replication. Daughter cells always tend to lose plasmids that do not provide an advantage, as these are source of metabolic burden related to the presence of extra-proteins to be expressed in the plasmid[177–179]. In some instances, plasmid loss due to segregational instability has been circumvented by endowing plasmids with appropriate "addiction systems", as discussed in Chapter 1. Furthermore, bacteria transformed with plasmids can also suffer of structural stability, in which the plasmid is still present in the cells, but with mutations in the nucleotide sequence which inactivate expression of the GOI. Among the factors contributing to structural instability is the presence of IS-element native the chassis

for protein expression, which could occasionally "jump" in the CDS of the gene of interest thereby having deleterious effect on protein expression[68]. *C. metallidurans* is a bacterial species with formidable genome plasticity, which is due to the high number of mobile elements in the chromosomes that can be activated upon sensing of environmental stress[180]. As high expression of heterologous proteins in bacteria can be toxic to the cell, transposable elements could be the cause of no detectable expression of the SNAP-tag. Nevertheless, the high number of untransformed chloramphenicol resistant colonies on LB plates supplemented with chloramphenicol, suggests the use of antibiotic in liquid culture may not be sufficient for selection of plasmid-retaining clones, therefore suggesting in this case issues related to segregational instability. Moreover, inducible promoters that are functional in *E.coli* are reported to lack activity in other hosts[181], which introduces the variable of whether the P_{BAD} promoter is functional in *C. metallidurans* CH34.

Chromosomal integration is reported to lead to more stable strains for bioprocessing[185]. However, single chromosomal expression level is generally lower than multicopy plasmid-based expression[182], heavily depends on the site of integration[183] and as for plasmid-based expression systems, require extensive knowledge of performance of regulative elements like promoters.

Therefore, while plasmid-derived heterologous expression of the SNAP-tag likely failed due to segregational instability of the expression plasmid, no knowledge of activity of heterologous promoters and the variable of the transposon-mediated chromosomal location for the insertion of the SNAP-tag operon makes it challenging to postulate the reason for failure of protein expression. Nevertheless, it can be stated the lack of tools to efficiently modify the genomic DNA of *C. metallidurans* CH34, the paucity of knowledge regarding behaviour of regulative genetic elements like

promoters with a wide range of activity and plasmid copy numbers and stability, is a constraint that hampers the biotechnological applications of *C. metallidurans* CH34.

3.6 Conclusions

Conclusions

Firstly, the operon for autotransporter-mediated expression of the SNAP-tag was shown to be functional in *E. coli*. However, plasmid- and chromosomal-borne expression of the SNAP-tag in *C. metallidurans* NG7 failed. Expression from the plasmid system likely failed because of segregational instability of the pBBR1 plasmid while the negative outcome of expression from the chromosomal insertion could have happened because of unfavourable chromosomal location or inactive promoter. Nevertheless, lack of knowledge about promoter activities and lack of efficient tools for genomic modification of *C. metallidurans* CH34 are major limitations to promote use of this organism for biotechnological applications. These results highlighted the need for developing a toolbox for efficient genetic modification of this organism, which were addressed in the following chapters of this thesis.

4 -Exploring Plasmid Addiction Systems for Stable Expression of Heterologous Proteins in *C. metallidurans* CH34

4.1 Background: Plasmid Addiction Systems as Tools to Improve Plasmid Stability and Heterologous Protein Expression

High density cultures of genetically modified bacteria in bioreactors are necessary to produce economically viable products such as biopolymers, proteins, chemicals, and biofuels. Genetic modifications can be performed either by integrating the GOI in the chromosomal DNA or by introducing it into replicative plasmids, subsequently transformed in the bacterial host. Chromosomal integration, despite leading to a stable genotype, often results in low product yields due to copy number[179], while plasmid-based expression platforms often results in metabolic burden, decreased cell viability and plasmid loss[70]. To limit the latter, PAS have been proposed as a mean to promote plasmid stability while obtaining high products yields at the same time[184]. As discussed in section 1.6.1, different types of PAS can be used to attempt plasmid stabilization in bacterial hosts. Metabolism-based PAS are based on deletion of chromosomal genes essential for the growth of the organism and subsequent complementation of these genes on a plasmid, coupled with gene(s) for production of the product of interest. One of the early examples of metabolism-based PAS consisted in the deletion of KDPG-aldolase gene from *C. necator* H16 and complementation with the same gene coupled with a cyanophycin synthetase on a plasmid system[76]. On the one hand rational metabolism-based PAS is an attractive strategy in organisms where genetic tools for genome engineering are available but on the other hand, perturbation of known metabolic pathways without extensive knowledge of the physiology of a microorganism can often lead to unpredicted metabolic outcomes[185]. Evolution-based metabolic engineering has also been rising as an alternative strategy to the rational approach in order to obtain fit microbial strains for biotechnological applications[186,187]. Moreover, direct microbial evolution might be

the only option available for microbial strains where no appropriate selection is available, as reported for *Thermotoga sp*, where 5-FOA mediated evolution of uracil auxotrophic strains has previously been employed for development of a *pyrE*-based selection system[188].

In this chapter, I explored the possibility of exploiting evolution abilities of *C. metallidurans* NG7 to develop uracil auxotrophic strain for implementation of a metabolism-based PAS for stable expression of heterologous proteins. In Chapter 3, difficulties in working with the in-house strain of *C. metallidurans* (*C. metallidurans* NG7) were reported. Phenotypical and genotypical studies of *C. metallidurans* NG7 herein presented demonstrate that *C. metallidurans* NG7 lacks pMOL30 and contains an IncP-1α multidrug resistance plasmid. This genotype was unexpected as this strain was ordered from DSMZ as *C. metallidurans* CH34 and was supposed to contain plasmids pMOL30 and pMOL28, which are important for biotechnological applications (see Section 1.5.2). As in the previous chapter difficulty in the choice of appropriate selection marker for isolation of transformants of *C. metallidurans* NG7 were reported, the evolution approach employed for *Thermotoga sp.* was initially herein applied for evolution of an uracil auxotrophic strain of *C. metallidurans* NG7 for developing a metabolism-based PAS. The genotypic and phenotypic analysis of *C. metallidurans* NG7 carried out while performing the Plasmid Stability Test (PST) and Flow Cytometry (FC), highlighted that this strain is an unsuitable chassis for biotechnological applications. Therefore, the evolution strategy was repeated for development of uracil auxotrophy-based PAS for *C. metallidurans* CH34.

4.2 Experimental Strategy

4.2.1 Evolution of Uracil Auxotrophic Strains of *C. metallidurans* Species

The main goal of this section was to develop a metabolism-based Plasmid Addiction System (PAS) for stable maintenance of plasmids for heterologous protein expression. The uracil biosynthesis pathway was targeted for development of uracil auxotrophic strains, which would then be transformed with a plasmid for complementation of the auxotrophy. The experimental strategy was based on direct evolution of *C. metallidurans* strains on SGMM agar plates supplemented with 5-FOA. PyrE and PyrF, the central enzymes of the pyrimidine biosynthesis pathway, convert orotic acid to orotidine 5-phosphate and orotidine 5'-phosphate to uridine 5'-phosphate, respectiveley[189]. Deletion of the *pyrE* and *pyrF* genes is widely reported to result in uracil auxotrophy in yeast and a variety of prokaryotes and both have been used as positive or negative selection markers[190–193]. 5-FOA is converted to 5-fluorouridine 5 phosphate (5-FOMP) and 5-fluoroorotidine monophosphate (5-FUMP) by the enzymes encoded by *pyrE* and *pyrF*, respectively (Figure 29). Further enzymatic conversions (not shown in Figure 29) of 5-FUMP into 5-fluorouracil, which is toxic to the cell, leads to cell death. If the chromosomal copy of the *pyrE* or *pyrF* are inactivated and an exogenous source of uracil is added to the media, the 5-FOA cannot be metabolised into its toxic derivatives and cells survive. Following construction of the uracil auxotroph stains, a plasmid for the complementation of the auxotrophy, and carrying the *mRFP1* gene, was delivered in *C. metallidurans* CH34 and *C. metallidurans* NG7. Plasmid Stability Test (PST) was performed to assess plasmid stability, by calculating the percentage of the total population of cells of each strain growing on SGMM agar plates with antibiotic. Flow Cytometry (FC) was also used to calculate the percentage of live cells expressing mRFP1, as well as the Relative

Median Fluorescent Intensity to determine the fold-change in expression between the complemented uracil auxotrophs and their wild type counterpart (Figure 30).

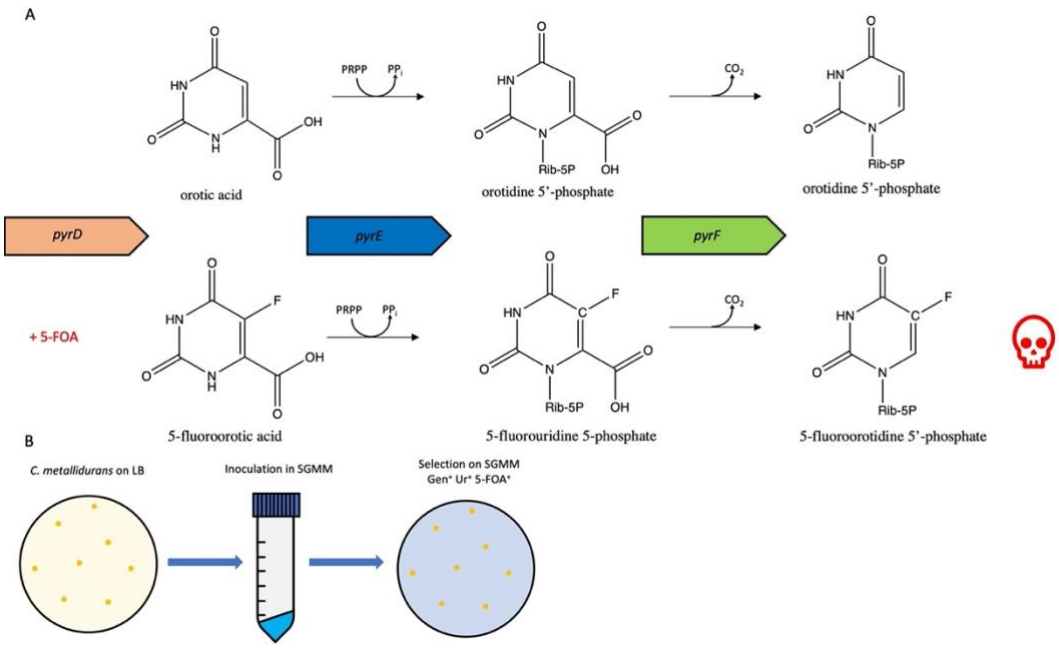

Figure 29-Graphical representation of experimental strategy for evolution of uracil auxotroph strains of *C. metallidurans* species: A) Genomic arrangements and functions of genes for synthesis of pyrimidines targeted for the evolution of uracil auxotrophic strains of *C. metallidurans* species: *pyrD* **(**light orange**),** *pyrE* (blue) and *pyrF* (green), code for enzymes responsible for production of intermediates of the uracil synthesis pathway. Addition of 5-FOA to the culture media and its metabolization generate toxic chemicals, leading to cell death. B) The protocol developed for generating uracil auxotrophic strains was based on initial growth of *C. metallidurans* on LB plate. A single colony was picked and grown in SGMM for 48 hours. The whole culture was then plated on SGMM agar plates supplemented with gentamycin, uracil and 5-FOA.

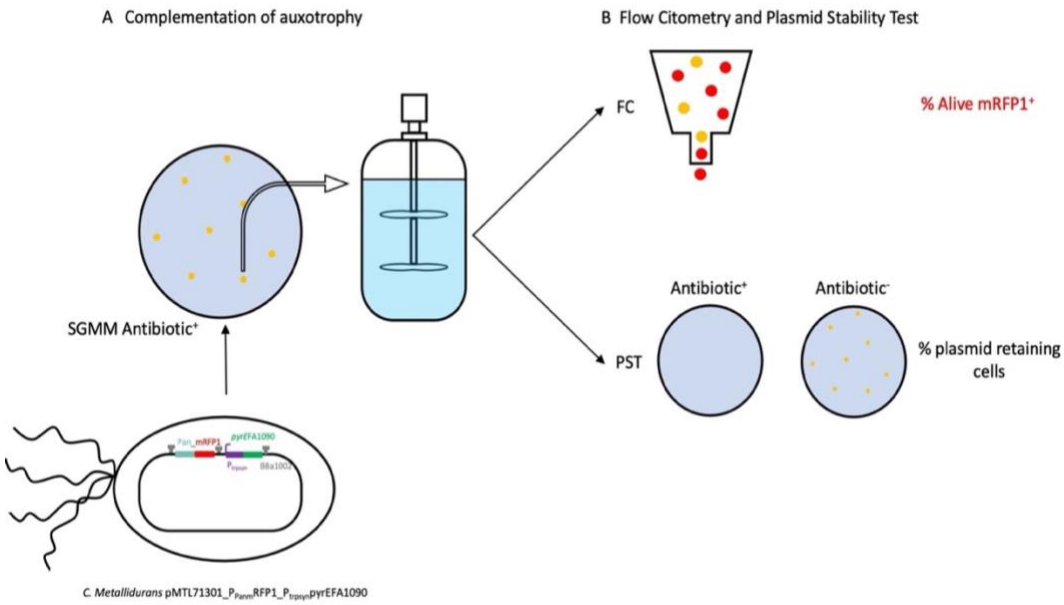

Figure 30-Graphical representation of experimental workflow for analysis of the *pyrE*-based Plasmid Addiction System: A) *C. metallidurans* uracil auxotrophs and *C. metallidurans* wild type were transformed with pMTL71301_P_{pan}*mRFP1*_P_{trpsyn}*pyrE*FA1090 plasmid for complementation of the auxotrophy and constitutive expression of *mRFP1*. Two independent biological replicates from the uracil auxotrophs and the wild type were inoculated in a bioreactor operated in continuous mode. B) Every 24 hours a culture sample was collected, and cells were analysed *via* FC to obtain the percentage of cells expressing mRFP1 (labelled as red circles), and *via* PST to study the percentage of cells retaining the plasmid.

4.3 Aims of the Study

The overall aim of this study was to develop a Plasmid Addiction System for Stable plasmid segregation and protein expression in *C. metallidurans*. This was done by:

i) Exploiting the genome plasticity of *C. metallidurans* to obtain uracil auxotrophic strains *via* a directed evolution approach

ii) Complementation of the auxotrophy with an expression plasmid containing a heterologous *pyrE* gene and expressing the mRFP1 protein.

iii) Assess plasmid maintenance and protein expression while growing the complemented uracil auxotrophic strains in bioreactors, using Plasmid Stability Test (PST) and Flow Cytometry (FC).

iv) Use the stabilization determinants of the IncP-1α plasmid, to stabilize in-house mini RK2 expression plasmids.

4.4 Materials & Methods

4.4.1 Phenotypic Analysis of *C. metallidurans* NG7 & *C. metallidurans* CH34: Heavy Metal & antibiotic Minimal Inhibitory Concentration Test (MIC) & Megaplasmid Extraction

The purpose of the phenotypic analysis was to study whether *C. metallidurans* CH34 and *C. metallidurans* NG7 showed difference resistance behaviour toward heavy metals and antibiotics. As the heavy metal resistance determinants of *C. metallidurans sp.* are present on the megaplasmids, these were extracted from both *C. metallidurans* CH34 and *C. metallidurans* NG7 for further comparison.

Cupriavidus metallidurans NG7 and CH34 were thawed from cryostocks stored at -80 ˚C and grown on SGMM agar plates until colonies were visible. Single colonies were patched on a fresh SGMM agar plate to obtain enough biomass and were then streaked on SGMM plates supplemented with either 20mM $ZnSO_4 \cdot 7H_2O$, 6mM $CdCl_2$ x $5H_2O$, 8mM $CuSO_4$, 50 mM $NiCl_2$ x $6H_2O$ as described by Van Houdt and colleagues[193]. Tc 20 µg/mL, Kan 1500 µg/mL and Chl 400 µg/mL were also tested for MIC.

Extraction of the megaplasmids was based on the method of Andrup *et al.,*[194] and was performed in collaboration with Ann Provoost from SCK-CEN, (Mol, Belgium). 10 mL of liquid LB were inoculated with single colonies of *C. metallidurans* NG7 or *C. metallidurans* CH34 for 12-14 hours (OD_{600} ~1). 8 mL of the pre-culture were collected by centrifugation at 6000 rpm for 10 minutes and the supernatant was discarded. The pellet was resuspended by pipetting in 300 µL of E-Buffer (15% wt/vol Sucrose, 40mM Tris-hydroxide, 2mM EDTA, pH 7.9) and transferred to a 2 mL Eppendorf tube (Eppendorf®). 600 µL of lysis buffer 3% wt/vol

Sodium dodecyl sulphate ($CH_3(CH_2)_{11})SO_4Na$, 50 mM Tris, pH 12.5) were added, the tubes were gently inverted 20 times and the samples were incubated at 65 ˚C for 30 minutes. 30 µL of proteinase K (Qiagen®, initial concentration 20 mg/mL) were added and the tube was again inverted 20 times and incubation at 65 ˚C for 90 minutes followed. 1mL of phenol was added, the tube was inverted 40 times and the mixture was loaded in a pre-spun Phase Lock Tube Heavy (Quantabio®) and centrifuged for 5 minutes at 1500 rpm. Aqueous phase was collected and transferred into a new 2 mL Eppendorf tube. DNA mixtures could be stored at -20 ˚C at this stage. 40 µL of DNA were loaded on a 0.5% Certified Megabase Agarose Gel (BioRad ®) in 1X TBE buffer [1 mM Tris, 1 mM Boric Acid (H_3BO_3), 002 mM EDTA]. Gel electrophoresis was carried out for 24 hours at 4-6 ˚C at 100 V in a 23 cm-long 0.5% Certified Megabase Agarose Gel (Biorad®) in 1X Tris-Borate EDTA buffer. The gel was then transferred to a bath with water and Ethidium Bromide (30 µL/ L H_2O) for 5-10 minutes and then transferred in a water bath with distilled water for 1.5 hours.

4.4.2 5-FOA Minimal Inhibitory Concentration Test (MIC)

The scope of this experiment was to investigate the MIC of 5-FOA for isolation of uracil auxotrophic strains of *C. metallidurans sp.* To do so, three single colonies of *C. metallidurans* NG7 were grown LB media for 48 hours. These were washed twice in PBS and eventually resuspended in SGMM minimal media at OD_{600} 0.5 and 5-FOA in DMSO (stock solution 50 mg/mL) was supplemented at concentrations 25 µg/mL, 50 µg/mL, 75 µg/mL, 100 µg/mL, 200 µg/mL, 300 µg/mL, 400 µg/mL, 500 µg/mL and 600 µg/mL. 800 µL of *C. metallidurans* NG7 with the different concentrations of 5-FOA were transferred to MTP-48-B plates (m2p labs) and a BioLector Pro® with integrated light scattering reader (m2p labs) was used for measuring biomass growth.

Cells were grown at 30 ˚C fir 72 hours at 800 rpm. A 5-points calibration curve between OD_{600} values of *C. metallidurans* CH34 in SGMM and the light scattering values obtained with the same samples and measured with the BioLector, was used to convert light scattering readings in OD_{600}

4.4.3 Growth of *C. metallidurans* for Isolation of Uracil Auxotrophs Generated via Evolution Experiments on 5-FOA

For generation of uracil auxotrophs (strains with inactivated *pyrE* gene) of *C. metallidurans* NG7 and *C. metallidurans* CH34 by evolution on 5-FOA (Chapter 4), three independent colonies of the respective wild type strains were grown in LB media as described, cells were collected by centrifugation at 4000 rpm and washed in PBS twice. Pellets were resuspended in 300 µL of PBS and plated in three separate SGMM agar plates supplemented with 10 µg/mL gentamycin, 500 µg/mL of 5-FOA and 20 µg/mL uracil.

4.4.4 Construction of Plasmids for *pyrE*-Based Plasmid Addiction System

Plasmids pMTL71101_P_{Pan}*mRFP1*_P_{trpsyn}*pyrE*FA1090 & pMTL71301_P_{Pan}*mRFP1*_P_{trpsyn}*pyrE*FA1090 were generated for complementation of the auxotrophy of uracil auxotroph strains of *C. metallidurans* NG7 and *C. metallidurans* CH34 respectively. pMTL71101_P_{Pan}*mRFP1* & pMTL71301_P_{Pan}*mRFP1* were also generated as negative control. A schematic representation of the cloning procedure of pMTL71101_P_{Pan}*mRFP1*_P_{trpsyn}*pyrE*FA1090 is reported in Figure 31. A two-step cloning strategy was employed. i) pMTL71101 was digested with *Not*I and *Asc*I. pUC57_P_{Pan} was used as template for PCR amplification of the Pan promoter with

primer pairs Pan_71101NotI_Fw/Pan_RFP_Rv. The fragments were assembled for generation of pMTL71101_P_{Pan}*mRFP1*.Following, ii) pMTL71101_P_{Pan}*mRFP1* was digested with *Fse*I and *Asc*I, while genomic DNA of *N. gonorrhoeae* FA1090 was used as template for amplification of the P_{trpsyn}*pyrE*FA109*0* fragment with primer pairs P_{trpsyn}_PyrEFA1090_71101FseI_Fw/PyrEFA1090_BBa0012_71101AscI_Rv. The forward primer contained a spacer sequence for inclusion of the P_{trpsyn} promoter upstream the *pyrE* CDS. The reverse primer included a spacer for addition of the double terminator BBa0012 (Biobrick) downstream the *pyrE* sequence. The fragments were assembled for generation of pMTL71101_P_{Pan}*mRFP1*_P_{trpsyn}*pyrE*FA1090.

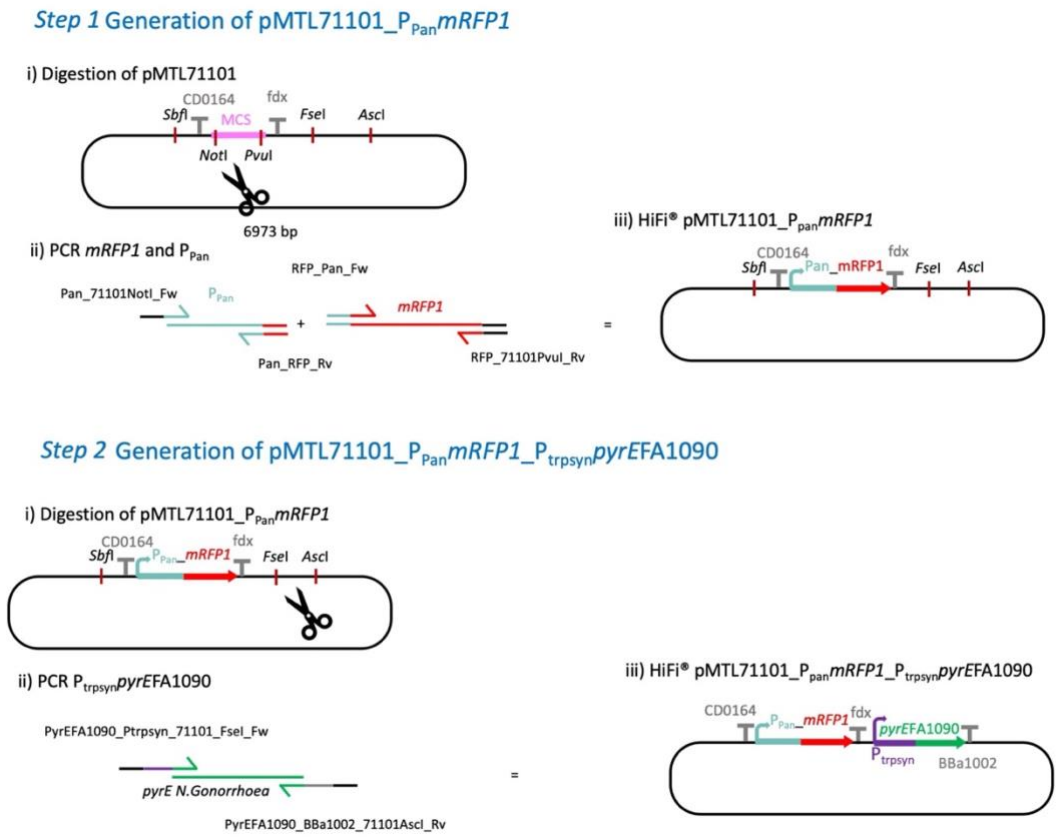

Figure 31-Two-step cloning for generation of plasmid pMTL71101_P$_{Pan}$*mRFP1*_P$_{trpsyn}$*pyrE*FA1090: Details of the cloning procedure are in the text. The colour coding is: pink for the Multiple Cloning Site (MCS), light green for the P_{pan} promoter, red for the *mRFP1* gene, purple for the P_{trpsyn} promoter and dark green for the *pyrE* gene from *N. gonorrhoea* FA1090. The transcription terminator sequences are labelled in grey. A detailed description of the cloning steps is reported in the text.

Plasmid pMTL71301_P$_{Pan}$*mRFP*1_P$_{trpsyn}$*pyrE*FA1090 was created in the following way: pMTL71301 was digested with *Not*I and *Asc*I while the P$_{Pan}$*mRFP*1_P$_{trpsyn}$*pyrE*FA1090 fragment was amplified via PCR with primer pairs Pan_71301NotI_Fw/ PyrEFA1090_71301AscI_Rv. pMTL71101_P$_{Pan}$*mRFP*1_P$_{trpsyn}$*pyrE*FA1090 & pMTL71301_P$_{Pan}$*mRFP*1_P$_{trpsyn}$*pyrE*FA1090 were transformed by means of electroporation into *C. metallidurans* NG7/NG7 Δ*pyrE* & *C. metallidurans* CH34/CH34 Δ*pyrE* to generate *C. metallidurans* NG7_*mRFP*1, *C. metallidurans* NG7

Δ*pyrE_mRFP*1, *C. metallidurans* CH34_*mRFP*1 and *C. metallidurans* CH34 Δ*pyrE_mRFP*1.

4.4.5 Construction of Plasmids pMTL74301Low and pMTL74301Low_*parCBADE*

pMTL74311 was considered for cloning of the *parCBADE* genes. This is an in-house mini RK2 shuttle vector with a R271C mutation in the *trfA* plasmid replication initiator gene that makes it a high copy plasmid (~ 40 copies/cell) in *C. necator* H16[151] and the ColE1 RNA II origin for replication in *E. coli*. In order to test this plasmid, in the first instance the R271C mutation had to be reversed to resume the low-copy feature of mini RK2 (thereby obtaining pMTL74311Low) and secondly, the *parCBADE* system was cloned in the modular vector pMTL74311Low, whilst also deleting the ColE1 RNA II origin of replication (generating pMTL74301Low_*parCBADE*). The control plasmid was also built by eliminating the ColE1 RNA II origin *via* site-directed mutagenesis. A schematic representation of the cloning procedure of pMTL74301Low and pMTL74301Low_*parCBADE* is reported in Figure 32. A two steps procedure was followed. i) the C271R mutation on the *trfA* gene[195] of pMTL74311 was reverted. This was done by using primer pairs trfa271mut_Fw/Rv by means of inverse PCR. Following, the PCR mixture was incubated with the Q5® Site-Directed Mutagenesis Kit following manufacturer recommendations for generation of pMTL74311Low. ii) pMTL74311Low was digested with *Asc*I and *Fse*I to eliminate the ColE1 RNA II origin of replication. The *parCBADE* operon was amplified from gDNA of *C. metallidurans* NG7 with primer pairs ParCBADE_74301AscI_Fw/ParCABDE_74301FseI_BBa0012_Rv. The two fragments were then assembled for generation of pMTL74301Low_*parCBADE*. For generation of the pMTL74301Low control plasmid, pMTL74311Low was used as

template for inverse PCR with primer pair 74301_Fw/Rv, with primer pairs designed back-to-back. The Q5® Site Directed Mutagenesis Kit was then used for generation of pMTL74301Low.

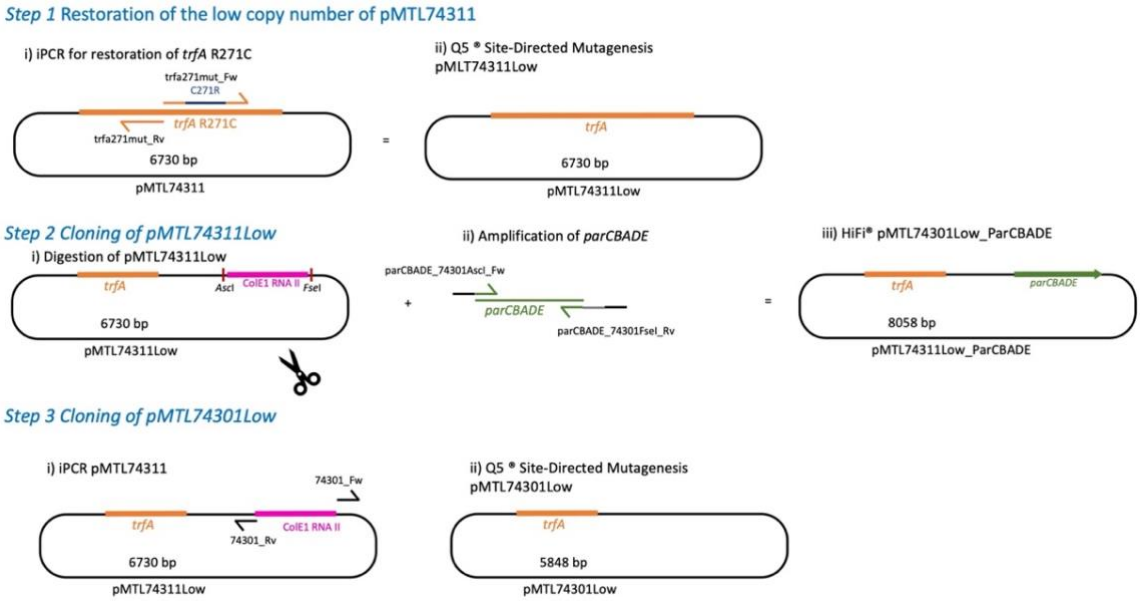

Figure 32-Cloning strategy for pMTL74301Low & pMTL74301Low*_parCBADE:* *Step 1*: for clarity, only the *trfA* gene (orange) is displayed in the pMTL74311 plasmid. *Step 2:* the ColE1 RNAII replication origin is also shown in pink. The *parCBADE* operon was isolated by PCR from IncP-1α (green) and the plasmid pMTL74311Low*_parCBADE* was created. In step 3 the control plasmid pMTL74311Low was generated as described in the main text. Detailed description of the cloning steps is in the text.

4.4.6 Complementation of Uracil Auxotrophy

The aim of this experiment was to confirm that the genomic deletion of a portion of the *pyrE* gene was responsible for the lack of growth shown by both strains of *C. metallidurans*. To do so, pMTL71101_P_{pan}*mRFP1*_P_{trpsyn}*pyrE*FA1090 and pMTL71301_P_{pan}*mRFP1*_P_{trpsyn}*pyrE*FA1090 were electroporated in electrocompetent *C. metallidurans* NG7 and *C. metallidurans* CH34, resulting in strains *C. metallidurans* NG7_Δ*pyrE_mRFP1* and *C. metallidurans* CH34_Δ*pyrE_mRFP1*. The plasmids pMTL71101_P_{pan}*mRFP1* and

pMTL71301_P_{pan}*mRFP1* were also electroporated in the respective *C. metallidurans* uracil auxotroph strains as negative controls. Transformants were selected on SGMM agar minimal media lacking uracil and supplemented with chloramphenicol (for *C. metallidurans* NG7_Δ*pyrE_mRFP1*) or tetracycline (for *C. metallidurans* CH34 Δ*pyrE_mRFP1*). The outcome expected was growth and absence of growth for the cells transformed with the P_{pan}*mRFP1*_P_{trpsyn}*pyrE*FA1090 & P_{pan}*mRFP1* plasmids, respectively

4.4.7 Continuous Growth in Bioreactors of Complemented Uracil Auxotrophic Strains

Continuous growth of *C. metallidurans* strains was performed to assess stability of the plasmids generated in Section 4.4.4. *C. metallidurans* NG7*_mRFP1* and *C. metallidurans* NG7 Δ*pyrE_mRFP1* was carried out using Multifors 2® parallel bioreactors (Infors HT) as follows. Two independent colonies for each strain were initially inoculated in 5 mL SGMM with appropriate selection (Chloramphenicol 500 µg/mL for *C. metallidurans* NG7*_mRFP1* and *C. metallidurans* NG7 Δ*pyrE_mRFP1* & tetracycline 20 µg/mL for *C. metallidurans* CH34*_mRFP1* and *C. metallidurans* CH34 Δ*pyrE_mRFP1*) at 30 ˚C for 48 hours. A setback for each culture at OD_{600} 0.1 was performed in 250 mL E-Flask supplemented with 25 mL SGMM media supplemented with the appropriate selection. After 48 hours, the cultures were inoculated at OD_{600} 0.1 in Multifors 2®. *C. metallidurans* NG7-related strains were inoculated in MM media with 0.4% Na-Gluconate as carbon source, while for *C. metallidurans* CH34-related strains MM media with 2% Na-Gluconate was used. The cultures were grown up to late exponential phase in the bioreactors (~OD_{600} 2.5) and the feed rate was subsequently fixed at $\mu = 0.1\ hr^{-1}$. Growth conditions were set as

follows: Compressed air flow set at 0.5 l/min, 30 ˚C and stirring facilitated by two Rushton impellers at 500 rpm. Dissolved oxygen and pH were monitored by means of an optical probe (Mettler Toledo) and a pH probe (Mettler Toledo).

4.4.8 PST of Bacterial Strains Grown in Continuous in Bioreactor Settings

Study of PAS for *C. metallidurans* NG7*_mRFP1*, *C. metallidurans* NG7 Δ*pyrE_mRFP1*, was performed by means of PST t following the procedure of Miles-Misra[196] with the due adaptations. Samples were withdrawn every 24 hours from the bioreactors. The samples were serially diluted in PBS and a 20 µL drop was inoculated on to SGMM and SGMM agar plates supplemented with gentamycin and chloramphenicol respectively. The CFU was calculated for both types of plates and the percentage of cells retaining the plasmid was calculated with the formula $\%\ of\ plasmid\ retaining\ cells = 100x\frac{CFU\ SGMM\ Gen^{+}Cm^{+}}{CFU\ SGMM\ Gen^{+}}$ where CFU SGMM Gen^{+} Cm^{+} and CFU SGMM correspond to the CFU calculated on SGMM supplemented with gentamycin and chloramphenicol and with no SGMM supplemented only with gentamycin.

Study of PAS for *C. metallidurans* CH34*_mRFP1* and *C. metallidurans* CH34*_* Δ*pyrE_mRFP1* was performed as before with the following differences: replica plating was perfromed on SGMM agar plates supplemented with 20 µg/mL uracil and gentamycin (SGMM Gen^{+} Ur^{+}) and SGMM agar plates supplemented with tetracycline plus gentamycin. Addition of uracil served the purpose to account for plasmid loss due to cross feeding, which was not previously taken into consideration. The percentage of cells retaining the plasmid was eventually calculated with the formula $\%\ of\ plasmid\ retaining\ cells = 100x\frac{CFU\ SGMM\ Gen^{+}\ Tc^{+}}{CFU\ SGMM\ Gen^{+}\ Ur^{+}}$ where CFU

SGMM Gen^+ Tc^+ and CFU SGMM Gen^+ Ur^+ correspond to the CFU calculated on SGMM plates supplemented with tetracycline and with no tetracycline respectively but with addition of uracil.

4.4.9 PST of IncP-1α in *C. metallidurans* NG7, pMTL74301Low/ pMTL74301Low_*parCBADE* in *C. metallidurans* CH34 & *C. metallidurans* AE126

C. metallidurans NG7 and *C. metallidurans* CH34/AE126 transformed with plasmids pMTL74301Low and pMTL74301Low_*parCBADE* were grown in 5mL LB media in 50 mL Falcon tubes supplemented with tetracycline for 48 hours. Cells were collected by centrifugation at 4500 rpm for 6 minutes and resuspended in fresh LB media twice. In the last wash cells were resuspended at OD_{600} 0.05 and inoculated in in 250 mL E-Flasks with 25 mL LB media. Each day for 8 days the cells were resuspended in 25 mL of fresh LB media at OD_{600} 0.05, and the aliquot was diluted serially, and 20 µL spotted on LB Gen^+ and LB Gen^+ Tc^+ in accordance to the Miles-Misra methodology. Plasmid stability was then calculated with the formula $\%\ of\ plasmid\ retaining\ cells = 100x\frac{CFU\ LB\ Gen^+\ Tc^+}{CFU\ LB\ Gen^+}$.

The purpose of this experiment was to test if *parCBADE* was sufficient to confer stability to pMTL74311Low plasmid in *C. metallidurans* CH34. Stability of pMTL74301Low_*parCBADE* was also assessed in *C. metallidurans* AE126, which is isogenic to *C. metallidurans* CH34 but from which pMOL30 was cured[44]. The only difference between *C. metallidurans* AE126 and *C. metallidurans* NG7 is the presence of IncP-1α. Therefore, direct comparison of stability of pMTL74311Low_*parCBADE* in *C. metallidurans* CH34 and *C. metallidurans* AE126 would allow to gather more

information on the role of the *parCBADE* system in providing stability of the in-house mini RK2 in *C. metallidurans* CH34 and of IncP-1α in *C. metallidurans* NG7. Interpretation of the results would then be in accordance with the following rationale:

i) If no plasmid loss was to be seen in either strain, it could be concluded the parCBADE alone is enough to provide efficient segregation of in-house mini RK2 to the daughter cells and post-segregational killing of plasmid-less cells in *C. metallidurans* CH34.

ii) If plasmid instability was to be seen in *C. metallidurans* CH34, but not in *C. metallidurans* AE126, plasmid loss could be blamed on incompatibility of parCBADE with the native systems involved in segregation of pMOL30 to the daughter cells. This would also highlight parCBADE alone would suffice to provide stability of pMTL74311Low in *C. metallidurans* AE126 and IncP-1α in *C. metallidurans* NG7.

iii) If plasmid instability was to be seen in both strains, it could be concluded additional stabilization determinants to the *parCBADE* system would be required to stabilize pMTL74311Low in *C. metallidurans sp*.

4.4.10 Flow Cytometry (FC) of Bacterial Strains Grown in Continuous Bioreactor Settings

Flow cytometry was used to investigate expression of *mRFP1* from strains *C. metallidurans* NG7*_mRFP1* & *C. metallidurans* NG7*_ΔpyrE_mRFP1*. Samples were withdrawn at 0, 168 and 336 hours for *C. metallidurans* NG7*_mRFP1* & *C. metallidurans* NG7*_ΔpyrE_mRFP1*, washed twice in PBS and resuspended in PBS at OD_{600} 0.1. Each sample was stained separately in 500 µL of PBS supplemented with

10 μM Syto9 (Thermofisher) and 5 μM Yoyo-1 (Thermofisher) for 30 minutes in the dark at RT. All centrifugation steps were performed at 1000 rpm. Three samples for each strain were prepared, namely unstained sample (Negative Control, no staining), Only Yoyo-1 (live staining) and Only Syto-9 (all cells staining). MoFlo Astrios (Beckman Coulter) flow cytometer was used along with laser at 488nm 200mV for scattering profile and Yoyo-1/Syto-9, while laser 561nm 200mV was used for excitation of mRFP1. Filters were set to detect emission wavelengths between 513/526nm and 614/620 for Syto-9/Yoyo-1 and mRFP1 respectively. Data analysis was performed with Kaluza (Beckman Coulter). FFS and SSC heights were used to identify cell populations, while plot of SSC height against SSC area was used to distinguish and gate singlets from doublets in the cell population. Syto-9 was used to discriminate cells against debris, while singlets negative to Yoyo-1 (live cells) were gated to detect mRFP1 fluorescence over time. Percentage of mRFP1 positive cells for the duplicates of both strains were taken into consideration and plotted against time. rMFI was eventually calculated by dividing the MFI of *C. metallidurans* NG7*_ΔpyrE_mRFP1* by the MFI of *C. metallidurans* NG7*_mRFP1*. Standard deviation was used to check within the experiment variation (n=2).

Firstly, Live/dead cells were discriminated with Yoyo-1® and Syto9® (Thermofisher) to check for any possible effect of the complementation on cell viability and secondly, a direct comparison between the two strains was performed by comparing the live cells expressing mRFP1 ($Yoyo1^{-}/mRFP1^{+}$). Syto9 and Yoyo-1®, the fluorophores herein selected to discriminate live/dead cells, are DNA staining both emitting in the green region of the spectrum. The most used combination of fluorophores for measurement of live/dead cells are Syto9® and Propidium Iodide[197], emitting in the green and red spectra respectively, allowing staining of live and dead

cells in the same tube. Since the complementation plasmid was built with the *mRFP1* gene to monitor protein expression over time Yoyo-1® was used as a membrane impermeable counterstain which implied that the two DNA staining methods had to be performed in separate tubes. Therefore, validation of the staining protocol was performed to verify that the totality of the events detected could be attributed to cells rather than a mixture of cells and debris. This was done with the sample stained with Syto9®. The overall strategy for FC data analysis followed the same initial procedure for all the different staining. Briefly, individual cells within populations were identified using Forward Scattering (FSC) and Side Scattering (SSC) and singlets were discriminated from doublets by means of density plot of SSC Area vs SSC Height. Finally, the tubes with unstained sample, stained with Syto9® or Yoyo-1® were analysed as follows:

i) *Unstained samples:* this sample had the purpose to establish the threshold for determination of samples positive to Syto9 ($Syto9^+$). Following singlets gating, the threshold for Syto9 negative cells ($Syto9^-$) was established.

ii) *Syto9®-stained samples:* this sample had the purpose of separating cells from debris and validating my staining protocol. After gating of singlets, the threshold for Syto9- events previously set was applied to this sample. If no Syto9- events were recognized, the protocol was considered valid as the whole sample was considered to be composed of cells.

iii) *Yoyo-1®-stained samples*: this sample had the purpose of discriminating the fraction of live cells expressing mRFP1. Following determination of singlets, $Yoyo\text{-}1^-$ cells were considered as live cells

and the fraction of mRFP1^{+}/Yoyo-1^{-} cells (live cells expressing *mRFP1*) from *C. metallidurans* NG7*_mRFP1* and *C. metallidurans* NG7*_*Δ*pyrE_mRFP1* were further compared to study *via* determination of the relative Median Fluorescence Intensity of mRFP1 expression between the two strains.

4.6 Results & discussion

4.6.1 Comparison of the Phenotypic and Genotypic Differences between *C. metallidurans* NG7 and *C. metallidurans* CH34

In this section the phenotypic and genotypic differences between *C. metallidurans* NG7 and *C. metallidurans* CH34 were investigated by means of a combined *in silico* and wet-lab approach. In Chapter 3, our in-house strain of *C. metallidurans* (ordered from DSMZ in 2015, prior to my arrival in the lab) was re-named *C. metallidurans* NG7 since it displayed different antibiotic-resistance properties compared to those described in the literature. Indeed, *C. metallidurans* NG7 showed resistance to all the antibiotics reported to be active against *C. metallidurans* CH34 (tetracycline, kanamycin, and piperacillin) and showed sensitivity to chloramphenicol only at concentrations of 400 μg/mL.

Firstly, a phenotypic analysis was performed on *C. metallidurans* NG7 and *C. metallidurans* CH34 to assess for presence/absence of pMOL30 and pMOL28 as described in Section 4.4.1. The megaplasmid content of both *C. metallidurans* CH34 and *C. metallidurans* NG7 was further extracted and compared using agarose gel electrophoresis. Secondly, while investigating plasmid stability of the complementation plasmid pMTL71101_P_{Pan}*mRFP1*_P_{trpsyn}*pyrE*FA1090 (see section 4.6.3), *C. metallidurans* NG7 and *C. metallidurans* CH34 were sent for Illumina whole-genome sequencing and genomic data were subsequently analysed as reported in section 2.3.

The phenotypic analysis showed *C. metallidurans* NG7 was unable to grow on SGMM agar media in the presence of Zn^{2+}, Cd^{2+}, and Cu^{2+}, but could grow on agar minimal media supplemented with either Ni^{2+}, tetracycline, kanamycin, or piperacillin, thereby

suggesting loss of pMOL30 as well as acquisition of genes involved in antibiotic resistance (Table 7). Extraction and analysis of the megaplasmid content with agarose gel electrophoresis, confirmed the band relative to pMOL30 (233 kb) was missing, and an additional band of ~65Kb was observed (Figure 33A). Illumina sequencing reads of *C. metallidurans* NG7 were assembled against the genome of *C. metallidurans* CH34, which was used as reference, and SNPs, InDels and SV were called against the sequences deposited on NCBI (see section 2.3 for accession numbers and details of the parameters employed). The data highlighted the absence of pMOL30 and presence of an additional plasmid of 60kb which had 100% homology with IncP-1α[198], a multidrug resistance plasmid clade belonging to the IncP-1 incompatibility group which is described to be present in 5-8 copies per cell in *E. coli*[199] (Table 8). IncP-1α was initially isolated in the Burns Unit of the Birmingham Accident Hospital in 1969 from *Klebisella aerogenes*[200] and was later discovered to be abundant in a variety of environments, ranging from clinical to agricultural and industrial settings[201], which are typically associated with the use of considerable amounts of antibiotics and/or heavy metals. IncP-1α plasmids have a mosaic-like structure which has evolved by homologous recombination of different segments deriving from other plasmids and can be divided into a backbone and a non-backbone section[201]. The backbone bears the *oriV* origin of replication, the *trfA* replication initiation gene[192], the origin of transfer *oriT* along with the *traJ* gene involved in plasmid replication and conjugation, respectively and the *parCBADE* genes involved in plasmid segregation and post-segregational killing[196]. Among non-backbone sequences are Coding Sequences (CDS) coding for tetracycline (*tetR* & *tetA*) and kanamycin (*aphaA*)[198] resistance, which are believed to have been integrated in the plasmid as the result of a transposition event (Figure 33B). Furthermore, two transposition events were clearly

still visible as presence of a Tn1 transposon, which gives β-lactamase resistance cassette and a IS*21*, which contains several genes of unknown function[198]. Besides the lack of pMOL30 and the additional IncP-1α plasmid, three other SNPs were found in *C. metallidurans* NG7. One mutation involved amino acid change E132G in a tyrosine type recombinase integrase (Rmet_3675), one was an intergenic variant and the last another point mutation, leading to L181P substitution in Rmet_RS07710, which codes for a Nickel Transporter (Table 8).

Table 7-growth of *C. metallidurans* NG7 and *C. metallidurans* CH34 on SGMM agar supplemented with different selective agents

Genomic location of resistance genes	**Selection**	***C. metallidurans* NG7**	***C. metallidurans* CH34**
pMOL30	Zn^{2+}	-	+
	Cd^{2+}	-	+
	Cu^{2}	-	+
pMOL28	Ni^{2+}	+++	+
//	Tc	+++	-
	Kan	+++	-
	Pip	+++	+++
	Chl	+-	+-

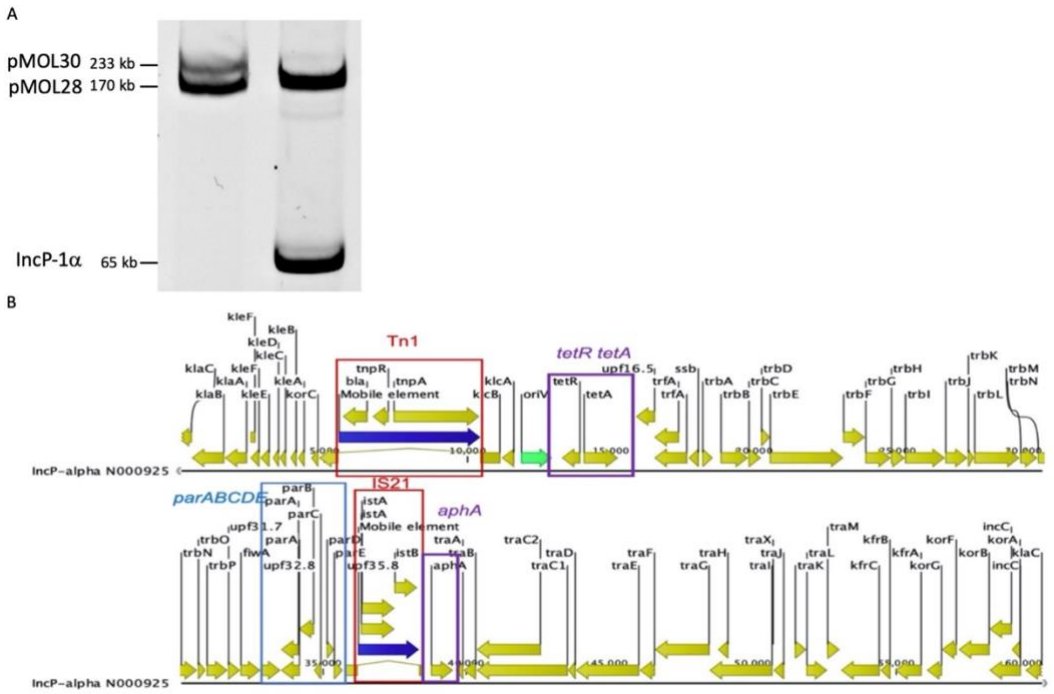

Figure 33-Megaplasmid content of *C. metallidurans* CH34 and organization of the IncP-1α plasmid: A) Agarose gel electrophoresis showing the megaplasmid content of *C. metallidurans* NG7: First and second lane refer to *C. metallidurans* CH34 and *C. metallidurans* NG7, respectively. B) Organisation of IncP-1α plasmid. Tetracycline and kanamycin resistances genes, highlighted with purple boxes, are thought to be part of the original backbone structure, while β-lactamase resistance gene was introduced by the integration of a Tn1 transposon (red box, Tn1). Another transposition event due to IS21 resulted in insertion of genes whose functions are still under investigation. A toxin-antitoxin and multimer resolution system are also present (*parCBADE*, blue box).

Table 8-List of mutations of *C. metallidurans* NG7 filtered against *C. metallidurans* CH34

Chromosome	Region	Type	CDS
IncP-1α		Acquisition of Plasmid	
pMOL30		Loss of Plasmid	
CHR1	1654515	Point Mutation A>G, E132G	Rmet_3675 Tyrosine type recombinase integrase
CHR2	1171984	Point Mutation C>G	Intergenic
	1654515	Point Mutation T>C L181P	Rmet_RS07710 Nickel Transporter

4.6.2 5-FOA Mediated Evolution of Uracil Auxotrophic Strains of *C. metallidurans* NG7 and *C. metallidurans* CH34 species

4.6.2.1 Minimal Inhibitory concentration of 5-FOA

Before embarking on the directed evolution study, it was necessary to establish the Minimal Inhibitory Concentration (MIC) of 5-FOA for *C. metallidurans* NG7. This experiment was done in *C. metallidurans* NG7 only as it was the strain of *C. metallidurans* initially available in our lab. The experimental procedure followed is reported in section 4.4.2. The OD_{600} values measured at the end of the experiment (72 hours) are reported in Figure 34, for each concentration of 5-FOA tested (25 µg/mL, 50 µg/mL, 75 µg/mL, 100 µg/mL, 200 µg/mL, 300 µg/mL, 400 µg/mL, 500 µg/mL and 600 µg/mL). As expected, a dose-dependent effect of 5-FOA on bacterial growth was observed. However, as no significant differences were detected in the OD_{600} values measured between 300 and 600 µg/mL 5-FOA, 500 µg/mL of 5-FOA was eventually used in the evolution experiments of both *C. metallidurans* NG7 and *C. metallidurans* CH34.

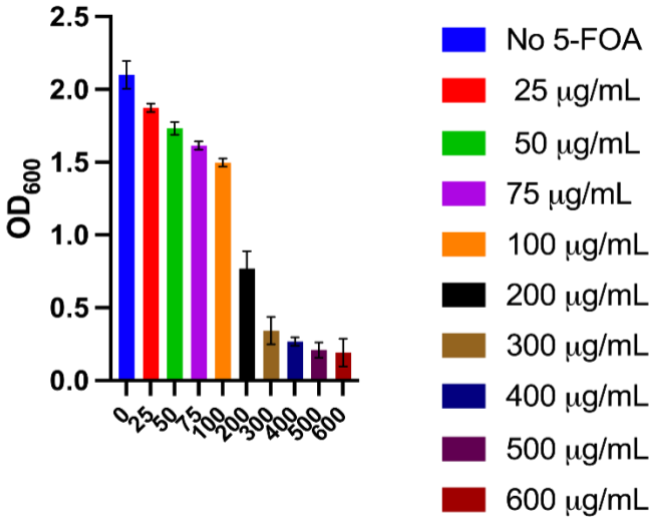

Figure 34-Toxicity assay of 5-FOA in liquid cultures of *C. metallidurans* NG7 in SGMM: *C. metallidurans* NG7 grown in 0.4% SGMM with 5-FOA at different concentrations OD_{600} values taken at the endpoint of the experiment (72 hours). Error bars represent standard deviation (n=3).

4.6.2.2 5-FOA-Mediated Evolution of Uracil Auxotroph Strains of *C. metallidurans* NG7 & *C. metallidurans* CH34

The aim of this section was to isolate uracil auxotrophs on SGMM agar media supplemented with 500 µg/mL 5-FOA as described in 4.4.3. All the colonies isolated on 5-FOA uracil plates for both the *C. metallidurans* NG7 and *C. metallidurans* CH34 strains were shown to be uracil auxotrophs by means of replica plating (Figure 35A show replica plates of the uracil auxotrophs of *C. metallidurans* NG7 only). cPCR was performed on the *pyrE* and *pyrF* loci with primer pairs pyrE400Up_Fw/pyrE400Dw_Rv & pyrF400Up_Fw/pyrF400Dw_Rv, which anneal outside the *pyrE* and *pyrF* genes, respectively. cPCR and Sanger sequencing of the *pyrE* locus confirmed InDels in some of the isolates (Figure 35A) and further Illumina whole-genome sequencing showed a wide range of mutations occurring in *pyrE*. *C. metallidurans* NG7 Δ*pyrE* isolates 2-4 showed a 1bp insertion (causing a frameshift mutation), a 101 bp deletion and insertion of ISRme6 IS element respectively. The

only Δ*pyrE* isolate of *C. metallidurans* CH34 sent for whole-genome sequencing also displayed a 101 bp deletion of the *pyrE* gene (Table 9).

Despite none of the isolates screened by cPCR and/or Illumina sequencing showing mutations in the *pyrF* gene, *pyrE* is reported in the literature to be in some cases a preferential site of mutation for achieving uracil auxotrophy. Fluctuation tests experiments for calculation of mutation rates in *S. acidocaldarius* and *Thermus thermophilus* focusing on the *pyrE/F* locus showed higher mutation rate for *pyrE* than *pyrF*[188,202]. This has been attributed to *pyrE* being a preferential mutation site by causing disruptive polar effects on downstream *pyrF*. Furthermore, point mutations and insertions of IS element were found to be 20-fold and 3-fold more likely in *pyrE* rather than *pyrF* in different thermophilic bacteria[203,204]. The data herein reported suggested that the *pyrE* gene is the preferred site of mutation when 5-FOA-mediated evolution is used to generate uracil auxotrophs in *C. metallidurans* NG7 (and probably also in *C. metallidurans* CH34), with mutations ranging from SNPs and InDels to transposon insertions. The uracil auxotroph isolates of *C. metallidurans* NG7 and *C. metallidurans* CH34 number 3 and 27 were further considered for the downstream complementation, PST and FC experiments since they were characterised by ~100 bp deletions, which were considered to be the most stable type of mutation amongst those observed in the *pyrE* gene due to their low probability of reverting to wild type. These strains will be from now on referred to as *C. metallidurans* NG7 Δ*pyrE* and *C. metallidurans* CH34 Δ*pyrE*, respectively.

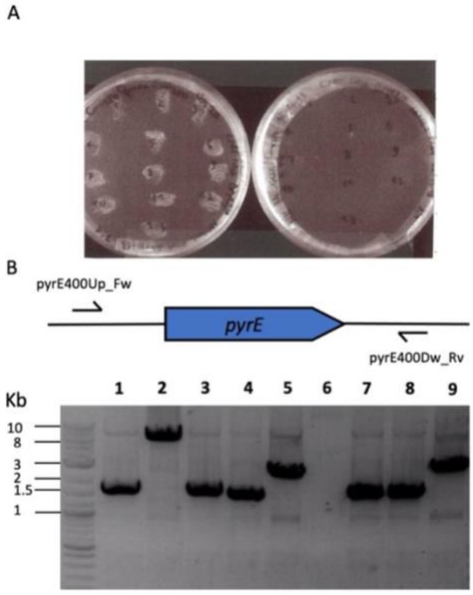

Figure 35-Replica plating and cPCR of uracil auxotroph strains of *C. metallidurans* NG7: A) Replica plating of isolates of *C. metallidurans* NG7 from SGMM 5-FOA uracil agar plates on SGMM agar plates with uracil (left) and without uracil (right). B) agarose gel electrophoresis of cPCR amplicons of FOA resistant isolates of *C. metallidurans* NG7. Lane 1 control (gDNA of *C. metallidurans* NG7), Lanes 2- 9) uracil auxotrophs. cPCR was performed with primers pyrE400Up_Fw and pyrE400Dw_Rv to amplify the *pyrE* gene.

Table 9-List of mutations of isolates of *C. metallidurans* NG7 & *C. metallidurans* CH34 evolved on SGMM agar media supplemented with 5-FOA

Strain	Type of Mutation	Region	Chromosome	Features	CDS	product
NG7 Δ*pyrE*_2	SNP-Insertion	155133	CHR1	1bp frameshift mutation	Rmet_0150 *pyrE*	Orotate phosphoribosyltransferase
	Deletion	pMOL30	pMOL30	Curing of the plasmid	Plasmid with heavy metal resistance features	
	Insertion	IncP-1α	/	Acquisition of IncP-1α	Plasmid with antibiotic resistance features	
NG7 Δ*pyrE*_3	Deletion	154777-154878	CHR1	101 bp deletion	Rmet_0150 *pyrE*	Orotate phosphoribosyltransferase
	Deletion	pMOL30	pMOL30	Curing of the plasmid	Plasmid with heavy metal resistance features	
	Insertion	IncP-1α	/	Acquisition of IncP-1α	Plasmid with antibiotic resistance features	
NG7 Δ*pyrE*_4	Insertion	154643-154742	CHR1	Insertion Rmet6448 Transposase ISRme6	Rmet_0150 *pyrE*	Orotate phosphoribosyltransferase
	Deletion	pMOL30	pMOL30	Curing of the plasmid	Plasmid with heavy metal resistance features	
	Insertion	IncP-1α	/	Acquisition of IncP-1α	Plasmid with antibiotic resistance features	
CH34 Δ*pyrE*_27	SNP-Substitution	154686	CHR1	T>A, Amino acid change L>P	Rmet_0150 *pyrE*	Orotate phosphoribosyltransferase
CH34 Δ*pyrE*_27	Deletion	154700-154800	CHR1	Deletion 100 bp		

4.6.3 Complementation of Uracil Auxotrophy of *C. metallidurans* NG7 Δ*pyrE* & *C. metallidurans* CH34 Δ*pyrE*

4.6.3.1 Cloning of the Complementation & Expression Plasmids

To complement uracil auxotrophy, determined by 5-FOA-mediated disruption of the *pyrE* gene, plasmids pMTL71301_P_{pan}*mRFP1*_P_{trpsyn}*pyrE*FA1090, pMTL71301_P_{pan}*mRFP1*, pMTL71101_P_{pan}*mRFP1*_P_{trpsyn}*pyrE*FA1090 & pMTL71101_P_{pan}*mRFP1* were constructed as reported in section 4.4.4 and shown in Figure 31. Sanger sequencing was used to confirm the nucleotide sequence of the plasmid. The plasmids only differed in their antibiotic resistance cassettes, which are Tc^+ for pMTL71301 and Cat^+ for pMTL71101. These two different backbones were employed as *C. metallidurans* NG7 was found to be susceptible only to chloramphenicol (section 3.5.1), while the use of tetracycline is widely reported in the literature for selection of transformants or recombinant clones of *C. metallidurans* CH34[205,206]. These plasmids carry the P_{pan} strong constitutive[63] and P_{trpsyn}[207] promoters, controlling expression of *mRFP1* and heterologous *pyrE* from *N. gonorrhoeae* FA1090, respectively, and were used to perform FC and PST experiments.

4.6.3.2 Complementation of Uracil Auxotrophy in *C. metallidurans* NG7 and *C. metallidurans* CH34

C. metallidurans NG7 and *C. metallidurans* CH34 were electroporated with plasmids pMTL71101_P_{pan}*mRFP1*_P_{trpsyn}*pyrE*FA1090 and pMTL71301_P_{pan}*mRFP1*_P_{trpsyn}*pyrE*FA1090 respectively as described in section 4.4.6. As expected, cells transformed with the complementation plasmids (I.E carrying the *pyrE* gene from *N. gonorrhoeae* FA1090) showed presence of pink colonies, while transformation of plasmid deprived of the complementation gene, failed to produce any transformants. These results showed that growth was restored, and cells were able to express mRFP1 (Figure 36).

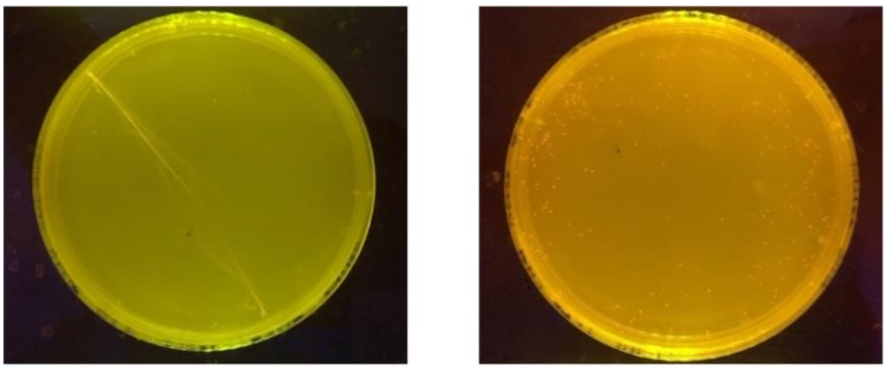

Figure 36-Complementation test of *C. metallidurans* NG7 under blue light: Left panel; *C. metallidurans* NG7 Δ*pyrE* transformed with pMTL71101_P_{Pan}*mRFP*1. Right panel: *C. metallidurans* NG7 Δ*pyrE* transformed with complementation plasmid pMTL73101_P_{Pan}*mRFP*1_P_{trpsy}*pyrE (*strain *C. metallidurans* NG7_Δ*pyrE_mRFP1*).

4.6.4 Plasmid Stability & Protein Expression Tests in Complemented strains of *C. metallidurans* NG7 and CH34

The aim of these experiments was to test if the complemented uracil auxotroph strains, described in the previous section, were able to retain the complementation plasmid and express mRFP1 during continuous growth in bioreactors. Based on the

observations reported in the previous section, where a plasmid encoding the *pyrE* gene was essential to restore growth of uracil auxotroph strains, it was expected that plasmids should be retained during continuous cultivation.

4.6.4.1 Plasmid Stability Test (PST) and Flow Cytometry (FC) to Study Plasmid Stability and Protein Expression of *C. metallidurans* NG7_Δ*pyrE_mRFP*1 During Continuous Growth in Bioreactor Setup

The aim of this section was to test if *C. metallidurans* NG7_Δ*pyrE_mRFP1* (I.E uracil auxotrophic *C. metallidurans* NG7 transformed with pMTL71101_P_{pan}*mRFP1*_P_{trpsyn}*pyrE*FA1090) was capable of stable plasmid maintenance and expression of mRFP1 when grown in continuous heterotrophic conditions. *C. metallidurans* NG7 was also transformed with plasmid pMTL71101_P_{pan}*mRFP*1 to obtain *C. metallidurans* NG7_*mRFP1* which was used as a control strain. Following, two independent cultures of each strain, *C. metallidurans* NG7_*mRFP1* and *C. metallidurans* NG7_Δ*pyrE_mRFP1* were inoculated in 500 mL bioreactors and grown for 336 hours (14 days), cell cultures were periodically sampled and subjected to PST and FC to test for segregational instability and protein expression respectively (see section 4.4.7 & 4.4.8 for details). In the first instance, growth of the two strains showed to be comparable as estimated by OD_{600} (Figure S4). The control strain *C. metallidurans* NG7_*mRFP*1 showed dramatic plasmid instability. Indeed, at the start of the experiment in continuous growth, only ~4% of the cells appeared to retain the expression plasmid, compared to ~97% of plasmid-retaining cells for *C. metallidurans* NG7_Δ*pyrE_mRFP*1 ($p<0.00001$ Mann-Whitney test). While plasmid was completely lost in *C. metallidurans*_NG7_*mRFP1* after 24 hours (not shown), *C. metallidurans* NG7_Δ*pyrE_mRFP1* showed stable plasmid maintenance throughout

the duration of the experiment (and Figure 37). The fact that the wild type strain showed dramatic instability of pMTL71101_P_{pan}_*mRP1* further points at segregational instability as the main factor leading to lack of expression of the SNAP-tag in Chapter 3.

Table 10-Results of the PST of *C. metallidurans* NG7*_mRFP1* & *C. metallidurans* NG7_Δ*pyrE_mRFP1*: Standard deviation (n=2) is reported between brackets

	Plasmid-retaining cells (%)	
Hours	***C. metallidurans* NG7*_mRFP1***	***C. metallidurans* NG7_Δ*pyrE_mRFP1***
0	4 (± 5.65.22)	97.5 (± 0.70)
168	0 (± 0)	99.5 (± 0.70)
336	0 (± 0)	97.5 (± 2.12)

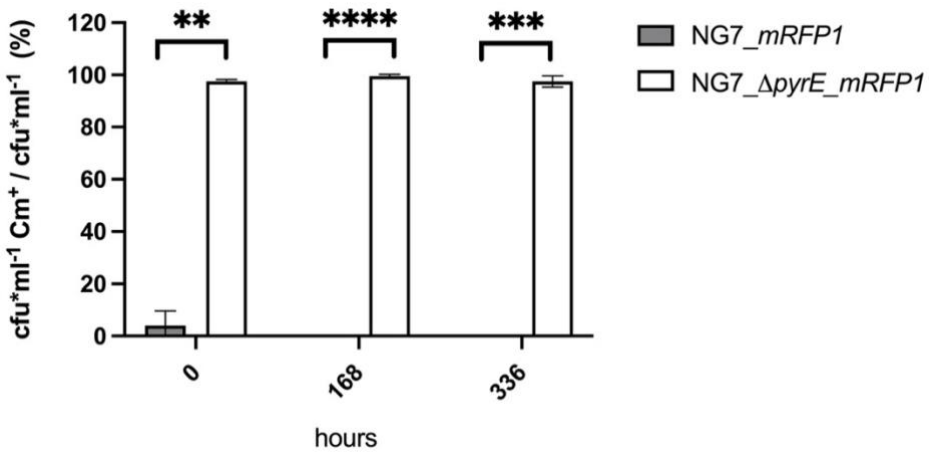

Figure 37-Plasmid Stability Test of *C. metallidurans* NG7*_mRFP1* & *C. metallidurans* NG7*_ΔpyrE_mRFP1*: The strains under investigation were grown in continuous for 336 hours (2 weeks) with 0.4% SGMM. Every 24 hours cells were collected, serially diluted and 20 µL of each dilution were plated on SGMM Gen^+ or SGMM Gen^+ Cm^+ plates using the Miles-Misra method. The percentage of cells retaining the plasmid was eventually calculated. Statistical significance was calculated with Mann-Whitney test: ** $p<0.01$, *** $p<0.0001$, **** $p<0.00001$. Error bars represent standard deviation (n=2).

The following section describes the results of the validation of the staining protocol for FC and refers to the experimental section 4.4.11. Dot plots relative to the samples of *C. metallidurans* NG7*mRFP1* and *C. metallidurans* NG7*_ΔpyrE_mRFP1* at 0 and 336 hours are reported as example. In first instance, the unstained sample showed all events generated were singlets and the threshold for $Syto9^+$ events was established (Figure 38). Secondly, samples stained with Syto9 generated only $Syto9^+$ signal when analysed *via* FC, thereby indicating the totality of the signal generated was due to the presence of cells, which validated my staining protocol (Figure 39). Lastly, samples stained only with Yoyo-1 were analysed and further considered for comparison of live cells ($Yoyo\text{-}1^-$) and live cells expressing mRFP1 ($Yoyo\text{-}1^-$, $mRFP1^+$). Representative dot plots are visible in Figure 38.

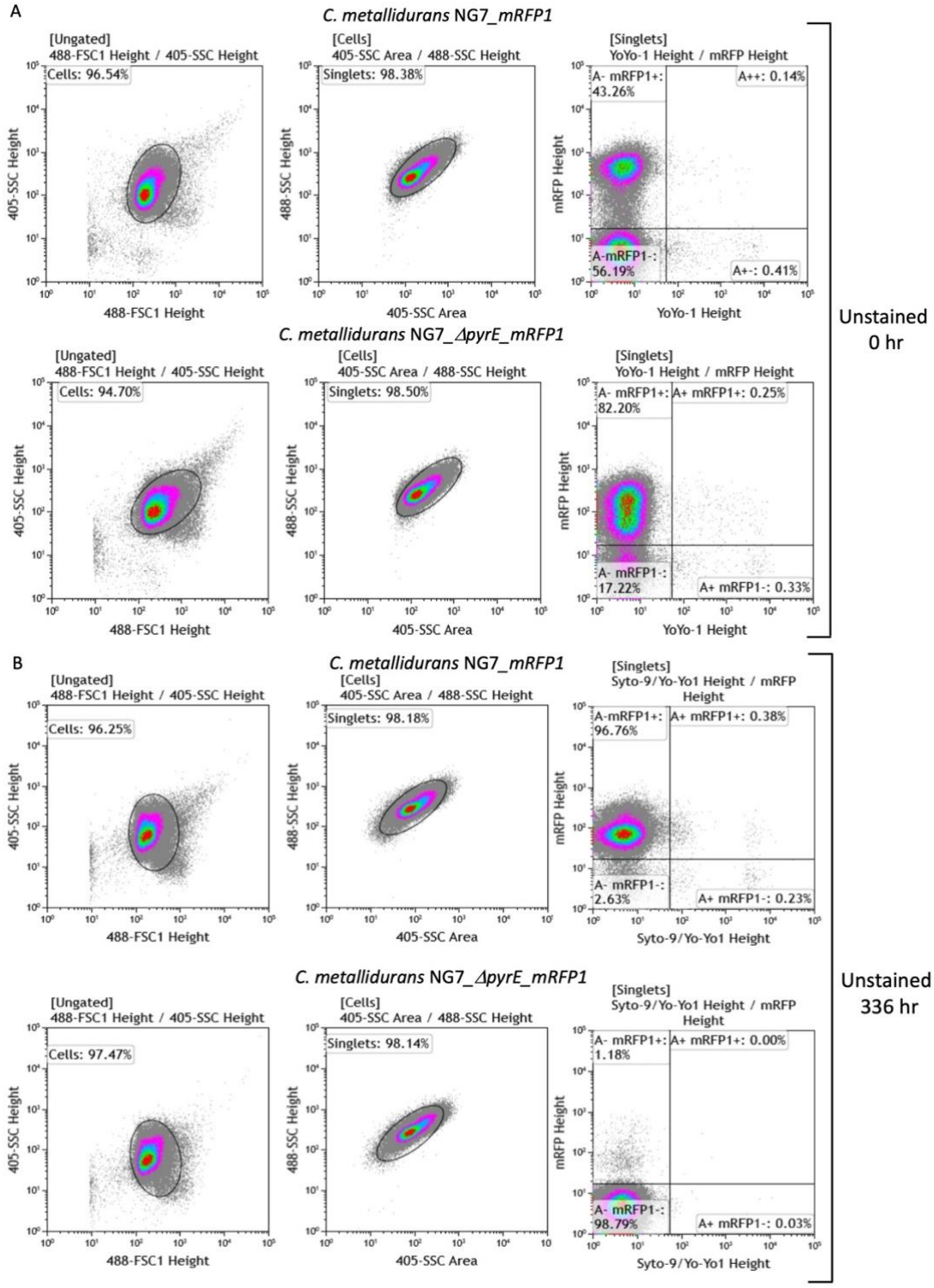

Figure 38-dot plot of unstained *C. metallidurans* NG7*_mRFP1* & *C. metallidurans* NG7*_ΔpyrE_mRFP1*: A) 0 hours & B) 336 hours. Top and bottom panels are relative to *C. metallidurans* NG7*_mRFP1* & *C. metallidurans* NG7*_ΔpyrE_mRFP1*, respectively. From left to right panels represents dot plots of FSC/SSC, singlets, and dot plot of Syto9/Yoyo-1 signal vs mRFP1 signal.

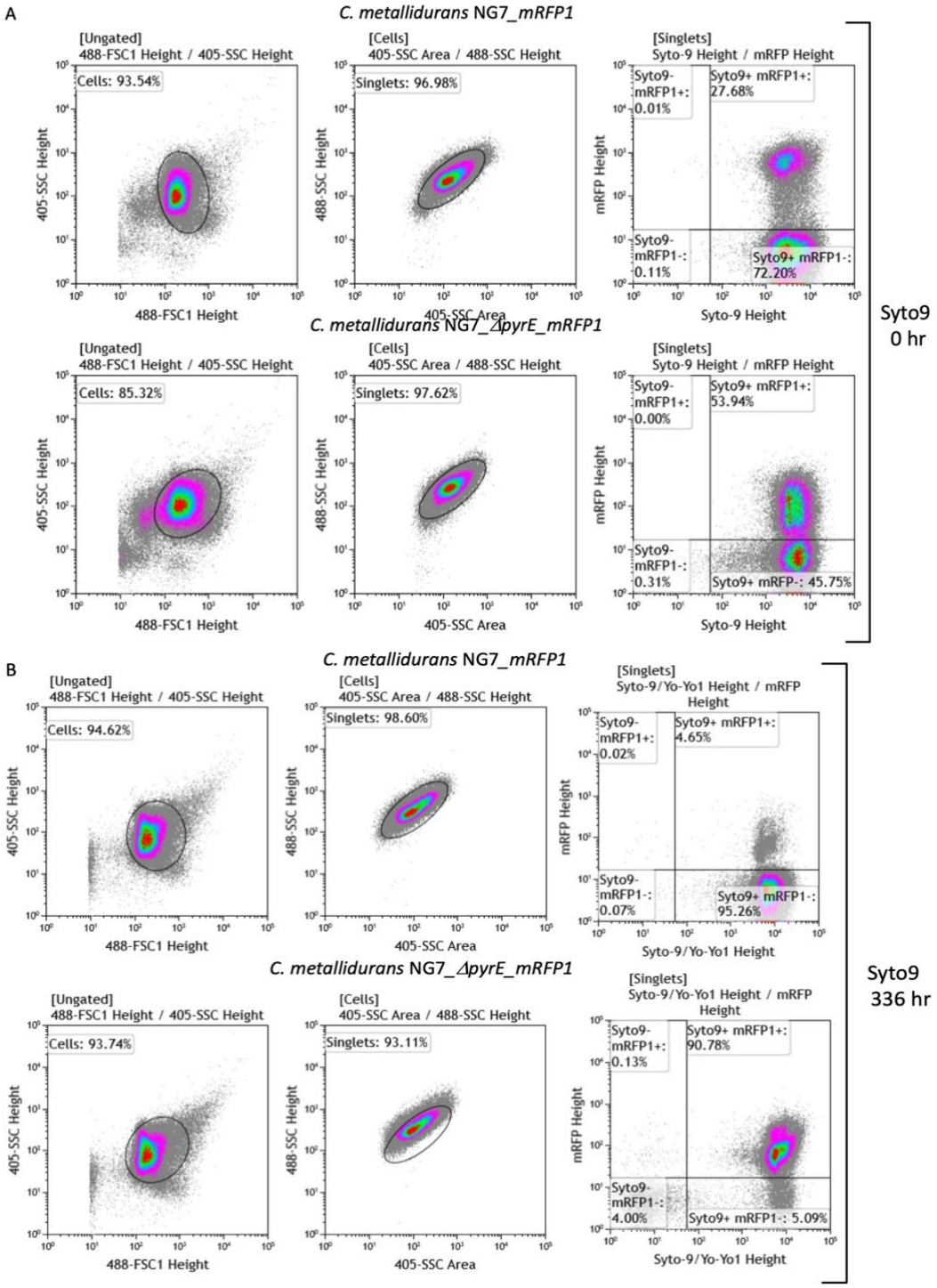

Figure 39-dot plot of Syto9-stained *C. metallidurans* NG7*_mRFP1* & *C. metallidurans* NG7_Δ*pyrE_mRFP1*: A) 0 hours & B) 336 hours. Top and bottom panels are relative to C. *metallidurans* NG7_mRFP1 & *C. metallidurans* NG7*_ΔpyrE_mRFP1*, respectively. From left to right panels represents dot plots of FSC/SSC, singlets and Syto9 signal vs mRFP1 signal.

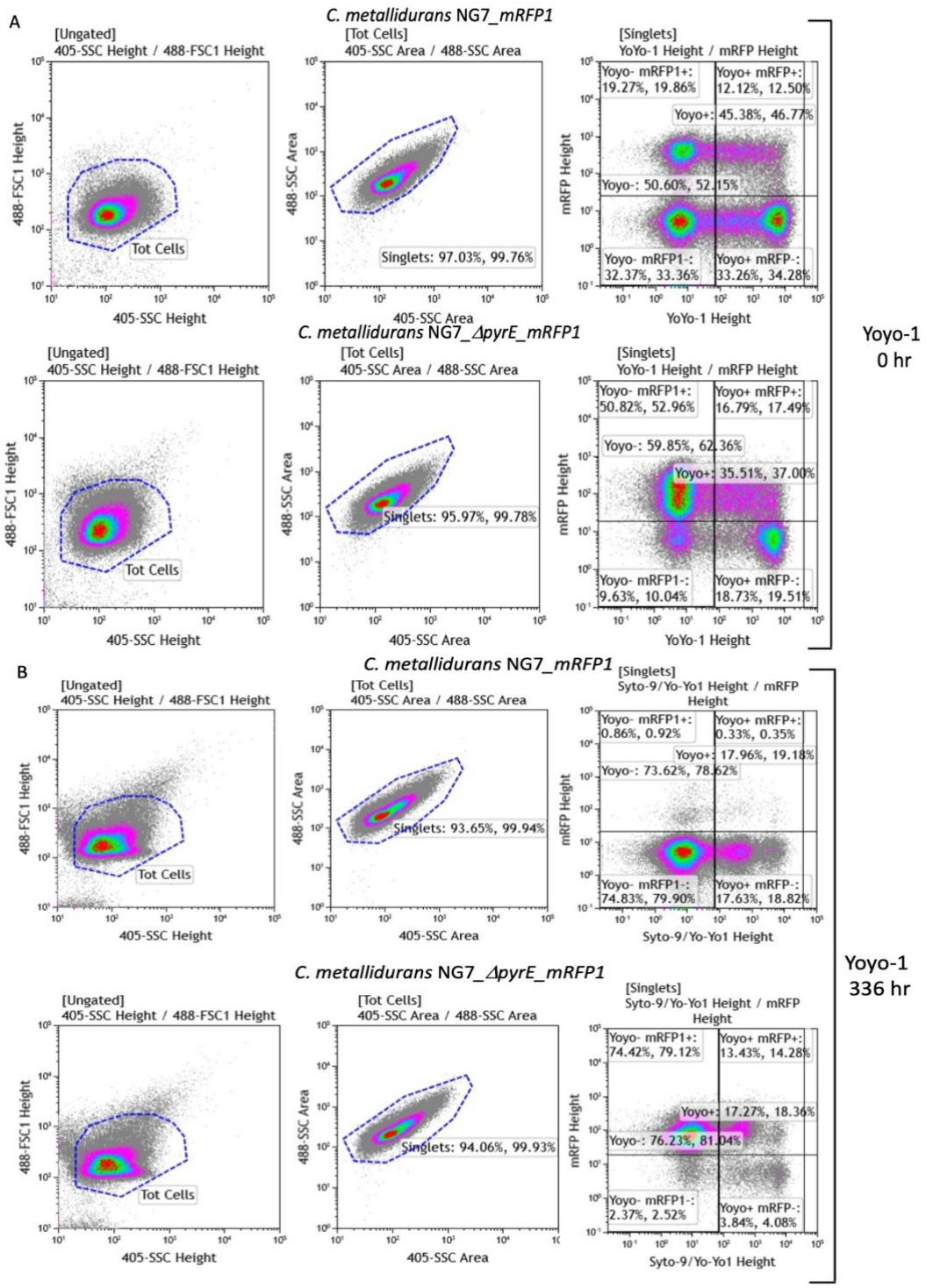

Figure 40-dot plot of Yoyo-1-stained C. *metallidurans* NG7*_mRFP1* & C. *metallidurans* NG7_Δ*pyrE_mRFP1:* A) 0 hours & B) 336 hours. Top and bottom panels are relative to *C. metallidurans* NG7*_mRFP1* & *C. metallidurans* NG7*_*Δ*pyrE_mRFP1*, respectively. From left to right panels represents dot plots of FSC/SSC, singlets, and Yoyo-1-stained cells.

Following optimization of the staining protocol, the independent biological replicates of *C. metallidurans* NG7_*mRFP1* and *C. metallidurans* NG7_Δ*pyrE_mRFP1* were pooled and analysed for i) comparison of the live cells and ii) difference in mRFP1 expression. No statistical difference in the number of live cells between the different strains was found (Figure 41A). However, the percentage of live cells expressing mRFP1 was found to be statistically different between *C. metallidurans* CH34 NG7_Δ*pyrE_mRFP1* and *C. metallidurans* CH34 NG7_*mRFP1* with the former being always above 70 % (Figure 41B).

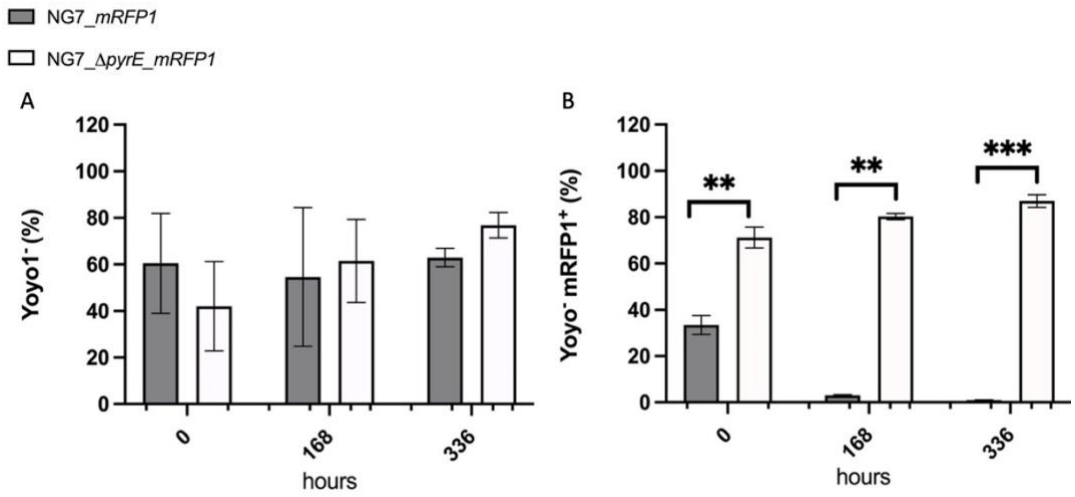

Figure 41-Percentage live cells (Yoyo-1-) and live cells expressing mRFP1 (Yoyo-1$^-$, mRFP1$^+$): Samples were stained with Syto9 and Yoyo-1. Yoyo-1 was used to discriminate between live and dead cells by means of FC. A) comparison of live cells of *C. metallidurans* NG7_*mRFP1* (dark gray) & *C. metallidurans* NG7_Δ*pyrE_mRFP1* (white). B) live cells expressing *mRFP1* (Yoyo-1$^-$/mRFP1$^+$) of *C. metallidurans* NG7_*mRFP1* (dark grey) & *C. metallidurans* NG7_Δ*pyrE_mRFP1* (white). Statistical significance was calculated by means of Mann-Whitney test: ** $p<0.01$, *** $p<0.0001$, **** $p<0.00001$. Error bars represent standard deviation (n=2).

Next, to have a better insight on the difference in mRFP1 expression, the relative Median Fluorescence Intensity (rMFI) of *C. metallidurans* NG7_Δ*pyrE_mRFP1* compared to *C. metallidurans* NG7_*mRFP1* was calculated and a histogram of the mRFP1 intensity against the number of cells (cell count) with a given intensity of mRFP1 was also built (herein shown only for the sample at 336 hours). The shift of the mRFP1 intensity reported in the histogram correlating mRFP1 intensity with the number of events and the rMFI of *C. metallidurans* CH34 NG7_Δ*pyrE_mRFP1* compared to *C. metallidurans* CH34 NG7_*mRFP1* highlighted a difference of over 30-fold in the rMFI of the complemented auxotrophic strain compared to the control strain between time 0 and 336 hours (Figure 42A, Figure 42B and Table 11).

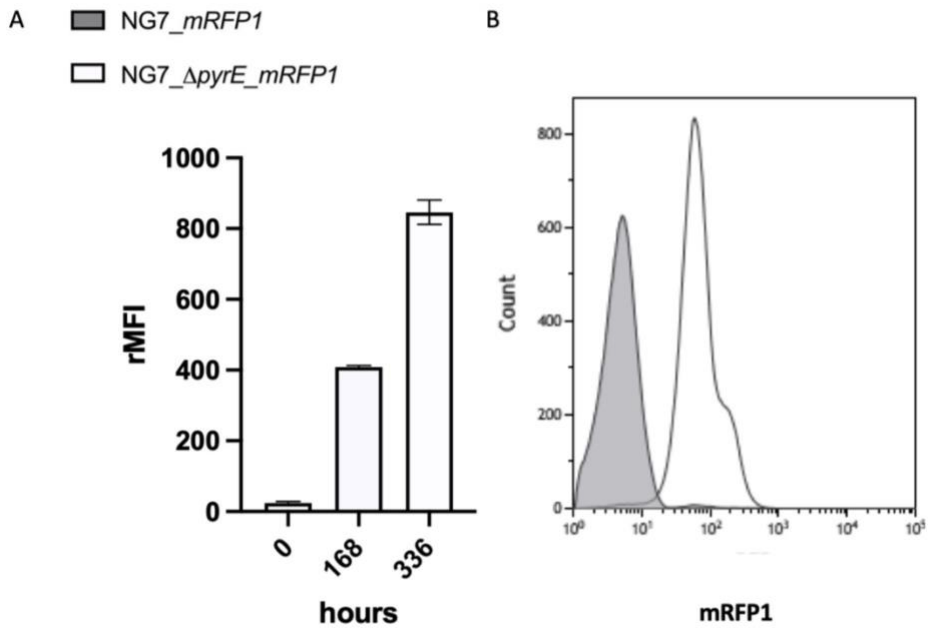

Figure 42-rMFI of *C. metallidurans* NG7_Δ*pyrE_mRFP1*& histogram of mRFP1 intensity: A) rMFI of *C. metallidurans* NG7_Δ*pyrE_mRFP1* throughout duration of the experiment. Error bars represent standard deviation (n=2). B) Histogram correlating mRFP1 intensity with the number of events for the samples collected at 336 hours. Error bars represent standard deviation (n=2). NG7_*mRFP1* and NG7_Δ*pyrE_mRFP1* in the legend represent strains *C. metallidurans* NG7_*mRFP1* and *C. metallidurans* NG7_Δ*pyrE_mRFP1* respectively.

Table 11-rMF1 of mRFP1 for *C. metallidurans* NG7_Δ*pyrE_mRFP1* and fold difference of the rMFI between time 0 and 336 hours*:* Standard deviation calculated from 2 replicates (n=2) is reported

Strain	**rMFI**		
	0 hours	**168 hours**	**336 hours**
C. metallidurnas NG7_Δ*pyrE_mRFP1*	24.84 ± 4.299	408.714 ± 3.98	846.666 ± 34.395
Fold-difference between rMFI at 0 hours and 336 hours	34.084		

Despite *C. metallidurans* NG7_Δ*pyrE_mRFP1* appeared to be efficient in terms of plasmid maintenance and mRFP1 expression compared to *C. metallidurans* NG7_*mRFP1* in the conditions tested, the presence of the multidrug resistance IncP-1α plasmid makes manipulation of this strain challenging as well as posing a potential environmental and health hazard. Furthermore, lack of pMOL30 significantly reduces *C. metallidurans* CH34 NG7 resistance to some heavy metals, which is a desirable trait for biotechnological and bioremediation processes. Altogether, these limitations hinder the use of this *C. metallidurans* strain in further downstream applications.

4.6.5 Plasmid Stability Test in *C. metallidurans* CH34 Δ*pyrE_mRFP1*

The aim of this section was to test if *C. metallidurans* CH34_Δ*pyrE_mRFP1* (I.E uracil auxotrophic *C. metallidurans* CH34 transformed with pMTL71301_P_{pan}*mRFP1*_P_{trpsyn}*pyrE*FA1090) was capable of stable plasmid maintenance and expression of mRFP1 when grown in continuous heterotrophic conditions. This experiment was started at the beginning of the early outbreak of the COVID-19 pandemic and PST could only be performed for 48 hours before the first

national lockdown was proclaimed in the UK, which made the laboratory inaccessible for three months. Compared to the previous experiment performed in *C. metallidurans* NG7 strains, the following differences were tested:

i) The percentage of Na-gluconate was increased from 0.4% to 2% since high cell density is a desirable trait in industrial context

ii) Replica plating for the PST was performed by adding uracil on SGMM Gen^{+} plates to account for "social cheaters". In mono-species bacterial cultures, typical of a biotechnological context, cells are in constant cooperation and communication with each other. This cooperation is often defined by the presence of "public goods", namely products synthesised by the bacterial cells and secreted in the culture medium that are available to the whole microbial community. The cooperative fraction of the population will produce a certain public good that will be exploited by a subpopulation of cheaters, which is unable to synthetize that specific chemical. In the short term, cheaters have a fitness advantage over the cooperators since they do not need to invest energy to produce the public good. However, when the subpopulation of cooperators becomes too small to sustain growth of the cheaters, these start to die off and are replaced by cooperators. Eventually, the total population will reach a state where the fractions of cooperators and cheaters are in equilibrium with each other[208,209].

During continuous growth, the subpopulation of the *C. metallidurans* CH34_Δ*pyrE_mRFP1* culture that retained the plasmid kept decreasing throughout the duration of the experiment (Figure 43, Table 12), while no significant differences

in terms of growth could be observed between this strain and the control (Figure S5). Complete plasmid loss in continuous setup has been suggested to be caused by the lower growth rates of cells bearing the plasmid, due to the metabolic burden plasmid replication and protein expression have on the host cells[210]. The fact that plasmid loss was observed in continuous in *C. metallidurans* CH34_Δ*pyrE_mRFP1*, even though uracil auxotrophy should have ensured the plasmid to be stably maintained throughout the generations, might be explained by the presence of social cheaters cross-feeding on uracil. Pure cultures of *P. aeruginosa* grown on casein as sole carbon and energy source, were shown to degrade casein via extracellular proteases for which expression is quorum-sensing-dependent. However, during continuous growth, mutants defective for expression of these protease (I.E social cheater) were noticed to arise and benefit from the catabolism of the casein but eventually reached an equilibrium between the cheaters and cooperative fraction of the culture[211]. Therefore, it is possible that plasmid loss in pure cultures of complemented uracil auxotrophic strain of *C. metallidurans* CH34 was due to opportunistic cheaters cross-feeding on uracil. This implied, an equilibrium between cheaters and cooperative cells could have been eventually reached, so that only a fraction of the total bacterial population still retained the plasmid, resulting in lower-than-expected protein expression levels.

Table 12-results of the PST of *C. metallidurans* CH34_*mRFP1* & *C. metallidurans* CH34_Δ*pyrE_mRFP1*

	Plasmid-retaining cells (%)	
Hours	***C. metallidurans* CH34_*mRFP1***	***C. metallidurans* CH34_Δ*pyrE_mRFP1***
0	18.35 (± 11.22)	56.62 (± 0.73)
24	14.77 (± 0.31)	44.87 (± 24.29)
48	8.88 (± 7.85)	30.98 (± 3.12)

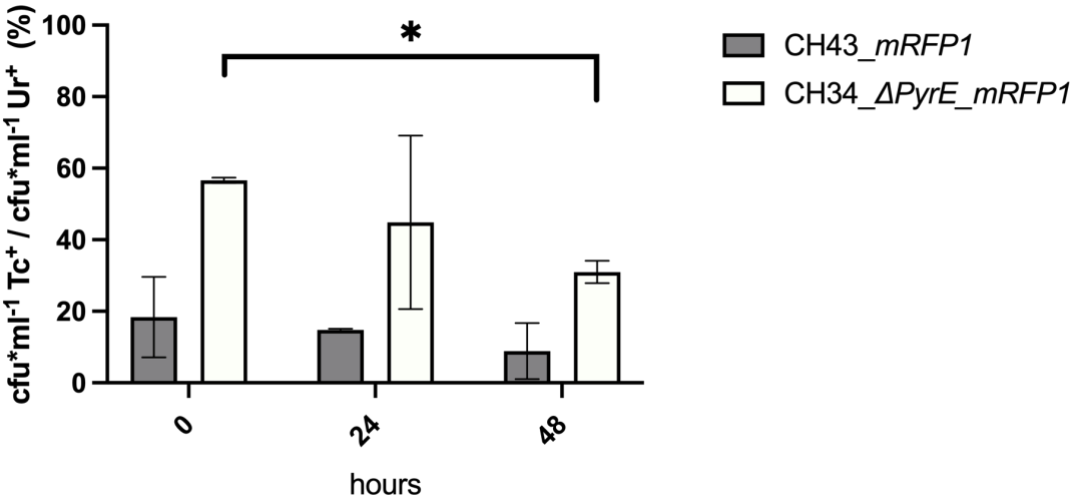

Figure 43-Plasmid Stability Test of *C. metallidurans* CH34 & *C. metallidurans* CH34_Δ*pyrE_mRFP1*: *C. metallidurans* Strains were transformed with plasmids pMTL71301_P_{Pan}*mRFP1* & pMTL71301_ P_{Pan}*mRFP1*_P_{trpsyn}*pyrE*FA1090, respectively and grown in continuous for 48 hours with 2% SGMM. Every 24 hours culture samples were collected, serially diluted and 20 µL of each dilution were spotted on SGMM Gen^+ Ur^+ and SGMM Gen^+ Tc^+. The percentage of cells retaining the plasmid was then calculated. Statistical significance was assessed with Mann-Whitney test. * $p<0.05$ with error bars representing standard deviation (n=2). CH34_*mRFP1* and CH34_Δ*pyrE_mRFP1* in the legend represent strains *C. metallidurans* CH34_*mRFP1* and *C. metallidurans* CH34_Δ*pyrE_mRFP1* respectively.

C. metallidurans CH34 Δ*pyrE_mRFP1* showed significant plasmid loss during continuous growth, while *C. metallidurans* NG7_Δ*pyrE_mRFP1* displayed

significantly improved stability, compared to its wild type counterpart. Stability/expression experiments of *C. metallidurans* CH34_Δ*pyrE_mRFP1* and *C. metallidurans* NG7_Δ*pyrE_mRFP1* cannot be directly compared because of the difference in concentrations of the carbon source used. Therefore, it could not be inferred whether the loss of the complementation/expression plasmid observed with *C. metallidurans* CH34_Δ*pyrE_mRFP1* was the result of genetic differences between the *C. metallidurans* CH34 and *C. metallidurans* NG7 (pMOL30^{-}, IncP-1α^{+}) strains or a consequence of the "social cheating" behaviour adopted by a sub-population of cells.

As the episomal complementation of uracil auxotrophy in *C. metallidurans* CH34 did not improve plasmid stability significantly, when this strain was grown to high cell densities under heterotrophic conditions, an alternative approach was considered. Due to the intrinsic problem of cross-feeding, and the time-consuming protocols to achieve uracil auxotrophic strains and their subsequent complementation, strategies involving partitioning and toxin/antitoxin (TA) systems were explored next.

4.6.6 Use of the Multimer resolution & Toxin/Antitoxin System from IncP-1α for development of a PAS in *C. metallidurans* CH34

4.6.6.1 Stability of IncP-1α in *C. metallidurans* CH34

As *C. metallidurans* NG7 was cultivated without selection multiple times for various experiments, it was reasonable to assume that IncP-1α plasmid was stably maintained and propagated in this strain. Stability of this multidrug resistant plasmid has been studied extensively between the 1980's and 1990's. Deletion experiments identified the major stability determinants to be *IncC,* and *korB* gene members of the active partitioning systems[212] and the *parCBADE* gene cluster[213]. *parCBADE* is

composed of two divergent operons. Of these, *parCBA* is involved in plasmid segregation since it encodes proteins that play a role in resolving plasmid multimers, a major cause of plasmid instability[214,215], while the *parDE* operon codes for a TA system that is known to trigger post-segregational killing of plasmid-less cells[216]. This system was shown to be the minimal region necessary for stabilising a different range of plasmids in prokaryotes[213,217]. Roberts *et al.* demonstrated that cloning of the *parCBADE* in mini RK2 backbones resulted in plasmid stability in the absence of selection in a number of bacterial species, including *E. coli* TG1, *P. aeruginosa* PA01161Nal, *A. tumefaciens* A348, in both LB and M9 media for over 100 generations. On the other hand, using only *parDE* was insufficient for plasmid stabilization in LB, although it did improve plasmid maintenance in minimal media with some bacterial strains[199]. In the same study, different plasmid types than RK2 were successfully stabilised, thereby demonstrating the potential universality of the system. Therefore, I decided to clone the *parCBADE* cluster in a mini RK2 plasmid to test if these stabilization determinants would suffice to provide plasmid stability in *C. metallidurans* CH34. To confirm stability of IncP-1α in *C. metallidurans* NG7, I firstly performed a PST. To do so, *C. metallidurans* NG7 was grown in 25 mL LB media in the absence of selection in 250 mL E-Flasks. The cultures were re-inoculated in fresh media every day to stimulate cell division. The presence of the plasmid was also tested daily, by replica plating randomly picked bacterial colonies obtained from the liquid cultures on LB Gen^+ & LB Gen^+ Tc^+. As it can be observed in Figure 44, IncP-1α plasmid proved to be stable for the whole duration of the experiment (8 days) suggesting that *parCBADE*, alone or in combination with other stability determinants

already present in the plasmid backbone, may be promoting efficient segregation and maintenance of IncP-1α.

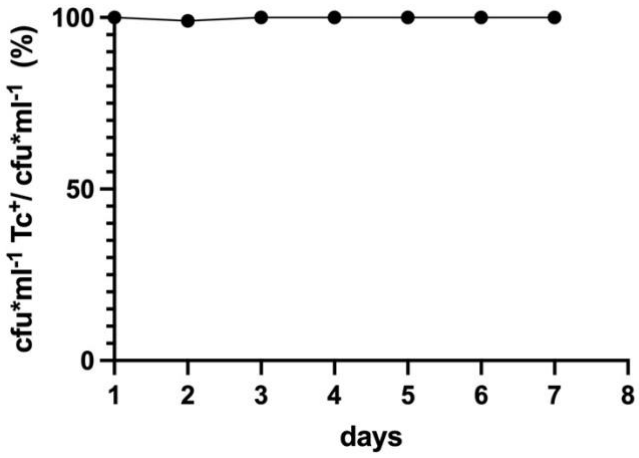

Figure 44-Plasmid stability test of IncP-1α in *C. metallidurans* NG7: *C. metallidurans* NG7 was grown in LB media in E-Flasks for 8 days with daily media change. Cells were replica plated on LB Gen^+ and LB Gen^+ Tc^+ to calculate plasmid stability (n=3).

4.6.6.2 PST of pMTL74301Low_*parCBADE* in *C. metallidurans* CH34 & *C. metallidurans* AE126

pMTL74301Low and pMTL74301Low_*parCBADE* were successfully cloned. These were then transformed in *C. metallidurans* CH34 and AE126 and tested for PST, as previously described in section 4.4.10. As can be seen in Figure 45, both plasmids were lost, regardless of the strains, over the course of the experiment. Therefore, loss of pMTL74301Low_*parCBADE* was deemed to be due to lack of other genes necessary for stabilization of IncP-1α plasmid in *C. metallidurans* NG7. It is possible that members of the active partitioning system *IncC & korB* might be necessary for stabilization of mini RK2 in *C. metallidurans* CH34. Deletion of these genes from an otherwise intact IncPα R995Δ*incC* plasmid led to high instability in *P. putida* despite the presence of a functional copy of the *parCBADE* system[212].

Nevertheless, there is evidence pointing towards an additive stabilization mechanism of the *incC/parCBADE* systems for plasmid maintenance, rather than a strict reciprocal dependence. Indeed, stability analysis of R995 with deletions in both *incC* and *parCBADE* loci showed that plasmid variants R995Δ*incC*Δ*par*, R995Δ*incC* and R995Δ*par* were retained by 6%, 75% and 98% of the cells in *P. aeruginosa* cultures, respectively[212]. Therefore, it is possible additional stabilization determinants are needed to provide segregational stability to mini RK2 plasmids in *C. metallidurans* CH34.

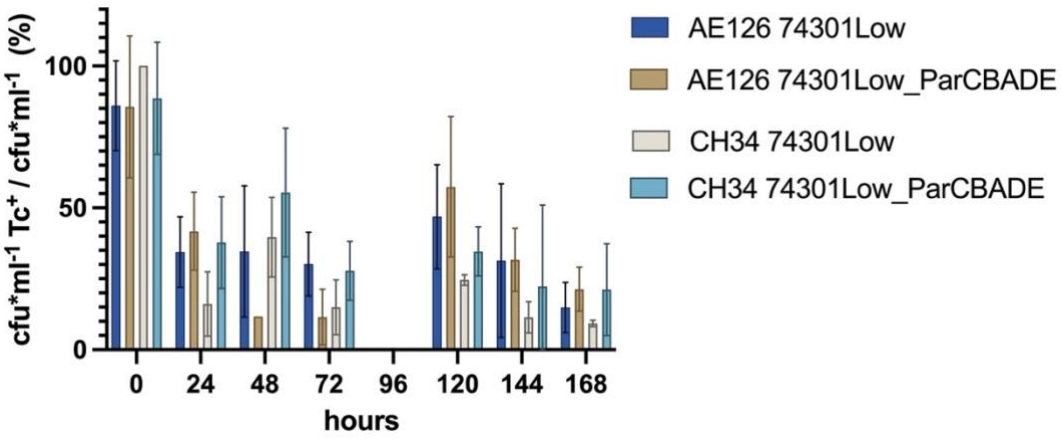

Figure 45-Plasmid Stability Test of pMTL74311_*parCBADE* in *C. metallidurans* CH34 & AE126: Both strains were transformed with plasmid pMTL74301Low and pMTL74301_parCABDE and grown in LB in E-Flask with daily media change for 8 days. Cells were replica plated on LB Gen^+ and LB Gen^+ Tc^+ to calculate plasmid stability. The percentage of cells retaining the plasmid was eventually calculated. Error bars represent SD (n=3).

4.7 Conclusions

Firstly, it was discovered that the *in-house* strain of *C. metallidurans* NG7 lacked pMOL30 and had an additional IncP-1α multidrug resistance plasmid. This made this strain less appealing for biotechnological applications due to the presence of drug-resistance determinants and lack of desirable traits (I.E heavy metal resistance genes in pMOL30).

Secondly, the 5-FOA mediated evolution strategy was successful in obtaining uracil auxotrophic strains of *C. metallidurans* NG7 and *C. metallidurans* CH34 and further complementation in *trans* of the *pyrE* gene on a pBBR1 plasmid, showed that growth could be restored in minimal media. The uracil auxotrophy-based PAS was tested for plasmid maintenance and protein expression in continuous growth conditions in *C. metallidurans* NG7 and *C. metallidurans* CH34.

Almost complete plasmid loss was observed in *C. metallidurans* NG7 wild type strains compared to the complemented uracil auxotrophs. This strongly suggested failure to express the SNAP-tag from a plasmid platform in Chapter 3 was due to segregational instability of the pBBR1 expression plasmid pMTL71101_P_{BAD}_*SNAP_aidA-C* plasmid.

C. metallidurans CH34_Δ*pyrE_mRFP1* was unable to show stable plasmid maintenance for the duration of the experiment (disrupted by the Covid19 global pandemic) most likely due to social cheaters using the excess of uracil secreted in the medium. Therefore, an alternative PAS based on the *parCBADE* stabilization determinants of the multidrug resistance IncP-1α plasmid was studied. The *mrs* (*parCBA*) and *psk* (*parDE*) systems of IncP-1α were not sufficient to confer stability to our in-house mini RK2 plasmid when *C. metallidurans* was grown in continuous conditions. This highlights the importance of developing reliable molecular tools to

introduce chromosomal insertions in *C. metallidurans* CH34 for metabolic engineering and heterologous protein expression purposes. Since the CRISPR-Cas system has become the most popular molecular biology technique for editing genomes of a variety of species across the kingdoms of biology, the next chapter of this thesis is concerned with the feasibility of employing the CRISPR-Cas9 technology for generation of insertions & deletions in the genome of *C. metallidurans* CH34 for carrying out physiological studies and investigating potential bioprocessing applications.

5 -Development of promoter libraries & a CRISPR-Cas9 Tool for Marker-Free Genome Modifications in *C. metallidurans* CH34

5.1 Background: Strategies to Achieve Successful Editing With CRISPR-cas9 in Bacterial Genomes

Despite the exceptional potential of *C. metallidurans* CH34 as an industrial microbial chassis, the literature lacks proof-of-concept studies highlighting the versatility of this microorganism for biotechnological applications. One of the major limitations hindering the progress of such studies, is the scarcity of genetic tools for heterologous protein expression and genome modification. The most used technology for genome modification of *C. metallidurans* CH34 is a suicide plasmid-based homologous recombination (HR), which is highly inefficient and time consuming (See section 1.6.3.1). Since its discovery, spCas9 systems have been extensively used for establishment of efficient and robust technologies for isolation of recombinant strains of prokaryotic and eukaryotic origin[218,219]. Development of successful CRISPR-spCas9 technologies for selection of HR-mediated recombinant isolates in *C. glutamicum*[220], *R. sphaeroides*[221], *M. capsulatus*[222], *C. necator* H16[223] and *Clostridia sp.*[84] were all shown to be dependent on two main factors. On the one hand, the avoidance of toxicity of Cas9 by tightly controlling its expression via use of inducible promoters[223] and/or orthogonal synthetic riboswitches[84] to achieve transient expression. On the other hand, the use of strong constitutive promoters for expression of sgRNA. However, as different microbes respond dramatically differently to regulation sequences such as promoters, optimization of CRISPR-Cas systems must be performed prior to its successful application to different bacterial hosts. Another limitation, is the necessity of using conjugation as means for plasmid delivery, which is a long and tedious process when compared to electroporation[224]. Furthermore, when using conjugation, good counterselection against *E. coli* is required, by either using plates with antibiotics to which the target organism is resistant and *E. coli* is

susceptible or by using the 2,6-Diaminoimelic acid auxotrophic *E.coli* MFDPir strain[225].

In summary i) knowledge of regulatory elements like active promoters in the host is essential along with ii) optimization of expression of components of the CRISPR-Cas system for successful implementation in novel bacterial strains of industrial interest.

5.2 The Use of Riboswitches for Tight Control of Protein Expression

Riboswitches are a type of short regulatory RNA (sRNA) sequences. sRNA were first discovered as non-coding RNA that were able to regulate expression of specific genes in *E.coli*[226]. These molecules are typically 50-500 nucleotide-long *trans*-acting elements which bind with non-perfect base matching the target mRNA(s) and regulate its expression at post-transcriptional level[227]. On the contrary, riboswitches are *cis*-acting elements which are placed on the 5' UTR of the co-transcribed gene and are composed of an aptamer domain, specific for a ligand, and an expression domain needed for regulation of the downstream gene[227]. Depending on the characteristics of the riboswitch, upon binding of the ligands, riboswitch regulation varies from transcription and translation initiation/termination and RNA degradation. Therefore, sRNA and Riboswitches can be used to regulate synthetic genetic circuits and are of great interest for the synthetic biology and biotechnology community. In particular, riboswitches offer an alternative to the use of inducible promoters, which have been traditionally employed to control expression of heterologous proteins upon presence of an inducer molecule, such as the P_{BAD} promoter[228,229]. Inducible promoters require multiple protein-based factors to be functional: codon usage optimisation for production of proteins necessary for their functioning; protein folding and membrane

permeability to the required inducer might differ greatly depending on the expression system[227]. Indeed, some inducible promoters that proved to have an ON/OFF response in presence and absence of an inducer molecule in *E.coli,* failed to be functional in other hosts[181]. On the contrary, synthetic riboswitches can be engineered as orthogonal genetic systems affected exclusively by the presence of a specific inducer, thereby generating a predictable outcome regardless of the host. Theophylline-dependent synthetic riboswitches have been engineered which have an ON/OFF regulation for heterologous protein expression in a vast array of microorganisms[230] and have been used to date in many microorganisms as an alternative to inducible promoter systems[231]. Once transcribed, theophylline-dependent riboswitches form a stem-loop that sequesters the RBS, thereby preventing translation. Upon addition of theophylline, the secondary structure is relaxed, and the ribosome binding site sequence becomes available for translation to occur (Figure 53 shows the mechanism of action of a theophylline-inducible riboswitch controlling expression of the *mRFP1* gene).After discovery of the TCT8-4 theophylline dependent aptamer[232], subsequent studies generated libraries of theophylline-sensitive riboswitches with different mutations located between the ligand domain and the Shine-Dalgarno sequence. These were studied with β-Galactosidase as reporter gene, in order to quantify the ability of the synthetic riboswitch to repress protein expression in absence of theophylline[29,232,32]. Eventually, five synthetic theophylline-dependent riboswitches named E[231] and F-I[84] were built and tested in different hosts such as *E. coli, Agrobacterium tumefaciens, Acinetobacter baumanni, Mycobacterium smegmatis, Bacillus subtilis and Streptococcus pyogenes*[231] demonstrating that theophylline-dependent riboswitches were capable of regulating expression of β-Galactosidase to a certain extent but regulation level still differed depending on the host.

5.3 Aim of the Study

The overall goal of this study was to develop genetic tools for protein expression and genetic modifications in *C. metallidurans* CH34. This was performed by:

i) Developing a library of constitutive promoters with a wide range of expression levels that can be used to express heterologous proteins in *C. metallidurans* CH34

ii) Testing of theophylline-dependent riboswitches E^{231} and $F\text{-}I^{84}$ to tightly regulate expression of Cas9 in *C. metallidurans* CH34.

iii) Using the newly developed promoter and riboswitch libraries for optimization of a CRISPR-Cas9 system for selection of recombinant *C. metallidurans* CH34 clones.

iv) Exploiting the CRISPR-Cas9 Riboswitch system to generate *pilAE, pilA* and *pilE* knockout strains to investigate whether type IV pili may be involved in EET in *C. metallidurans* CH34 (see Chapter 6).

5.4 Materials & Methods

5.4.1 Construction of CRISPR plasmids

Firstly, it was investigated if the RiboCas system developed by Cañadas et al[84]., could be used to select for recombinant clones of *C. metallidurans* CH34 *phaC1* gene (Rmet_1356). The RiboCas regulon of Cañadas and colleagues was composed of two modules. The first section was involved in regulation of *cas9* and it was composed of the P_{fdx} promoter from *C. sporogenes*, Riboswitch E^{231} (hereafter referred to as RBE), *cas9* and CD0164 terminator from *C. difficile.* The second module was instead engaged in expression of the sgRNA and it was constructed of P_{AraE} from

C. acetobutylicum, RNA scaffold (SIBS RNA, for the formation of the riboprotein complex between *cas9* and the sgRNA)[233], and the terminator of the *fdx* gene of *C. difficile*. This system, together with the sgRNA and homology arms to target *phaC1* was cloned in pMTL74311 for generation of pMTL74311_RiboCas_Δ*phaC1* as follows (Figure 46, plasmid map in figure S11)[6]. pMTL74311 was digested with *Eco*RI and *Asc*I and the digested fragment was isolated via agarose gel electrophoresis and subsequently purified. pRECas1_Cpas_sgRNAonly*phaC1* was used as template for PCR amplification of the RiboCas regulon containing *cas9* under control of the P_{fdx} promoter in the non-leading strand and the P_{AraE} in the leading strand controlling expression of the sgRNA with primer pairs RiboCas_74311EcoRI_Fw/RiboCas_AraE_Rv. The SIBS RNA scaffold was amplified from the same template with primer pairs SIBS_sgPhaC1SpeI_Fw/SIBS_LHAPhaC1_Rv. The forward primer was synthetized with addition of the sgRNA targeting *phaC1* gene as oligonucleotide spacer. Left and right homology arms were amplified with primer pairs LHA_PhaC1_Fw/Rv and RHA_PhaC1_Fw/Rv respectively. The fragments were assembled for generation of pMTL74311_RiboCas_Δ*phaC1*.

[6] Experiment performed in collaboration with Dr. marco Garavagla (marco.garavaglia@nottingham.ac.uk)

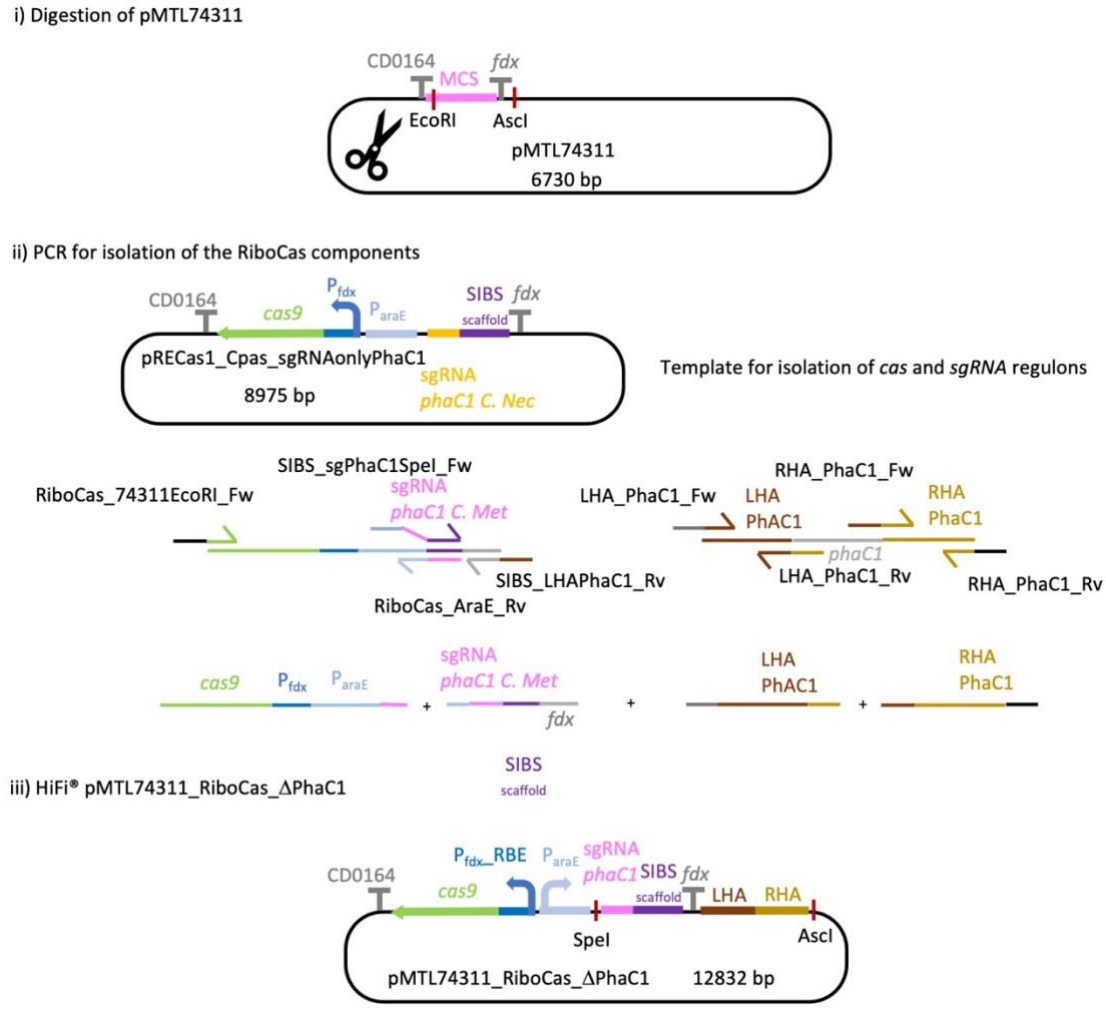

Figure 46-Cloning strategy of pMTL74311_RiboCas_Δ*phaC1*: detailed description is in the text**.** The colour coding is: pink for the multiple cloning site, gray for the terminator sequences, light green for *cas9*, blue for the P_{fdx} promoter, azure for P_{araE}, pink for the sgRNA targeting *phaC1*, brown and gold for the LHA and RHA respectively.

To create suitable vectors for the study of the P_{fdx} riboswitch library in *C. metallidurans* CH34, plasmids pMTL71101_P_{fdx}_RBx_*mRFP1*[7] (x stands for the riboswitch cloned in the specific plasmid), prepared by Dr. Garavaglia (unpublished results), were used for subcloning in pMTL71301. Plasmid pMTL71301 and pMTL71101_P_{fdx}_RBx_*mRFP1* were digested with *Sbf*I and *Xho*I. The DNA bands relative to the digested pMTL71301 and the P_{fdx}_RBx_*mRFP1* digested fragments

7

were ligated as already described in section 2.2. This procedure was performed for cloning of vectors pMTL71301_P_{fdx}_RBD_*mRFP1*, pMTL71301_P_{fdx}_RBE_*mRFP1*, pMTL71301_P_{fdx}_RBF_*mRFP1*, pMTL71301_P_{fdx}_RBF_*mRFP1*, pMTL71301_P_{fdx}_RBG_*mRFP1*, pMTL71301_P_{fdx}_RBH_*mRFP1*, pMTL71301_P_{fdx}_RBI_*mRFP1*, pMTL71301_P_{fdx}_RBJ_*mRFP1*, pMTL71301_P_{fdx}_L_*mRFP1.*

Next, a P_{BAD}-riboswitch library was constructed to investigate the expression profile of a hybrid promoter-riboswitch regulon as double inducible system for protein expression. A schematic representation of the cloning procedure of the P_{BAD}-riboswitch library can be seen in Figure 47-General cloning strategy for the riboswitch library under control of the P_{BAD} promoter pMTL71301 was digested with *Sbf*I and *Xho*I, separated via agarose gel electrophoresis and purified as already described in section 2.2. The P_{BAD} promoter and *mRFP1* protein were amplified via PCR from pMTL71301_P_{BAD}_*mRPF1*. *mRFP1* amplification was performed with primer pairs designed with homology arms to the digested backbone (Reverse) and the P_{BAD} promoter. Forward primers were also endowed of a spacer sequence for insertion of the riboswitch of interest upstream the *mRFP1*. Amplification of the P_{BAD} promoter was performed with primer pairs AraC_pbad_gt_Fw/Rv. Amplification of *mRFP1* was done by using the common reverse primer Rb_RFP_Rv and with forward primers Rb_Dx_RFP_Fw (x stands for the riboswitch of interest, Table 4). All fragments were eventually assembled thereby generating plasmids pMTL71301_P_{BAD}_RBD_*mRFP1*, pMTL71301_P_{BAD}_RBE_*mRFP1*, pMTL71301_P_{BAD}_RBF_*mRFP1*, pMTL71301_P_{BAD}_RBG_*mRFP1*, pMTL71301_P_{BAD}_RBH_*mRFP1*, pMTL71301_P_{BAD}_RBI_*mRFP1*, pMTL71301_P_{BAD}_RBG_*mRFP1*,

pMTL71301_P_{BAD}_RBI_*mRFP1*, pMTL71301_P_{BAD}_RBJ_*mRFP1*, pMTL71301_P_{BAD}_L_*mRFP1*.

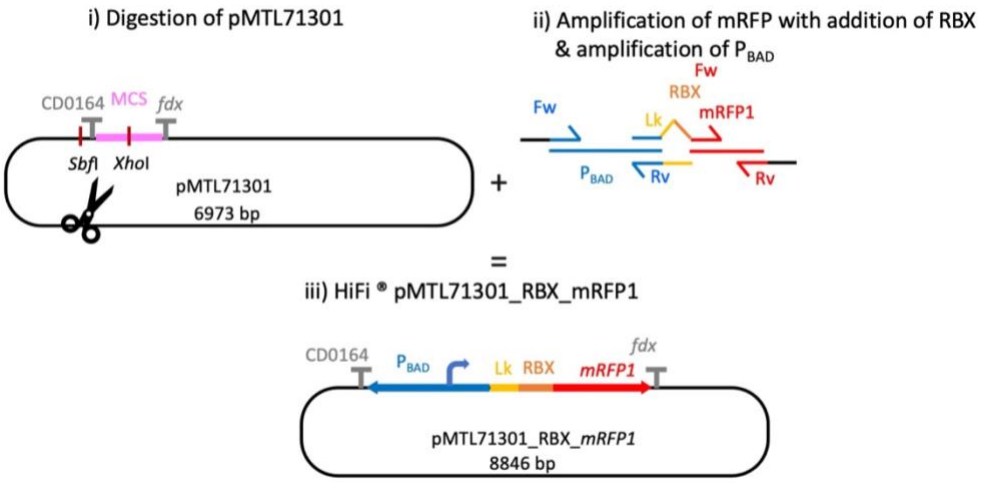

Figure 47-General cloning strategy for the riboswitch library under control of the P_{BAD} promoter: Detailed description is in the test. The colour coding is: pink for the MCS, gray for the terminator sequences, blue for the P_{BAD} promoter, yellow for the linker, brown for the RBX, and red for the *mRFP1*.

Following this, a constitutive promoter library was built. A schematic representation of the cloning procedure of can be seen in Figure 48. pMTL71301 was digested with *Not*I and *Nhe*I, run and purified from 1% agarose gel as already described. Depending on the length of the promoters used, their sequence was either amplified via PCR from a DNA template (promoter >100bp) or included as spacers in the primers for *mRFP1* amplification (promoter <100bp). Amplification of *mRFP1* was performed with primer pairs with the reverse primer endowed of homology arms for the digested backbone and forward primer with homology arms for the promoter under scrutiny. The template used for amplification of *mRFP1* was pMTL71301_P_{BAD}_*mRP1*. Briefly, isolation of the promoter and/or *mRFP1* amplicons for assembly in pTML71301 was performed as follows: P_{Pan} was amplified from pUT57 template with primer pairs Pan_71301NotI_Fw/Pan_*mRFP1*_Rv and *mRFP1* with mRFP_Pan_Fw/mRFP1_71301NheI_Rv. P_{λ} was added to *mRFP1* as

spacer with primer pairs λmRFP1NotI_Fw/mRFP1_71301NheI_Rv. P_{OA0284} was amplified from gDNA of *C. metallidurans* NA4 with primer pairs POA0284_mRFP1NotI_Fw/POA0284_mRFP1_Rv and *mRFP1* with mRFP_POA0284_Fw/mRFP1_71301NheI_Rv. P_{ARAE} was amplified from pRECas1-IIE with primer pairs AraE_71301NotI_Fw/AraE_mRFP1_Rv and *mRFP1* with primer pairs mRFP1_AraE_Fw/ mRFP1_71301NheI_Rv respectively. J23119 was added to *mRFP1* as a spacer with primer pairs mRFP1J23119NotI_Fw/ mRFP1_71301NheI_Rv and lastly, P_{trpsyn} was added to *mRFP1* as a spacer with primer pairs mRFP1_Ptrpsyn_71301NotI_Fw/mRFP1_71301NheI_Rv. Therefore, plasmids pMTL71301_P_{pan}*mRFP1*, pMTL71301_P_{λ}*mRFP1*, pMTL71301_P_{OA0284}*mRFP1*, pMTL71301_P_{AraE}*mRFP1*, pMTL71301_P_{J23119}*mRFP1* and pMTL71301_P_{trpsyn}*mRFP1* were assembled and transformed in *E. coli* DH5α.

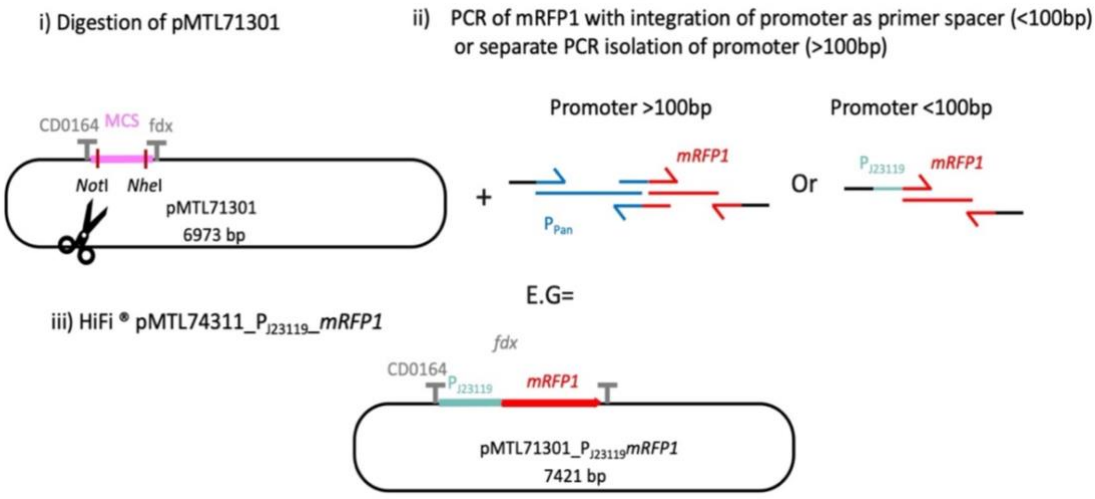

Figure 48-General cloning strategy for the constitutive promoter library: Detailed description is in the test. The example given shows cloning of the P_{J23119} promoter. Since PJ23119 is smaller than 100bp, its sequences was included in the forward primer for amplification of *mRFP1*. The colour coding is: pink for the MCS, gray for the terminators, blue for the P_{Pan}, light green for P_{J23119}, red for *mRFP1*.

Next, to investigate if the promoter tested could lead to expression of the CRISPR-*cas9* components and subsequent genome editing in *C. metallidurans* CH34,

plasmid pMTL74311_RBIC9_Δ*pyrE* was cloned to target the *pyrE* gene. To do so, pMTL74301 was digested with *Eco*RI and *Asc*I and gel purification of digested backbone fragment. *cas9* was isolated via PCR from pMTL74311_*cas9*_Δ*phaC*1[8] with primers Cas9RBI_74311EcoRI_Fw and Cas9RBI_J23119_Rv. This plasmid contains P_{BAD}-RBI for expression of *cas9* and P_{AraE} for expression of the sgRNA. The reverse primer binds on the *pfdx* terminator sequence downstream of *araC* and includes the nucleotide sequence of the P_{J23119} promoter for expression of the sgRNA. Amplification of the SIBS RNA scaffold was performed with primers SIBS_J23119_Fw/ SIBS_LHAPyrE_Rv, with the forward primer having the sgRNA targeting *pyrE* and inserted as a spacer together with a unique *Spe*I restriction site. Amplification of 800bp right and left homology arms from the genome of *C. metallidurans* CH34 was performed with primer pairs LHAPyrE_SIBS_fw/LHAPyrE_RHA_Rv and RHAPyrE_LHA_Fw/RHAPyrE_74311AscI_Rv. All the fragments were then assembled in pMTL74311 with the NEBuilder® HiFi® DNAAassembly Cloning kit (Figure 49).

[8] Cloned by Dr Marco Garavaglia for targeting of *phaC1* of *C. Necator* H16

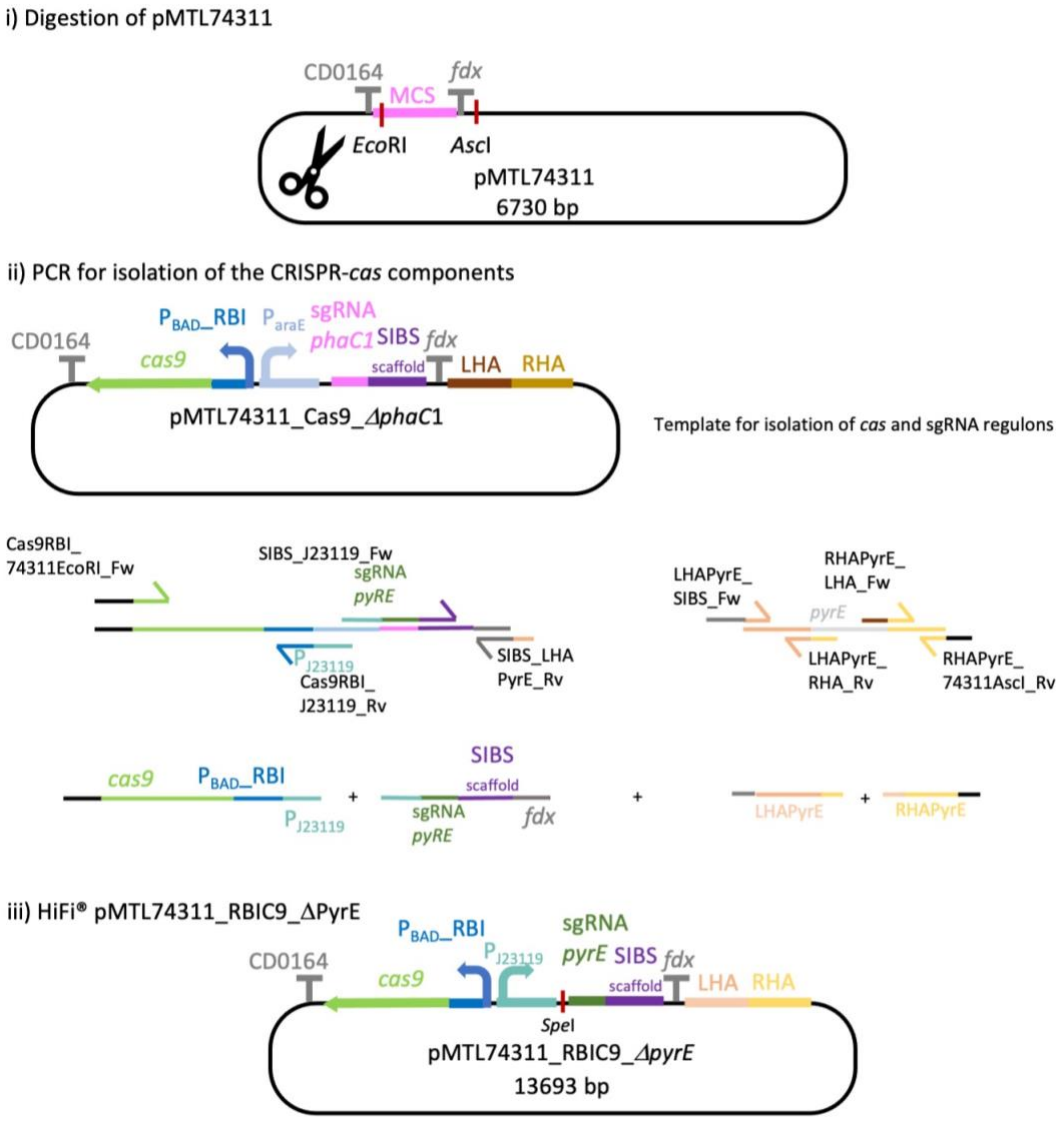

Figure 49-Cloning strategy of pMTL74311_RBIC9_Δ*pyrE:* Detailed description is in the test. The colour coding is: green for *cas9*, blue for P_{BAD}_RBI, tale for P_{J23119}, dark green for sgRNA*pyrE*, purple for the SIBS scaffold RNA, pink and yellow for LHA and RHA respectively.

Following, plasmids pMTL74311_RBIC9_Δ*pilA*, pMTL74311_RBIC9_Δ*pilE* and pMTL74311_RBIC9_Δ*pilAE* were built to obtain knockouts of *pilA*, *pilE* and *pilAE* loci, respectively. Plasmids pMTL74311_P_{BAD}RBIC9_Δ*pilAE*::*gfp* and pMTL74311_P_{BAD}RBIC9_Δ*pilAE*::λ*gfp* were also created to determine the ability of the CRISPR-Cas9 system to perform insertions, a necessary feature to develop recombinant strains for metabolic engineering. The strategy used to construct

pMTL74311_RBIC9_Δ*pilAE* is herein reported as an example. pMTL74311_RBIC9_Δ*pyrE* was digested with *Asc*I/*Spe*I and the fragments containing the CRISPR-*cas* module, and the SIBS RNA scaffold were separated via agarose gel electrophoresis and purified as reported in section 2.2. The SIBS scaffold was amplified from the correct digested fragment of the plasmid pMTL74311_RBIC9_Δ*pyrE* via PCR with the primer pair sgRNA_RBIC9SpeI_Fw/SIBS_LHAPilA_Rv. The forward primer included the sgRNA for targeting the *pilAE* locus and a *Spe*I restriction site as spacers. Left and right homology arms were amplified by means of PCR with primer pairs LHAPilA_SIBS_Fw/LHAPilA_RHA_Rv & RHAPilA_LHA_Fw/RHAPilA_RBIC9AscI_Rv, respectively. RHAPilA_RBIC9AscI_Rv also introduced an *Asc*I restriction site. The fragments were then assembled in the digested backbone via the NEBuilder® HiFi DNA Assembly Cloning kit for generation of pMTL74311_RBIC9_Δ*pilAE* (Figure 50, all the plasmid maps for the validation experiments of the CRISPR-Cas9 system are reported in Figures S13-15).

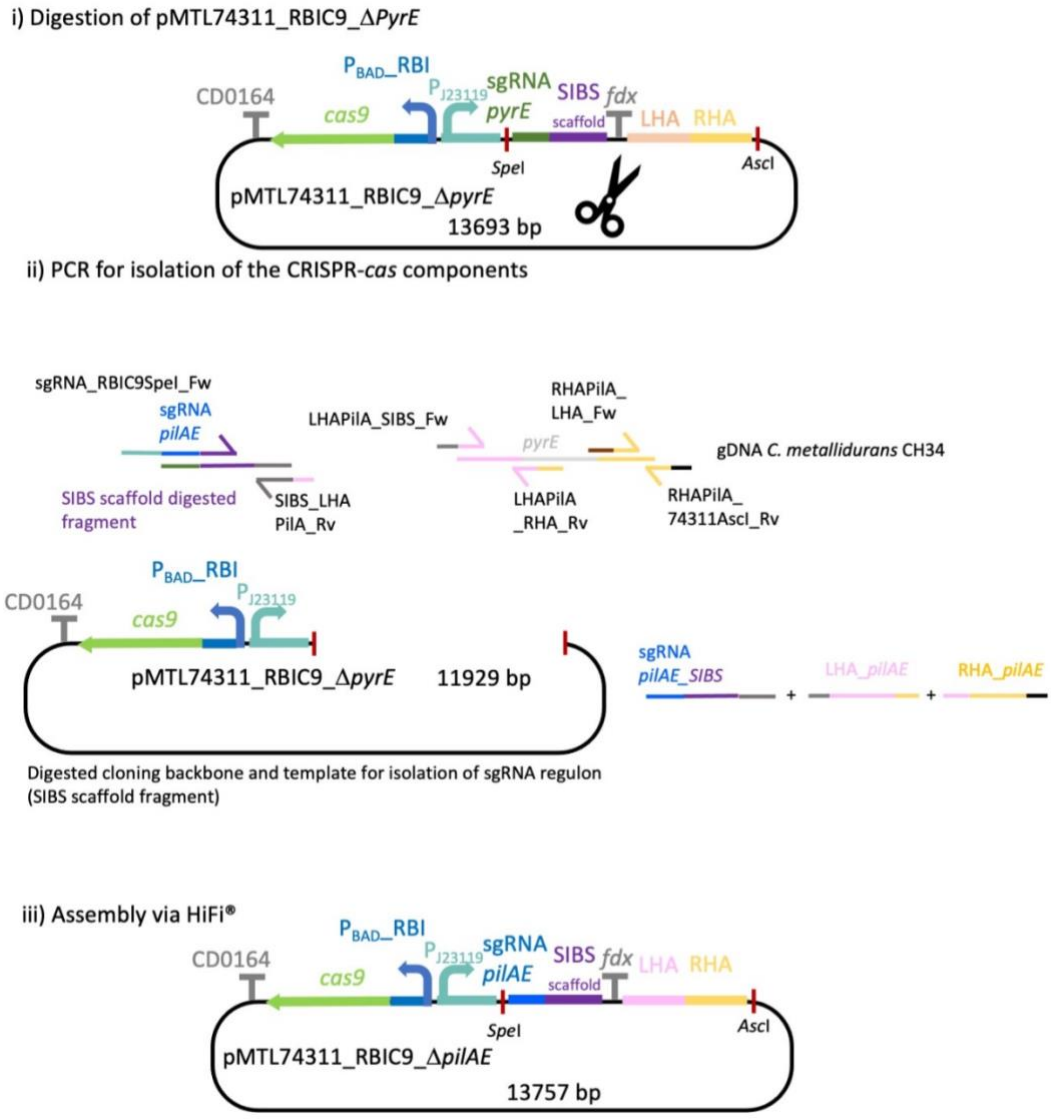

Figure 50-cloning strategy for pMTL74311_RBIC9_Δ*pilAE:* Detailed description is in the test. The colour coding is: gray for the terminators, green for *cs9*, blue for P_{BAD}_RBI, teal for P_{J23119}, light bllue for sgRNA targeting *pilAE*, purplle for the SIBS scaffold and pink and yellow for the LHA and RHA respectively.

5.4.2 PST of pMTL71301 and pMTL74311 in *C. metallidurans* CH34

The aim of this experiment was to find a suitable cloning vector for delivery of the CRISPR-Cas9 system in *C. metallidurans* CH34, which would then be cured after editing. To do so, the in-house plasmids pMTL71301 (pBBR1 replicon) and pMTL74311 (IncP-1 replicon, the origin of replication of RK2 plasmids) (Figure S12 with relevant restriction sites) were electroporated in *C. metallidurans* CH34. After

selection of successful transformants on LB Tc^+ agar plates, three biological replicates for each strain were subjected to PST (See section **Error! Reference source not found.**). Briefly, three independent single colonies were grown in LB media in E-Flasks without selection, changing the media daily to dilute the cultures. Samples were taken every 24 hours, serially diluted and subjected to the Miles-Misra methodology[237] by plating on LB Gen^+ and LB Gen^+ Tc^+ agar plates and calculating the percentage of cells retaining the plasmid.

5.4.3 Study of Promoter and Riboswitch Libraries

This section describes the materials and methods used to study the expression level of *mRFP1* reporter gene under the control of different regulatory elements. *C. metallidurans* CH34 was electroporated with the plasmids for the riboswitch or constitutive promoter libraries, which construction can be found in section 5.4.1. Cultures from three single colonies deriving from three independent transformation events were set up in 5 mL LB media supplemented with tetracycline. Following this the cultures were resuspended to OD_{600} 0.05 in fresh LB media and 200 µL was distributed in a black bottom 96 well plate (Thermo Scientific™). The plates were incubated in a Cytomat 2C incubator at 30 ˚C, 800 rpm for 48 hours and were fed into a Molecular Devices SpectraMax i3 plate reader using a PreciseSCARA robotic arm OD^{600}. mRFP1 expression levels were monitored every 2 hours. mRFP1 was excited at 585 nm and emission was detected at 620 nm and OD measurement was done at 600 nm. mRFP1 levels (Arbitrary Units, A.U.) at the end of the experiment were plotted for each plasmid construct for the constitutive promoter and riboswitch library. mRFP1 expression levels for the P_{fdx} promoter library were studied by addition of

5mM theophylline. For the P_{BAD} library, 0.1% arabinose was also added to the LB. Activation ratios were calculated as follows:

P_{fdx} promoter library: $Activation\ ratio = \frac{mRFP1\ A.U\ (+Theophylline)}{mRFP1\ A.U\ (-Theophylline)}$

P_{BAD} promoter library: $Activation\ ratio = \frac{mRFP1\ A.U\ (+Theophylline + Arabinose)}{mRFP1\ A.U\ (-Theophylline + Arabinose)}$

5.4.4 Protocol for Isolation & Confirmation of Recombinant Clones with the CRISPR-Cas9 System

The protocol for isolation of recombinant clones was adapted from the work of Cañadas and colleagues[84] and can be visualized in Figure 51-Protocol for isolation of recombinant clones of *C. metallidurans* CH34 after delivery of the RiboCas system. To do so, *C. metallidurans* CH34 was grown as already described in LB media. Plasmids pMTL74311_RBIC9_Δ*pyrE*, pMTL74311_RBIC9_Δ*pilAE* and pMTL74311_RBIC9_Δ*pilAE::gfp* were delivered via conjugation, plasmid pMTL74311_RBIC9_Δ*pilAE::λgfp* was delivered via both conjugation and electroporation, while pMTL74311_RBIC9_Δ*pilE* and pMTL74311_RBIC9_*ΔpilA* were delivered via electroporation only. Following, is a detailed protocol for isolation of recombinant clones of *C. metallidurans* CH34 with the optimized CRISPR-Cas9 system.

Selection of transformants & isolation of Mother Colonies: 3-5 days after delivery of the plasmid, transformants were selected on LB Tc^+ Gen^+ agar plates. Two colonies for each transformation event were streaked on LB Tc^+ Gen^+ agar plates to generate the Mother Colonies with enough biomass for induction.

Induction of the Mother Colonies: 1 μL loop was used to resuspend the mother colonies in 100 μL of PBS. These were then plated on LB Induction agar plates (LB IND, supplemented with tetracycline, gentamycin, 5mM theophylline, 0.1% arabinose) and incubated at 30 ˚C for 3-5 days.

Confirmation of recombinant isolates: Isolates growing on the LB induction agar plates were then streaked on LB Gen^+ agar plates and subjected to colony PCR with

primers pair external to the homology arms and primer pairs with one primer external to the homology arms and the other primer inside the deleted genes.

Curing of CRISPR-Cas9 plasmids: Recombinant clones were grown overnight in LB Gen+ at 30 ˚C 200 rpm, serially diluted, plated on LB Gen^+ agar plates and incubated at 30 ˚C for 24 hours. 48 isolates were resuspended in 100 µL of PBS and replica plated on LB Tc^+ Gen^+ and LB Gen^+ to verify plasmid loss.

Storage of the recombinant isolates: cPCR was performed again on isolates which lost the plasmid (not growing on LB Tc^+ Gen^+ agar plates). These were then grown overnight in LB Gen+ and eventually cryo-stocks were prepared as described in section 2.1.2. To obtain the Δ*pyrE* knockouts, the following modifications were made to the protocol.

cPCR was performed for screening of knockouts in the *pilAE* locus of *C. metallidurans* CH34, according to the following strategy:

a) *C. metallidurans* CH34 Δ*pilAE* was the first knockout attempted and it was screened with primers PilAUp2_Fw/PilEDw_Rv (OUT_OUT2), which were initially found to amplify unspecific product on the negative control. Therefore, knockout mutants *C. metallidurans.* CH34 Δ*pilA* and *C. metallidurans* CH34 Δ*pilE* were screened with primer pairs PilA_Up3_Fw/RHA_Dw4_Rv (OUT_OUT) binding outside *pilA* and *pilE* homology arms to confirm the respective deletions. *C. metallidurans* CH34 gDNA and the plasmid delivered for induction of the CRISPR-Cas9 system were used as positive and negative controls, respectively (Figure S8).

b) Internal primers to the deleted genes were also used to perform cPCR to exclude the presence of mixed populations of knockout and *wild type* strains. For confirmation of *C. metallidurans* CH34 Δ*pilAE/*Δ*pilA* primer pairs PilA_Up3_Fw/PilA_Sq_Rv (OUT_InPilA) were used with PilA_Sq_Rv binding inside the CDS of *pilA*. *C. metallidurans* Δ*pilE* knockouts were confirmed via cPCR with primer pairs PilA_Up3_Fw/PilE_Sq_Rv (OUT_InPilE) with PilE_Sq_Rv binding in the CDS of *pilE*. *C. metallidurans* CH34 gDNA. The plasmid delivered for induction of the CRISPR-Cas9 system were used as positive and negative controls, respectively (Figure S8).

For generation of Δ*pyrE* knockouts of *C. metallidurans* CH34 with the CRISPR-Cas9 system, four independent experiments were performed. For each experiment, plasmid pMTL74311_RBIC9_Δ*pyrE* (Figure 58A) was delivered in *C. metallidurans* CH34. The protocol used was the same as for generation of the other knockouts with the following differences.

Selection of transformants & isolation of Mother Colonies: selection of transformants was performed on SGMM Tc^+ Gen^+ Ur^+ agar plates

Induction of the Mother Colonies: Induction was performed on SGMM Tc^+ Gen^+ Ur^+ Th^+ Ar^+ agar plates.

Confirmation of recombinant isolates: confirmation of recombination was firstly performed by replica plating onto SGMM Gen^+ Ur^+ agar plates and SGMM Gen^+ (Figure 58B). Secondly, cPCR was further performed on 12 randomly selected colonies to visualize the size of the *pyrE* locus with primer pairs LHAUp_pyrE_Fw and RHAPyrE_Rv, which bind outside of the left homology arm and external to the 3' end of the deletion, respectively (**Error! Reference source not found.**, Figure

58C). Lastly, PCR bands showing the correct deletions were purified and confirmed via Sanger sequencing with primers pyrE_Fw and RHA_pyrE_Rv (Figure 58D).

Curing of CRISPR-Cas9 plasmids: Recombinant clones were grown overnight in SGMM Gen^+ Ur^+ at 30 ˚C 200 rpm, serially diluted, plated on SGMM Gen^+ Ur^+ agar plates and incubated at 30 ˚C for 24-48 hours. 48 isolates were resuspended in 100 µL of PBS and replica plated on SGMM Gen^+ Tc $^+$ Ur^+ and SGMM Gen^+ Ur^+ to verify plasmid loss.

Storage of the recombinant isolates: this was performed as before, but growth of isolates was done by using SGMM Gen^+ Ur^+ liquid media.

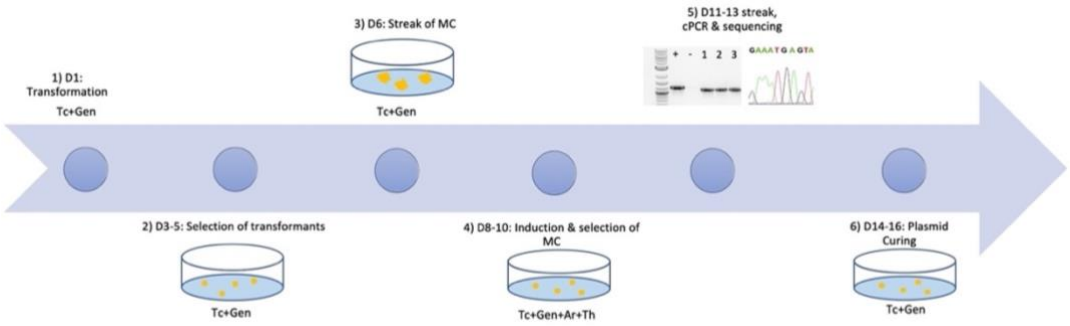

Figure 51-Protocol for isolation of recombinant clones of *C. metallidurans* CH34 after delivery of the RiboCas system: 1) After plasmid delivery (Day 1), 2) colonies grew in 3-5 days and were then 3) streaked plates Tc^+ Gen^+ agar plates to form the mother colonies (Day 6). 4) The mother colonies were induced by plating on plates Tc^+ Gen^+ with addition of theophylline and incubated until growth was observed (Day 8-10). 5) Colonies growing on the plates used for the induction were then streaked on Gen^+ plates, screened by cPCR and sent for sanger sequencing (Days 11-13). Eventually 6) the clones which underwent recombination were subjected to plasmid curing (Day 14-16).

Table 13-List & role of primers used to screen for recombinant clones of *C. metallidurans* CH34

Primer pairs	Primer name	Primers pair function
pyrE	LHAUp_pyrE_Fw & RHAPyrE_Rv	Amplify *pyrE* locus. Bind outside of the left homology arm (Fw) and external to the 3' end of the deletion (Rv).
OUT_OUT	PilA_Up3_Fw	Amplify *pilAE* locus with primers pairs binding outside homology arms
	RHA_Dw4_Rv	
OUT_OUT2	PilAUp2_Fw	Amplify *pilAE* locus with primers pair binding outside and inside LHA & RHA respectively
	PilEDw_Rv	
OUT_InPilA	PilA_Up3_Fw	Amplify *pilA* locus with primers pairs binding outside the LHA and inside *pilA*. Used to confirm pure knockout population
	PilA_sq_Rv	
OUT_InPilE	PilA_Up3_Fw	Amplify *pilE* locus with primers pairs binding outside the LHA and inside *pilE*. Used to confirm pure knockout population
	PilE_Sq_Rv	

5.4.5 Confocal Microscopy of *C. metallidurans* CH34 Δ*pilAE::λgfp*

Super-resolution confocal microscopy was performed to visualize GFP expression in *C. metallidurans* CH34 Δ*pilAE::gfp*; and *C. metallidurans* CH34 Δ*pilAE::λgfp* CH34. The strains were grown according to Section 2.1.2. Cells were resuspended at OD_{600} 0.5 and collected by centrifugation at 4000 rpm for 5 minutes. After two washes in PBS, cell membranes were stained with 5 μM FM® 4-64 (ThermoFisher) dye in PBS for 30 minutes in the dark. After staining, cells were collected by centrifugation

at 2000 rpm for 10 minutes, washed twice in PBS and eventually resuspended in 100 μL of Fluoromount-G™ water based Mounting Medium (ThermoFisher). 5 μL of cell suspension was placed on an 18 mm Borosilicate Glass Square Coverslip (FisherScientific) and mounted on a Frosted Microscope slide (ThermoScientific). Images were taken with a Zeiss Elyra Super Resolution Microscope using a Plan-Apochromat 63x/1.4 Oil DIC M27 objective. SIM (Structured Illumination Microscopy) mode was used with following settings. Two tracks were setup for lasers 488 nm at 4% and 8% power, 100 ms and 200 ms exposure for GFP and FM® 4-64 respectively. SRM (Super Resolution Microscopy) and SIM (Structured Illumination Microscopy) grating periods were 28 μm and 42 μm for the green and red tracks respectively while bandpass filters employed were BP 495-550 + LP 750 for the green channel and LP 655 for the red channel. Channel shift was corrected by using Zen Channel Alignment Tool.

5.5 Results and Discussion

5.5.1 PST of pMTL71301 and pMTL74311 for Selection of Curable Plasmid for Cloning of CRISPR-Cas9 system

PST was performed as reported in section 5.4.2 as shown in Figure 52. Plasmid pMTL74311 was completely lost after 48 hours of continuous culture in the absence of selection as 0% of the cells screened displayed plasmid maintenance. Nevertheless, pMTL71301 was still detectable in the cultures after seven days. The choice of plasmid to be used for CRISPR-Cas9 mediated genome engineering of prokaryotes is often overlooked. One common approach to limit Cas9 toxicity is based on transient transformation of the editing plasmid by using temperature-sensitive replicons. However, these plasmids cannot be used in *C. metallidurans* CH34 as they need a temperature of 37-42 ˚C to be cured[19] and *C. metallidurans* CH34 undergoes Temperature Induced Mortality & Mutagenesis at 37 ˚C[20], the maximum temperature at which growth can be observed. Therefore, as pMTL74311 could be easily cured from *C. metallidurans* CH34, it was chosen as expression platform for the CRISPR-Cas9 system.

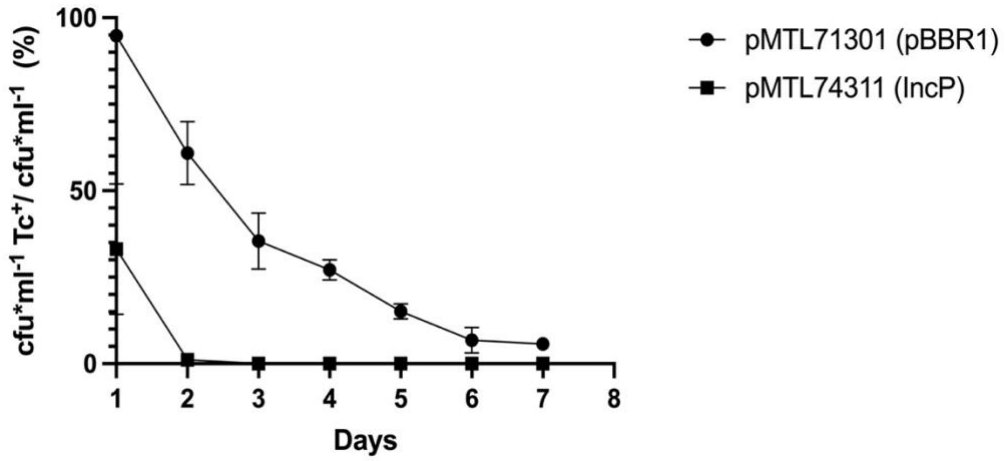

Figure 52-plasmid stability test of pMTL71301 (pBBR1) and pMTL74311 (RK2) in *C. metallidurans* CH34: The percentage of plasmid retaining cells is reported. Error bars represents SD (n=3).

5.5.2 Development of a Protocol for Isolation of Recombinant Clones via the RiboCas System for Generation of *C. metallidurans* CH34 Δ*phaC1*

Firstly, the RiboCas system was cloned into plasmid pMTL74311_RiboCas_Δ*phaC*1 for targeting of the *phaC1* gene (section 5.4.1). After conjugation of the RiboCas plasmid in *C. metallidurans* CH34, a protocol for induction of the genome editing system and screening of the isolates was developed as reported in section 5.4.4 and in Figure 51-Protocol for isolation of recombinant clones of *C. metallidurans* CH34 after delivery of the RiboCas system Despite cPCR being performed for more than 150 isolates grown on LB Tc^+ Gen^+ 5mM theophylline (growth media selective for the recombinant clones), no edited clones were detected. This suggested either the RiboCas in the current configuration was not functional, or the efficiency was too low for rapid selection of recombinant clones.

5.5.3 Optimization of Expression of *cas9* and sgRNA

Since the RiboCas system, as used by Cañadas and colleagues, with P_{fdx} and P_{AraE} controlling expression of *cas9* and sgRNA respectively, could not be used as a selection tool for efficient isolation of HR-mediated recombinant clones of *C. metallidurans* CH34, it was hypothesized this was likely to be due to expression of the RiboCas components not being at optimal levels. Therefore, a new experimental strategy was developed based on fine tuning of expression of the CRISPR-Cas9 components and is summarised as follows:

i) Test of theophyilline induced riboswitches E^{231} and $F\text{-}J^{84}$ under control of the P_{fdx} and P_{BAD} promoters to screen for the combination with the best activation ratio (The fold difference between the maximum and the minimum expression level in the presence and absence of inducers respectively) for tight control of expression of toxic proteins.

ii) Test of a variety of synthetic and heterologous constitutive promoters to screen for suitable candidates (with optimal features being short nucleotide sequence and strong expression) for transcription of the sgRNA.

iii) Identify the Promoter_Riboswitch combination with the best activation ratio to obtain relatively high transient expression of *cas9* and couple this with a strong constitutive promoter, allowing for expression of the

sgRNA at sufficiently high levels to isolate recombinant clones of *C. metallidurans* CH34.

5.5.3.1 Design of the Riboswitch Library

In order to optimize the expression of the CRISPR-Cas9 components, the *mRFP1* reporter gene was cloned under the control of i) synthetic theophylline-dependent riboswitches E[231] and F-J[84], which were placed downstream of either the constitutive P_{fdx} or inducible P_{BAD} promoters[9] and ii) a list of in-house constitutive promoters for optimization of expression of the sgRNA. A general diagram of the design of the genetic construct with the mechanism of action of the theophylline is shown in Figure 53.

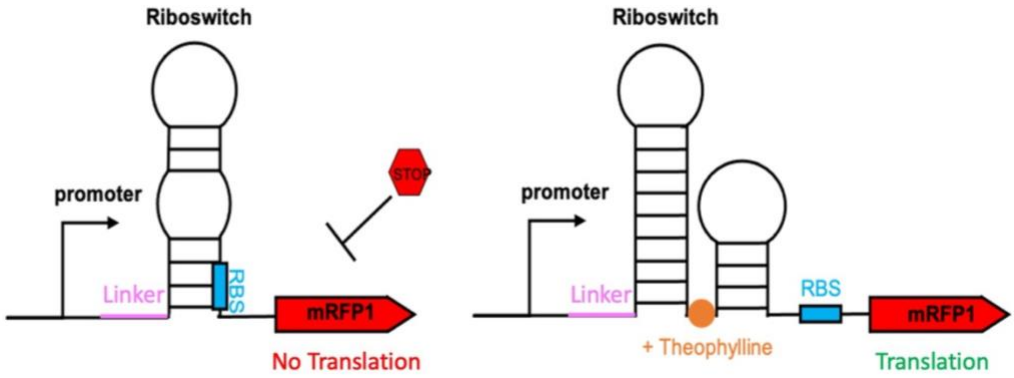

Figure 53-Mechanism to control *mRFP1* expression by means of theophylline-dependent Riboswitches: The *mRFP1* gene was cloned downstream of the regulatory cassettes including either the p_{BAD} or P_{fdx} promoters and each of the tested riboswitch. When theophylline is absent, the riboswitch adopts the OFF conformation and the RBS is sequestered, preventing translation to occur (left panel). When theophylline is added to the system, the secondary structure unfolds, releasing the RBS that becomes accessible for ribosome binding and translation of the mRNA encoding the mRFP1 fluorescent protein. The linker sequence, RBS, theophylline and *mRFP1* cassettes are coloured in pink, blue, orange, and red respectively.

[9]Design and cloning of the Riboswitch library was done in collaboration with Dr. Marco Garavaglia. marco.garavaglia@nottingham.ac.uk

The riboswitches were designed to be fused to a linker region, connecting the promoter sequence to the "core" riboswitch sequence[84]. A construct lacking any riboswitch (L, Linker), but maintaining the RBS was also used as control. Plasmid pMTL71301 was chosen in virtue of its higher stability when compared to pMTL74311 (the backbone assigned for delivery of the CRISPR-Cas9 system) for cloning of the Riboswitch Library. In *C. necator* H16, pMTL74311 was shown to have roughly the same number of copies as pMTL71301 (data not published, obtained in our laboratory by Dr. Ehsaan). Therefore, these two plasmids were likely to yield comparable expression levels of the reporter gene.

P_{BAD} was chosen to include a second control element to minimise basal expression, with the aim to prevent the harmful effects resulting from untimed expression of the toxic protein Cas9. The inducible promoter P_{BAD} is routinely used to control the expression of heterologous proteins in *C. necator* H16[234] and should therefore be active also in the closely related species *C. metallidurans*. The rationale behind the choice of the promoter-riboswitch combination to be used for *cas9* expression was based on the identification of the system that would display the highest activation ratio, which was measured by dividing the expression levels of mRPF1 observed in the presence of theophylline (ON state) by the expression levels in the absence of theophylline (OFF state) (Figure 53). To this end, each of the reporter plasmids carrying the Riboswitch library were electroporated in *C. metallidurans* CH34 as described in section 2.1.8. Table 3 and section 9.1.2 reports the plasmids used in this study and the sequences of the riboswitches respectively.

5.5.3.2 Study of the Riboswitch Library Under Control of the P_{BAD} and P_{fdx} Promoters

The P_{fdx}-Riboswitch and P_{BAD}-Riboswitch plasmids were electroporated into *C. metallidurans* CH34 with the final aim to select the combination of promoter-riboswitch showing a high activation ratio and moderate maximum expression level of the reporter gene. Firstly, the P_{fdx}-riboswitch library was tested. The P_{fxd} promoter showed expression of mRFP1, while all the riboswitches tested showed repression abilities in *C. metallidurans* CH34 despite having different degrees of leakiness. This experiment suggests that leakiness of the P_{fdx}RBE (present in the RiboCas system for control of *cas9* expression) may have been one of the factors that prevented the successful selection of recombinant clones (Figure 54).

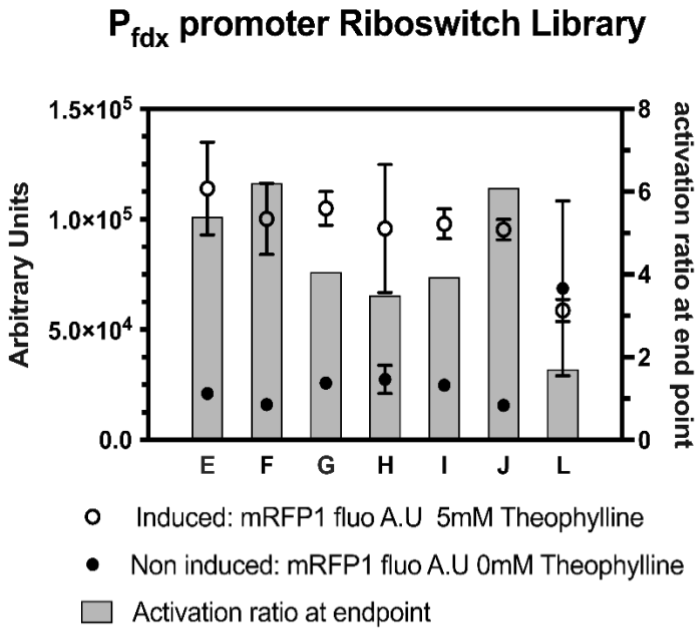

Figure 54-Testing of the P_{fdx} promoter riboswitch library: mRFP1 fluorescence is measured in Arbitrary Units. Empty and full circles represent the mRFP1 A.U. (measured on the left y axis) obtained in ON (5mM Theophylline) and OFF status. Grey bars represent the activation ratios (measured on the right y axis) Error bars represent SD (n=3).

Next, the P_{BAD}-Riboswitch library was tested in presence of arabinose only (OFF state), to provide information regarding the ability of the riboswitch alone to control expression at posttranscriptional level and in presence of both arabinose and theophylline (ON state). When the fluorescence intensity (A.U.) was plotted for each construct, it was noticed that the construct P_{BAD}RBE, P_{BAD}RBG, P_{BAD}RBI, P_{BAD}RBJ all exhibited very good repression of mRFP1 expression in the OFF state. However, P_{BAD}RBE/J and P_{BAD}RBF were excluded from further consideration. Indeed, the former showed a low activation ratio, which is not ideal since sub-optimal Cas9 expression levels are likely to result in the unsuccessful selection of recombinant clones, while the latter displayed high variability in terms of the maximal mRFP1 expression levels recorded in the ON state (Figure 55).

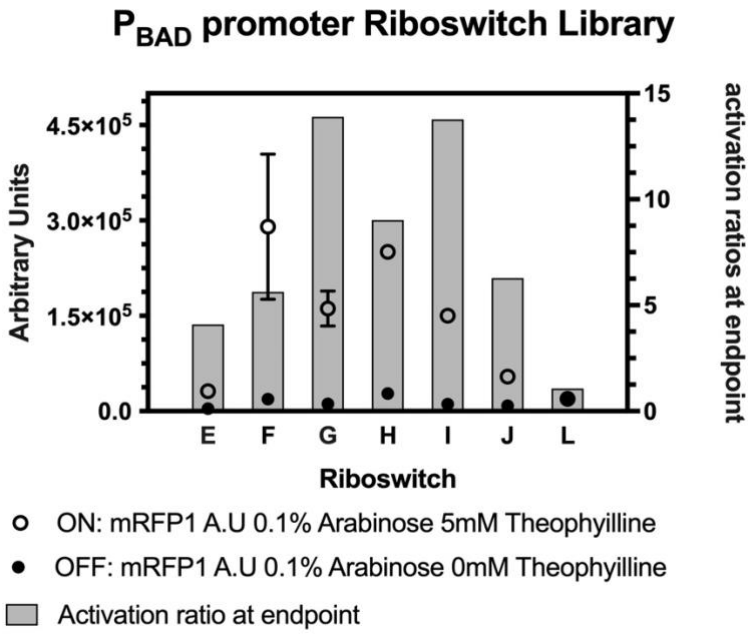

Figure 55-P_{BAD} promoter riboswitch library: mRFP1 fluorescence is measured in Arbitrary Units. Empty and full circles represent the mRFP1 A.U obtained in ON (0.1% Arabinose, 5mM Theophylline) and OFF (0.1% Arabinose) states. Empty and full circles represent the mRFP1 A.U (relative to the left y axis). obtained in ON (5mM Theophylline) and OFF status. Gray bars represent the activation ratios (relative to the right y axis) Error bars represent SD (n=3).

To provide a clearer comparison between the P_{fdx}RBJ and P_{BAD}RBI, the promoter-riboswitch combinations showing the lowest mRFP1 expression in the OFF state, the mRFP1 levels (A.U.) in the absence of theophylline were compared via a Mann-Whitney test. It can be noted that the mRFP1 expression levels measured in the OFF state for the P_{fdx}RBJ construct were approximately 1.4 times higher than those observed with P_{BAD}RBI, under the same experimental condition. Despite the difference in expression levels in the OFF state was statistically non-significant, P_{BAD}RBI was selected as the regulatory cassette to control expression of *cas9* since it showed good repression in absence of theophylline and sufficiently high activation ratio to ensure transient expression of *cas9*.

Table 14-comparison of P_{fdx}RBJ and P_{BAD}RBI leaky expression levels of mRFP1: SD and Activation ratios are also displayed. Error is represented by SD. Mann-Whitney test was performed to check for statistical significance (n=3).

Genetic construct	mRFP1 A.U. in OFF state	SD	Activation ratio	p-value
P_{fdx}RBJ	$1.564*10^4$	1549.469	1.709	n.s
P_{BAD}RBI	$1.089*10^4$	2384.570	13.771	

The relative contribution of both the P_{BAD} and RBI elements in regulation of the mRFP1 protein was further investigated. The P_{BAD}_RBI system lacking both inducers (OFF_OFF) showed virtually no expression of mRFP1. Addition of only theophylline (Th_OFF) resulted in a small increase of expression, which can be attributed to background leakiness of the P_{BAD} promoter[235] (statistically non-significant). However, while addition of only arabinose (OFF_Ar) resulted in a small significantl increased production of mRFP1 ($p<0.00001$), the dramatic difference in expression levels in the OFF_Ar and Th_Ar status (when both inducers were added, $p<0.001$), suggested the riboswitch effectively prevented translation by sequestering the RBS. These results strongly indicate that the P_{BAD}_RBI combination can be used as a reliable ON/OFF system to ensure tight regulation of *cas9* expression and toxic proteins (Figure 56).

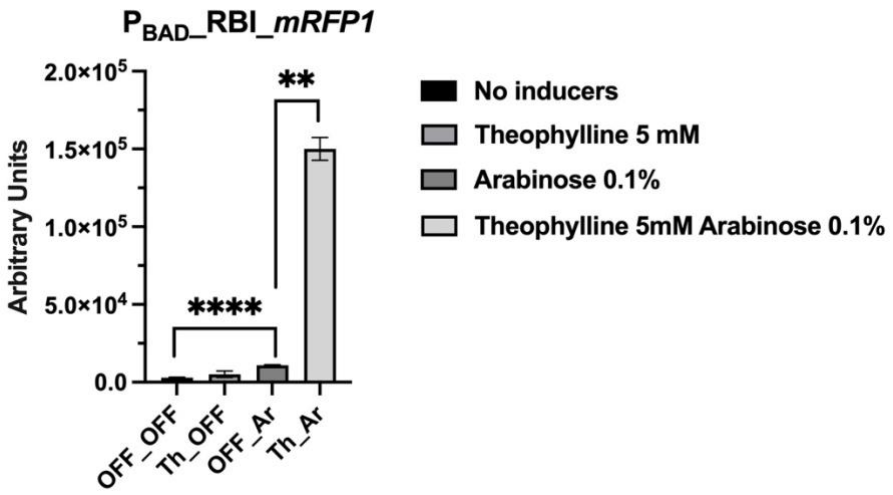

Figure 56-Separate contribution of RBI and P_{BAD} in supressing expression of mRFP1: OFF_OFF, Th_OFF, OFF_Ar and Th_Ar indicate the absence of both inducers, presence of only 5mM theophylline, presence of only 0.1% arabinose or presence of both the inducers. Two tailed Mann-Whitney test was used to calculate statistical significance. ** $p<0.01$, *** $p<0.0001$, **** $p<0.00001$. Error bars represent Standard Deviations (n=3).

5.5.3.3 Construction and Analysis of a Constitutive Promoter library for Expression of sgRNA

The aim of this section was to test protein expression level of few constitutive promoters in *C. metallidurans* CH34. pMTL71301_P_{pan}*mRFP1*, pMTL71301_P_{λ}*mRFP1*, pMTL71301_P_{OA0284}*mRFP1*, pMTL71301_P_{AraE}*mRFP1*, pMTL71301_P_{J23119}*mRFP1* and pMTL71301_P_{trpsyn}*mRFP1* were successfully cloned, delivered in *C. metallidurans* CH34 and studied for expression level of *mRFP1*. The results of these experiments showed that the promoters tested were characterised by different levels of strength. While some promoters showed low to mid activity, such as P_{trpsyn}, λ and P_{AraE}, P_{Pan} and P_{J23119} displayed strong constitutive expression (Figure 57). Since P_{J23119} is a synthetic promoter of only 35 bp and can be easily cloned by designing primers with the promoter sequence as spacer region, while P_{Pan} is 400 bp long, the former was chosen to express the sgRNAs. Considering that

the availability of molecular tools for *C. metallidurans* CH34 is still very limited, the screening of this promoter library provides valuable information for the scientific community interested in using this species for biotechnological and synthetic biology applications. Promoters with low activities are still useful tools that can be used for complementation of auxotrophies[236] or expression of toxic or difficult-to-purify proteins to avoid formation of inclusion bodies and improve the yield of soluble protein[237].

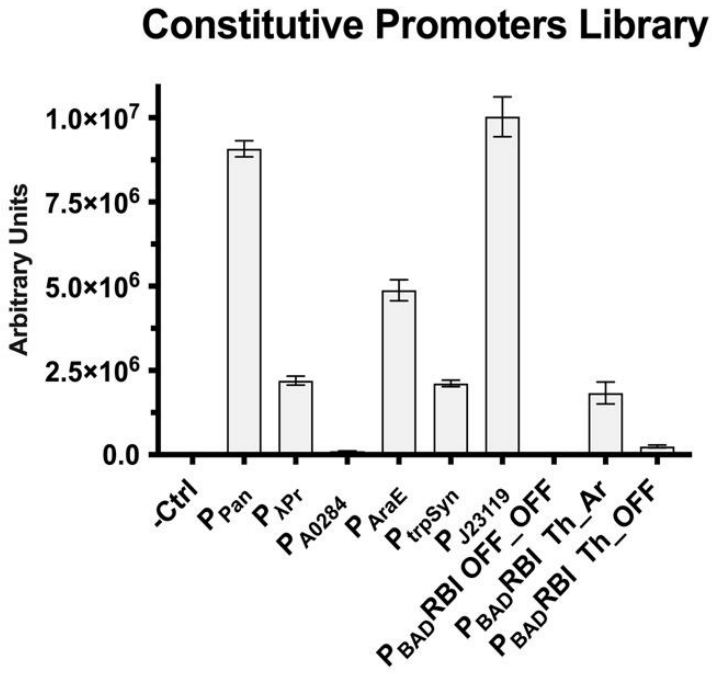

Figure 57-Screening of a constitutive promoter library in *C. metallidurans* CH34: mRFP1 fluorescence is measured in Arbitrary Units. Error bars represent SD (n=3). 5mM Theophylline is added to the growth media.

With the information gathered in the current section the ultimate combination of P_{BAD}_RBI and P_{J23119} was therefore chosen for controlling expression of *cas9* and the sgRNA, respectively. Indeed, the former construct allowed for tight repression and optimal transient expression of *cas9*, while the latter showed high constitutive expression and is small, which is an important feature since plasmid size is inversely correlated with transformation efficiency. These DNA constructs were therefore

cloned in the pMTL74311 (RK2) vector to obtain an easily curable platform for expression of the components of the CRISPR-Cas9 system.

5.5.4 Testing the Optimized CRISPR-Cas9 system by Generation of a *pyrE* Knockout Strain of *C. metallidurans* CH34

The aim of this experiment was to assess the ability of the optimized CRISPR-Cas9 system to generate marker-less recombinant clones of *C. metallidurans* CH34. Based on the results of the promoter and riboswitch libraries, the double-repressed system formed by the P_{BAD}RBI promoter and the constitutive promoter P_{J23119} were chosen for expression of *cas9* and sgRNA respectively. *pyrE* was selected as target for the pilot experiment in virtue of the simplicity of screening based on the mutant's phenotype. As reported in section 4.2.1, replica plating of bacterial colonies on minimal media agar plates with or without uracil can be used to quickly select for uracil auxotrophs, thereby allowing identification of recombinant clones, even in case of low selection efficiency of Cas9. The one-plasmid system pMTL74311_P_{BAD}RBIC9_Δ*pyrE* (Figure 58A), containing all the elements for expression of the CRISPR system and the homology arms for recombination was cloned and delivered to *C. metallidurans* CH34 via conjugation. The plasmid was built so to promote recombination between the homology arms of the plasmid and genomic DNA, eventually leading to deletion of a ~100bp portion at the 5' of the *pyrE* gene between bases 35-130. The choice of the fragment length and location was based on the genome sequencing data of the uracil auxotrophic isolates evolved on SGMM agar plates supplemented with uracil and 5-FOA (see section 4.6.3, and Table 9). As deletions of ~100bp were observed at the 5' end of the *pyrE* gene in the evolved strain *C. metallidurans* CH34 Δ*pyrE,* the targeting sgRNA was chosen as close as possible

to this region to ensure *cas9*-mediated Double Strand Break (DSB) and following recombination would eventually lead to uracil auxotrophy. Small deletions and design of the homology arms in proximity of the cutting site were reported to show increased selection efficiency of recombinant clones in higher eukaryotes, compared to when homology arms were designed far from the editing sites [238,239]. Therefore, the homology arms for recombination were designed to be within 30 base pairs of the cutting site, resulting in the deletion of a small (~100bp) fragment of the *pyrE* gene, rather than the whole CDS.

After delivery of pMTL74311_RBIC9_Δ*pyrE* (Figure 58A), transformants grew on selection plates. After induction of the mother colonies some of the isolates subjected to replica plating, grew on SGMM Gen^+ Ur^+ agar plates but not on SGMM Gen^+, indicating successful selection of uracil auxotrophs (Figure 58A). Following, isolates screened for *pyrE* knockout by cPCR with primer pairs LHAUp_pyrE_Fw and RHAPyrE_Rv showed auxotrophy was due to a deletion in the *pyrE* locus (Figure 58C). Lastly, PCR bands showing the correct deletions were purified and confirmed via Sanger sequencing with primers pyrE_Fw and RHA_pyrE_Rv (Figure 58D) which showed deletion in the *pyrE* locus occurred accordingly to the design of the homology arms in pMTL74311_RBIC9_Δ*pyrE*. All but one of the induced Mother Colonies produced knockouts and overall selection efficiency was of 60 ± 14.9 % (SD, n=4) (Table 15). The one mother colony which failed to produce knockouts, did not show any growth on induction plates, suggesting Cas9 selection may be, in some cases, 100% efficient to prevent growth of non-recombinant clones. However, this is not the case for all the mother colonies tested which showed different efficiencies of recombination among the induced isolates tested. Evolution of bacterial cells is well reported to cause loss of performance in recombinant bacterial strains due to mutation

of recombinant DNA sequences [240,241,242] suggesting that "escapees" might be able to circumvent Cas9 selection, probably by inactivating the portion of the *cas9* gene coding for its endonuclease activity or promoter sequences. *C. metallidurans* CH34 is described as "master survivalist"[43] due to its ability to rearrange its genome in response to challenging environmental conditions, its resistance to high concentration of heavy metals and the ability to metabolize a vast array of pollutants, using them as carbon sources [43,52,180]. In Chapter 4 of this thesis, I showed that plating *C. metallidurans* CH34 in the presence of 5-FOA and uracil results in isolation of uracil auxotrophs by means of *pyrE* loss of function due to the emergence of SNPs, InDels or Structural Variants. Likewise, it is possible that *cas9* may act as an environmental stressor, triggering mutations in *C. metallidurans* CH34 that could either produce catalytically inactive variants of Cas9 or prevent its expression.

Table 15-Summary of *pyrE* knockout experiment: error represent the SD (n=4)

Target	Exp. number	MC	Mutants/Isolates screened	Selection efficiency	Overall efficiency
pyrE	**1**	1	12/12	54 %	60% ± 14.7
		2	1/12		
	2	3	//	100%	
		4	12/12		
	3	5	2/12	58%	
		6	12/12		
	4	7	3/12	29.1%	
		8	4/12		

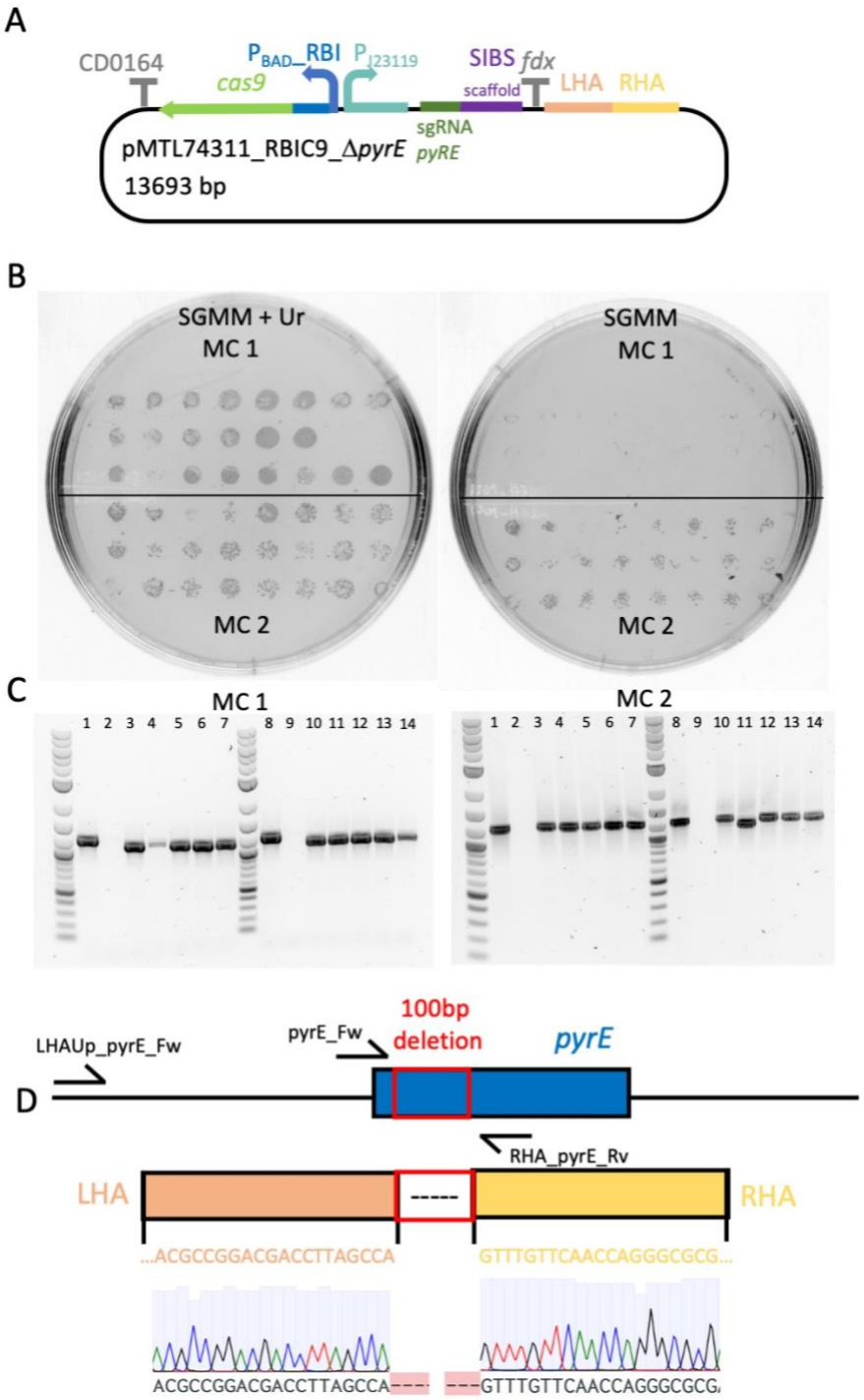

Figure 58-CRISPR-Cas9-mediated isolation of *pyrE* knockouts of *C. metallidurans* CH34: A) Organization of plasmid pMTL74311_RBIC9_Δ*pyrE*. B) Replica plating of isolates of C .metallidurans CH34 on SGMM agar plates with and without uracil (left and right panel, respectively). cPCR identifying the 100bp nucleotide deletion on the *pyrE* gene. D) schematic of the strategy for deletion of the *pyrE* gene and location of the primers used for cPCR amplification of the *pyrE* locus and for Sanger sequencing. The Sanger sequencing chromatogram of a representative isolate is also shown in the bottom panel (D).

5.5.5 Validation of the CRISPR-Cas9 System in *C. metallidurans* CH34: Targeting of Type IV Pili in *C. metallidurans* CH34

One of the aims of my PhD project was to investigate the EET mechanisms *C. metallidurans* CH34 exploits to transmit electrons to solid extracellular electron acceptors, like electrode surfaces[52,148]. However, the lack of molecular tools for the modification of the *C. metallidurans* CH34 genome has so far limited the possibility of performing fast and scarless genome editing for physiological studies. Therefore, to validate the CRISPR-Cas9 system, I decided to target some genes hypothesized to be involved in EET in *C. metallidurans* CH34. In the early 2000's *G. sulfureducens* was shown to be capable of EET, by using type IV pili encoded by the *pilA* gene for transmission of electrons to solid $Fe(OH)_3$[138]. A few years later, *C. metallidurans* CH34 was found to be responsible of biomineralization for solid gold particles from aqueous gold in solution. This process eventually resulted in precipitation of solid gold and formation of biofilms on the gold grains where proteinaceous structures were connecting the cells in the biofilm. These pili were hypothesized to be conductive "nanowires" thought to be responsible for "channelling" excess electrons to the outside of the cell, aiding in the respiration process[51]. Therefore, I firstly conducted a bioinformatic analysis by searching for significant homology of *G. sulfureducens* PilA (GSU1496) with the proteome of *C. metallidurans* CH34. pBLAST was used for this task and two proteins were found to be 46.03% (Rmet_0472, coding for *pilA*) and 60.53% (Rmet_0473, coding for *pilE*) identical to GSU1496. The sequences of these proteins were aligned, and it was observed high conservation of the N-terminal region between the pilins of *C. metallidurans* CH34 and *G. sulfureducens,* highlighting the

possibility that Rmet_0472 & Rmet_0473 might be involved in EET in *C. metallidurans* CH34 (Figure 59).

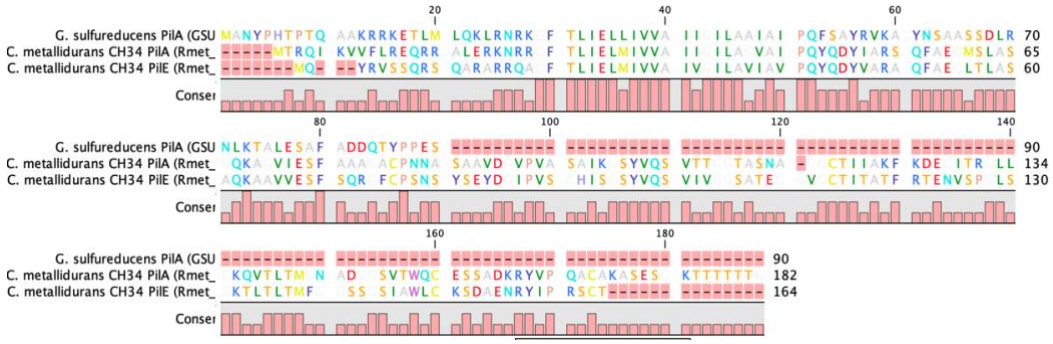

Figure 59-Alignment of primary amino acid sequence of *pilA* from *G. sulfureducens* and *pilA/E* from *C. metallidurans* CH34.

Therefore, with the aim of studying if type IV pili were involved in EET in *C. metallidurans* CH34, Δ*pilA*, Δ*pilE* & Δ*pilAE* knockouts were built by employing the CRISPR-Cas9 tool optimized and tested for deletion of the *pyrE* gene. Plasmid pMTL74311_P_{BAD}RBIC9_Δ*pilAE* was delivered to *C. metallidurans* CH34 via conjugation. However, electroporation was also investigated as a method for delivery of all the other plasmids. This was done because conjugation has been reported to induce the SOS response genes, which eventually can lead to recombination of DNA and unwanted mutations[243] and subsequent isolation of non-isogenic mutants. Furthermore, using this method would save a considerable amount of time (approximately 2 days), particularly when employing a quick protocol for preparation of electrocompetent cells, as described for *P. aeruginosa* POA1[150]. All the knockouts obtained were screened by cPCR, which was carried out as described in section 5.4.4.

The MCs induced to target the *pilAE* locus resulted in 100% editing efficiency. However, recombination of isolates from induction of MC2 resulted somehow in deletion of about 300 bp in the LHA, while MC1 showed only 4 colonies growing on LB IND plates, all of which displayed the intended modification (Figure S8). When

plasmids were delivered by electroporation to target the *pilA* and *pilE* loci, efficiency of selection was 12.5% for both targets. *GFP* was also inserted successfully with 50% efficiency by replacing the *pilAE* region. However, no GFP expression was detected using Super Resolution Confocal Microscopy. In *P. aeruginosa*, presence of the PilA protein was suggested to be required for its own regulation as a complex interaction between the two-component system *pilS-pilA* results in autoregulation of expression of the *pilA* gene[244]. Thereby, it is possible that fine regulation of expression of the *pilA/E* genes may also occur in *C. metallidurans* CH34 and subsequent deletion of *pilAE locus* may have impaired expression from their native promoter, resulting in no production of GFP. As expression of GFP was not detected under control of the native regulatory sequence insertion of *GFP* under control of the λ constitutive promoter was attempted. Initially, plasmid pMTL74311_P_{BAD}RBIC9_Δ*pilAE*::λ*GFP* was electroporated in *C. metallidurans* CH34, resulting in low transformation efficiency. While only 4 out of the 10 mother colonies induced produced isolates on LB IND plates, none of these carried the desired mutation. The same plasmid was also delivered by conjugation, with approximately a 10^2-fold increase in transformation efficiency (Figure 60A). Two mother colonies were induced and a total of 2 out of 93 isolates were confirmed by cPCR to be Δ*pilAE*::λ*GFP* mutants (2.03% efficiency). Therefore, conjugation could be used as delivery method for the CRISPR-Cas9 plasmids herein developed for the genomic integration of toxic proteins to obtain a higher amount of transformants where electroporation fails. *C. metallidurans* CH34 Δ*pilAE*::λ*GFP* was visualized under Super-resolution Confocal Microscopy as described in section 5.4.5. The wild type strain was used to measure basal fluorescence

levels, which were used as reference for comparison with *C. metallidurans* CH34 Δ*pilAE*::λ*GFP* (Figure 60B).

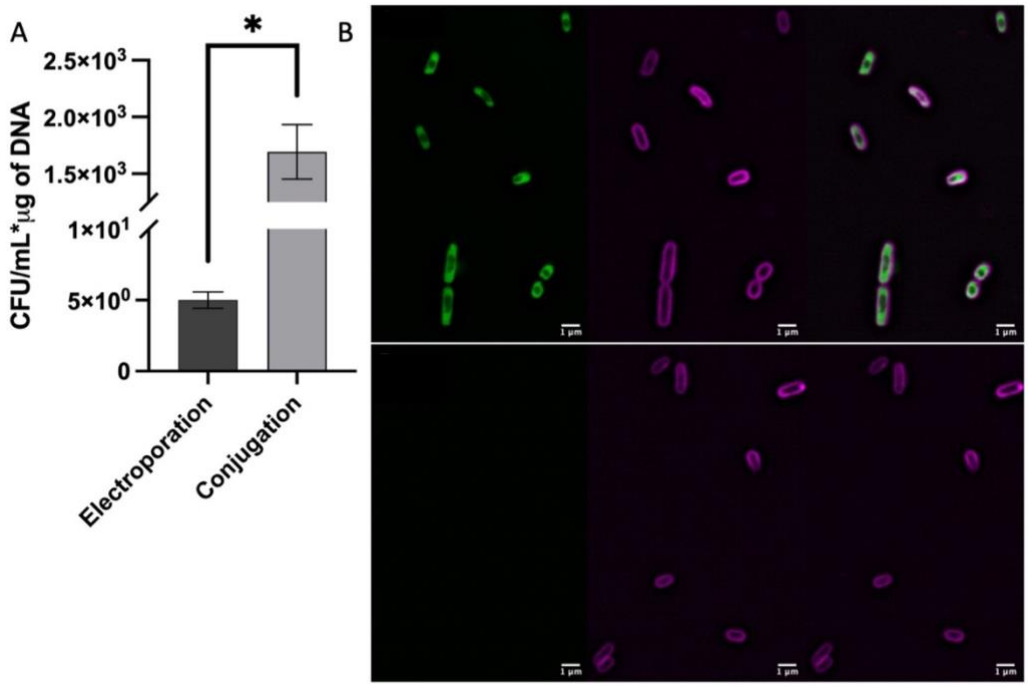

Figure 60-transformation efficiencies of pMTL74311_Δ*pilAE::λGFP* delivered by electroporation or conjugation and confocal microscopy images of *C. metallidurans* CH34 Δ*pilAE::λGFP*: A) Comparison of transformation efficiency of the plasmid pMTL74311_P_{BAD}RBIC9_Δ*pilAE*::λ*GFP* between electroporation and conjugation B) confocal microscopy of *C. metallidurans* CH34 _Δ*pilAE*::λ*GFP* (top panel) and) *C. metallidurans* CH34 wild type (bottom panel). Panels from left to right represent GFP, FM4-64 and overlay channels.

Results of the validation knockout experiments in terms of *cas9*-mediated selection efficiencies are presented in Table 16, while representative agarose gel electrophoresis pictures of the cPCR products confirming *pilE* and *pilA, pilAE::GFP* and *pilAE::*λ*GFP* knockouts are reported in Figure S8 of the supplementary material. Three biological replicates for each of the type IV pili knockouts were conserved for the analysis of potential off-target mutations and future electrophysiological studies.

Table 16-summary of the validation experiments of the CRISPR-Cas9 system herein developed: *Selection efficiency is calculated from 2 mother colonies growing on LB Tc^+ plates from the same transformation event. Delivery of the plasmid was performed by either conjugation (Conj.) or electroporation (Electr.).

Target	Delivery	Mutants/screened	Selection efficiency*
pilAE	Conj.	16/16	100%
pilA	Electr.	3/24	12.5%
pilE	Electr.	3/24	12.5%
pilAE::GFP	Electr.	12/24	50%
pilAE::λGFP	Electr.	0/24	0%
pilAE::λGFP	Conj.	2/93	2.04%

5.5.6 Off-Target Study: Whole Genome Analysis of the Impact of the CRISPR-Cas9 system on *C. metallidurans* CH34

C. metallidurans CH34 wild type and the 3 biological replicates of knockout strains Δ*pilAE*, Δ*pilA* and Δ*pilE* were sent for whole genome Illumina sequencing. The trimmed reads were reassembled and aligned to the reference genome of *C. metallidurans* CH34. SNPs, InDels and SV were called for *C.metallidurans* CH34 wild type using the sequences deposited in the GeneBank database (see Material and Methods section 2.3 for accession numbers and variant calling details) as reference genome. Following this, all the variants found in the knockout strains were filtered against the variants of *C. metallidurans* CH34 used as parental strain to identify any potential off-target mutations. *C. metallidurans* CH34 wild type was found to have 16 variations when compared to the sequence deposited in GeneBank. Three out of 16 variations were in intergenic regions, one of which corresponded to a 375 nucleotides deletion. Notably, 25% of all the variants consisted of inversion or deletion of genes involved in the mobilisation of transposable elements such as Rmet_3142 and Rmet_3143, coding for an IS481 family transposase and a generic transposase, respectively and Rmet_2172 and Rmet_12045, coding for a site-specific integrase and a tyrosine type integrase/recombinase (Table S10 in the supplementary material). This confirmed the tendency of this bacterial species to mutate and constantly evolve, in a process that is mediated by the numerous mobile genetic elements[180] present in its genome.

All the mutants but Δ*pilA#1* displayed only the correct precise deletion relative to the target that Cas9 was programmed to cleave when the variants were filtered against the wild type used as parental strain. One SNP and one complex variant were identified in intergenic regions and two SNPs and one substitution were found in Rmet_5844,

which codes for a Polysaccharide Biosynthesis Tyrosine Kinase (Table S10 in the supplementary material). The effects of conjugation as the mean to deliver the CRISPR-Cas9 plasmid was also assessed but did not seem to promote genome rearrangements as no increase in the number of variants was detected in comparison with strains generated via electroporation of the CRISPR-Cas9 plasmid. Nevertheless, conjugation in *C. metallidurans* CH34 is reported to induce genomic changes. Indeed, the *C. metallidurans* MSR33 strain, which was obtained by conjugal transfer of the IncP-1β pTP6 plasmid to *C. metallidurans* CH34, in the attempt to increase its resistance to inorganic mercury for bioremediation purposes, was found to be resistant also to other heavy metals such as cadmium, nickel and cobalt. A genomic comparison of the MSR33 strain with the wild type revealed an array of mutations ranging from InDels to SNPs that were likely to be the result of the conjugation process and eventually caused an unanticipated phenotype[245]. Therefore, as conjugation of plasmids can pose a considerable risk for the introduction of undesired mutations, the creation and optimization of the CRISPR-Cas9 system using electroporation, as demonstrated in this study, should be regarded as the "gold standard" tool for the generation of isogenic *C. metallidurans* CH34 mutants that can be used for bioprocessing or physiological studies.

5.6 Conclusions

In this chapter I successfully built libraries of constitutive promoters and riboswitches under the control of the P_{BAD} inducible system. This was in turn of paramount importance to optimize a functional CRISPR-Cas9 system for robust selection of recombinant clones of *C. metallidurans* CH34. This work represents to my knowledge the first successful attempt to generate a genetic toolbox for *C. metallidurans* CH34.

Access to constitutive promoters with extended range of activities is fundamental in the context of engineering heterologous metabolic pathways as it makes adjustment of gene expression to the desired level more facile[234]. Moreover, the use of inducible promoters with minimal basal activity is vital for manufacturing of a vast array of products[246]. The CRISPR-Cas9 system was shown to be compatible with electroporation, thereby speeding up the process of gene-editing and it was not found to introduce off-target mutations in the genome of *C. metallidurans* CH34.

In the next chapter, the double knockout strain *C. metallidurans* CH34 Δ*pilAE* herein generated was studied by means of the technique of Cyclic Voltammetry to shed light on the role of the *pilA/E* genes in EET in *C. metallidurans* CH34. Nevertheless, despite the single pilin knockouts *C. metallidurans* CH34 Δ*pilA* and *C. metallidurans* CH34 Δ*pilE* were also successfully isolated, the number of mutants screened had to be reduced due to limited accessibility to the laboratory facility as aftermath of the Covid-19 global pandemic.

6 -Study of Electrophysiological Properties of *Cupriavidus metallidurans* CH34 biofilms grown on Screen-Printed-Carbon-Electrodes using Cyclic Voltammetry

6.1 Background: Consideration on the Methodologies for the Study of Electroactive Bacteria

In section 1.7.4 the potential of *C. metallidurans* CH34 for its use in BES for generation of electricity was discussed. One of the main aspects to improve for BES to become attractive from a commercial point of view is to maximize the transfer of electrons between bacteria and the electrode. This is necessarily tied with understanding of the basic mechanisms the organism under investigation uses for transmission of electrons to solid surfaces outside the cell. There are only three published studies considering *C. metallidurans* CH34 for application in BES, which are herein described in chronological order. Firstly, *C. metallidurans* CH34 was screened as possible biocatalyst at the cathode during polarization experiment in MES, but it was found to consume non-significant amount of currents when compared to an abiotic control[53]. In a second study, *C. metallidurans* CH34 was able to produce anodic current in MFC coupled with toluene degradation in potentiostatic mode[52]. In the most recent publication, *C. metallidurans* CH34 and *Azospira oryzae* were enriched from sulphate-reducing sludge in a MFC in galvanostatic mode (i.e without polarization of the fuel cell) and produced anodic current[148]. Nevertheless, none of these studies aimed to investigate the mechanisms underlying EET, but all intended to highlight the potential of this microorganisms for biotechnological applications ranging from electrosynthesis to wastewater treatment. The only (indirect) investigation on the possible mechanisms of EET used by *C. metallidurans* CH34 comes from a study of gold detoxification and biomineralization. In the late 2000s and early 2010s, two research groups aimed to answer the question if and how *C. metallidurans* CH34 was involved in the process of biomineralization of gold. While it was firstly discovered to associate on biofilms on secondary gold grains in the Tomakin Park Gold Mine,

Australia[145], later findings highlighted the soluble fraction of gold that enters the cells undergoes a detoxification process involving a set of copper-specific resistance genes (the *cup/cop* cluster). These code for an array of proteins that included efflux pumps, cytochromes C and oxidoreductase proteins[247] involved in detoxification of Cu. It was further shown that the biofilm formed on Au grains contained proteinaceous structures labelled as nanowires, which were thought to aid respiration by "breathing" excess electrons on the gold surface[51] (Figure 15) in similar fashion to the mechanisms used by *G. sulfureducens* to reduce extracellular Fe(III) precipitates[138] and anodic electrodes in MFCs[248,249]. Therefore, it can be said that despite *C. metallidurans* CH34 is an ideal candidate for applications in BES such as bioremediation of heavy metal contaminated waters with simultaneous production of electricity, the current lack of knowledge on the mechanisms for EET currently limits the potential application in this field.

While interesting for research on electroactive bacteria, BES can be difficult to setup to laboratories not specialized in studies of microbial electrophysiology. However, considerable interest also lies in miniaturization of BES for applications where maximization of power output is not the end goal[250–252]. Screen Printing technology is used for fabrication of cheap electrochemical devices focused on environmental sensing built in a wide variety of configurations that includes the classical three-electrodes setup. The printing process involve the use of different inks. Graphite based inks are widely employed due to their conductivity and further have similar properties to conventional electrodes used in MFCs such as low background signals[253]. In the literature, there are examples where SPEs were functionalised with bacteria for applications such as biosensing[250,254] or for study of microbial metabolism as performed by Estevez-Canales and colleagues[255]. Estevaz-Canales and

collaborators used SPCEs as inexpensive and simple to set up platform for the study of electrophysiological properties of the model organism *G. sulfureducens* in different physiological conditions. However, this study aimed specifically to reproduce chronoamperometric and CV curves that were already extensively characterized in *G. sulfureducens* growing in MFC[256]. To the best of my knowledge there are no previous reports using SPE for *de-novo* pilot investigation of RedOx centres of non-model electroactive bacteria. Therefore, this chapter is focused on assessment of the potential of SPCEs for study of *C. metallidurans* CH34 as representative organism of novel electroactive prokaryote.

6.2 Aim of the Study

The goals of this study were to investigate the role of type IV pili and the mechanisms of EET between *C. metallidurans* CH34 and terminal extracellular electron acceptor. This was performed by:

i) Creating and optimizing a protocol for exploration of the electrochemical activity of *C. metallidurans* CH34. This was done by Cyclic Voltammetry studies of SPCEs functionalized with biofilm of *C. metallidurans* CH34.

ii) Providing information of the type of EET mechanisms used by *C. metallidurans* CH34.

iii) To exploiting the optimized protocol for investigation of the role of the *pilA/E* in EET in *C. metallidurans* CH34.

6.3 Material & Methods

6.3.1 Electrode Batch Test

This experiment was performed with the aim to understand variability of electrochemical parameters of the electrode batch. Zensor TE-100 SPCE were used for all the following studies. Initial electrodes batch test was performed by covering the WE, CE and RE with 1mM ferricyanide (FCI^{+}) and cycling at a scan rate of 100mV/s between 0.6 V and -0.4 V Vs Ag/AgCl in aerobic conditions with a Autolab Potentiostat (Metrohm DropSens).

The second electrode batch test was performed in AnO_2 conditions in an anaerobic cabinet (Don Whitley Scientific) with a μStat-i 400s portable potentiostat (Metrohm DropSens). Pretreatment was performed by repetitive cycling by performing CV between 0.6 V and -0.6 V at 100 mV/s for 70 cycles (see section 6.4.2.2).

6.3.2 Cyclic Voltammetry Experiments on Biofilm-Modified SPCE

Following experiments were all performed in AnO_2 conditions with a μStat-i-400s portable potentiostat (Metrohm DropSens). For study of electrophysiological properties, *C. metallidurans* CH34 was grown for 48 hours in 7.5 mL SGMM in 50 mL falcon tube, washed twice in PBS and resuspended in PBS pH 6.9 at OD_{600} 3.5. 4 mL of the culture was placed into 20 mL scintillation vial (Starstedt) and transferred into AnO_2 cabinet (Don Whitley Scientific). SPCE were washed with ddH_2O, sterilized with 70% ethanol, rinsed again in ddH_2O, transferred to the scintillation vial (Starstedt) and incubated for 24 hours in AnO_2 conditions. After incubation the electrode was gently rinsed with PBS pH 6.9 2% Na-Gluconate, 200 μL of PBS pH 6.9 2% Na-Gluconate were then placed so to cover the WE, CE and RE and CV

measurements were taken by performing CV between 0.6 and -0.6 V at 1 mV/s, 5 mV/s or 20 mVs (specified in the text in Chapter 6). For scan rate studies CV experiments were performed at 5 mV/s, 10 mV/s, 15 mV/s, 20 mV/s, 30 mV/s, 50 mV/s and 100 mV/s vs Ag/AgCl. This was performed to study if the EET was due to soluble electron carriers or electrochemical active chemical spices adsorbed on the electrode surface. A negative control was used by incubating the SPCE with PBS pH 6.9 with no cells. The two samples were then treated the same way and 2 scans were taken for each sample.

6.3.3 Cyclic Voltammetry Data Analysis

Dropview 8400 software (Metrohm DropSens) was used for recording of voltammograms. Polynomial fitting baseline subtraction tool was used for subtraction of the baseline from current peaks. Data were exported in excel and transferred to Prism 9 (GraphPad) for figure generation and statistical analysis).

6.3.4 Confocal Microscopy: Live-Dead Staining of Biofilm-Modified SPCE

After Cyclic Voltammetry experiments, the SPCE used for the study of electrophysiological properties of *C. metallidurans* CH34, were removed from AnO_2 conditions and stained for 30 minutes in the dark at RT with 5µM Syto9 and 20 µM PI. After staining, the electrodes with the staining solution were placed in 35mm Nunc™ Glass Bottom Dishes (Thermofisher) and imaged using a Zeiss Elyra Super Resolution Microscope using a Plan-Apochromat 20X objective. Excitation of Syto9 and PI was performed with lasers 488 nm and 561 nm while detection was obtained in the windows 499-570 and 588-685 respectively. power of both lasers was setup at 1%. The Z-stack was obtained by scanning 17 slices of 16 µm each.

6.4 Results

6.4.1 Electrodes Batch Test: Peak Currents and Peak Potential Variability

To assess if the purchased Screen-Printed Carbon Electrodes were suitable for study of the electrophysiological properties of *C. metallidurans* CH34, the variability of the electrode's batch in terms of peak currents and peak potentials was tested. CV was performed with a water solution containing 1mM ferricyanide (FCI^+), a well characterized chemical species widely used in electrochemical experiments to study electrode performance[257] as reported in section 6.3.1. Five electrodes were tested as representative of the batch and peak current (I_{pa} I_{pc}), the peak potentials (E_{pa}, E_{pc}) and peak separation (ΔE)were calculated as illustrated in Figure 61A, while Figure 61B shows an overlay of the voltammogram obtained for each replicate. The I_{Ox}, I_{Rd} and ΔE values of each replicate were pooled for calculation of the average and standard deviation for assessment of batch variability (Figure 61C-E, Table 17). Variability of the electrode batch was eventually deemed acceptable for downstream electrophysiological experiments. It is noteworthy the peak potential separation was found to be greater than 59 mV, the expected values for diffusion-limited reversible RedOx reactions. However, this is a theoretical value that can be observed only in ideal conditions[154].

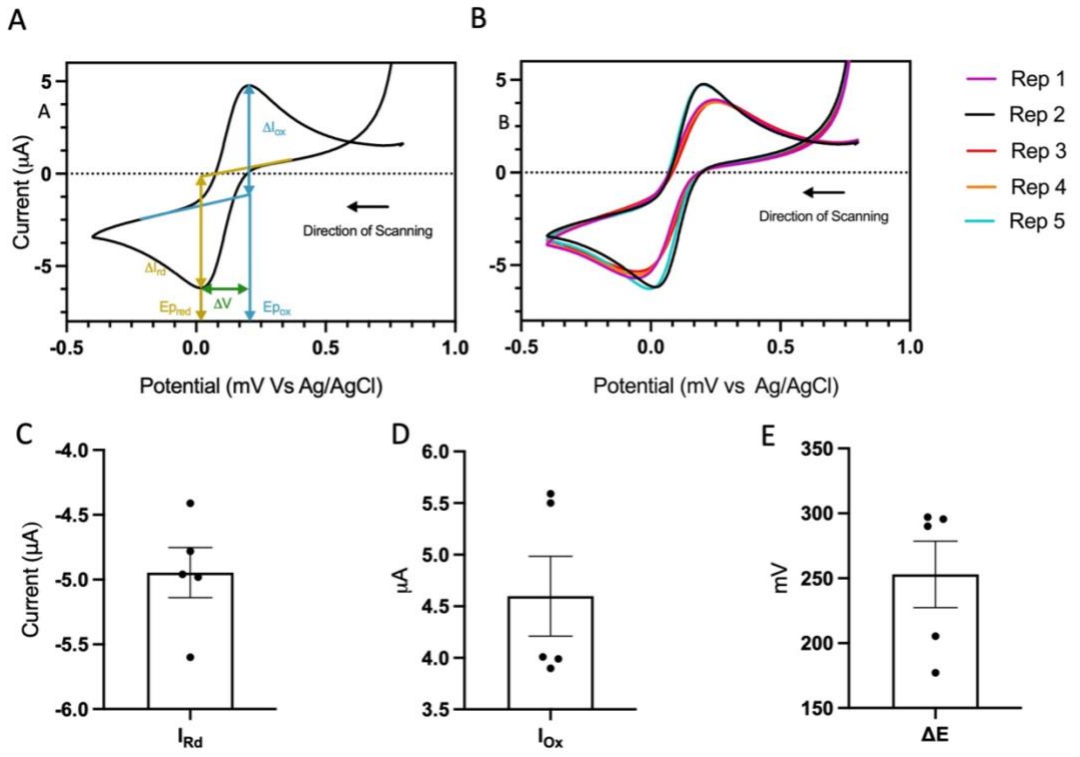

Figure 61-Electrode batch test in 1mM FCI: A) Representative voltammogram of one of the replicates with methodology for calculation of current peaks (I_{pa}, I_{pc}), peak potentials (E_{pa}, Ep_{pc}) and peak separation (ΔE). B) Overlay of the replicates of the electrode batch test. C)-E Bar diagram of the reduction/oxidation peaks and peak potential variation respectively. Bars represent SD (n=5).

Table 17-descriptive statistics of the batch test experiment of the SPCEs

	ΔI_{rd}	ΔIox	ΔE
Minimum	-5.6	3.9	177.2
Maximum	-4.41	5.59	297
Range	1.19	1.69	119.8
Mean	-4.94	4.59	253
St. Deviation	0.413	0.866	57.29

6.4.2 Study of Involvement of Type IV pili in Extracellular Electron Transfer in *C. metallidurans* CH34 on SPCEs by Means of Cyclic Voltammetry

6.4.2.1 Experimental Strategy

The strategy adopted for the study of electrophysiological properties of *C. metallidurans* CH34 is described in this section. The protocol was adapted from the study where SPCEs were used for qualitative assessment of RedOx activities in *G. sulfureducens*[8]. The authors grew *G. sulfureducens* in conditions previously well established to induce expression of the nanowires by supplementing the media with appropriate electron donor/acceptor and performing growth at 25 ˚C[138,248]. Cells were then positioned on the SPCE, and voltammetry measurements were immediately performed. However, on the contrary to *G. sulfureducens,* there is no information available in the literature on the conditions necessary to promote EET mechanisms in *C. metallidurans* CH34 that can be related to specific RedOx proteins. Therefore, incubation of the cells was performed in absence of oxygen in PBS for 24 hours. With the aim to maintain the cells physiologically stable and limit the availability of terminal electron acceptor, which is known to induce EET in electroactive biofilms[258]. The protocol followed for study of RedOx centres in *C. metallidurans* CH34 was developed as follows (Figure 62 and section 2.12.4 of M&M for the detailed protocol):

i) *C. metallidurans* strains were grown on LB Gen^+ agar plates.

ii) Single colonies were inoculated in SGMM and grown in aerobic conditions for 48 hours at 30 ˚C while shaking at 200 rpm.

iii) Bacterial cultures were collected by centrifugation and incubated overnight in PBS pH 6.9 in AnO_2 conditions to promote formation of biofilm onto the electrode.

iv) The biofilm-modified SPCE were connected to a portable potentiostat in AnO_2 conditions, supplemented of PBS 2% Na-Gluconate pH 6.9, and CV scans were performed at 5 mV/s (as described by Canales *et al.*[255]) between 0.6 V and -0.6 V followed by data analysis. Two consecutive scans were taken.

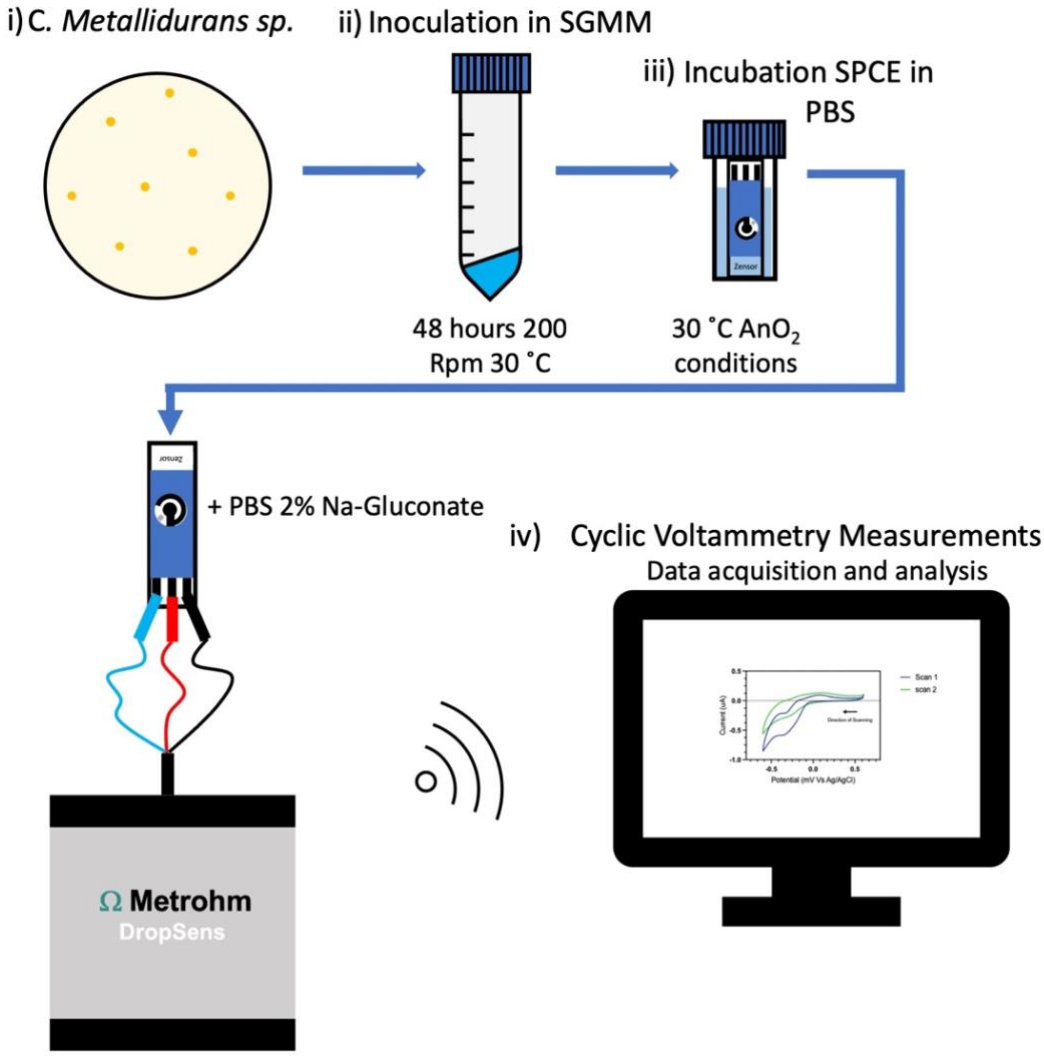

Figure 62-Protocol designed for study of RedOx centres of *C. metallidurans* CH34: i) growth of *C. metallidurans sp.* on LB Gen^+ plates, ii) inoculation of single colony in SGMM and growth for 48 hours at 200 rpm and 30 ˚C, iii) collection of cells by centrifugation and resuspension in AnO_2 conditions in PBS pH 6.9, iv) data acquisition and analysis.

6.4.2.2 Protocol Optimization for Assessment of RedOx Peaks of Biofilm-Modified SPCEs

In this section, the protocol previously described to analyse electrochemical properties of *C. metallidurans* CH34 was optimized and tested to reveal RedOx mechanisms of *C. metallidurans* CH34 biofilms. *C. metallidurans* CH34 was incubated in AnO_2 conditions in PBS with the SPCEs as described above. A negative (abiotic) control was also used to determine the background signal. The protocol is described in detail in section 6.3.2. While the negative control did not produce any measurable RedOx peak (black voltammogram in Figure 63), the voltammogram related to the biofilm-modified SPCE showed a reduction and an oxidation peaks at -0.3 V and 0.1 V respectively in the first scan (blue voltammogram in Figure 63), which peak separation and peak ratio visually different from 1, suggested an irreversible RedOx mechanisms. However, the second scan showed lower current peaks and a shift toward more positive potentials for both the reduction and oxidation peaks. As this happened with all the replicates tested, it meant there was a consistent change in either the chemistry of the electrode or a change in the biology of the biofilm.

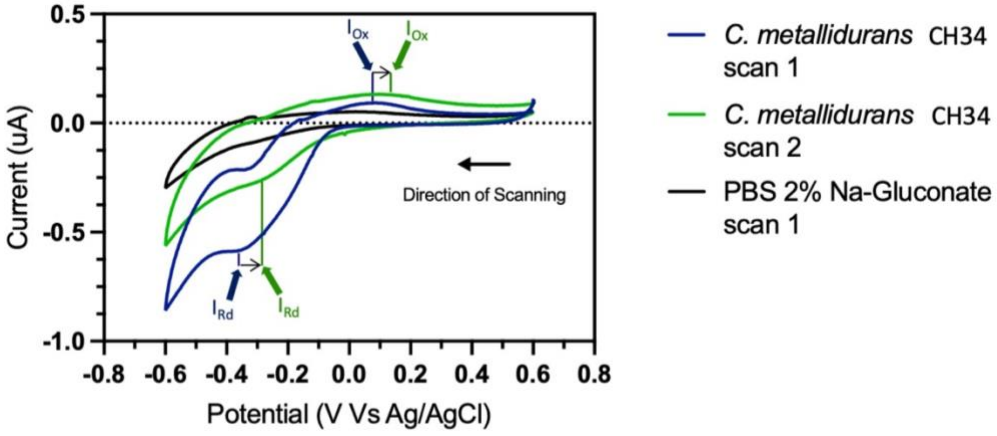

Figure 63-Representative CV scan from the optimization experiments for analysis of RedOX centres of *C. metallidurans* CH34 biofilm: First (blue) and second scan (green) for the biofilm-modified SPCE are shown. I_{Rd} and I_{Ox} of each scan are also shown with relative colours. Shift of the current peaks toward more positive potentials is indicated by black arrows. Only first scan for the negative control (black) is shown.

A literature study highlighted that adsorption of impurities during printing of SPCEs is a documented phenomenon that can impair electron transfer kinetics and electrode performance[259]. Different treatments have been proposed to "activate" carbon-based electrodes such as heat[260], plasma treatment[261] and voltammetry-based methodologies[262], which involves preconditioning by performing repetitive scanning at a given potential window before starting the experiment[155]. To test whether lack of pre-treatment was indeed the cause of unstable electrochemical response observed in the experiment mentioned above, repetitive potential cycling was further considered as preconditioning methodology in virtue of its simplicity in the attempt to improve the reproducibility of the voltammograms. Briefly, one biofilm-modified SPCE and one bare electrode incubated in PBS pH 6.9 (negative control) were treated as previously described. Prior to perform the CV scans to obtain information on the biofilm activity, repetitive cycling at 100mV/s from 0.6 V to -0.6 V was performed in AnO_2 conditions for 70 cycles using PBS 2% Na-Gluconate pH 6.9 as electrolyte. During electrode pre-treatment it was observed that the shape of the voltammogram

of both the biofilm-modified and bare electrode kept changing for the whole duration of the experiment until scan number 50 (Figure 64). Moreover, the shape of the voltammograms of the first scan of the biofilm-modified and the control SPCEs (pink voltammogram in Figure 64), resemble the voltammogram of the pilot experiment showed in Figure 63. This experiment demonstrated the change of the voltammogram shape was due to the chemistry of the electrode, rather than the biofilm. From here on, prior to any CV experiment, pre-treatment of the SPCEs was performed by repetitive scanning as just described in the text above.

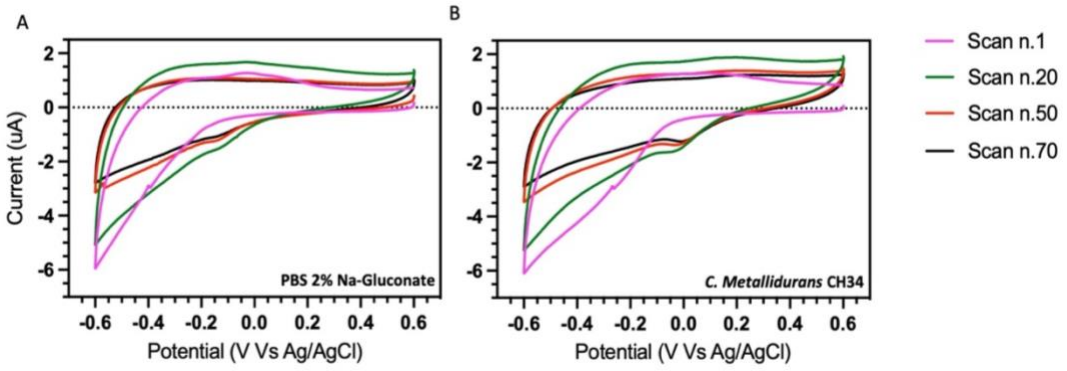

Figure 64-CV scans of the pre-treatment experiments of the biofilm-modified and bare SPCE: Scan number 1 (pink), 20 (dark green), 50 (red) and 70 (black) are shown for the A) negative control and B) biofilm-modified SPCE.

6.4.2.3 Study of the RedOx centres and Involvement of Type IV Pili in Extracellular Electron Transfer in Biofilms of *C. metallidurans* CH34

The optimized protocol for study of biofilm-modified SPCEs was next exploited to determine whether lack of type IV pili would result in either significantly smaller or complete absence of RedOx peaks. The rationale behind the experiment followed the idea that if *pilA/E* genes were responsible for EET in *C. metallidurans* CH34, a faradaic current peak related to the pili would either be lacking or showing

reduced magnitude during the CV scan as it could be noticed from study of *G. sulfureducens* biofilm *pilA* knockout[256]. For these reasons, CV experiments were firstly performed on *C. metallidurans* CH34 to test if the protocol developed produced any RedOx peaks (n=4). The scan rate of 20 mV/s was eventually used for future experiments. The biofilm-modified SPCE showed a cathodic (reductive) peak at 0.05 V and an anodic (oxidative) peak at 0.3 V which were further confirmed by subtraction of the baseline (Figure 65A and Figure 65B respectively) and the negative control also showed two smaller RedOx peaks with reduction and oxidation peak at -0.1V and 0.1V respectively.

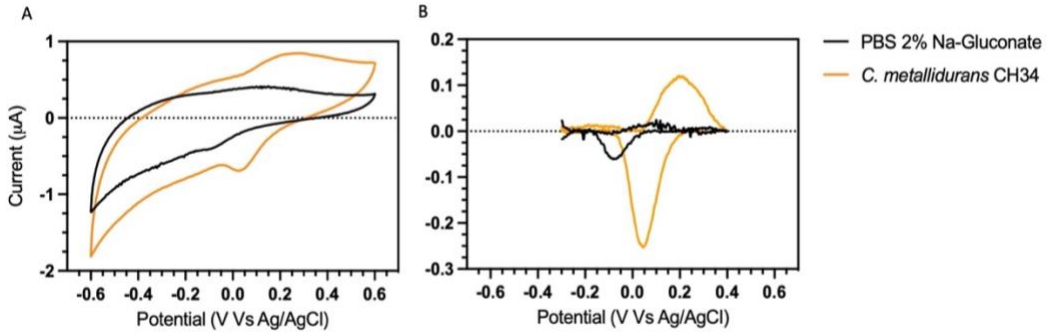

Figure 65-Representative CV scans of *C. metallidurans* CH34 biofilm-modified SPCE and negative control at 20mV/s: A) Representative voltammograms of *C. metallidurans* biofilm on the SPCE (orange) and PBS 2% Na-Gluconate (black) and B) current peaks after baseline subtraction.

Variability of the peak potentials was noticed among the replicates (n=4) as 50% of the biofilm-modified SPCE showed both peaks shifted circa 0.140V toward more positive potentials (supplementary Figure S16). It was reasoned this could have been caused by i) degradation over time of the electrode stock or ii) a phenomenon called biofouling where bacterial biofilm growing on the RE might destabilize the electrode system by altering the potential applied on the WE[263]. Therefore, I firstly tested if the electrode batch still exhibited reproducible current peaks and peak potential. To do so, I performed the FCI^{+} test as described in section 2.12.3. The

following adjustment were made compared to the first test in order to reproduce the conditions used to test the biofilm-modified SPCE:

i) The electrode batch test was performed under AnO_2 conditions.

ii) the electrodes were tested for peak currents and peak potential with and without pretreatment (n=5) to further verify the effect of the preconditioning on reproducibility.

As it could be observed by the voltammograms, there seemed to be a stabilization effect of the electrochemical response of the electrodes after preconditioning compared to the ones that did not undergo preconditioning treatment (Figure 66A & Figure 66B respectively, only 3 representative replicates are shown). The stabilization effect was also visible when plotting the values of each replicate for current peaks and peak potentials as bar diagram, which showed values grouping around the median with a lower SD. However, no significant difference (Mann-Whitney test) was found regarding the height of the current peaks or the variation in the peak potential (Figure 66C & Figure 66D).

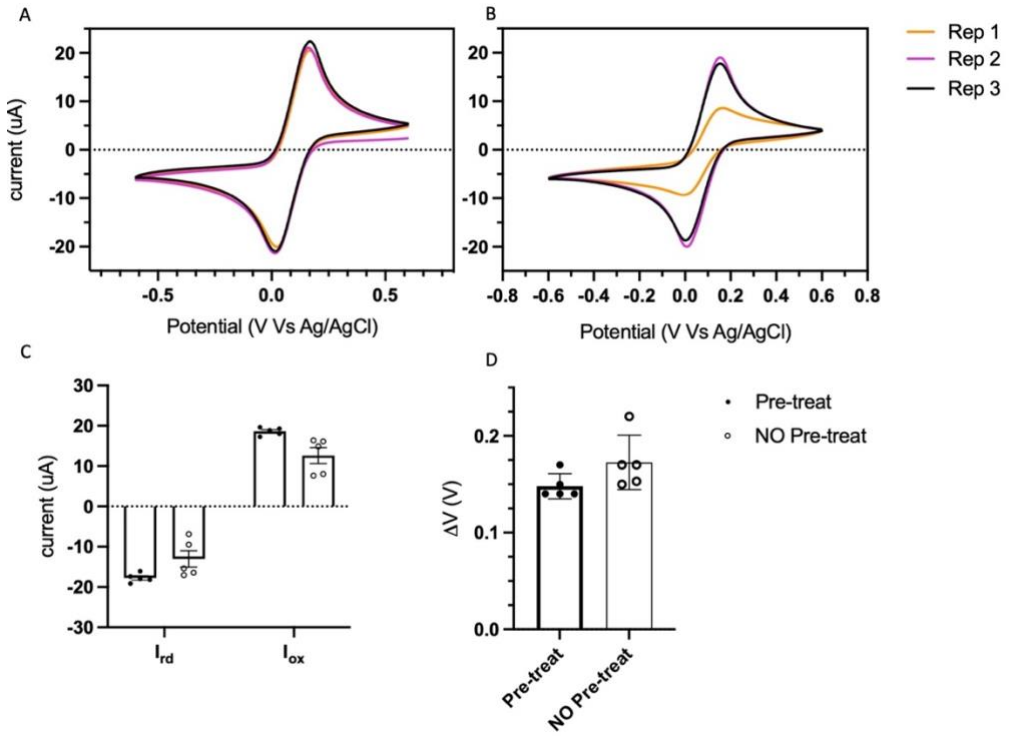

Figure 66-Cyclic voltammograms and bar graphs of electrode batch test in AnO_2 conditions: representative voltammograms of electrodes tested with 1mM FCI^+ with the portable bipotentiostat in AnO_2 conditions with (A) and without (B) preconditioning and bar diagram of the current peaks (C) and peak potentials (D) with and without pretreatment. Bars represent SD (n=5).

Provided the electrode's batch was still fit to obtain reproducible data, the fact that i) variability of the peak potential of the biofilm-modified SPCE was observed (Figure S16) and ii) RedOx peaks could also be noticed in the negative control (Figure 65 & FigureS16), it could be possible that shifts of the peak potentials of the biofilm-modified SPCEs may have also happened toward more negative potentials (I.E overlapping with the peaks observed in the negative control). Therefore, a Mann-Whitney test was performed between the current peaks observed in the biofilm-modified SPCE and the negative control. The absolute values of both current peaks obtained from CV scans of the biotic SPCE were significantly higher than the respective values of the negative control ($p<0.05$), thereby confirming the presence of RedOx centres involved in EET in *C. metallidurans* CH34 (Figure 67).

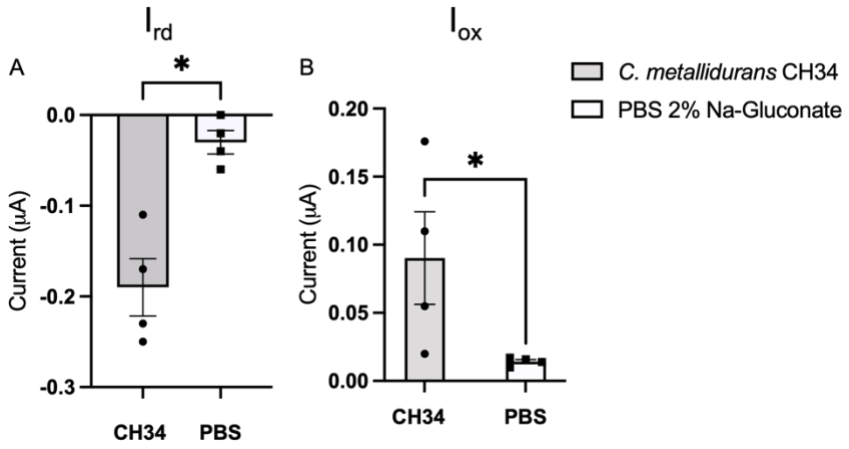

Figure 67-Peak currents of biofilm-modified SPCE and negative control: (A) I_{Rd} (B) I_{ox} currents. Significance of the difference in the current peaks between the biofilm-modified SPCE and negative control is highlighted metallidurans CH34. n=4, error bars represent SD. *p<0.05.

To further confirm the presence of the RedOx peaks were due to biological activity, the biofilm-modified and abiotic electrode were stained with Syto9® and Propidium Iodide (PI) as described in section 2.11.3 and observed by means of confocal microscopy by taking overview scans of the horizontal plane and z-stacks of the WE. The confocal microscopy displayed mostly live cells growing as a monolayer (z-stack) onto the electrode surface on the biofilm-modified SPCE and absence of cells in the negative control activity (Figure S17). This further supported the hypothesis that RedOx couples observed were due to biological activity.

Next, to estimate if the nature of the electron transfer was MET or DET, a scan rate study was performed by means of CV at 5mV/s, 10mV/s, 15 mV/s, 20 mV/s, 30 mV/s, 50 mV/s and 100 mV/s vs Ag/AgCl. The value of the cathodic and anodic peak currents was plotted against the square root of the scan rate. A linear relationship between the cathodic peak and the square root of the scan rate suggested a diffusion controlled EET system. However, the anodic current peaks showed no linear relationship with either the square root of the scan rate (Figure 68B) or the scan rate (Figure S18) and displayed reduced intensity when compared to the cathodic current

peaks. Furthermore, shifting of the cathodic and anodic peaks toward more negative and positive potentials respectively could also be observed (Figure 68C) which has been reported in the literature to be due to sluggish charge transfer rate and solution resistance[264]. These observations suggested the phenomenon observed was that of a E_rC_i described in section 6.3.4.2.

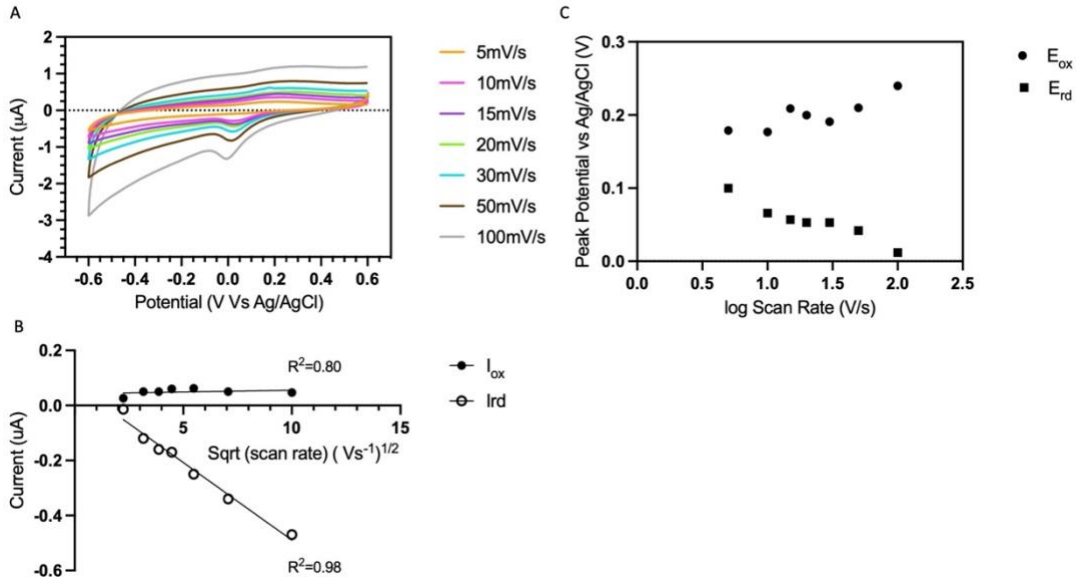

Figure 68-Results of the scan rate experiment of the biofilm-modified SPCE: A) Voltammograms at different scan rates B) plot of the anodic and cathodic current peaks with the square root of the scan rate and C) plot of the peak potentials with the $\log_{10}$ of the scan rate.

However, this is a textbook interpretation for a system where all the components are defined. Microbial cells, despite answering to the same theory, are much more complex to understand and care should be taken in draw conclusions from (relatively) straightforward scan rate experiments, which often showed mixed mass-transfer behaviour in the literature[256,265,266]. In the case of *Shewanella* MR1, data obtained from CV experiments showed a linear relationship between reduction and oxidation current peaks and the scan rate as well as small peak separation (<20 mV) and shift of the peak potentials, which hinted at EET mechanisms liked to species

adsorbed on the electrode surface[118]. Since *Shewanella* is reported to be capable of EET via both soluble mediators and membrane bound cytochrome, it was initially postulated the mechanism witnessed was consistent with adsorption of cytochromes to the electrode surface. However, CV analysis of media filtered of all the bacteria and change of media resulted in RedOx response and depletion of catalytic activity respectively, thereby highlighting the presence of soluble electron carriers being pivotal for current generation. Eventually, In-depth analysis of the electrode surface via spectroscopic techniques showed flavins could be adsorbed at the interface of the electrode, thereby reconciling MET mechanism with the adsorption-controlled electron transfer behaviour observed in the CV experiments of *Shewanella* biofilms[265]. In *Geobacter sulfureducens*, which can form thick (>50 μm) biofilms, a mixed behaviour could be observed under acetate oxidizing conditions with anodic current that seemed to arise from surface-adsorbed mechanisms and diffusion-limited at scan rates <0.5 V/s and >0.5 V/s respectively. This complex interaction resulting in a "bimodal behaviour" was discussed to be due to RedOx molecules confined in the biofilm[256]. This complex "bimodal" behaviour is typical of well-established and thick biofilms of *Geobacter*[256] and showed similarities to the catalytic response of glucose oxidase enzymes trapped in a redox conductive epoxy cement which displayed symmetric RedOx current peaks at slow scan rates typical of adsorbed species, but displayed classic diffusion-limited behaviour at high scan rates[267].

The confocal microscopy data herein presented relative to the biofilm of *C. metalliduranas* CH34 showed the presence of a monolayer of cells (Figure S17, z-stack). This excludes the complex interplay of RedOx molecules trapped in thick biofilms and limits data interpretation to the presence of soluble RedOx mediators of a E_rC_i system. Moreover, During CV scans at 5mV/s an additional anodic peak was

observed in the biofilm-modified SPCE (Figure 69A & Figure 69B) that could not be visualized at higher scan rates. As described in section 6.3.1, when potential at the WE is changed, a capacitative current would flow due to rearrangement of the double layer. This capacitiative current is reported to occasionally overlap faradaic currents for low cell coverage of the electrode or for low electrocatalytic activity of the biofilm[266].

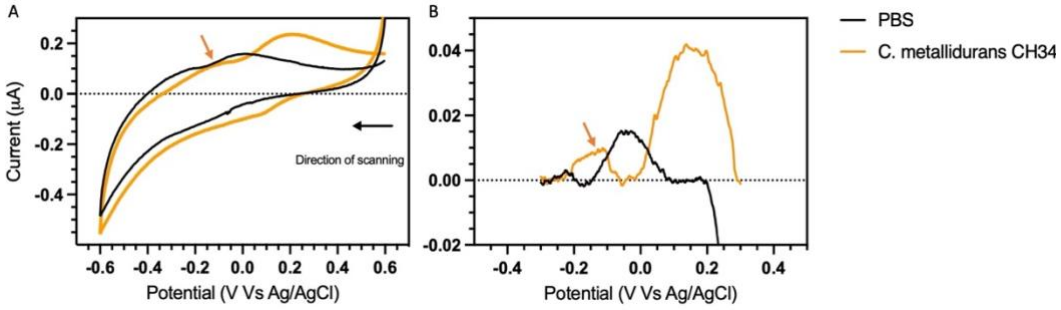

Figure 69-CV scans of *C. metallidurans* CH34 biofilm-modified SPCE and negative control at 5 mV/s: A) voltammogram and B) voltammogram with baseline subtraction of the anodic track only between 0.3 and -0.3V. The additional oxidative peak is highlighted by an orange arrow. The orange and black tracks refer to the biofilm-modified SPCE and the negative control respectively.

Therefore, in the attempt to resolve potential RedOx peaks with low electrochemical activity, CV experiments were repeated at 1 mV/s. Two RedOx couples namely $RedOx^1$ and $RedOx^2$ were observed (Figure 70A and Figure 70B), with a peak potential of 0.3 V and -0.16 V respectively which were not present in the negative control (Figure 70C). Both the RedOx centres showed no peak separation and a ratio $I_{rd}/I_{ox} \neq 1$, thereby indicating two electrochemically active species adsorbed on the electrode surface are responsible for EET in *C. metallidurans* CH34.

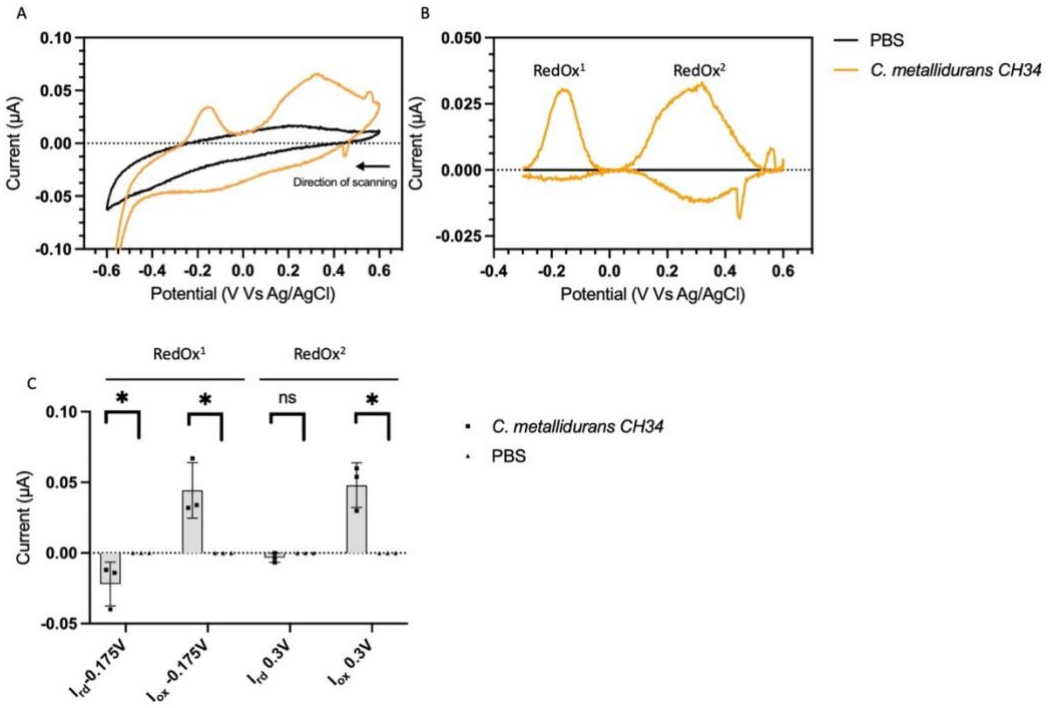

Figure 70-representative CV scans of *C. metallidurans* CH34 biofilm-modified SPCE and negative control at 1mV/s: A) CV scan at 1mV/s of *C. metallidurans* CH34 biofilm-modified SPCE and negative control with B) baseline subtraction. C) Peak current of *C. metallidurans* CH34 biofilm-modified SPCE and negative control. Error bars represent SD, Mann-Whitney one tailed test, * $p<0.05$. The orange and black tracks refer to the biofilm-modified SPCE and the negative control respectively.

Next, the strain *C. metallidurans* CH34 Δ*pilAE* was tested by performing CV at 1 mV/s to study involvement of the *pilA* and *pilE* in the process of EET. No difference in the shape of the voltammogram (Figure 71) was shown, thereby indicating type IV pili are not involved in EET in *C. metallidurans* CH34 in the conditions tested. The other knockout strains *C. metallidurans* CH34 Δ*pilA* and *C. metallidurans* CH34 Δ*pilE* could not be studied due to time constraints to access laboratory facilities during the Covid-19 pandemic.

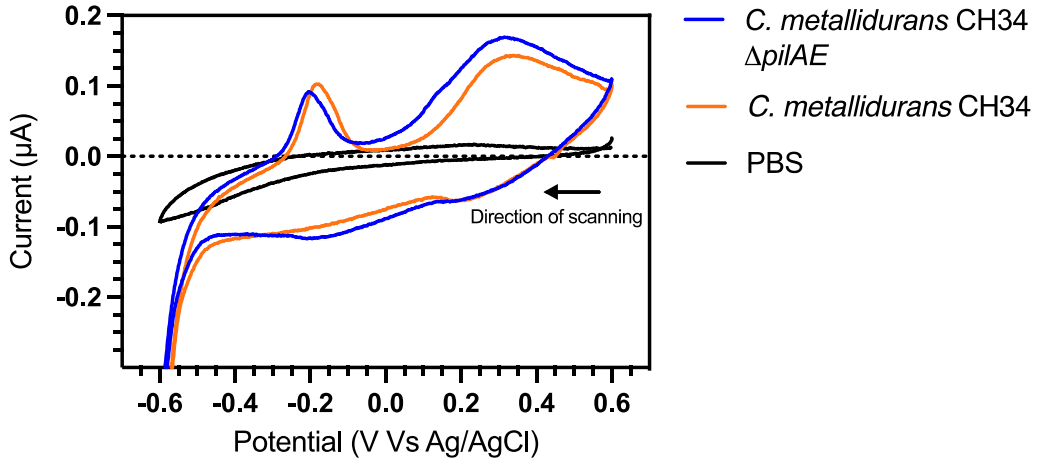

Figure 71-Cyclic Voltammetry of *C. metallidurans* CH34 and *C. metallidurans* CH34 Δ*pilAE* biofilm-modified SPCE and negative control at 1 mV/s: Blue, orange, and black tracks correspond to the voltammograms of SPCEs modified with biofilms of *C. metallidurans* CH34 Δ*pilAE, C. metallidurans* CH34 wild type and negative control (PBS only) respectively. n=3, only one voltammogram is shown for clarity.

Traditionally, studies on the electron transfer mechanisms in bacteria is performed in long-term experiment in BES after observation of current production (electrogens organisms, in MFC) or consumption (electrotrophic organisms, in MES). This implies that the bacteria are well adapted for EET mechanisms and possible RedOx proteins are expressed and active. Estevez-Canales and colleague previously employed cheap SPCE as biosensing platform by exploiting EET mechanisms of *G. sulfureducens*[255]. In this study, *Geobacter sulfureducens* was grown in fumarate-limiting conditions. well established to promote EET [138] prior to electrochemical analysis. CV scans resulted in RedOx couple, however exhibiting different shape when compared to voltammograms obtained from thick biofilms matured during polarizing conditions in MFC setup [256,268]. Electroactive biofilms are shown to display different organization and electrochemical behaviour depending on the growth conditions. For example, Zhang and co-workers studied the phenotype of *Geobacter* biofilms under intermittent polarization experiments, by changing the frequencies at

which the biofilm was left under polarization or at open circuit potential. The biofilm adopted a mushroom-like organization and a flat and uniform structure if alternate and constant polarization was applied respectively. Cyclic voltammetry of the biofilm grown in the different conditions also revealed dramatic changes in the shape of the voltammograms and current intensities. While short polarization times increased the stored charge and current intensities, longer polarization intervals (300 seconds) resulted in dramatic reduction of the aforementioned parameters and produced a voltammogram with redox peaks of low intensity and no peak separation (Figure S14 from publication), similar to what observed in this study[270]. Furthermore, electroactive bacteria are reported to store charges by using polymers such as PHA[271,272], or cytochromes[273,274] as electron sinks.

SPCEs are known to be inherently unsuitable for long term polarization experiments due to degradation of the pseudo reference electrode, which can cause potential drift[275,276]. Therefore, the experiments herein presented were performed by incubating cells in AnO_2 in PBS without polarization of the electrode followed by CV to individuate potential RedOx centres and to investigate on the possible role of type IV pili in EET.

6.5 Conclusions

A methodology for the study of bacterial EET in AnO_2 conditions by using cheap disposable SPCEs was herein developed and used to characterize EET mechanisms of *C. metallidurans* CH34 and to investigate on the role of the *pilA/E* genes in current generation. The results herein reported suggested *pilA/E* genes were not involved in EET in the conditions tested and that *C. metallidurans* CH34 was capable of EET by means of a diffusion-limited E_rC_i mechanism and two RedOx molecules characterized by quasi-reversible electron transfer mechanism adsorbed to the electrode surface which.

7 -Summary & Discussion

7.1 Context of this Thesis

In engineering, the concept of a standard implies establishment of a technical requirement, process, practice, or method. By using standards, engineers around the world can ensure development of safe, compatible, and consistent products. Synthetic biology aims to integrate the principle of "standardization" to living organisms to exploit their features for the benefit of human society. In relation to synthetic biology, the use of standards allow for conformity to environmental and safety regulations, predictability of experimental outcomes and it can result in boosting knowledge transfer and innovation of the field[277]. Another fundamental aspect to implementation of prokaryotic chassis in synthetic biology, is that thorough knowledge of the metabolic and molecular processes of the cell are necessary to improve or program a cell for efficient industrial-scale processes. Therefore, rational design and characterization of genetic parts and application-specific physiological studies are fundamental aspects for the design of recombinant strains with improved outcome.

Due to its metabolic flexibility, *C. metallidurans* CH34 represents the archetype of a suitable prokaryote for biotechnological applications. Being capable of withstanding high concentrations of heavy metals, using BTEX as carbon source, growing with lithoautothrophic lifestyle as well as the ability to perform extracellular electron transfer, frames its relevance in applications such as bioremediation, MFC, MES and bioprocessing. Nevertheless, only a few studies at academic level focus on *C. metallidurans* CH34 as a suitable chassis for industrial applications. The main reasons behind the (surprising) scarcity of publications highlighting the biotechnological potential of this remarkable prokaryote are the absence of i) experimental studies unravelling the mechanism of industrially relevant metabolic features other than resistance to heavy metals and ii) genetic toolboxes that can be

used by research groups to tailor genetic circuits of expected outcomes. Therefore, in the work presented in this thesis I aimed to address some of these shortfalls by implementing novel genetic tools to make *C. metallidurans* CH34 a more desirable organism for synthetic biology applications and study in more details the basic physiological mechanisms of EET, which knowledge can be exploited to increase electron density at the electrode surface in MFCs to eventually generate commercial-level power densities. Furthermore, a synthetic biology strategy to improve electron density transfer between the cell and the electrode was proposed.

7.2 Outcome of the Thesis

In Chapter 3 of this work, I aimed at creating a strain of *C. metallidurans* CH34 with enhanced biofilm formation at the electrode surface for increased EET. The strategy involved electrode surface modification with O^6-benzylguanine and outer membrane expression of the SNAP-tag under control of a P_{BAD} inducible promoter. Expression studies were performed in the in-house strain of *C. metallidurans* NG7, which was so re-named because of the different phenotype observed regarding antibiotic resistance when compared to *C. metallidurans* CH34. Expression in *C. metallidurans* NG7 failed from both plasmid system and chromosomal transposon-mediated insertion. In the case of the plasmid-driven expression, circumstantial evidence such as background growth of colonies not transformed with the expression plasmid on selection plates and the following discovery in part 2 of the presence of the multi-drug resistance IncP-1α plasmid pointed towards plasmid loss as the possible main cause of lack of expression. Nonetheless, chromosomal insertion of the SNAP-tag also resulted in no expression which could be either blamed on inactivity

of the P_{BAD} promoter or random insertion of the transposon in "transcriptionally inactive" sections of the bacterial chromosome[183].

To circumvent the problem of plasmid loss, Plasmid Addiction Systems were proposed in Chapter 4 as standard biological parts that could be used to couple plasmid maintenance and protein expression in *C. metallidurans* CH34. It is noteworthy this strategy was initially developed to circumvent the issue of segregational instability in *C. metallidurans* NG7. Nevertheless, development of stable plasmids remains an invaluable weapon against plasmid and product loss regardless of the bacterial chassis. Furthermore, the issue of plasmid instability in *C. metallidurans* CH34 was already brought to attention by Biondo and colleagues[56]. Uracil auxotrophy-based PAS and the *parCBADE* system from IncP-1α were exploited to create a stabilization technology for mini pBBR1 and RK2 expression plasmids respectively and the strength of the systems was tested in continuous settings, which drives dilution of plasmid-harbouring compared to plasmid-less cells due to the higher metabolic burden the formers are exposed to. None of the strategies herein employed were successful to achieve stable plasmid maintenance, which highlighted the need of an efficient genome editing tool to perform chromosomal integration of heterologous genes and metabolic pathways and the consequent necessity to develop a library of regulatory elements to fine tune synthetic genetic pathways.

Following, in Chapter 5 I successfully developed a CRISPR-Cas9 tool for genome editing of *C. metallidurans* CH34. A preliminary step was to optimize the expression level of the sgRNA and Cas9, pivotal to minimize toxicity of Cas9 and improve the overall efficiency of the system[84,221,222]. This was done by designing and testing a library of constitutive promoters and inducible promoters. Eventually, constitutive promoters with a wide range of activity and a hybrid ON/OFF system composed of

the inducible P_{BAD} and ncRNAs riboswitches for complete repression of expression in absence of the inducers were characterized and optimized. Beside the goal of optimizing expression of the CRISPR components, this is to my knowledge the first comprehensive library of constitutive promoters and inducible promoters for *C. metallidurans* CH34. Eventually, the optimized system proved to be robust, but with efficiency of isolation of recombinant clones ranging between 2% and 100%. However, it should be pointed out the lowest efficiency was found when screening isolates with chromosomal integration of constitutively expressed *GFP*, which toxicity is reported in the literature[278]. Moreover, deletions of genes coding from type 4 pili in *C. metallidurans* were performed[51]. This was done with the double scope of validating the CRISPR-Cas9 system and obtaining K.O strains of for study of EET mechanisms. Following this, a time-honoured electrochemistry technique called Cyclic Voltammetry was applied to examine electron exchange mechanisms between the electrode surface and *C. metallidurans* biofilms. Comparison of *C. metallidurans* CH34 wild type and *C. metallidurans* CH34 Δ*pilAE* did not find evidence of involvement of the type IV pili in the transfer of electrons under the conditions tested but highlighted the presence of different RedOx centres likely to be involved in both MET and DET. Two of these centres are likely to be outer membrane cytochromes forming direct contact between the cell and the electrode surface or polymers involved in electron storage and release[271–274] while the other RedOx centre displayed characteristics of soluble mediators responsible for a E_rC_i mechanism. These data represent a first interpretation of the mechanisms *C. metallidurans* CH34 uses for extracellular electron transfer and shed light on the intricate multi-component systems likely to be composed of cytochromes and diffusive mediators which carry out

oxidation and reduction under limitation of carbon source and terminal electron acceptor.

7.3 Limitations and Future work

One of the main goals of this thesis was the development of an initial toolbox for genome editing of *C. metallidurans* CH34 which could serve as starting point for the synthetic biology community to implement this microorganism in biotechnological applications, where genome engineering can result in creation of efficient bacterial strains. While characterization of constitutive and inducible promoters was successful, more should be done in the future to expand the toolbox that can be used for design of genetic circuits with predictable outcomes. Issues such as stepwise expression where expression levels can be correlated with the concentration of the inducer in inducible systems, tight repression of gene expression and design of true orthogonal genetic parts with chassis-independent behaviour, are among the main points to be addressed to achieve a real and comprehensive standardized genetic toolbox for heterologous protein expression. Firstly, the P_{BAD}_Riboswitch library should be further tested for dose-response characterization of expression of mRFP1 thus providing expression profiles of the extensively used P_{BAD} promoter under control of the orthogonal theophylline-dependent riboswitch. Secondly, the library of constitutive and inducible promoters should be expanded. Ideally application-specific synthetic inducible promoters should be engineered with activation depending on the presence of inducer molecule in the media/environment rather than from the addition of external chemicals, which can significantly raise the cost of biotechnological processes. To further develop modular orthogonal regulatory sequences, more effort should aim at characterizing synthetic ncRNA in *C. metallidurans* CH34, in similar fashion to what

herein performed for the theophylline-dependent riboswitch which previously showed regulation of expression across several bacteria genera[231]. On the aspect of gene editing, the necessity of high-throughput multiplex technologies should be developed for *C. metallidurans* CH34 in order to boost extensive genetic modifications that can accelerate physiological studies and biotechnological applications[279]. While these aspects altogether represent a good starting point, they do not by any means represent a comprehensive list of the necessary tools and effort for exploitation of *C. metallidurans* CH34. Indeed, achievement of this task is a multidisciplinary effort that cannot be accomplished by one researcher alone. The need for genome scale metabolic models, design of novel synthetic nucleic acid sequences and models for predictions of outcomes of bioprocessing, requires instead expertise in the field of mathematics, biophysics, informatics, and chemistry.

While some of the electrophysiological aspects of *C. metallidurans* CH34 were herein unravelled, the technical limitation and the restrictions posed by Covid-19 limited the amount of work that could be carried out during the final phase of my PhD. The monolayer biofilm of *C. metallidurans* CH34 grown on disposable Screen-Printed-Carbon-Electrodes was characterized for EET in non-optimal conditions for achievement of high current densities, normally correlated with the presence of type IV e-pili in thick biofilm of *G. sullfureducens sp*[280]. More precisely, to be able to study the involvement of nanowires in EET in *G. sulfureducens*, growth in MFC with polarized anode is required for several weeks to achieve thick biofilm and nanowire-related high current densities, which was impossible with the SPCEs and the instrumentations available. Therefore, the work herein performed was instrumental to understand polarization potentials to be set for deeper study of EET mechanisms and represents for the first time a qualitative characterization of the RedOx mechanisms

C. metallidurans CH34 uses to store and release charge under limitation of carbon source and terminal electron acceptor. However, future studies in MFC with polarized anodes will be pivotal to gain insight into EET mechanism that can be improved by means of synthetic biology approaches for commercial applications in BES.

8 -Bibliography

1.McCormick, K., & Kautto, N. (2013). The bioeconomy in Europe: An overview. *Sustainability*, *5*(6), 2589-2608.

2. Chisti, Yusuf. "Growing the bioeconomy." (2010): 198.

3. Lokko, Y., Heijde, M., Schebesta, K., Scholtès, P., Van Montagu, M., & Giacca, M. (2018). Biotechnology and the bioeconomy—Towards inclusive and sustainable industrial development. *New biotechnology*, *40*, 5-10.

4. Blancquaert, D., Van Daele, J., Strobbe, S., Kiekens, F., Storozhenko, S., De Steur, H., ... & Van Der Straeten, D. (2015). Improving folate (vitamin B9) stability in biofortified rice through metabolic engineering. *Nature Biotechnology*, *33*(10), 1076-1078.

5. Ye, X., Al-Babili, S., Kloti, A., Zhang, J., Lucca, P., Beyer, P., & Potrykus, I. (2000). Engineering the provitamin A (β-carotene) biosynthetic pathway into (carotenoid-free) rice endosperm. *Science*, *287*(5451), 303-305.

6. dos Reis, S. P., Marques, D. N., Barros, N. L. F., Costa, C. D. N. M., & de Souza, C. R. B. (2018). Genetically engineered food crops to abiotic stress tolerance. In *Genetically engineered foods* (pp. 247-279). Academic Press.

7. Goeddel, D. V., Kleid, D. G., Bolivar, F., Heyneker, H. L., Yansura, D. G., Crea, R., ... & Riggs, A. D. (1979). Expression in Escherichia coli of chemically synthesized genes for human insulin. *Proceedings of the National Academy of Sciences*, *76*(1), 106-110.

8. Meehl, M. A., & Stadheim, T. A. (2014). Biopharmaceutical discovery and production in yeast. *Current opinion in biotechnology*, *30*, 120-127.

9. Sanchez-Garcia, L., Martín, L., Mangues, R., Ferrer-Miralles, N., Vázquez, E., & Villaverde, A. (2016). Recombinant pharmaceuticals from microbial cells: a 2015 update. *Microbial cell factories*, *15*(1), 1-7.

10. Murphy, C., Rettedal, E., Lehouritis, P., Devoy, C., & Tangney, M. (2017). Intratumoural production of TNFα by bacteria mediates cancer therapy. *PloS one*, *12*(6), e0180034.

11. Hillson, N. J., Hu, P., Andersen, G. L., & Shapiro, L. (2007). Caulobacter crescentus as a whole-cell uranium biosensor. *Applied and environmental microbiology*, *73*(23), 7615-7621.

12. Beller, H. R., Lee, T. S., & Katz, L. (2015). Natural products as biofuels and bio-based chemicals: fatty acids and isoprenoids. *Natural product reports*, *32*(10), 1508-1526.

13. Rani, N., Sangwan, P., Joshi, M., Sagar, A., & Bala, K. (2019). Microbes: a key player in industrial wastewater treatment. In *Microbial wastewater treatment* (pp. 83-102). Elsevier.

14. Nguyen, T. H., Ghorbel, E., Fares, H., & Cousture, A. (2019). Bacterial self-healing of concrete and durability assessment. *Cement and Concrete Composites*, *104*, 103340.

15. Gleizer, S., Ben-Nissan, R., Bar-On, Y. M., Antonovsky, N., Noor, E., Zohar, Y., ... & Milo, R. (2019). Conversion of Escherichia coli to generate all biomass carbon from CO2. *Cell*, *179*(6), 1255-1263.

16. Deng, D., Zhang, Y., & Liu, Y. (2015). A Geobacter strain isolated from rice paddy soil with higher bioelectricity generation capability in comparison to Geobacter sulfurreducens PCA. *RSC Advances*, *5*(55), 43978-43989.

17. Claassens, N. J., Sousa, D. Z., dos Santos, V. A., De Vos, W. M., & van der Oost, J. (2016). Harnessing the power of microbial autotrophy. *Nature Reviews Microbiology*, *14*(11), 692-706.

18. Du, J., Shao, Z., & Zhao, H. (2011). Engineering microbial factories for synthesis of value-added products. *Journal of Industrial Microbiology and Biotechnology*, *38*(8), 873-890.

19. Liu, F., Monroe, E., & Davis, R. W. (2019). Engineering microbial consortia for bioconversion of multisubstrate biomass streams to biofuels. In *Biofuels-Challenges and opportunities*. London: IntechOpen.

20. Zheng, T., Li, J., Ji, Y., Zhang, W., Fang, Y., Xin, F., ... & Jiang, M. (2020). Progress and prospects of bioelectrochemical systems: electron transfer and its applications in the microbial metabolism. *Frontiers in Bioengineering and Biotechnology*, *8*, 10.

21. Potter, M. C. (1911). Electrical effects accompanying the decomposition of organic compounds. *Proceedings of the royal society of London. Series b, containing papers of a biological character*, *84*(571), 260-276.

22. Munoz-Cupa, C., Hu, Y., Xu, C., & Bassi, A. (2021). An overview of microbial fuel cell usage in wastewater treatment, resource recovery and energy production. *Science of the Total Environment*, *754*, 142429.

23. Gude, V. G. (2015). Energy and water autarky of wastewater treatment and power generation systems. *Renewable and sustainable energy reviews*, *45*, 52-68.

24. Rabaey, K., & Verstraete, W. (2005). Microbial fuel cells: novel biotechnology for energy generation. *TRENDS in Biotechnology*, *23*(6), 291-298.

25. Cabau-Peinado, O., Straathof, A. J., & Jourdin, L. (2021). A general model for biofilm-driven microbial electrosynthesis of carboxylates from CO2. *Frontiers in microbiology*, *12*, 669218.

26. Jourdin, L., Sousa, J., van Stralen, N., & Strik, D. P. (2020). Techno-economic assessment of microbial electrosynthesis from CO2 and/or organics: An interdisciplinary roadmap towards future research and application. *Applied Energy*, *279*, 115775.

27. Zhang, D., Yang, F., Shimotori, T., Wang, K. C., & Huang, Y. (2012). Performance evaluation of power management systems in microbial fuel cell-based energy harvesting applications for driving small electronic devices. *Journal of Power Sources*, *217*, 65-71.

28. Pham, T. H., Rabaey, K., Aelterman, P., Clauwaert, P., De Schamphelaire, L., Boon, N., & Verstraete, W. (2006). Microbial fuel cells in relation to conventional anaerobic digestion technology. *Engineering in Life Sciences*, *6*(3), 285-292.

29. Bird, L. J., Kundu, B. B., Tschirhart, T., Corts, A. D., Su, L., Gralnick, J. A., ... & Glaven, S. M. (2021). Engineering Wired Life: Synthetic Biology for Electroactive Bacteria. *ACS Synthetic Biology*, *10*(11), 2808-2823.

30. Lovley, D. R., & Holmes, D. E. (2022). Electromicrobiology: the ecophysiology of phylogenetically diverse electroactive microorganisms. *Nature Reviews Microbiology*, *20*(1), 5-19.

31. Babauta, J., Renslow, R., Lewandowski, Z., & Beyenal, H. (2012). Electrochemically active biofilms: facts and fiction. A review. *Biofouling*, *28*(8), 789-812.

32. Chu, N., Liang, Q., Zhang, W., Ge, Z., Hao, W., Jiang, Y., & Zeng, R. J. (2020). Waste C1 gases as alternatives to pure CO2 improved the microbial electrosynthesis of C4 and C6 carboxylates. *ACS Sustainable Chemistry & Engineering*, *8*(23), 8773-8782.

33. Banner, A., Toogood, H. S., & Scrutton, N. S. (2021). Consolidated bioprocessing: synthetic biology routes to fuels and fine chemicals. *Microorganisms*, *9*(5), 1079.

34. Lee, S. Y., & Kim, H. U. (2015). Systems strategies for developing industrial microbial strains. *Nature biotechnology*, *33*(10), 1061-1072.

35. Kelly, J. R., Rubin, A. J., Davis, J. H., Ajo-Franklin, C. M., Cumbers, J., Czar, M. J., ... & Endy, D. (2009). Measuring the activity of BioBrick promoters using an in vivo reference standard. *Journal of biological engineering*, *3*(1), 1-13.

36. Lee, J. W., Choi, S., Park, J. H., Vickers, C. E., Nielsen, L. K., & Lee, S. Y. (2010). Development of sucrose-utilizing Escherichia coli K-12 strain by cloning β-fructofuranosidases and its application for L-threonine production. *Applied microbiology and biotechnology*, *88*(4), 905-913.

37. Park, J. H., Lee, K. H., Kim, T. Y., & Lee, S. Y. (2007). Metabolic engineering of Escherichia coli for the production of L-valine based on transcriptome analysis and in silico gene knockout simulation. *Proceedings of the national academy of sciences*, *104*(19), 7797-7802.

38. Yim, H., Haselbeck, R., Niu, W., Pujol-Baxley, C., Burgard, A., Boldt, J., ... & Van Dien, S. (2011). Metabolic engineering of Escherichia coli for direct production of 1, 4-butanediol. *Nature chemical biology*, *7*(7), 445-452.

39. Nikel, P. I., Chavarria, M., Danchin, A., & de Lorenzo, V. (2016). From dirt to industrial applications: Pseudomonas putida as a synthetic biology chassis for hosting harsh biochemical reactions. *Current opinion in chemical biology*, *34*, 20-29.

40. Wendisch, V. F., Brito, L. F., Lopez, M. G., Hennig, G., Pfeifenschneider, J., Sgobba, E., & Veldmann, K. H. (2016). The flexible feedstock concept in industrial biotechnology: metabolic engineering of Escherichia coli, Corynebacterium glutamicum, Pseudomonas, Bacillus and yeast strains for access to alternative carbon sources. *Journal of biotechnology*, *234*, 139-157.

41. Gu, Y., Xu, X., Wu, Y., Niu, T., Liu, Y., Li, J., ... & Liu, L. (2018). Advances and prospects of Bacillus subtilis cellular factories: from rational design to industrial applications. *Metabolic engineering*, *50*, 109-121.

42. Fernández-Cabezón, L., & Nikel, P. I. (2020). Advanced metabolic engineering strategies for the development of sustainable microbial processes. In *New and Future Developments in Microbial Biotechnology and Bioengineering* (pp. 225-246). Elsevier.

43. Janssen, P. J., Van Houdt, R., Moors, H., Monsieurs, P., Morin, N., Michaux, A., ... & Mergeay, M. (2010). The complete genome sequence of Cupriavidus metallidurans strain CH34, a master survivalist in harsh and anthropogenic environments. *PloS one*, *5*(5), e10433.

44. Mergeay, M., Nies, D., Schlegel, H. G., Gerits, J., Charles, P., & Van Gijsegem, F. (1985). Alcaligenes eutrophus CH34 is a facultative chemolithotroph with plasmid-bound resistance to heavy metals. *Journal of bacteriology*, *162*(1), 328-334.

45. Mergeay, M., & Van Houdt, R. (Eds.). (2015). *Metal Response in Cupriavidus metallidurans: Volume I: From Habitats to Genes and Proteins*. Springer.

46. Reith, F., Rogers, S. L., McPhail, D. C., & Webb, D. (2006). Biomineralization of gold: biofilms on bacterioform gold. *science*, *313*(5784), 233-236.

47. Coenye, T., Spilker, T., Reik, R., Vandamme, P., & LiPuma, J. J. (2005). Use of PCR analyses to define the distribution of Ralstonia species recovered from patients with cystic fibrosis. *Journal of Clinical Microbiology*, *43*(7), 3463-3466.

48. Monsieurs, P., Mijnendonckx, K., Provoost, A., Venkateswaran, K., Ott, C. M., Leys, N., & Van Houdt, R. (2014). Genome sequences of Cupriavidus metallidurans strains NA1, NA4, and NE12, isolated from space equipment. *Genome announcements*, *2*(4), e00719-14.

49. Mergeay, M., & Van Houdt, R. (Eds.). (2015). *Metal Response in Cupriavidus metallidurans: Volume I: From Habitats to Genes and Proteins*. Springer.

50. Millacura, F. A., Cárdenas, F., Mendez, V., Seeger, M., & Rojas, L. A. (2017). Degradation of benzene by the heavy-metal resistant bacterium Cupriavidus metallidurans CH34 reveals its catabolic potential for aromatic compounds. *bioRxiv*, 164517.

51. Fairbrother, L., Etschmann, B., Brugger, J., Shapter, J., Southam, G., & Reith, F. (2013). Biomineralization of gold in biofilms of Cupriavidus metallidurans. *Environmental Science & Technology*, *47*(6), 2628-2635.

52. Espinoza Tofalos, A., Daghio, M., González, M., Papacchini, M., Franzetti, A., & Seeger, M. (2018). Toluene degradation by Cupriavidus metallidurans CH34 in nitrate-reducing conditions and in Bioelectrochemical Systems. *FEMS microbiology letters*, *365*(12), fny119.

53. de Campos Rodrigues, T., & Rosenbaum, M. A. (2014). Microbial electroreduction: screening for new cathodic biocatalysts. *ChemElectroChem*, *1*(11), 1916-1922.

54. Diels, L., Spaans, P. H., Van Roy, S., Hooyberghs, L., Ryngaert, A., Wouters, H., ... & Tsezos, M. (2003). Heavy metals removal by sand filters inoculated with metal sorbing and precipitating bacteria. *Hydrometallurgy*, *71*(1-2), 235-241.

55. Corbisier, P., Thiry, E., & Diels, L. (1996). Bacterial biosensors for the toxicity assessment of solid wastes. *Environmental Toxicology and Water Quality: An International Journal*, *11*(3), 171-177.

56. Biondo, R., da Silva, F. A., Vicente, E. J., Souza Sarkis, J. E., & Schenberg, A. C. G. (2012). Synthetic phytochelatin surface display in Cupriavidus metallidurans CH34 for enhanced metals bioremediation. *Environmental science & technology*, *46*(15), 8325-8332.

57. Valls, M., Atrian, S., de Lorenzo, V., & Fernández, L. A. (2000). Engineering a mouse metallothionein on the cell surface of Ralstonia eutropha CH34 for immobilization of heavy metals in soil. *Nature biotechnology*, *18*(6), 661-665.

58. Panich, J., Fong, B., & Singer, S. W. (2021). Metabolic engineering of Cupriavidus necator H16 for sustainable biofuels from CO2. *Trends in biotechnology*, *39*(4), 412-424.

59. Alagesan, S., Hanko, E. K., Malys, N., Ehsaan, M., Winzer, K., & Minton, N. P. (2018). Functional genetic elements for controlling gene expression in Cupriavidus necator H16. *Applied and environmental microbiology*, *84*(19), e00878-18.

60. Xiong, B., Li, Z., Liu, L., Zhao, D., Zhang, X., & Bi, C. (2018). Genome editing of Ralstonia eutropha using an electroporation-based CRISPR-Cas9 technique. *Biotechnology for biofuels*, *11*(1), 1-9.

61. Hu, M., Xiong, B., Li, Z., Liu, L., Li, S., Zhang, C., ... & Bi, C. (2020). A novel gene expression system for Ralstonia eutropha based on the T7 promoter. *BMC microbiology*, *20*(1), 1-7.

62. Riley, L. A., & Guss, A. M. (2021). Approaches to genetic tool development for rapid domestication of non-model microorganisms. *Biotechnology for Biofuels*, *14*(1), 1-17.

63. Ribeiro-dos-Santos, G., Biondo, R., Quadros, O. D. F., Vicente, E. J., & Schenberg, A. C. G. (2010). A metal-repressed promoter from gram-positive Bacillus subtilis is highly active and metal-induced in gram-negative Cupriavidus metallidurans. *Biotechnology and bioengineering*, *107*(3), 469-477.

64. Sybesma, W., Starrenburg, M., Kleerebezem, M., Mierau, I., de Vos, W. M., & Hugenholtz, J. (2003). Increased production of folate by metabolic engineering of Lactococcus lactis. *Applied and Environmental Microbiology*, *69*(6), 3069-3076.

65. Qi, L. S., Larson, M. H., Gilbert, L. A., Doudna, J. A., Weissman, J. S., Arkin, A. P., & Lim, W. A. (2013). Repurposing CRISPR as an RNA-guided platform for sequence-specific control of gene expression. *Cell*, *152*(5), 1173-1183.

66. Lynch, S. A., Desai, S. K., Sajja, H. K., & Gallivan, J. P. (2007). A high-throughput screen for synthetic riboswitches reveals mechanistic insights into their function. *Chemistry & biology*, *14*(2), 173-184.

67. Lino, C. A., Harper, J. C., Carney, J. P., & Timlin, J. A. (2018). Delivering CRISPR: a review of the challenges and approaches. *Drug delivery*, *25*(1), 1234-1257.

68. Friehs, K. (2004). Plasmid copy number and plasmid stability. *New trends and developments in biochemical engineering*, 47-82.

69. Ensley, B. D. (1986). Stability of recombinant plasmids in industrial microorganisms. *Critical Reviews in Biotechnology*, *4*(3), 263-277.

70. Bentley, W. E., Mirjalili, N., Andersen, D. C., Davis, R. H., & Kompala, D. S. (1990). Plasmid-encoded protein: the principal factor in the "metabolic burden" associated with recombinant bacteria. *Biotechnology and bioengineering*, *35*(7), 668-681.

71. Meade, J., Bartlow, P., Trivedi, R. N., Akhtar, P., Ataai, M. M., Khan, S. A., & Domach, M. M. (2015). Effect of plasmid replication deregulation via inc mutations on E. coli proteome & simple flux model analysis. *Microbial Cell Factories*, *14*(1), 1-13.

72. Bennett, P. M. (2008). Plasmid encoded antibiotic resistance: acquisition and transfer of antibiotic resistance genes in bacteria. *British journal of pharmacology*, *153*(S1), S347-S357.

73. Kasai, Y., Inoue, J., & Harayama, S. (2001). The TOL plasmid pWW0 xylN gene product from Pseudomonas putida is involved in m-xylene uptake. *Journal of Bacteriology*, *183*(22), 6662-6666.

74. Lund, B. A., Leiros, H. K. S., & Bjerga, G. K. (2014). A high-throughput, restriction-free cloning and screening strategy based on ccd B-gene replacement. *Microbial Cell Factories*, *13*(1), 1-7.

75. Morin, C. E., & Kaper, J. B. (2009). Use of stabilized luciferase-expressing plasmids to examine in vivo-induced promoters in the Vibrio cholerae vaccine strain CVD 103-HgR. *FEMS Immunology & Medical Microbiology*, *57*(1), 69-79.

76. Voss, I., & Steinbüchel, A. (2006). Application of a KDPG-aldolase gene-dependent addiction system for enhanced production of cyanophycin in Ralstonia eutropha strain H16. *Metabolic engineering*, *8*(1), 66-78.

77. Schneider, J. C., Jenings, A. F., Mun, D. M., McGovern, P. M., & Chew, L. C. (2005). Auxotrophic markers pyrF and proC can replace antibiotic markers on protein production plasmids in high-cell-density Pseudomonas fluorescens fermentation. *Biotechnology progress*, *21*(2), 343-348.

78. Jarboe, L. R., Zhang, X., Wang, X., Moore, J. C., Shanmugam, K. T., & Ingram, L. O. (2010). Metabolic engineering for production of biorenewable fuels and chemicals: contributions of synthetic biology. *Journal of Biomedicine and Biotechnology*, *2010*.

79. Baker, T. A., Bell, S. P., Gann, A., Levine, M., Losick, R., & Inglis, C. H. S. L. P. (2008). *Molecular biology of the gene*. San Francisco, CA, USA:: Pearson/Benjamin Cummings.

80. Palazzo, A. F., & Lee, E. S. (2015). Non-coding RNA: what is functional and what is junk?. *Frontiers in genetics*, *6*, 2.

81. Fitz, E., Wanka, F., & Seiboth, B. (2018). The promoter toolbox for recombinant gene expression in Trichoderma reesei. *Frontiers in Bioengineering and Biotechnology*, *6*, 135.

82. Salis, H. M., Mirsky, E. A., & Voigt, C. A. (2009). Automated design of synthetic ribosome binding sites to control protein expression. *Nature biotechnology*, *27*(10), 946-950.

83. Isaacs, F. J., Dwyer, D. J., Ding, C., Pervouchine, D. D., Cantor, C. R., & Collins, J. J. (2004). Engineered riboregulators enable post-transcriptional control of gene expression. *Nature biotechnology*, *22*(7), 841-847.

84. Cañadas, I. C., Groothuis, D., Zygouropoulou, M., Rodrigues, R., & Minton, N. P. (2019). RiboCas: a universal CRISPR-based editing tool for Clostridium. *ACS synthetic biology*, *8*(6), 1379-1390.

85. Wang, Q., Zhang, J., Al Makishah, N. H., Sun, X., Wen, Z., Jiang, Y., & Yang, S. (2021). Advances and perspectives for genome editing tools of Corynebacterium glutamicum. *Frontiers in Microbiology*, *12*, 654058.

86. Ehsaan, M., Kuit, W., Zhang, Y., Cartman, S. T., Heap, J. T., Winzer, K., & Minton, N. P. (2016). Mutant generation by allelic exchange and genome resequencing of the biobutanol organism Clostridium acetobutylicum ATCC 824. *Biotechnology for biofuels*, *9*(1), 1-20.

87. Kleihues, L., Lenz, O., Bernhard, M., Buhrke, T., & Friedrich, B. (2000). The H2 sensor of Ralstonia eutropha is a member of the subclass of regulatory [NiFe] hydrogenases. *Journal of bacteriology*, *182*(10), 2716-2724.

88. Zoropogui, A., Gambarelli, S., & Coves, J. (2008). CzcE from Cupriavidus metallidurans CH34 is a copper-binding protein. *Biochemical and biophysical research communications*, *365*(4), 735-739.

89. Lambert, J. M., Bongers, R. S., & Kleerebezem, M. (2007). Cre-lox-based system for multiple gene deletions and selectable-marker removal in Lactobacillus plantarum. *Applied and environmental microbiology*, *73*(4), 1126-1135.

90. Leibig, M., Krismer, B., Kolb, M., Friede, A., Götz, F., & Bertram, R. (2008). Marker removal in staphylococci via Cre recombinase and different lox sites. *Applied and environmental microbiology*, *74*(5), 1316-1323.

91. Jinek, M., Chylinski, K., Fonfara, I., Hauer, M., Doudna, J. A., & Charpentier, E. (2012). A programmable dual-RNA–guided DNA endonuclease in adaptive bacterial immunity. *science*, *337*(6096), 816-821.

92. Westermann, L., Neubauer, B., & Köttgen, M. (2021). Nobel Prize 2020 in Chemistry honors CRISPR: a tool for rewriting the code of life. *Pflügers Archiv-European Journal of Physiology*, *473*(1), 1-2.

93. Ishino, Y., Shinagawa, H., Makino, K., Amemura, M., & Nakata, A. (1987). Nucleotide sequence of the iap gene, responsible for alkaline phosphatase isozyme

conversion in Escherichia coli, and identification of the gene product. *Journal of bacteriology*, *169*(12), 5429-5433.

94. Van Soolingen, D., De Haas, P. E., Hermans, P. W., Groenen, P. M., & Van Embden, J. D. (1993). Comparison of various repetitive DNA elements as genetic markers for strain differentiation and epidemiology of Mycobacterium tuberculosis. *Journal of clinical microbiology*, *31*(8), 1987-1995.

95. Mojica, F. J., Díez-Villaseñor, C., García-Martínez, J., & Soria, E. (2005). Intervening sequences of regularly spaced prokaryotic repeats derive from foreign genetic elements. *Journal of molecular evolution*, *60*(2), 174-182.

96. Alkhnbashi, O. S., Shah, S. A., Garrett, R. A., Saunders, S. J., Costa, F., & Backofen, R. (2016). Characterizing leader sequences of CRISPR loci. *Bioinformatics*, *32*(17), i576-i585.

97. Jansen, R., Embden, J. D. V., Gaastra, W., & Schouls, L. M. (2002). Identification of genes that are associated with DNA repeats in prokaryotes. *Molecular microbiology*, *43*(6), 1565-1575.

98. Pourcel, C., Salvignol, G., & Vergnaud, G. (2005). CRISPR elements in Yersinia pestis acquire new repeats by preferential uptake of bacteriophage DNA, and provide additional tools for evolutionary studies. *Microbiology*, *151*(3), 653-663.

99. Barrangou, R., Fremaux, C., Deveau, H., Richards, M., Boyaval, P., Moineau, S., ... & Horvath, P. (2007). CRISPR provides acquired resistance against viruses in prokaryotes. *Science*, *315*(5819), 1709-1712.

100. Brouns, S. J., Jore, M. M., Lundgren, M., Westra, E. R., Slijkhuis, R. J., Snijders, A. P., ... & Van Der Oost, J. (2008). Small CRISPR RNAs guide antiviral defense in prokaryotes. *Science*, *321*(5891), 960-964.

101. Mojica, F. J., Díez-Villaseñor, C., García-Martínez, J., & Almendros, C. (2009). Short motif sequences determine the targets of the prokaryotic CRISPR defence system. *Microbiology*, *155*(3), 733-740.

102. Collias, D., & Beisel, C. L. (2021). CRISPR technologies and the search for the PAM-free nuclease. *Nature communications*, *12*(1), 1-12.

103. Zheng, Y., Li, J., Wang, B., Han, J., Hao, Y., Wang, S., ... & Peng, W. (2020). Endogenous type I CRISPR-Cas: from foreign DNA defense to prokaryotic engineering. *Frontiers in bioengineering and biotechnology*, *8*, 62.

104. DiCarlo, J. E., Norville, J. E., Mali, P., Rios, X., Aach, J., & Church, G. M. (2013). Genome engineering in Saccharomyces cerevisiae using CRISPR-Cas systems. *Nucleic acids research*, *41*(7), 4336-4343.

105. Cong, L., Ran, F. A., Cox, D., Lin, S., Barretto, R., Habib, N., ... & Zhang, F. (2013). Multiplex genome engineering using CRISPR/Cas systems. *Science*, *339*(6121), 819-823.

106. Vyas, V. K., Barrasa, M. I., & Fink, G. R. Candida albicans CRISPR system permits genetic engineering of essential genes and gene families. Sci. Adv. 1, e1500248 (2015).

107. Friedland, A. E., Tzur, Y. B., Esvelt, K. M., Colaiácovo, M. P., Church, G. M., & Calarco, J. A. (2013). Heritable genome editing in C. elegans via a CRISPR-Cas9 system. *Nature methods*, *10*(8), 741-743.

108. Jiang, W., Zhou, H., Bi, H., Fromm, M., Yang, B., & Weeks, D. P. (2013). Demonstration of CRISPR/Cas9/sgRNA-mediated targeted gene modification in Arabidopsis, tobacco, sorghum and rice. *Nucleic acids research*, *41*(20), e188-e188.

109. Arroyo-Olarte, R. D., Bravo Rodríguez, R., & Morales-Ríos, E. (2021). Genome editing in bacteria: CRISPR-Cas and beyond. *Microorganisms*, *9*(4), 844.

110. Nelson, D. L., Lehninger, A. L., & Cox, M. M. (2008). *Lehninger principles of biochemistry*. Macmillan.

111. Lecomte, S. M., Achouak, W., Abrouk, D., Heulin, T., Nesme, X., & Haichar, F. E. Z. (2018). Diversifying anaerobic respiration strategies to compete in the rhizosphere. *Frontiers in Environmental Science*, *6*, 139.

112. Pester, M., Knorr, K. H., Friedrich, M. W., Wagner, M., & Loy, A. (2012). Sulfate-reducing microorganisms in wetlands–fameless actors in carbon cycling and climate change. *Frontiers in microbiology*, *3*, 72.

113. Kraft, B., Strous, M., & Tegetmeyer, H. E. (2011). Microbial nitrate respiration–genes, enzymes and environmental distribution. *Journal of biotechnology*, *155*(1), 104-117.

114.Rabus, R., Hansen, T. A., & Widdel, F. (2006). Dissimilatory sulfate-and sulfur-reducing prokaryotes. *The prokaryotes*, *2*, 659-768.

115. Myers, C. R., & Nealson, K. H. (1988). Bacterial manganese reduction and growth with manganese oxide as the sole electron acceptor. *Science*, *240*(4857), 1319-1321.

116. Lovley, D. R., & Phillips, E. J. (1988). Novel mode of microbial energy metabolism: organic carbon oxidation coupled to dissimilatory reduction of iron or manganese. *Applied and environmental microbiology*, *54*(6), 1472-1480.

117. Kim, B. H., Kim, H. J., Hyun, M. S., & Park, D. H. (1999). Direct electrode reaction of Fe (III)-reducing bacterium, Shewanella putrefaciens. *Journal of microbiology and biotechnology*, *9*(2), 127-131.

118. Von Canstein, H., Ogawa, J., Shimizu, S., & Lloyd, J. R. (2008). Secretion of flavins by Shewanella species and their role in extracellular electron transfer. *Applied and environmental microbiology*, *74*(3), 615-623.

119. Myers, J. M., & Myers, C. R. (2001). Role for outer membrane cytochromes OmcA and OmcB of Shewanella putrefaciens MR-1 in reduction of manganese dioxide. *Applied and environmental microbiology*, *67*(1), 260-269.

120. Marsili, E., Rollefson, J. B., Baron, D. B., Hozalski, R. M., & Bond, D. R. (2008). Microbial biofilm voltammetry: direct electrochemical characterization of catalytic electrode-attached biofilms. *Applied and environmental microbiology*, *74*(23), 7329-7337.

121. Holmes, D. E., Chaudhuri, S. K., Nevin, K. P., Mehta, T., Methé, B. A., Liu, A., ... & Lovley, D. R. (2006). Microarray and genetic analysis of electron transfer to electrodes in Geobacter sulfurreducens. *Environmental Microbiology*, *8*(10), 1805-1815.

122. Carlson, H. K., Iavarone, A. T., Gorur, A., Yeo, B. S., Tran, R., Melnyk, R. A., ... & Coates, J. D. (2012). Surface multiheme c-type cytochromes from Thermincola potens and implications for respiratory metal reduction by Gram-positive bacteria. *Proceedings of the National Academy of Sciences*, *109*(5), 1702-1707.

123. Köpke, M., Held, C., Hujer, S., Liesegang, H., Wiezer, A., Wollherr, A., ... & Dürre, P. (2010). Clostridium ljungdahlii represents a microbial production platform based on syngas. *Proceedings of the National Academy of Sciences*, *107*(29), 13087-13092.

124. Rabaey, K., Boon, N., Höfte, M., & Verstraete, W. (2005). Microbial phenazine production enhances electron transfer in biofuel cells. *Environmental science & technology*, *39*(9), 3401-3408.

125. Hernandez, M. E., Kappler, A., & Newman, D. K. (2004). Phenazines and other redox-active antibiotics promote microbial mineral reduction. *Applied and environmental microbiology*, *70*(2), 921-928.

126. Marritt, S. J., Lowe, T. G., Bye, J., McMillan, D. G., Shi, L., Fredrickson, J., ... & Butt, J. N. (2012). A functional description of CymA, an electron-transfer hub supporting anaerobic respiratory flexibility in Shewanella. *Biochemical Journal*, *444*(3), 465-474

127. Lower, B. H., Shi, L., Yongsunthon, R., Droubay, T. C., McCready, D. E., & Lower, S. K. (2007). Specific bonds between an iron oxide surface and outer membrane cytochromes MtrC and OmcA from Shewanella oneidensis MR-1. *Journal of bacteriology*, *189*(13), 4944-4952.

128. Schuetz, B., Schicklberger, M., Kuermann, J., Spormann, A. M., & Gescher, J. (2009). Periplasmic electron transfer via the c-type cytochromes MtrA and FccA of Shewanella oneidensis MR-1. *Applied and environmental microbiology*, *75*(24), 7789-7796.

129. Leys, D., Meyer, T. E., Tsapin, A. S., Nealson, K. H., Cusanovich, M. A., & Van Beeumen, J. J. (2002). Crystal structures at atomic resolution reveal the novel concept of "electron-harvesting" as a role for the small tetraheme cytochrome c. *Journal of Biological Chemistry*, *277*(38), 35703-35711.

130. McMillan, D. G., Marritt, S. J., Firer-Sherwood, M. A., Shi, L., Richardson, D. J., Evans, S. D., ... & Jeuken, L. J. (2013). Protein–protein interaction regulates the direction of catalysis and electron transfer in a redox enzyme complex. *Journal of the American Chemical Society*, *135*(28), 10550-10556.

131. Yang, Y., Xu, M., Guo, J., & Sun, G. (2012). Bacterial extracellular electron transfer in bioelectrochemical systems. *Process Biochemistry*, *47*(12), 1707-1714.

132. Kitayama, S. compositions, and activities of live Shewanella biofilms formed on graphite electrodes in electrochemical flow cells. *Appl. Environ. Microbiol*, (83), 00903-17.

133. Vargas, M., Malvankar, N. S., Tremblay, P. L., Leang, C., Smith, J. A., Patel, P., ... & Lovley, D. R. (2013). Aromatic amino acids required for pili conductivity and long-range extracellular electron transport in Geobacter sulfurreducens. *MBio*, *4*(2), e00105-13.

134. Yalcin, S. E., O'Brien, J. P., Gu, Y., Reiss, K., Yi, S. M., Jain, R., ... & Malvankar, N. S. (2020). Electric field stimulates production of highly conductive microbial OmcZ nanowires. *Nature chemical biology*, *16*(10), 1136-1142.

135. Yalcin, S. E., & Malvankar, N. S. (2020). The blind men and the filament: understanding structures and functions of microbial nanowires. *Current opinion in chemical biology*, *59*, 193-201.

136. Reardon, P. N., & Mueller, K. T. (2013). Structure of the type IVa major pilin from the electrically conductive bacterial nanowires of Geobacter sulfurreducens. *Journal of Biological Chemistry*, *288*(41), 29260-29266.

137. Childers, S. E., Ciufo, S., & Lovley, D. R. (2002). Geobacter metallireducens accesses insoluble Fe (III) oxide by chemotaxis. *Nature*, *416*(6882), 767-769.

138. Reguera, G., McCarthy, K. D., Mehta, T., Nicoll, J. S., Tuominen, M. T., & Lovley, D. R. (2005). Extracellular electron transfer via microbial nanowires. *Nature*, *435*(7045), 1098-1101.

139. Reguera, G., Nevin, K. P., Nicoll, J. S., Covalla, S. F., Woodard, T. L., & Lovley, D. R. (2006). Biofilm and nanowire production leads to increased current in Geobacter sulfurreducens fuel cells. *Applied and environmental microbiology*, *72*(11), 7345-7348.

140. Yi, H., Nevin, K. P., Kim, B. C., Franks, A. E., Klimes, A., Tender, L. M., & Lovley, D. R. (2009). Selection of a variant of Geobacter sulfurreducens with enhanced capacity for current production in microbial fuel cells. *Biosensors and Bioelectronics*, *24*(12), 3498-3503.

141. Liu, X., Walker, D. J., Nonnenmann, S. S., Sun, D., & Lovley, D. R. (2021). Direct observation of electrically conductive pili emanating from Geobacter sulfurreducens. *Mbio*, *12*(4), e02209-21.

142. Lebedev, N., Mahmud, S., Griva, I., Blom, A., & Tender, L. M. (2015). On the electron transfer through Geobacter sulfurreducens P il A protein. *Journal of Polymer Scince Part B: Polymer Physics*, *53*(24), 1706-1717.

143. Yan, H., Chuang, C., Zhugayevych, A., Tretiak, S., Dahlquist, F. W., & Bazan, G. C. (2015). Inter-Aromatic Distances in Geobacter Sulfurreducens Pili Relevant to Biofilm Charge Transport. *Advanced Materials*, *27*(11), 1908-1911.

144. Gu, Y., Srikanth, V., Salazar-Morales, A. I., Jain, R., O'Brien, J. P., Yi, S. M., ... & Malvankar, N. S. (2021). Structure of Geobacter pili reveals secretory rather than nanowire behaviour. *Nature*, *597*(7876), 430-434.

145. Reith, F., Rogers, S. L., McPhail, D. C., & Webb, D. (2006). Biomineralization of gold: biofilms on bacterioform gold. *science*, *313*(5784), 233-236.

146. Wiesemann, N., Mohr, J., Grosse, C., Herzberg, M., Hause, G., Reith, F., & Nies, D. H. (2013). Influence of copper resistance determinants on gold transformation by Cupriavidus metallidurans strain CH34. *Journal of bacteriology*, *195*(10), 2298-2308.

147. Wiesemann, N., Mohr, J., Grosse, C., Herzberg, M., Hause, G., Reith, F., & Nies, D. H. (2013). Influence of copper resistance determinants on gold transformation by Cupriavidus metallidurans strain CH34. *Journal of bacteriology*, *195*(10), 2298-2308.

148. Becerril-Varela, K., Serment-Guerrero, J. H., Manzanares-Leal, G. L., Ramírez-Durán, N., & Guerrero-Barajas, C. (2021). Generation of electrical energy in a microbial fuel cell coupling acetate oxidation to Fe3+ reduction and isolation of the involved bacteria. *World Journal of Microbiology and Biotechnology*, *37*(6), 1-15.

149. Simon, R. U. P. A. P., Priefer, U., & Pühler, A. (1983). A broad host range mobilization system for in vivo genetic engineering: transposon mutagenesis in gram negative bacteria. *Bio/technology*, *1*(9), 784-791.

150. Choi, K. H., Kumar, A., & Schweizer, H. P. (2006). A 10-min method for preparation of highly electrocompetent Pseudomonas aeruginosa cells: application for DNA fragment transfer between chromosomes and plasmid transformation. *Journal of microbiological methods*, *64*(3), 391-397.

151. Ehsaan, M., Baker, J., Kovács, K., Malys, N., & Minton, N. P. (2021). The pMTL70000 modular, plasmid vector series for strain engineering in Cupriavidus necator H16. *Journal of microbiological methods*, *189*, 106323.

152. De Lorenzo, V., Herrero, M., Jakubzik, U., & Timmis, K. N. (1990). Mini-Tn5 transposon derivatives for insertion mutagenesis, promoter probing, and chromosomal insertion of cloned DNA in gram-negative eubacteria. *Journal of bacteriology*, *172*(11), 6568-6572.

153. Fleetwood, F., Andersson, K. G., Ståhl, S., & Löfblom, J. (2014). An engineered autotransporter-based surface expression vector enables efficient display of Affibody molecules on OmpT-negative E. coli as well as protease-mediated secretion in OmpT-positive strains. *Microbial cell factories*, *13*(1), 1-14.

154. Bard, A. J., Faulkner, L. R., & White, H. S. (2022). *Electrochemical methods: fundamentals and applications*. John Wiley & Sons.

155. Elgrishi, N., Rountree, K. J., McCarthy, B. D., Rountree, E. S., Eisenhart, T. T., & Dempsey, J. L. (2018). A practical beginner's guide to cyclic voltammetry. *Journal of chemical education*, *95*(2), 197-206.

156. Wang, H., Sayed, S. Y., Luber, E. J., Olsen, B. C., Shirurkar, S. M., Venkatakrishnan, S., ... & Buriak, J. M. (2020). Redox flow batteries: how to determine electrochemical kinetic parameters. *ACS nano*, *14*(3), 2575-2584.

157. Logan, B. E., Wallack, M. J., Kim, K. Y., He, W., Feng, Y., & Saikaly, P. E. (2015). Assessment of microbial fuel cell configurations and power densities. *Environmental Science & Technology Letters*, *2*(8), 206-214.

158. Aghababaie, M., Farhadian, M., Jeihanipour, A., & Biria, D. (2015). Effective factors on the performance of microbial fuel cells in wastewater treatment–a review. *Environmental Technology Reviews*, *4*(1), 71-89.

159. Angelaalincy, M. J., Navanietha Krishnaraj, R., Shakambari, G., Ashokkumar, B., Kathiresan, S., & Varalakshmi, P. (2018). Biofilm engineering approaches for improving the performance of microbial fuel cells and bioelectrochemical systems. *Frontiers in Energy Research*, *6*, 63.

160. Min, D., Cheng, L., Zhang, F., Huang, X. N., Li, D. B., Liu, D. F., ... & Yu, H. Q. (2017). Enhancing extracellular electron transfer of Shewanella oneidensis MR-1 through coupling improved flavin synthesis and metal-reducing conduit for pollutant degradation. *Environmental science & technology*, *51*(9), 5082-5089.

161. Wang, V. B., Chua, S. L., Cao, B., Seviour, T., Nesatyy, V. J., Marsili, E., ... & Yang, L. (2013). Engineering PQS biosynthesis pathway for enhancement of bioelectricity production in Pseudomonas aeruginosa microbial fuel cells. *PloS one*, *8*(5), e63129.

162. Nosek, D., Jachimowicz, P., & Cydzik-Kwiatkowska, A. (2020). Anode modification as an alternative approach to improve electricity generation in microbial fuel cells. *Energies*, *13*(24), 6596.

163. Xu, H., Quan, X., Xiao, Z., & Chen, L. (2018). Effect of anodes decoration with metal and metal oxides nanoparticles on pharmaceutically active compounds removal and power generation in microbial fuel cells. *Chemical Engineering Journal*, *335*, 539-547.

164. Mollwitz, B., Brunk, E., Schmitt, S., Pojer, F., Bannwarth, M., Schiltz, M., ... & Johnsson, K. (2012). Directed evolution of the suicide protein O 6-alkylguanine-DNA alkyltransferase for increased reactivity results in an alkylated protein with exceptional stability. *Biochemistry*, *51*(5), 986-994.

165. Richins, R. D., Kaneva, I., Mulchandani, A., & Chen, W. (1997). Biodegradation of organophosphorus pesticides by surface-expressed organophosphorus hydrolase. *Nature biotechnology*, *15*(10), 984-987.

166. Lee, J. S., Shin, K. S., Pan, J. G., & Kim, C. J. (2000). Surface-displayed viral antigens on Salmonella carrier vaccine. *Nature biotechnology*, *18*(6), 645-648.

167. Biondo, R., da Silva, F. A., Vicente, E. J., Souza Sarkis, J. E., & Schenberg, A. C. G. (2012). Synthetic phytochelatin surface display in Cupriavidus metallidurans CH34 for enhanced metals bioremediation. *Environmental science & technology*, *46*(15), 8325-8332.

168. Tozakidis, I. E., Sichwart, S., & Jose, J. (2015). Going beyond E. coli: autotransporter based surface display on alternative host organisms. *New biotechnology*, *32*(6), 644-650.

169. Lee, J. S., Shin, K. S., Pan, J. G., & Kim, C. J. (2000). Surface-displayed viral antigens on Salmonella carrier vaccine. *Nature biotechnology*, *18*(6), 645-648.

170. Jose, J., Bernhardt, R., & Hannemann, F. (2002). Cellular surface display of dimeric Adx and whole cell P450-mediated steroid synthesis on E. coli. *Journal of biotechnology*, *95*(3), 257-268.

171. Singh, M., Kaur, N., & Comini, E. (2020). The role of self-assembled monolayers in electronic devices. *Journal of Materials Chemistry C*, *8*(12), 3938-3955.

172. Noyhouzer, T., & Mandler, D. (2011). Determination of low levels of cadmium ions by the under potential deposition on a self-assembled monolayer on gold electrode. *Analytica chimica acta*, *684*(1-2), 1-7.

173. Campbell, I. H., Rubin, S., Zawodzinski, T. A., Kress, J. D., Martin, R. L., Smith, D. L., ... & Ferraris, J. P. (1996). Controlling Schottky energy barriers in organic electronic devices using self-assembled monolayers. *Physical Review B*, *54*(20), R14321.

174. Van Houdt, R., Vandecraen, J., Leys, N., Monsieurs, P., & Aertsen, A. (2021). Adaptation of Cupriavidus metallidurans CH34 to toxic zinc concentrations involves an uncharacterized ABC-Type transporter. *Microorganisms*, *9*(2), 309.

175. Lipman, N. S., Jackson, L. R., Trudel, L. J., & Weis-Garcia, F. (2005). Monoclonal versus polyclonal antibodies: distinguishing characteristics, applications, and information resources. *ILAR journal*, *46*(3), 258-268.

176. Saavedra, J. T., Schwartzman, J. A., & Gilmore, M. S. (2017). Mapping transposon insertions in bacterial genomes by arbitrarily primed PCR. *Current protocols in molecular biology*, *118*(1), 15-15.

177. Silva, F., Queiroz, J. A., & Domingues, F. C. (2012). Evaluating metabolic stress and plasmid stability in plasmid DNA production by Escherichia coli. *Biotechnology advances*, *30*(3), 691-708.

178. Siegel, R., & Ryu, D. D. (1985). Kinetic study of instability of recombinant plasmid pPLc23trpAl in E. coli using two-stage continuous culture system. *Biotechnology and Bioengineering*, *27*(1), 28-33.

179. Popov, M., Petrov, S., Nacheva, G., Ivanov, I., & Reichl, U. (2011). Effects of a recombinant gene expression on ColE1-like plasmid segregation in Escherichia coli. *BMC biotechnology*, *11*(1), 1-12.

180. Van Houdt, R., Monsieurs, P., Mijnendonckx, K., Provoost, A., Janssen, A., Mergeay, M., & Leys, N. (2012). Variation in genomic islands contribute to genome plasticity in Cupriavidus metallidurans. *BMC genomics*, *13*(1), 1-11.

181. Schofield, D. A., Westwater, C., Hoel, B. D., Werner, P. A., Norris, J. S., & Schmidt, M. G. (2003). Development of a thermally regulated broad-spectrum promoter system for use in pathogenic gram-positive species. *Applied and environmental microbiology*, *69*(6), 3385-3392.

182. Tyo, K. E., Ajikumar, P. K., & Stephanopoulos, G. (2009). Stabilized gene duplication enables long-term selection-free heterologous pathway expression. *Nature biotechnology*, *27*(8), 760-765.

183. Schmid, M. B., & Roth, J. R. (1987). Gene location affects expression level in Salmonella typhimurium. *Journal of bacteriology*, *169*(6), 2872-2875.

184. Schneider, J. C., Jenings, A. F., Mun, D. M., McGovern, P. M., & Chew, L. C. (2005). Auxotrophic markers pyrF and proC can replace antibiotic markers on protein production plasmids in high-cell-density Pseudomonas fluorescens fermentation. *Biotechnology progress*, *21*(2), 343-348.

185. Bailey, J. E. (1991). Toward a science of metabolic engineering. *Science*, *252*(5013), 1668-1675.

186. Jamalzadeh, E., van Gulik, W. M., & Heijnen, J. J. (2010). Fumaric acid Uptake Mechanism in Saccharomyces cerevisiae: Aerobic vs. Anaerobic Conditions. *Journal of Biotechnology*, (150), 515-516.

187. Weikert, C., Sauer, U., & Bailey, J. E. (1997). Use of a glycerol-limited, long-term chemostat for isolation of Escherichia coli mutants with improved physiological properties. *Microbiology*, *143*(5), 1567-1574.

188. Han, D., & Xu, Z. (2017). Development of a pyrE-based selective system for Thermotoga sp. strain RQ7. *Extremophiles*, *21*(2), 297-306.

189. Turnbough Jr, C. L., & Switzer, R. L. (2008). Regulation of pyrimidine biosynthetic gene expression in bacteria: repression without repressors. *Microbiology and Molecular Biology Reviews*, *72*(2), 266-300.

190. Boeke, J. D., La Croute, F., & Fink, G. R. (1984). A positive selection for mutants lacking orotidine-5′-phosphate decarboxylase activity in yeast: 5-fluoro-orotic acid resistance. *Molecular and General Genetics MGG*, *197*(2), 345-346.

191. Tripathi, S. A., Olson, D. G., Argyros, D. A., Miller, B. B., Barrett, T. F., Murphy, D. M., ... & Caiazza, N. C. (2010). Development of pyrF-based genetic system for targeted gene deletion in Clostridium thermocellum and creation of a pta mutant. *Applied and environmental microbiology*, *76*(19), 6591-6599.

192. Sakaguchi, K., Funaoka, N., Tani, S., Hobo, A., Mitsunaga, T., Kano, Y., & Suzuki, T. (2013). The pyrE gene as a bidirectional selection marker in Bifidobacterium longum 105-A. *Bioscience of microbiota, food and health*, *32*(2), 59-68.

193. Van Houdt, R., Provoost, A., Van Assche, A., Leys, N., Lievens, B., Mijnendonckx, K., & Monsieurs, P. (2018). Cupriavidus metallidurans strains with different mobilomes and from distinct environments have comparable phenomes. *Genes*, *9*(10), 507.

194. Andrup, L., Barfod, K. K., Jensen, G. B., & Smidt, L. (2008). Detection of large plasmids from the Bacillus cereus group. *Plasmid*, *59*(2), 139-143.

195. Haugan, K., Karunakaran, P., Tøndervik, A., & Valla, S. (1995). The host range of RK2 minimal replicon copy-up mutants is limited by species-specific differences in the maximum tolerable copy number. *Plasmid*, *33*(1), 27-39.

196. Miles, A. A., Misra, S. S., & Irwin, J. O. (1938). The estimation of the bactericidal power of the blood. *Epidemiology & Infection*, *38*(6), 732-749.

197. Mah, T. F., Pitts, B., Pellock, B., Walker, G. C., Stewart, P. S., & O'Toole, G. A. (2003). A genetic basis for Pseudomonas aeruginosa biofilm antibiotic resistance. *Nature*, *426*(6964), 306-310.

198. Pansegrau, W., Lanka, E., Barth, P. T., Figurski, D. H., Guiney, D. G., Haas, D., ... & Thomas, C. M. (1994). Complete nucleotide sequence of Birmingham IncPα plasmids: compilation and comparative analysis. *Journal of molecular biology*, *239*(5), 623-663.

199. Roberts, R. C., & Helinski, D. R. (1992). Definition of a minimal plasmid stabilization system from the broad-host-range plasmid RK2. *Journal of Bacteriology*, *174*(24), 8119-8132.

200. Ingram, L. C., Richmond, M. H., & Sykes, R. B. (1973). Molecular characterization of the R factors implicated in the carbenicillin resistance of a sequence of Pseudomonas aeruginosa strains isolated from burns. *Antimicrobial agents and chemotherapy*, *3*(2), 279-288.

201. Norberg, P., Bergström, M., Jethava, V., Dubhashi, D., & Hermansson, M. (2011). The IncP-1 plasmid backbone adapts to different host bacterial species and evolves through homologous recombination. *Nature communications*, *2*(1), 1-11.

202 Grogan, D. W., & Hansen, J. E. (2003). Molecular characteristics of spontaneous deletions in the hyperthermophilic archaeon Sulfolobus acidocaldarius. *Journal of bacteriology*, *185*(4), 1266-1272.

203. Grogan, D. W., Carver, G. T., & Drake, J. W. (2001). Genetic fidelity under harsh conditions: analysis of spontaneous mutation in the thermoacidophilic archaeon Sulfolobus acidocaldarius. *Proceedings of the National Academy of Sciences*, *98*(14), 7928-7933.

204. Martusewitsch, E., Sensen, C. W., & Schleper, C. (2000). High spontaneous mutation rate in the hyperthermophilic archaeon Sulfolobus solfataricus is mediated by transposable elements. *Journal of bacteriology*, *182*(9), 2574-2581.

205. Alviz-Gazitua, P., Fuentes-Alburquenque, S., Rojas, L. A., Turner, R. J., Guiliani, N., & Seeger, M. (2019). The response of Cupriavidus metallidurans CH34 to cadmium involves inhibition of the initiation of biofilm formation, decrease in intracellular c-di-GMP levels, and a novel metal regulated phosphodiesterase. *Frontiers in microbiology*, *10*, 1499.

206. Van Houdt, R., Vandecraen, J., Leys, N., Monsieurs, P., & Aertsen, A. (2021). Adaptation of Cupriavidus metallidurans CH34 to toxic zinc concentrations involves an uncharacterized ABC-Type transporter. *Microorganisms*, *9*(2), 309.

207. Arikawa, H., & Matsumoto, K. (2016). Evaluation of gene expression cassettes and production of poly (3-hydroxybutyrate-co-3-hydroxyhexanoate) with a fine modulated monomer composition by using it in Cupriavidus necator. *Microbial cell factories*, *15*(1), 1-11.

208. Cavaliere, M., Feng, S., Soyer, O. S., & Jiménez, J. I. (2017). Cooperation in microbial communities and their biotechnological applications. *Environmental microbiology*, *19*(8), 2949-2963.

209. Wang, M., Schaefer, A. L., Dandekar, A. A., & Greenberg, E. P. (2015). Quorum sensing and policing of Pseudomonas aeruginosa social cheaters. *Proceedings of the National Academy of Sciences*, *112*(7), 2187-2191.

210. Ryan, W., & Parulekar, S. J. (1991). Recombinant protein synthesis and plasmid instability in continuous cultures of Escherichia coli JM103 harboring a high copy number plasmid. *Biotechnology and bioengineering*, *37*(5), 415-429.

211. Sandoz, K. M., Mitzimberg, S. M., & Schuster, M. (2007). Social cheating in Pseudomonas aeruginosa quorum sensing. *Proceedings of the National Academy of Sciences*, *104*(40), 15876-15881.

212. Siddique, A., & Figurski, D. H. (2002). The active partition gene incC of IncP plasmids is required for stable maintenance in a broad range of hosts. *Journal of bacteriology*, *184*(6), 1788-1793.

213. Saurugger, P. N., Hrabak, O., Schwab, H., & Lafferty, R. M. (1986). Mapping and cloning of the par-region of broad-host-range plasmid RP4. *Journal of Biotechnology*, *4*(6), 333-343.

214. Summers, D. K., Beton, C. W., & Withers, H. L. (1993). Multicopy plasmid instability: the dimer catastrophe hypothesis. *Molecular microbiology*, *8*(6), 1031-1038.

215. Field, C. M., & Summers, D. K. (2011). Multicopy plasmid stability: revisiting the dimer catastrophe. *Journal of Theoretical Biology*, *291*, 119-127.

216. Adamczyk, M., & Jagura-Burdzy, G. (2003). Spread and survival of promiscuous IncP-1 plasmids. *Acta Biochimica Polonica*, *50*(2), 425-453.

217. Roberts, R. C., Burioni, R., & Helinski, D. R. (1990). Genetic characterization of the stabilizing functions of a region of broad-host-range plasmid RK2. *Journal of bacteriology*, *172*(11), 6204-6216.

218. Mougiakos, I., Bosma, E. F., Ganguly, J., van der Oost, J., & van Kranenburg, R. (2018). Hijacking CRISPR-Cas for high-throughput bacterial metabolic engineering: advances and prospects. *Current Opinion in Biotechnology*, *50*, 146-157.

219. Hsu, P. D., Lander, E. S., & Zhang, F. (2014). Development and applications of CRISPR-Cas9 for genome engineering. *Cell*, *157*(6), 1262-1278.

220. Li, N., Wang, M., Yu, S., & Zhou, J. (2021). Optimization of CRISPR-Cas9 through promoter replacement and efficient production of L-homoserine in Corynebacterium glutamicum. *Biotechnology Journal*, *16*(8), 2100093.

221. Mougiakos, I., Orsi, E., Ghiffary, M. R., Post, W., de Maria, A., Adiego-Perez, B., ... & van der Oost, J. (2019). Efficient Cas9-based genome editing of Rhodobacter sphaeroides for metabolic engineering. *Microbial cell factories*, *18*(1), 1-13.

222. Tapscott, T., Guarnieri, M. T., & Henard, C. A. (2019). Development of a CRISPR/Cas9 system for Methylococcus capsulatus in vivo gene editing. *Applied and environmental microbiology*, *85*(11), e00340-19.

223. Xiong, B., Li, Z., Liu, L., Zhao, D., Zhang, X., & Bi, C. (2018). Genome editing of Ralstonia eutropha using an electroporation-based CRISPR-Cas9 technique. *Biotechnology for biofuels*, *11*(1), 1-9.

224. Corts, A. D., Thomason, L. C., Gill, R. T., & Gralnick, J. A. (2019). A new recombineering system for precise genome-editing in Shewanella oneidensis strain MR-1 using single-stranded oligonucleotides. *Scientific reports*, *9*(1), 1-10.

225. Ferrières, L., Hémery, G., Nham, T., Guérout, A. M., Mazel, D., Beloin, C., & Ghigo, J. M. (2010). Silent mischief: bacteriophage Mu insertions contaminate products of Escherichia coli random mutagenesis performed using suicidal transposon delivery plasmids mobilized by broad-host-range RP4 conjugative machinery. *Journal of bacteriology*, *192*(24), 6418-6427

226. Wassarman, K. M., Zhang, A., & Storz, G. (1999). Small RNAs in escherichia coli. *Trends in microbiology*, *7*(1), 37-45.

227. Villa*, J. K., Su*, Y., Contreras, L. M., & Hammond, M. C. (2018). Synthetic biology of small RNAs and riboswitches. *Microbiology spectrum*, *6*(3), 6-3.

228. Guzman, L. M., Belin, D., Carson, M. J., & Beckwith, J. O. N. (1995). Tight regulation, modulation, and high-level expression by vectors containing the arabinose PBAD promoter. *Journal of bacteriology*, *177*(14), 4121-4130.

229. Siegele, D. A., & Hu, J. C. (1997). Gene expression from plasmids containing the araBAD promoter at subsaturating inducer concentrations represents mixed populations. *Proceedings of the National Academy of Sciences*, *94*(15), 8168-8172.

230. Desai, S. K., & Gallivan, J. P. (2004). Genetic screens and selections for small molecules based on a synthetic riboswitch that activates protein translation. *Journal of the American Chemical Society*, *126*(41), 13247-13254.

231. Topp, S., Reynoso, C. M., Seeliger, J. C., Goldlust, I. S., Desai, S. K., Murat, D., ... & Gallivan, J. P. (2010). Synthetic riboswitches that induce gene expression in diverse bacterial species. *Applied and environmental microbiology*, *76*(23), 7881-7884.

232. Jenison, R. D., Gill, S. C., Pardi, A., & Polisky, B. (1994). High-resolution molecular discrimination by RNA. *Science*, *263*(5152), 1425-1429.

233. Ran, F. A. F. A., Hsu, P. D., Wright, J., Agarwala, V., Scott, D. A., & Zhang, F. (2013). Genome engineering using the CRISPR-Cas9 system. *Nature protocols*, *8*(11), 2281-2308.

234. Johnson, A. O., Gonzalez-Villanueva, M., Tee, K. L., & Wong, T. S. (2018). An engineered constitutive promoter set with broad activity range for Cupriavidus necator H16. *ACS Synthetic Biology*, *7*(8), 1918-1928.

235. Siegele, D. A., & Hu, J. C. (1997). Gene expression from plasmids containing the araBAD promoter at subsaturating inducer concentrations represents mixed populations. *Proceedings of the National Academy of Sciences*, *94*(15), 8168-8172.

236. Vidal, L., Pinsach, J., Striedner, G., Caminal, G., & Ferrer, P. (2008). Development of an antibiotic-free plasmid selection system based on glycine auxotrophy for recombinant protein overproduction in Escherichia coli. *Journal of biotechnology*, *134*(1-2), 127-136.

237. Duzenli, O. F., & Okay, S. (2020). Promoter engineering for the recombinant protein production in prokaryotic systems. *AIMS Bioengineering*, *7*(2), 62-81.

238. Yang, L., Guell, M., Byrne, S., Yang, J. L., De Los Angeles, A., Mali, P., ... & Church, G. (2013). Optimization of scarless human stem cell genome editing. *Nucleic acids research*, *41*(19), 9049-9061.

239. Singh, P., Schimenti, J. C., & Bolcun-Filas, E. (2015). A mouse geneticist's practical guide to CRISPR applications. *Genetics*, *199*(1), 1-15.

240. Bull, J. J., & Barrick, J. E. (2017). Arresting evolution. *Trends in Genetics*, *33*(12), 910-920.

241. Deatherage, D. E., Leon, D., Rodriguez, Á. E., Omar, S. K., & Barrick, J. E. (2018). Directed evolution of Escherichia coli with lower-than-natural plasmid mutation rates. *Nucleic acids research*, *46*(17), 9236-9250.

242. Renda, B. A., Hammerling, M. J., & Barrick, J. E. (2014). Engineering reduced evolutionary potential for synthetic biology. *Molecular BioSystems*, *10*(7), 1668-1678.

243. Baharoglu, Z., Bikard, D., & Mazel, D. (2010). Conjugative DNA transfer induces the bacterial SOS response and promotes antibiotic resistance development through integron activation. *PLoS genetics*, *6*(10), e1001165.

244. Kilmury, S. L., & Burrows, L. L. (2016). Type IV pilins regulate their own expression via direct intramembrane interactions with the sensor kinase PilS. *Proceedings of the National Academy of Sciences*, *113*(21), 6017-6022.

245. Millacura, F. A., Janssen, P. J., Monsieurs, P., Janssen, A., Provoost, A., Van Houdt, R., & Rojas, L. A. (2018). Unintentional genomic changes endow Cupriavidus metallidurans with an augmented heavy-metal resistance. *Genes*, *9*(11), 551.

246. Ruegg, T. L., Pereira, J. H., Chen, J. C., DeGiovanni, A., Novichkov, P., Mutalik, V. K., ... & Thelen, M. P. (2018). Jungle Express is a versatile repressor system for tight transcriptional control. *Nature communications*, *9*(1), 1-13.

247. Reith, F., Etschmann, B., Grosse, C., Moors, H., Benotmane, M. A., Monsieurs, P., ... & Brugger, J. (2009). Mechanisms of gold biomineralization in the bacterium Cupriavidus metallidurans. *Proceedings of the National Academy of Sciences*, *106*(42), 17757-17762.

248. Richter, L. V., Sandler, S. J., & Weis, R. M. (2012). Two isoforms of Geobacter sulfurreducens PilA have distinct roles in pilus biogenesis, cytochrome localization, extracellular electron transfer, and biofilm formation. *Journal of bacteriology*, *194*(10), 2551-2563.

249. Liu, X., Tremblay, P. L., Malvankar, N. S., Nevin, K. P., Lovley, D. R., & Vargas, M. (2014). A Geobacter sulfurreducens strain expressing Pseudomonas aeruginosa type IV pili localizes OmcS on pili but is deficient in Fe (III) oxide reduction and current production. *Applied and environmental microbiology*, *80*(3), 1219-1224.

250. Uria, N., Fiset, E., Pellitero, M. A., Muñoz, F. X., Rabaey, K., & del Campo, F. J. (2020). Immobilisation of electrochemically active bacteria on screen-printed electrodes for rapid in situ toxicity biosensing. *Environmental Science and Ecotechnology*, *3*, 100053.

251. Li, Z., Zhang, Y., LeDuc, P. R., & Gregory, K. B. (2011). Microbial electricity generation via microfluidic flow control. *Biotechnology and bioengineering*, *108*(9), 2061-2069.

252. Dávila, D., Esquivel, J. P., Sabate, N., & Mas, J. (2011). Silicon-based microfabricated microbial fuel cell toxicity sensor. *Biosensors and Bioelectronics*, *26*(5), 2426-2430.

253. Hayat, A., & Marty, J. L. (2014). Disposable screen printed electrochemical sensors: Tools for environmental monitoring. *Sensors*, *14*(6), 10432-10453.

254. Sudhakara Prasad, K., Arun, A. E., Rekha, P. E., Young, C. C., Chang, J. L., & Zen, J. M. (2009). A Microbial Sensor Based on Direct Electron Transfer at Shewanella Sp. Drop-Coated Screen-Printed Carbon Electrodes. *Electroanalysis: An International Journal Devoted to Fundamental and Practical Aspects of Electroanalysis*, *21*(14), 1646-1650.

255. Estevez-Canales, M., Berná, A., Borjas, Z., & Esteve-Núñez, A. (2015). Screen-printed electrodes: new tools for developing microbial electrochemistry at microscale level. *Energies*, *8*(11), 13211-13221.

256. Richter, H., Nevin, K. P., Jia, H., Lowy, D. A., Lovley, D. R., & Tender, L. M. (2009). Cyclic voltammetry of biofilms of wild type and mutant Geobacter sulfurreducens on fuel cell anodes indicates possible roles of OmcB, OmcZ, type IV pili, and protons in extracellular electron transfer. *Energy & Environmental Science*, *2*(5), 506-516.

257. Valentini, F., Amine, A., Orlanducci, S., Terranova, M. L., & Palleschi, G. (2003). Carbon nanotube purification: preparation and characterization of carbon nanotube paste electrodes. *Analytical chemistry*, *75*(20), 5413-5421.

258. Esteve-Núñez, A., Sosnik, J., Visconti, P., & Lovley, D. R. (2008). Fluorescent properties of c-type cytochromes reveal their potential role as an extracytoplasmic electron sink in Geobacter sulfurreducens. *Environmental microbiology*, *10*(2), 497-505.

259. McCreery, R. L. (2008). Advanced carbon electrode materials for molecular electrochemistry. *Chemical reviews*, *108*(7), 2646-2687.

260. Ranganathan, S., Kuo, T. C., & McCreery, R. L. (1999). Facile preparation of active glassy carbon electrodes with activated carbon and organic solvents. *Analytical chemistry*, *71*(16), 3574-3580.

261. Evans, J. F., & Kuwana, T. (1979). Introduction of functional groups onto carbon electrodes via treatment with radio-frequency plasmas. *Analytical Chemistry*, *51*(3), 358-365.

262. Engstrom, R. C. (1982). Electrochemical pretreatment of glassy carbon electrodes. *Analytical Chemistry*, *54*(13), 2310-2314.

263. Grattieri, M., Hasan, K., & Minteer, S. D. (2017). Bioelectrochemical systems as a multipurpose biosensing tool: Present perspective and future outlook. *ChemElectroChem*, *4*(4), 834-842.

264. Aoki, K. J., Chen, J., Liu, Y., & Jia, B. (2020). Peak potential shift of fast cyclic voltammograms owing to capacitance of redox reactions. *Journal of Electroanalytical Chemistry*, *856*, 113609.

265. Marsili, E., Baron, D. B., Shikhare, I. D., Coursolle, D., Gralnick, J. A., & Bond, D. R. (2008). Shewanella secretes flavins that mediate extracellular electron transfer. *Proceedings of the National Academy of Sciences*, *105*(10), 3968-3973.

266. Harnisch, F., & Freguia, S. (2012). A basic tutorial on cyclic voltammetry for the investigation of electroactive microbial biofilms. *Chemistry–An Asian Journal*, *7*(3), 466-475.

267. Gregg, B. A., & Heller, A. (1991). Redox polymer films containing enzymes. 2. Glucose oxidase containing enzyme electrodes. *The Journal of Physical Chemistry*, *95*(15), 5976-5980.

268. Fricke, K., Harnisch, F., & Schröder, U. (2008). On the use of cyclic voltammetry for the study of anodic electron transfer in microbial fuel cells. *Energy & Environmental Science*, *1*(1), 144-147.

269. Zhang, X., Prévoteau, A., Louro, R. O., Paquete, C. M., & Rabaey, K. (2018). Periodic polarization of electroactive biofilms increases current density and charge carriers concentration while modifying biofilm structure. *Biosensors and Bioelectronics*, *121*, 183-191.

270. Zhang, X., Prévoteau, A., Louro, R. O., Paquete, C. M., & Rabaey, K. (2018). Periodic polarization of electroactive biofilms increases current density and charge carriers concentration while modifying biofilm structure. *Biosensors and Bioelectronics*, *121*, 183-191.

271. Freguia, S., Rabaey, K., Yuan, Z., & Keller, J. (2007). Electron and carbon balances in microbial fuel cells reveal temporary bacterial storage behavior during electricity generation. *Environmental science & technology*, *41*(8), 2915-2921.

272. Nishio, K., Kimoto, Y., Song, J., Konno, T., Ishihara, K., Kato, S., ... & Nakanishi, S. (2014). Extracellular electron transfer enhances polyhydroxybutyrate productivity in Ralstonia eutropha. *Environmental Science & Technology Letters*, *1*(1), 40-43.

273. Liu, Y., & Bond, D. R. (2012). Long-distance electron transfer by G. sulfurreducens biofilms results in accumulation of reduced c-type cytochromes. *ChemSusChem*, *5*(6), 1047-1053.

274. Busalmen, J. P., Esteve-Núñez, A., Berná, A., & Feliu, J. M. (2008). C-type cytochromes wire electricity-producing bacteria to electrodes. *Angewandte Chemie International Edition*, *47*(26), 4874-4877.

275. Dawkins, R. C., Wen, D., Hart, J. N., & Vepsäläinen, M. (2021). A screen-printed Ag/AgCl reference electrode with long-term stability for electroanalytical applications. *Electrochimica Acta*, *393*, 139043.

276 Søpstad, S., Johannessen, E. A., Seland, F., & Imenes, K. (2018). Long-term stability of screen-printed pseudo-reference electrodes for electrochemical biosensors. *Electrochimica Acta*, *287*, 29-36.

277. Tas, H., Amara, A., Cueva, M. E., Bongaerts, N., Calvo-Villamañán, A., Hamadache, S., & Vavitsas, K. (2020). Are synthetic biology standards applicable in everyday research practice?. *Microbial Biotechnology*, *13*(5), 1304-1308.

278. Mittal, P., Brindle, J., Stephen, J., Plotkin, J. B., & Kudla, G. (2018). Codon usage influences fitness through RNA toxicity. *Proceedings of the National Academy of Sciences*, *115*(34), 8639-8644.

279. Abdelrahman, M., Wei, Z., Rohila, J. S., & Zhao, K. (2021). Multiplex genome-editing technologies for revolutionizing plant biology and crop improvement. *Frontiers in Plant Science*, *12*.

280. Yalcin, S. E., & Malvankar, N. S. (2020). The blind men and the filament: understanding structures and functions of microbial nanowires. *Current opinion in chemical biology*, *59*, 193-201.

9 -Appendix

9.1.1 Nucleotide Sequences of Promoters Used in This Study

The P_{Pan} promoter was ordered from Genescript in pUC57 vector as lyophilised DNA. Before, transformation in *E. Coli* DH5α it was resuspended in de-ionized H_2O according to manufacturer's instructions. All the other promoters were either added as spacers during PCRs or amplified by in-house plasmids.

P_{AraE}

TTTATATTTAGTCCCTTGCCTTGCCTACAAGGGATTTCCTATTCCTTTCAT
TTACAATTCATACGTATAAAATCCAAATTTTTCTTGACATTTATACACATA
AATATTATGATTTATATAGGTAATCGCTTTCATAAAATATATTACCCTTA
GGAAATCAAATGATTATAAGTCATATATGAAAACGTTATATATAATTGAT
ATGTTTACATTTGTAACTTAGATTTCTCTTTGATTTCCACATATATAAATC
TTAAGGAGGAGTTTTC

P_{J23119}

TTGACAGCTAGCTCAGTCCTAGGTATAATGCTAGC

P_{λ}

TAACACCGTGCGTGTTGACTATTTTACCTCTGGCGGTGATAATGGTTGC

P_{A0284}

GTCTTCATTCAAGGTTTTTCCCATGGACTGTTGTTCTAGTCGGCGTTACGT
CGAAACCTGAACGGCTAGTCAGTCAAGGCGACTCTTCGCCACTGCCTAG
CCGACATGGCGGGCAGTGGTATTCGCGCGGGTTCCCCGCGCGGCCATCTC
CCATCTATTTTTGCGACCTTTGTCATCAGGGAAACTGAGGGCGACTTACG
CTCGCGCGTTTCTCACGATGCAGGTCGTGTGTGCCTACATGCGCCGTAGA
AGCGCGTGGGGGAGGTCGC

P_{Pan}

GTTCGGTATCGAAAGCCGCTTTATCGAGCCGGGCTCATACAAGACATCG
ATCTGGTCAACGTCATTATCAAATTTTATGTCGGTGCCTCGTGCAGATTC
AGCCTATCATCAATACTATAAAAAGATCCTTTCCTATGTTCAAAAAAACG
GAGAAGAAATCGGAGATCCCCAAGAGGTTGCCGACCTCATTTATCAATT

GGCAACAAAACACGACATAAAGAATTTGCGATACCCGATCGGAAAGGGC
ATCAAGCTCACCCTGCTGTTCCGATCGCTTTTTCCTTGGTCTGCGTGGGAG
TCTATCCTGAAGAAAAAGCTAATTCAGCTGATCTAAATTATAATTATTAT
AATTTAGTATTGATTTTTATTTAGTATATGATATAATTAAGTCA

P_{BAD} (Includes *araC*)

TTATGACAACTTGACGGCTACATCATTCACTTTTTCTTCACAACCGGCAC
GGAACTCGCTCGGGCTGGCCCCGGTGCATTTTTTAAATACCCGCGAGAAA
TAGAGTTGATCGTCAAAACCAACATTGCGACCGACGGTGGCGATAGGCA
TCCGGGTGGTGCTCAAAAGCAGCTTCGCCTGGCTGATACGTTGGTCCTCG
CGCCAGCTTAAGACGCTAATCCCTAACTGCTGGCGGAAAAGATGTGACA
GACGCGACGGCGACAAGCAAACATGCTGTGCGACGCTGGCGATATCAAA
ATTGCTGTCTGCCAGGTGATCGCTGATGTACTGACAAGCCTCGCGTACCC
GATTATCCATCGGTGGATGGAGCGACTCGTTAATCGCTTCCATGCGCCGC
AGTAACAATTGCTCAAGCAGATTTATCGCCAGCAGCTCCGAATAGCGCC
CTTCCCCTTGCCCGGCGTTAATGATTTGCCCAAACAGGTCGCTGAAATGC
GGCTGGTGCGCTTCATCCGGGCGAAAGAACCCCGTATTGGCAAATATTG
ACGGCCAGTTAAGCCATTCATGCCAGTAGGCGCGCGGACGAAAGTAAAC
CCACTGGTGATACCATTCGCGAGCCTCCGGATGACGACCGTAGTGATGA
ATCTCTCCTGGCGGGAACAGCAAAATATCACCCGGTCGGCAAACAAATT
CTCGTCCCTGATTTTTCACCACCCCCTGACCGCGAATGGTGAGATTGAGA
ATATAACCTTTCATTCCCAGCGGTCGGTCGATAAAAAAATCGAGATAACC
GTTGGCCTCAATCGGCGTTAAACCCGCCACCAGATGGGCATTAAACGAG
TATCCCGGCAGCAGGGGATCATTTTGCGCTTCAGCCATACTTTTCATACT
CCCGCCATTCAGAGAAGAAACCAATTGTCCATATTGCATCAGACATTGCC
GTCACTGCGTCTTTTACTGGCTCTTCTCGCTAACCAAACCGGTAACCCCG
CTTATTAAAAGCATTCTGTAACAAAGCGGGACCAAAGCCATGACAAAAA
CGCGTAACAAAAGTGTCTATAATCACGGCAGAAAAGTCCACATTGATTA
TTTGCACGGCGTCACACTTTGCTATGCCATAGCATTTTTATCCATAAGATT
AGCGGATTCTACCTGACGCTTTTTATCGCAACTCTCTACTGTTTCTCCAT

P_{trpsyn}

CTGTTGACAATTAATCATCGAACTAGTTAACTAGTACGCACAACAGATCA
CAAGGAGGACGTTAT

9.1.2 Nucleotide Sequences of Riboswitches Used in this Study

Table 18-Sequence of Rioboswitches used in this study

Riboswitch & Nucleotide sequence (5'-3')	Reference
E GGUGAUACCAGCAUCGUCUUGAUGCCCUUGGCAGCACC CUGCUAAGGAGGUAACAACAAGAUG	Topp *et al.*,[234]
F GGUGAUACCAGCAUCGUCUUGAUGCCCUUGGCAGCACC CUGCUAAGGAGGCAACAACAUG	Cañadas *et al.*,[84]
G GGUGAUACCAGCAUCGUCUUGAUGCCCUUGGCAGCACC CUGCUAAGGAGGUAACAACAUG	Cañadas *et al.*,[84]
H GGUGAUACCAGCAUCGUCUUGAUGCCCUUGGCAGCACC CUGCUAAGGAGGUAACUUAAUG	Cañadas *et al.*,[84]
I GGUGAUACCAGCAUCGUCUUGAUGCCCUUGGCAGCACC CUGCUAAGGAGGUGUGUUAAUG	Cañadas *et al.*,[84]
J GGUGAUACCAGCAUCGUCUUGAUGCCCUUGGCAGCACC CUGCUAAGGAGGUCAACAAGAUG	Cañadas *et al.*,[84]
L //	Cañadas *et al.*,[84]

9.2 Supplementary Figures

Figure S1-Plasmid map of pMTL71101 and pMTL71101_P$_{BAD}$_*SNAP_aidA*-C

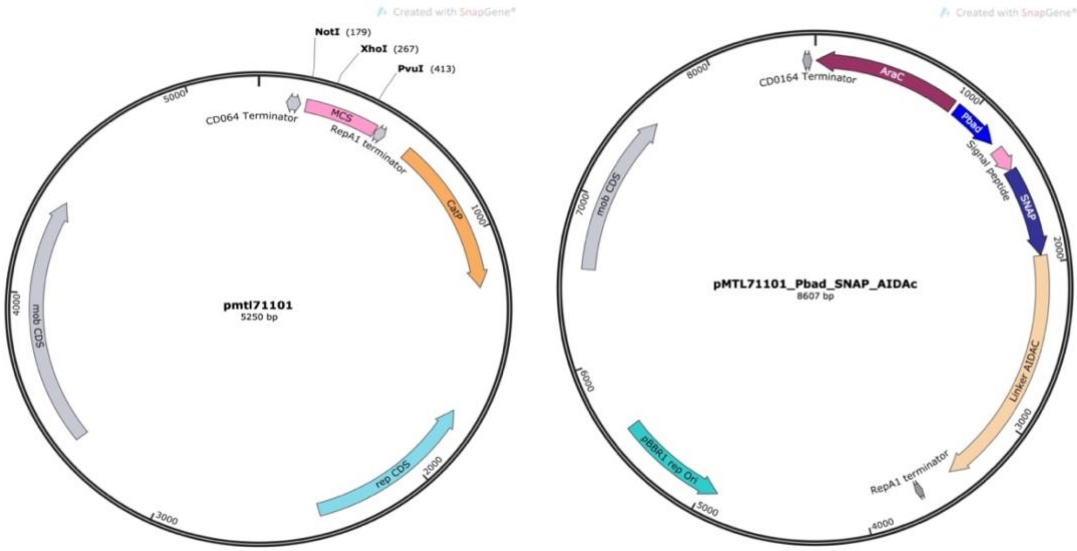

Figure S2-Plasmid maps of pMTL71101 with relative restriction sites and resulting pMTL71101_P$_{pan}$*mRFP1*_P$_{trpsyn}$*pyrE*FA1090

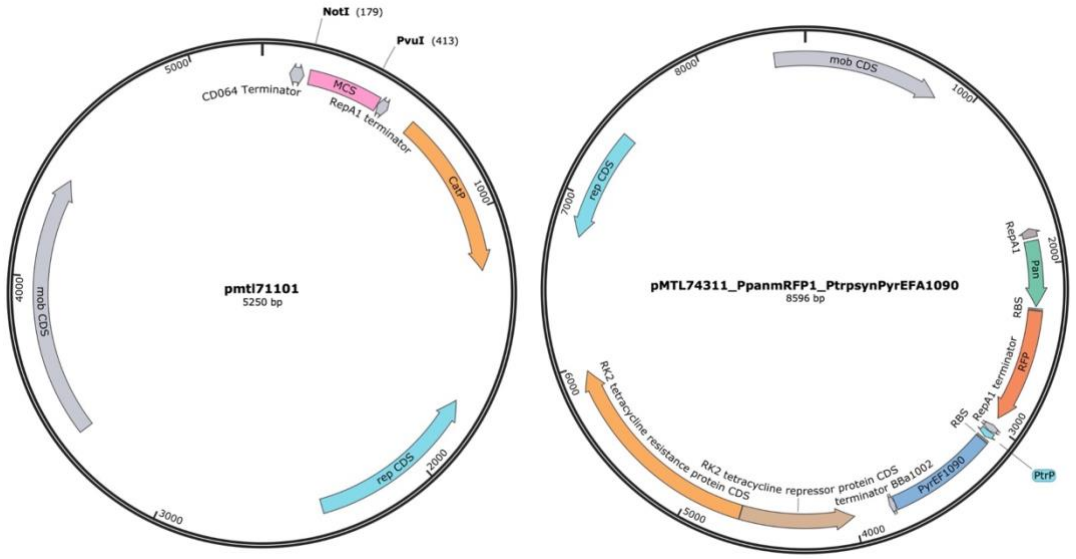

Figure S3-Plasmid maps of pMTL71301 with relative restriction sites and resulting pMTL71301_P_{pan}*mRFP1*_P_{trpsyn}*pyrE*FA1090

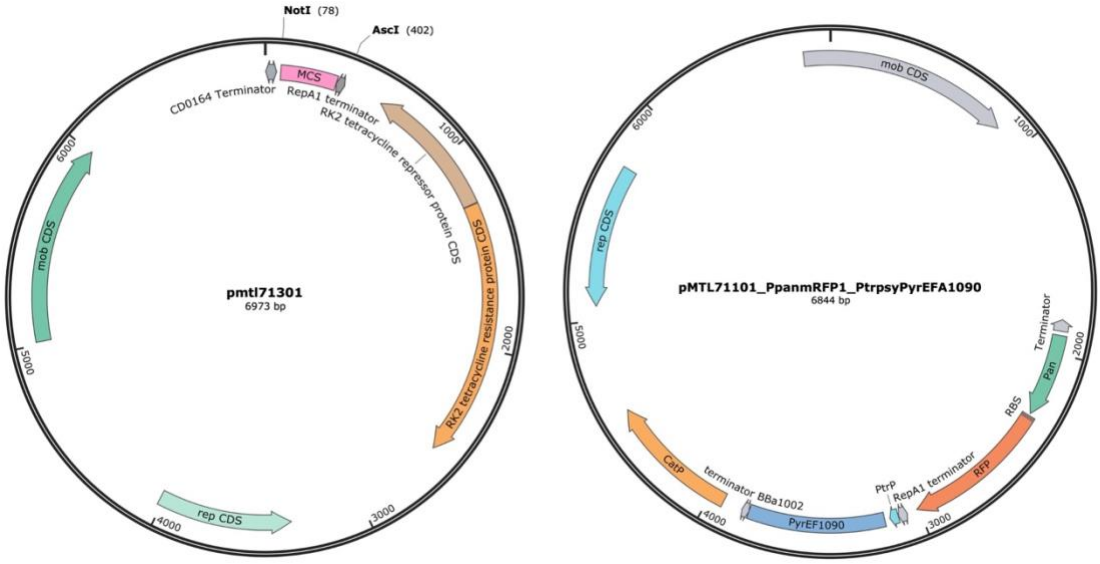

Figure S4-OD_{600} of *C. metallidurans* NG7*_mRFP1* and *C. metallidurans* NG7*_ΔpyrE_mRFP1*: measurements from growth in continuous

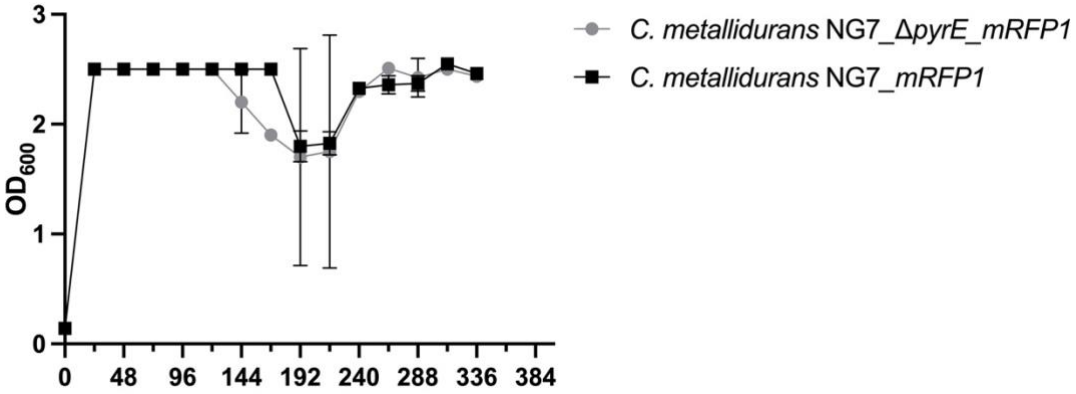

Figure S5-OD600 of *C. metallidurans* CH34_*mRFP1* and *C. metallidurans* CH34_Δ*pyrE_mRFP1*: Measurements from growth in continuous prior to beginning of Covid-19 pandemic

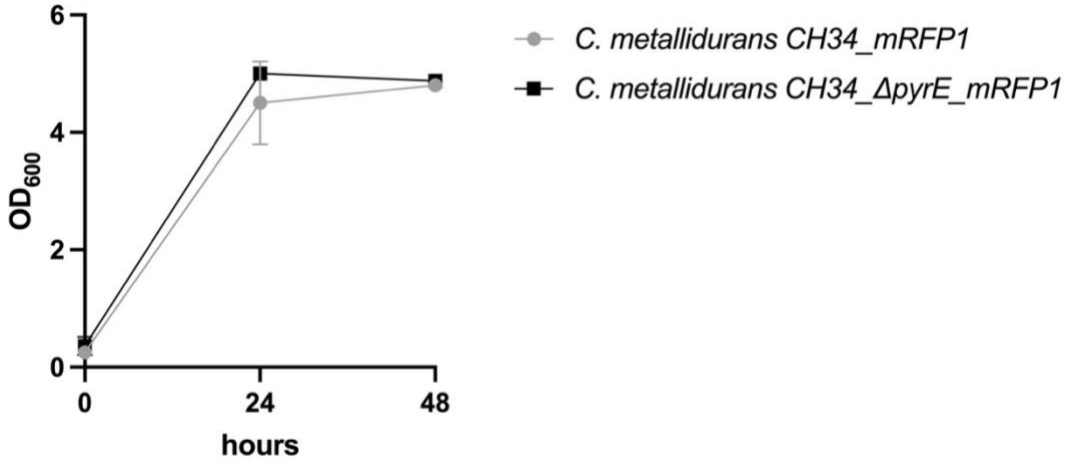

Figure S6-plasmid maps of A) pMTL74311 with related restriction sites, B) pMTL74301Low*_parCBADE* and C) pMTL74301Low

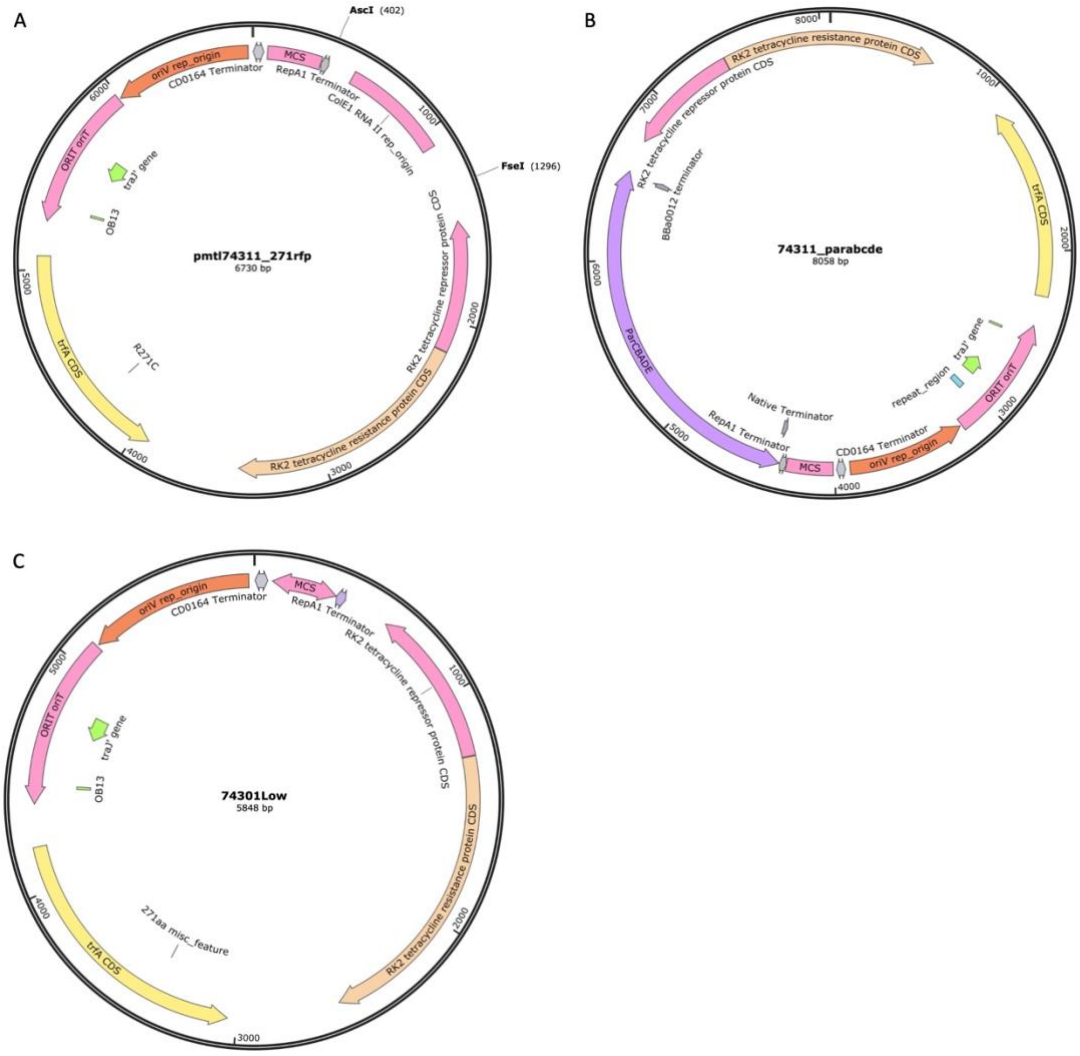

Figure S7-strategy for identification via cPCR of Δ*pilA/E* knockout strains of *C. metallidurans* CH34: PilAUp2_Fw/PilEDw_Rv (OUT_OUT2) were used for screening of Δ*pilAE* knockouts. Primers PilAUp3_Fw/RHA_Dw4_Rv (OUT_OUT) were used for screening of all the other knockouts. Primers PilA_Sq_Rv and PilE_Sq_Rv were then used in combination with PilAUp3_Fw for exclusion of wild type contamination from Δ*pilA*/Δ*pilAE* and Δ*pilE* strains, respectively.

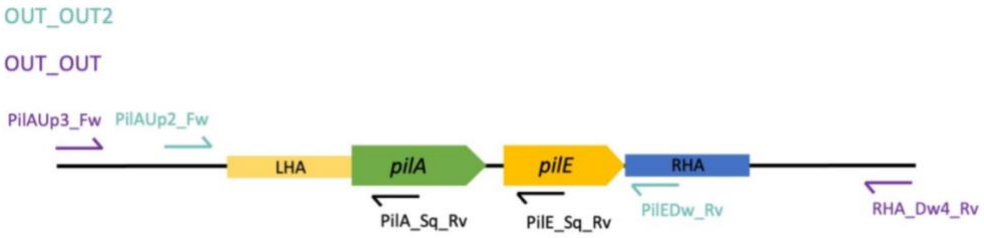

Figure S8 Agarose gel electrophoresis of representative knockout strains of *C. metallidurans* CH34 isolated from the induction plates of one of the mother colonies induced: cPCR of Δ*pilAE*, Δ*pilAE*::*GFP*, Δ*pilA*, Δ*pilE*, Δ*pilAE*::λ*GFP*. Genomic DNA of *C. metallidurans* CH34 and the respective plasmids for delivery of Cas9 were used as positive and negative control respectively (labelled as + and – in the figure).

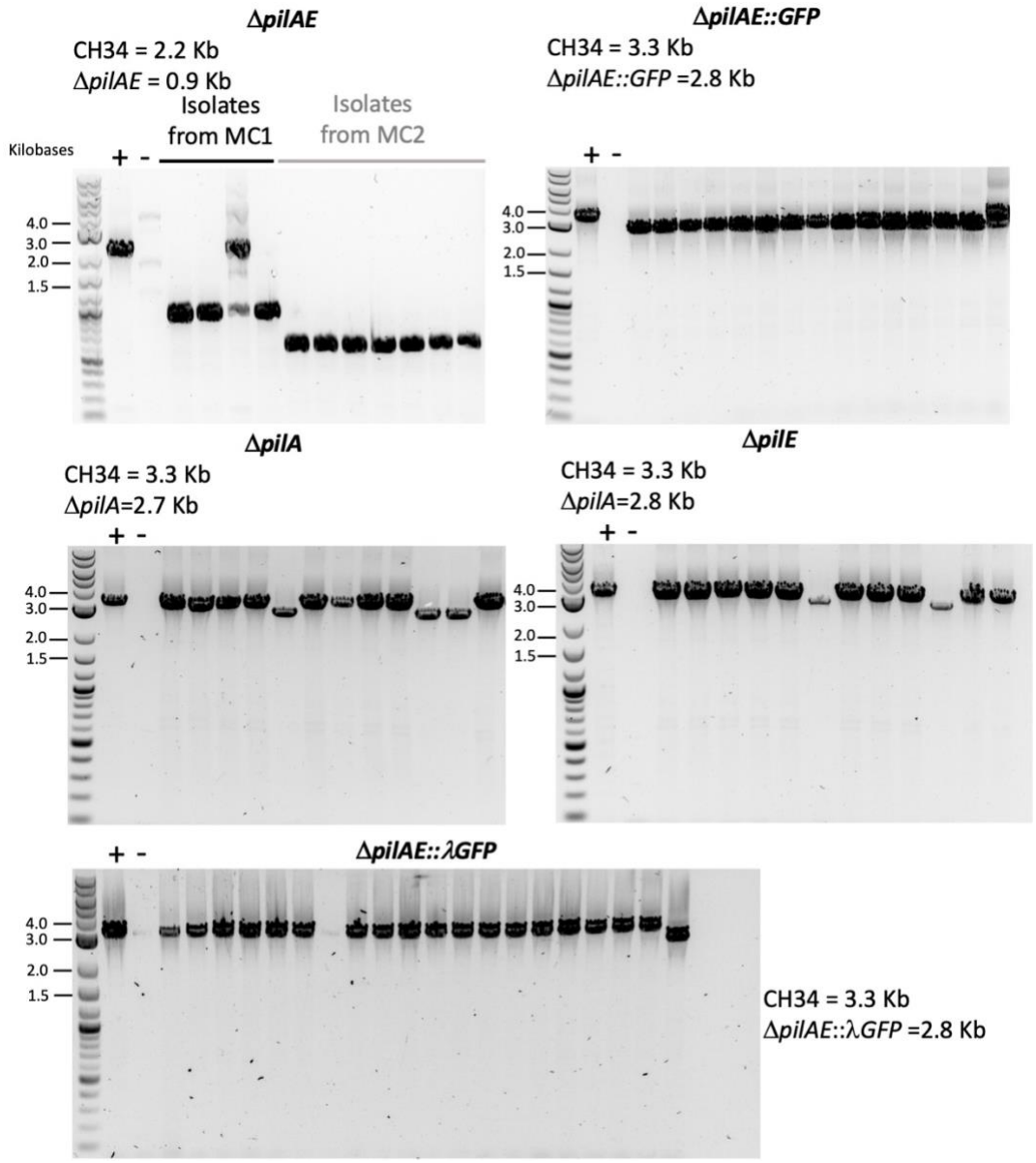

Table S9-List of Mutations of *C. metallidurans* CH34 wild type compared to sequences deposited in GeneBank

Strain	Type of Mutation	Region	Chromosme	Length (number of nucleotides)	CDS	Gene product
CH34 WT	SNP	1764297	Chromid	1	intergenic	Polihydroxyalkanoil acid synthase MFS transporter mercury II reductase mercury II reductase FUCS family protein UvrD helicase contain domain protein
		1816867			Rmet_5122	
		1874248^1874249	CHR1		Rmet_RS08660	
		2533709^2533710			Rmet_RS11620	
		2533760^2533761			Rmet_RS11620	
		3620760^3620761			Rmet_RS16815	
		3759195			Rmet_3478	
	Deletion	2329884..2330258	CHR1	375	Intergenic	hypothetical protein, AAA family ATPase, IS481 family transposase, transposase
		3403805..3407322	CHR1	3518	Rmet_3140-Rmet_3143	
	Inversion	2376693..>2376792	CHR1	237162	Rmet_2172	site specific integrase
		<2613755..2613854		237162	Rmet_12045	Tyrosine type integrase/recombinase
	Replacement	201288..201427	pMOL30	140	Intergenic	

Table S10-List of mutations of *C. metallidurans* CH34 mutants generated with CRISPR-Cas9 system

Strain	Type of Mutation	Region	Chromosme	Length (number of nucleotides)	CDS	Gene product
CH34 Δ*pilAE*#2	Deletion	501865..503157	CHR1	1293	Rmet_0472-_0473	*pilAE* type IV pili
CH34 Δ*pilAE*#3	Deletion	501865..503157	CHR1	1293	Rmet_0472-_0473	*pilAE* type IV pili
CH34 Δ*pilAE*#5	Deletion	501865..503157	CHR1	1293	Rmet_0472-_0473	*pilAE* type IV pili
CH34 Δ*pilA*#1	SNP (G>A)	36277	Chromid	1	Rmet_5844	Polysaccaride biosynthesis tyrosine autokinase
	SNP (G>T)	36281		1	Rmet_5844	Polysaccaride biosynthesis tyrosine autokinase
	Replacement	36277..36415	Chromid	139	Rmet_5844	Polysaccaride biosynthesis tyrosine autokinase
	SNP	501781	CHR1		Intergenic	
	Complex	802867..802931	Chromid	65	Intergenic	
CH34 Δ*pilA*#2	Deletion	501865..502413	CHR1	549	Rmet_0472	*pilA* type IV pili
CH34 Δ*pilA*#11	Deletion	501865..502413	CHR1	549	Rmet_0472	*pilA* type IV pili

Table S10-List of mutations of *C. metallidurans* CH34 mutants generated with CRISPR-Cas9 system: continuation from previous page

Strain	Type of Mutation	Region	Chromosme	Length (number of nucleotides)	CDS	Gene product
CH34 Δ*pilE*#3	Deletion	501865..503157	CHR1	495	Rmet_0473	*pilE* type IV pili
CH34 Δ*pilE*#6	Deletion	501865..503157	CHR1	495	Rmet_0473	*pilE* type IV pili
CH34 Δ*pilE*#11	Deletion	501865..503157	CHR1	495	Rmet_0473	*pilE* type IV pili

Figure S11-Maps of plasmids pMTL74311 & pMTL74311_RiboCas_Δ*phac1*

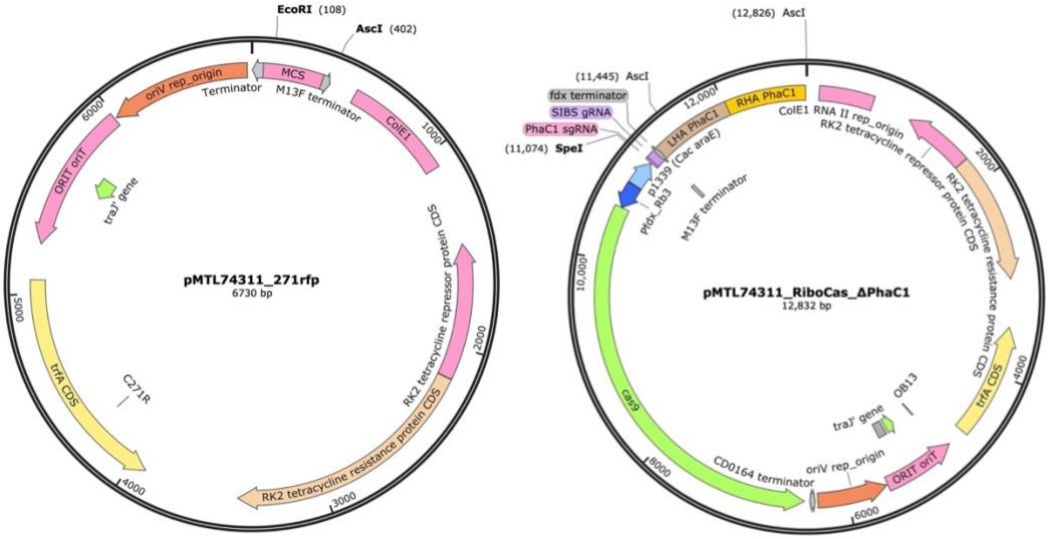

Figure S12-Maps of plasmids pMTL71301_P$_{J23119}$_*mRFP1* & pMTL71301_P$_{BAD}$RBI_*mRFP1*

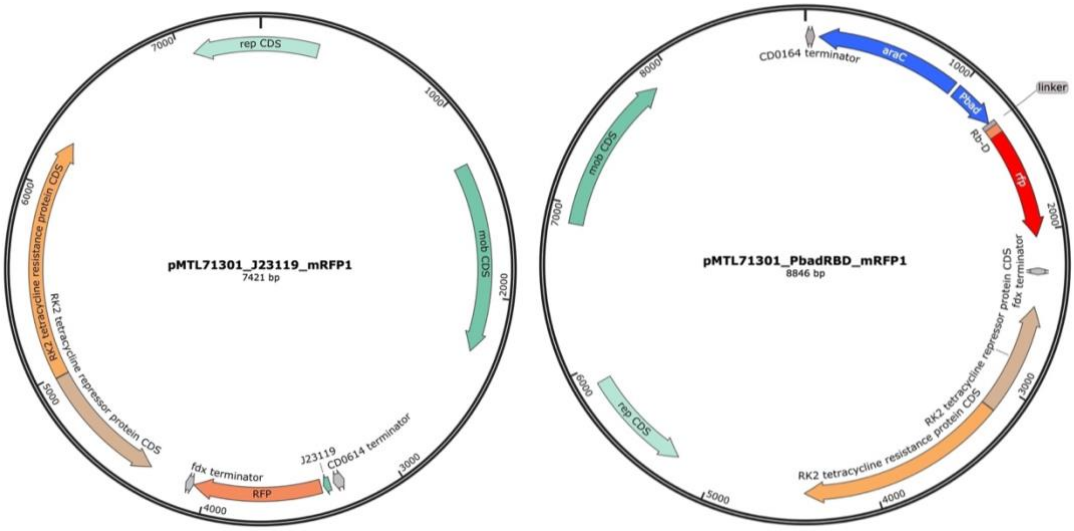

Figure S13-Maps of plasmids pMTL74311_RBIC9_Δ*pyrE* & pMTL74311_RBIC_Δ*pilAE*

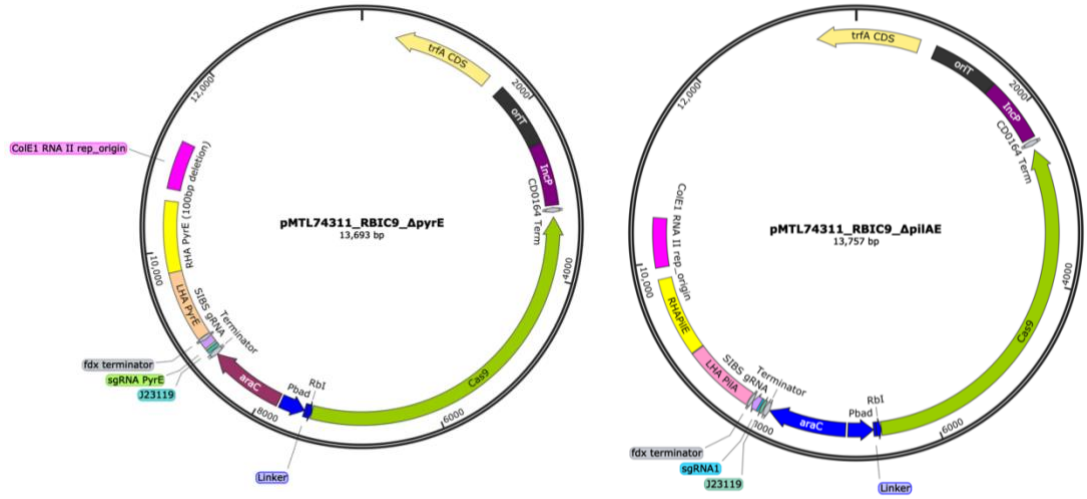

Figure S14: Maps of plasmids pMTL74311_RBIC9_Δ*pilE* & pMTL74311_RBIC9_Δ*pilA*

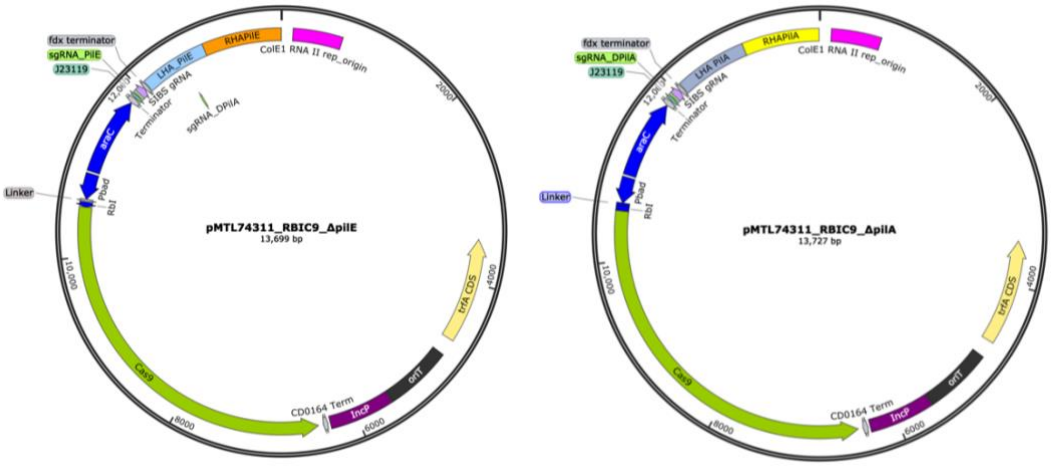

Figure S15: Maps of plasmids pMTL74311_RBIC9_Δ*pilAE*::*gfp* & pMTL74311_RBIC9_Δ*pilAE*::λ*gfp*

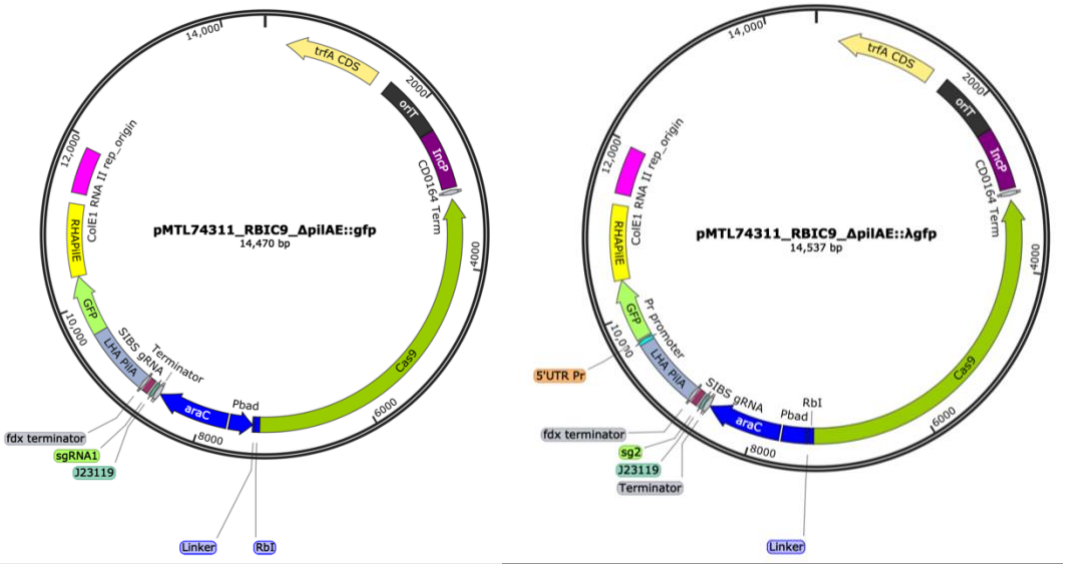

Figure S16-Cyclic voltammograms of biological replicates 2 and 3 of against the negative control for the biofilm-modified SPCE with *C. metallidurans* CH34showing shift of the current peaks in the biofilm-modified replicates: Black track is the abiotic SPCE, orange and purple tracks represent biological replicate 2 and 3 of the biofilm-modified SPCE.

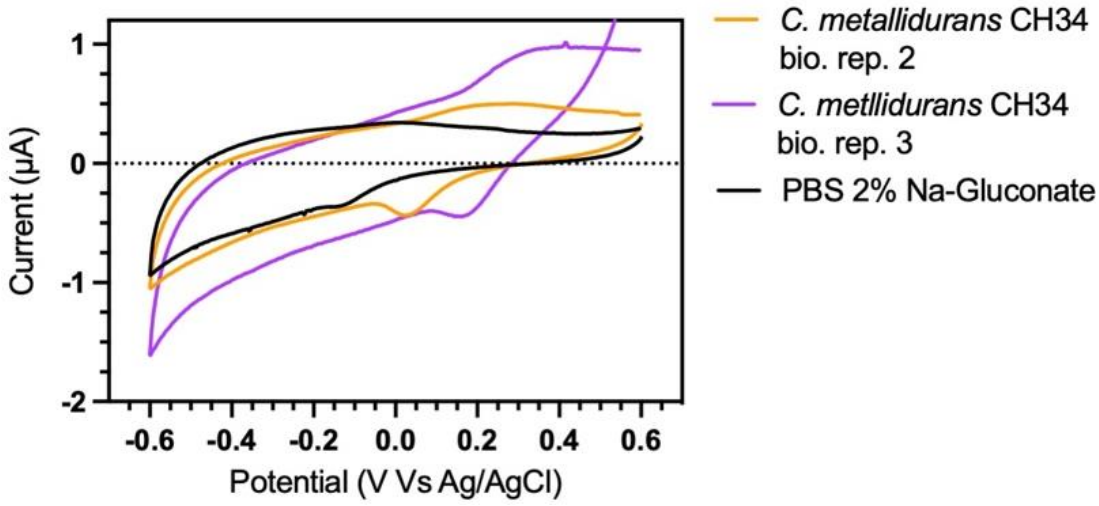

Figure S17-Confocal microscopy of Biofilm-modified SPCE stained with Syto9 and PI: seen from A) above and B) Z-stack. Scale bar (red) represents 20 μM.

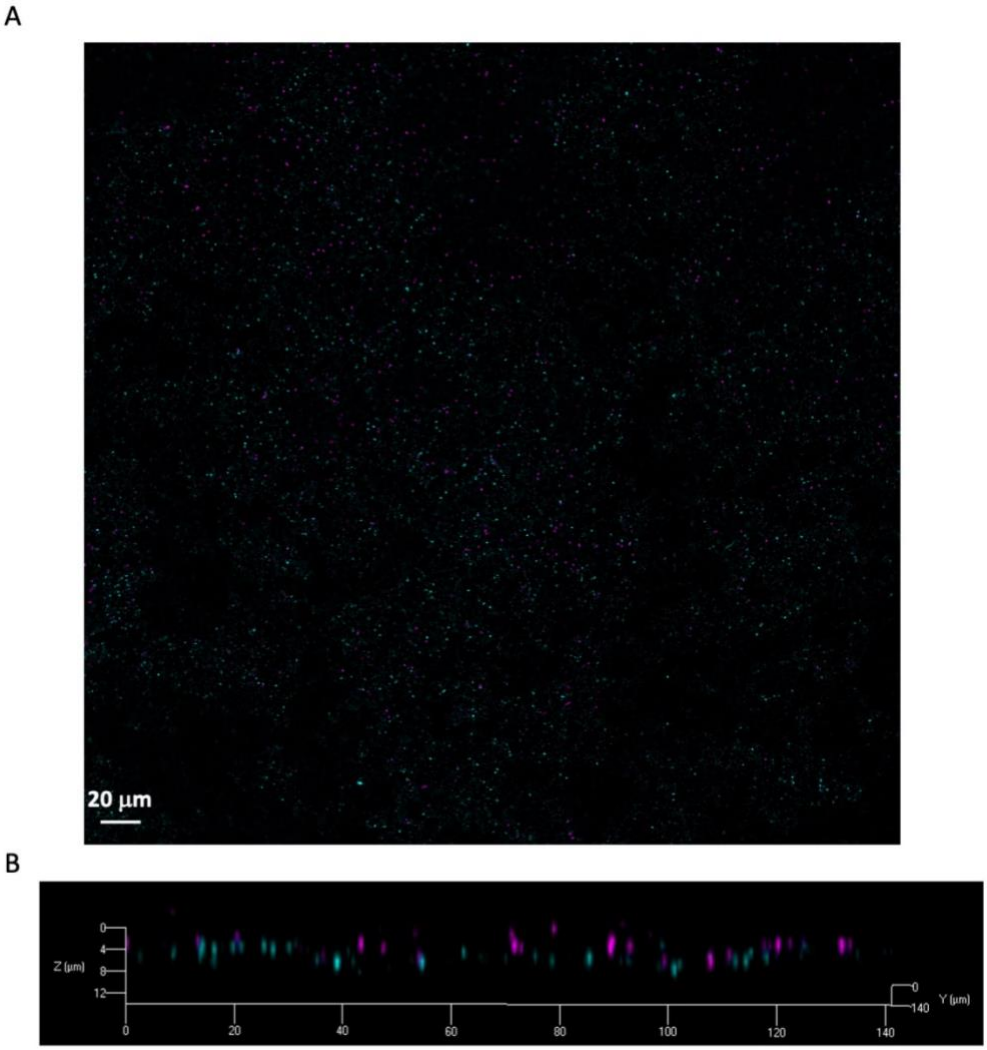

Figure S18 Plot of anodic I_{ox} current vs scan rate